ISSN 1949-8470 (online)

World Journal of Radiology

World J Radiol 2009 December 31; 1(1): 1-91

A peer-reviewed, online, open-access journal of Radiology

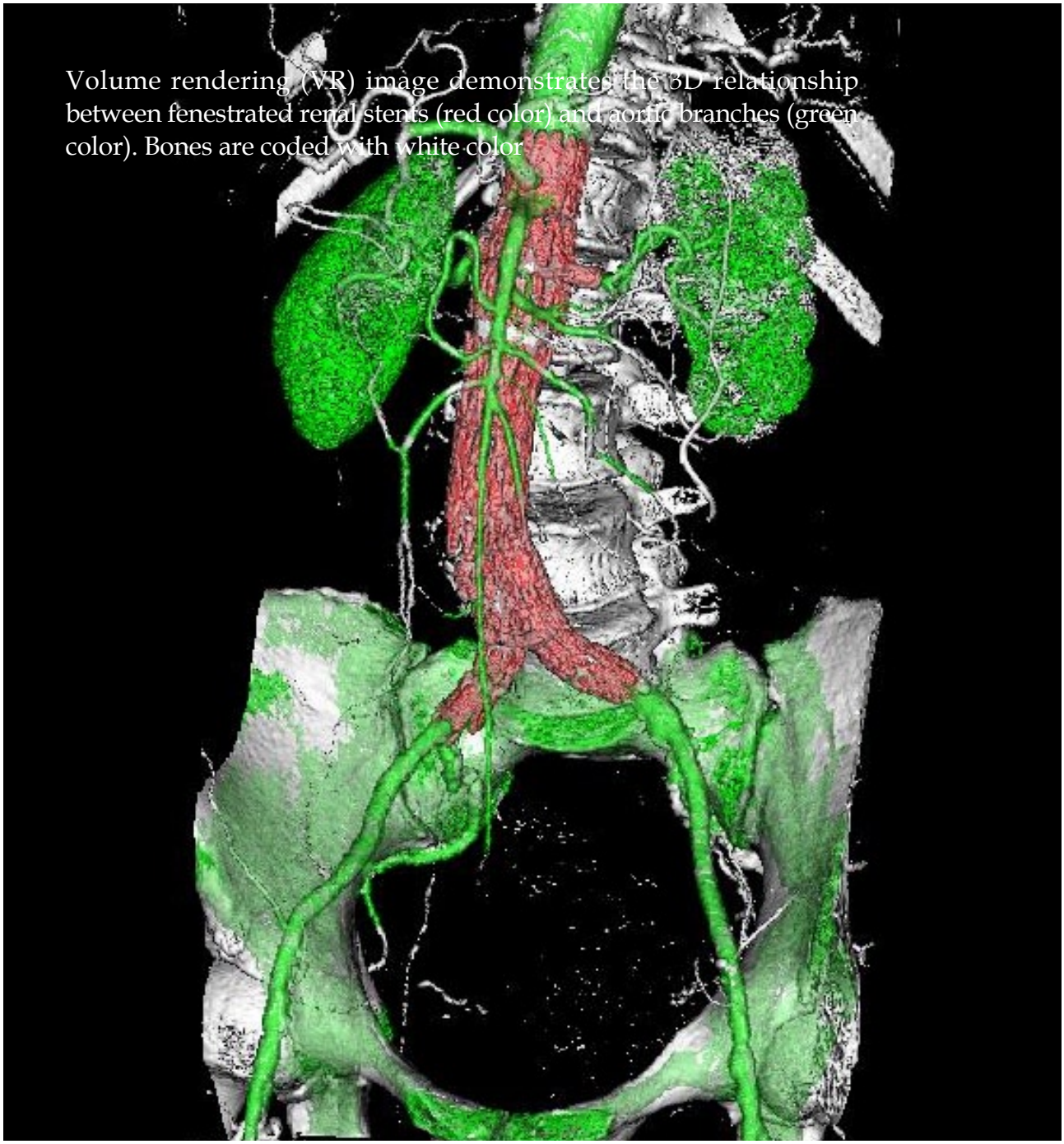

Volume rendering (VR) image demonstrates the 3D relationship between fenestrated renal stents (red color) and aortic branches (green color). Bones are coded with white color

WJR World Journal of Radiology

A peer-reviewed, online, open-access journal of Radiology

Editorial Board

2009-2013

The *World Journal of Radiology* Editorial Board consists of 303 members, representing a team of worldwide experts in radiology. They are from 38 countries, including Australia (3), Austria (4), Belgium (4), Brazil (2), Canada (9), Chile (1), China (23), Denmark (1), Egypt (4), Estonia (1), Finland (1), France (6), Germany (17), Greece (8), Hungary (1), India (9), Iran (5), Ireland (1), Israel (4), Italy (27), Japan (14), Lebanon (1), Libya (1), Malaysia (2), Mexico (1), Netherlands (4), New Zealand (1), Norway (1), Saudi Arabia (3), Serbia (1), Singapore (2), Slovakia (1), South Korea (16), Spain (8), Switzerland (5), Turkey (20), United Kingdom (15), and United States (76).

Youlia M Kirova, *Paris*
Géraldine Le Duc, *Grenoble Cedex*
Laurent Pierot, *Reims*
Frank Pilleul, *Lyon*
Pascal Pommier, *Lyon*

Germany

Ambros J Beer, *München*
Thomas Deserno, *Aachen*
Frederik L Giesel, *Heidelberg*
Ulf Jensen, *Kiel*
Markus Sebastian Juchems, *Ulm*
Kai U Juergens, *Bremen*
Melanie Kettering, *Jena*
Jennifer Linn, *Munich*
Christian Lohrmann, *Freiburg*
David Maintz, *Münster*
Henrik J Michaely, *Mannheim*
Oliver Micke, *Bielefeld*
Thoralf Niendorf, *Berlin-Buch*
Silvia Obenauer, *Duesseldorf*
Steffen Rickes, *Halberstadt*
Lars Victor B von Engelhardt, *Bochum*
Goetz H Welsch, *Erlangen*

Greece

Panagiotis Antoniou, *Alexandroupolis*
George C Kagadis, *Rion*
Dimitris Karacostas, *Thessaloniki*
George Panayiotakis, *Patras*
Alexander D Rapidis, *Athens*
Ioannis Tsalafoutas, *Athens*
Virginia Tsapaki, *Anixi*
Ioannis Valais, *Athens*

Hungary

Peter Laszlo Lakatos, *Budapest*

India

Anil Kumar Anand, *New Delhi*
Surendra Babu, *Tamilnadu*
Sandip Basu, *Bombay*
Kundan Singh Chufal, *New Delhi*
Shivanand Gamanagatti, *New Delhi*
Vimoj J Nair, *Haryana*
R Prabhakar, *New Delhi*
Sanjeeb Kumar Sahoo, *Orissa*

Iran

Vahid Reza Dabbagh Kakhki, *Mashhad*
Mehran Karimi, *Shiraz*
Farideh Nejat, *Tehran*
Alireza Shirazi, *Tehran*
Hadi Rokni Yazdi, *Tehran*

Ireland

Joseph Simon Butler, *Dublin*

Israel

Amit Gefen, *Tel Aviv*
Eyal Sheiner, *Be'er-Sheva*
Jacob Sosna, *Jerusalem*
Simcha Yagel, *Jerusalem*

Italy

Mohssen Ansarin, *Milan*
Stefano Arcangeli, *Rome*
Tommaso Bartalena, *Imola*
Filippo Cademartiri, *Parma*
Sergio Casciaro, *Lecce*
Laura Crocetti, *Pisa*
Alberto Cuocolo, *Napoli*
Mirko D'Onofrio, *Verona*
Massimo Filippi, *Milan*
Claudio Fiorino, *Milano*
Alessandro Franchello, *Turin*
Roberto Grassi, *Naples*
Stefano Guerriero, *Cagliari*
Francesco Lassandro, *Napoli*
Nicola Limbucci, *L'Aquila*
Raffaele Lodi, *Bologna*
Francesca Maccioni, *Rome*
Laura Martincich, *Candiolo*
Mario Mascalchi, *Florence*
Roberto Miraglia, *Palermo*
Eugenio Picano, *Pisa*
Stefania Romano, *Naples*
Luca Saba, *Cagliari*
Sergio Sartori, *Ferrara*
Mariano Scaglione, *Castel Volturno*
Lidia Strigari, *Rome*
Vincenzo Valentini, *Rome*

Japan

Shigeru Ehara, *Morioka*
Nobuyuki Hamada, *Chiba*
Takao Hiraki, *Okayama*
Akio Hiwatashi, *Fukuoka*
Masahiro Jinzaki, *Tokyo*
Hiroshi Matsuda, *Saitama*
Yasunori Minami, *Osaka*
Jun-Ichi Nishizawa, *Tokyo*
Tetsu Niwa, *Yokohama*
Kazushi Numata, *Kanagawa*
Kazuhiko Ogawa, *Okinawa*
Hitoshi Shibuya, *Tokyo*
Akira Uchino, *Saitama*
Haiquan Yang, *Kanagawa*

Lebanon

Aghiad Al-Kutoubi, *Beirut*

Libya

Anuj Mishra, *Tripoli*

Malaysia

R Logeswaran, *Cyberjaya*
Kwan-Hoong Ng, *Kuala Lumpur*

Mexico

Heriberto Medina-Franco, *Mexico City*

Netherlands

Jurgen J Fütterer, *Nijmegen*
Raffaella Rossin, *Eindhoven*
Paul E Sijens, *Groningen*
Willem Jan van Rooij, *Tilburg*

New Zealand

W Howell Round, *Hamilton*

Norway

Arne Sigmund Borthne, *Lørenskog*

Saudi Arabia

Mohammed Al-Omran, *Riyadh*
Ragab Hani Donkol, *Abha*
Volker Rudat, *Al Khobar*

Serbia

Djordjije Saranovic, *Belgrade*

Singapore

Uei Pua, *Singapore*
Lim CC Tchoyoson, *Singapore*

Slovakia

František Dubecký, *Bratislava*

South Korea

Bo-Young Choe, *Seoul*
Joon Koo Han, *Seoul*
Seung Jae Huh, *Seoul*
Chan Kyo Kim, *Seoul*
Myeong-Jin Kim, *Seoul*
Seung Hyup Kim, *Seoul*
Kyoung Ho Lee, *Gyeonggi-do*
Won-Jin Moon, *Seoul*
Wazir Muhammad, *Daegu*
Jai Soung Park, *Bucheon*
Noh Hyuck Park, *Kyunggi*
Sang-Hyun Park, *Daejeon*
Joon Beom Seo, *Seoul*
Ji-Hoon Shin, *Seoul*
Jin-Suck Suh, *Seoul*
Hong-Gyun Wu, *Seoul*

Spain

Eduardo J Aguilar, *Valencia*

Miguel Alcaraz, *Murcia*
Juan Luis Alcazar, *Pamplona*
Gorka Bastarrika, *Pamplona*
Rafael Martínez-Monge, *Pamplona*
Alberto Muñoz, *Madrid*
Joan C Vilanova, *Girona*

Switzerland

Nicolau Beckmann, *Basel*
Silke Grabherr, *Lausanne*
Karl-Olof Lövblad, *Geneva*
Tilo Niemann, *Basel*
Martin A Walter, *Basel*

Turkey

Olus Api, *Istanbul*
Kubilay Aydin, *İstanbul*
Işıl Bilgen, *Izmir*
Zulkif Bozgeyik, *Elazig*
Barbaros E Çil, *Ankara*
Gulgun Engin, *Istanbul*
M Fatih Evcimik, *Malatya*
Ahmet Kaan Gündüz, *Ankara*
Tayfun Hakan, *Istanbul*
Adnan Kabaalioglu, *Antalya*
Fehmi Kaçmaz, *Ankara*
Musturay Karcaaltincaba, *Ankara*
Osman Kizilkilic, *Istanbul*
Zafer Koc, *Adana*
Cem Onal, *Adana*
Yahya Paksoy, *Konya*
Bunyamin Sahin, *Samsun*
Ercument Unlu, *Edirne*
Ahmet Tuncay Turgut, *Ankara*
Ender Uysal, *Istanbul*

United Kingdom

K Faulkner, *Wallsend*
Peter Gaines, *Sheffield*
Balaji Ganeshan, *Brighton*
Nagy Habib, *London*
Alan Jackson, *Manchester*
Pradesh Kumar, *Portsmouth*
Tarik F Massoud, *Cambridge*
Igor Meglinski, *Bedfordshire*
Ian Negus, *Bristol*
Georgios A Plataniotis, *Aberdeen*
N J Raine-Fenning, *Nottingham*
Manuchehr Soleimani, *Bath*
MY Tseng, *Nottingham*
Edwin JR van Beek, *Edinburgh*
Feng Wu, *Oxford*

United States

Athanassios Argiris, *Pittsburgh*
Stephen R Baker, *Newark*
Lia Bartella, *New York*
Charles Bellows, *New Orleans*
Walter L Biffl, *Denver*
Homer S Black, *Houston*
Wessam Bou-Assaly, *Ann Arbor*
Owen Carmichael, *Davis*
Shelton D Caruthers, *St Louis*
Yuhchyau Chen, *Rochester*
Melvin E Clouse, *Boston*
Ezra Eddy Wyssam Cohen, *Chicago*
Aaron Cohen-Gadol, *Indianapolis*
Patrick M Colletti, *Los Angeles*
Kassa Darge, *Philadelphia*
Abhijit P Datir, *Miami*
Delia C DeBuc, *Miami*
Russell L Deter, *Houston*
Adam P Dicker, *Phil*
Khaled M Elsayes, *Ann Arbor*
Steven Feigenberg, *Baltimore*
Christopher G Filippi, *Burlington*
Victor Frenkel, *Bethesda*
Thomas J George Jr, *Gainesville*
Patrick K Ha, *Baltimore*
Robert I Haddad, *Boston*
Walter A Hall, *Syracuse*
Mary S Hammes, *Chicago*
John Hart Jr, *Dallas*
Randall T Higashida, *San Francisco*
Juebin Huang, *Jackson*
Andrei Iagaru, *Stanford*
Craig Johnson, *Milwaukee*
Ella F Jones, *San Francisco*
Csaba Juhasz, *Detroit*
Mannudeep K Kalra, *Boston*
Riyad Karmy-Jones, *Vancouver*
Daniel J Kelley, *Madison*
Amir Khan, *Longview*
Vikas Kundra, *Houston*
Kennith F Layton, *Dallas*
Rui Liao, *Princeton*
CM Charlie Ma, *Philadelphia*
Nina A Mayr, *Columbus*
Thomas J Meade, *Evanston*
Steven R Messé, *Philadelphia*
Feroze B Mohamed, *Philadelphia*
Koenraad J Mortele, *Boston*
Mohan Natarajan, *San Antonio*
John L Nosher, *New Brunswick*
Chong-Xian Pan, *Sacramento*
Dipanjan Pan, *St Louis*
Martin R Prince, *New York*
Reza Rahbar, *Boston*
Carlos S Restrepo, *San Antonio*
Veronica Rooks, *Honolulu*
Maythem Saeed, *San Francisco*
Edgar A Samaniego, *Palo Alto*
Jason P Sheehan, *Charlottesville*
William P Sheehan, *Willmar*
Charles Jeffrey Smith, *Columbia*
Dan Stoianovici, *Baltimore*
Dian Wang, *Milwaukee*
Jian Z Wang, *Columbus*
Liang Wang, *New York*
Shougang Wang, *Santa Clara*
Wenbao Wang, *New York*
Aaron H Wolfson, *Miami*
Ying Xiao, *Philadelphia*
Juan Xu, *Pittsburgh*
Benjamin M Yeh, *San Francisco*
Terry T Yoshizumi, *Durham*
Jinxing Yu, *Richmond*
Jianhui Zhong, *Rochester*

WJR World Journal of Radiology

Contents

Monthly Volume 1 Number 1 December 31, 2009

EDITORIAL

1 What is the purpose of launching *World Journal of Radiology?*
Ma LS

3 Incremental value of magnetic resonance imaging in the advanced management of prostate cancer
Wang L

TOPIC HIGHLIGHT

15 Contrast-enhanced ultrasound: The evolving applications
Xu HX

25 Detection of focal liver lesions in cirrhotic liver using contrast-enhanced ultrasound
Wong GLH, Xu HX, Xie XY

37 Contrast-enhanced ultrasound in the biliary system: Potential uses and indications
Xu HX

OBSERVATION

45 Neuroimaging in human prion disease: Searching in the mist
Ioannides P, Karacostas D

GUIDELINES FOR CLINICAL PRACTICE

50 Endovascular approach to acute aortic trauma
Karmy-Jones R, Teso D, Jackson N, Ferigno L, Bloch R

63 Endovascular stent graft repair of abdominal aortic aneurysms: Current status and future directions
Sun Z

REVIEW

72 Magnetic resonance imaging of the liver: New imaging strategies for evaluating focal liver lesions
Coenegrachts K

86 Contrast-enhanced harmonic ultrasound imaging in ablation therapy for primary hepatocellular carcinoma
Minami Y, Kudo M

Contents

World Journal of Radiology
Volume 1 Number 1 December 31, 2009

ACKNOWLEDGMENTS	I	Acknowledgments to reviewers of *World Journal of Radiology*
APPENDIX	I	Meetings
	I-V	Instructions to authors
ABOUT COVER		Sun Z. Endovascular stent graft repair of abdominal aortic aneurysms: Current status and future directions. *World J Radiol* 2009; 1(1): 63-71 http://www.wjgnet.com/1949-8470/full/v1/i1/63.htm
AIM AND SCOPE		*World Journal of Radiology* (*World J Radiol*, *WJR*, online ISSN 1949-8470, DOI: 10.4329) is a monthly peer-reviewed, online, open-access, journal supported by an editorial board consisting of 303 experts in radiology from 38 countries. The major task of *WJR* is to rapidly report the most recent improvement in the research of medical imaging and radiation therapy by the radiologists. *WJR* accepts papers on the following aspects related to radiology: Abdominal radiology, women health radiology, cardiovascular radiology, chest radiology, genitourinary radiology, neuroradiology, head and neck radiology, interventional radiology, musculoskeletal radiology, molecular imaging, pediatric radiology, experimental radiology, radiological technology, nuclear medicine, PACS and radiology informatics, and ultrasound. We also encourage papers that cover all other areas of radiology as well as basic research.
FLYLEAF	I-III	Editorial Board

NAME OF JOURNAL
World Journal of Radiology

LAUNCH DATE
December 31, 2009

SPONSOR
Beijing Baishideng BioMed Scientific Co., Ltd.,
Room 903, Building D, Ocean International Center,
No. 62 Dongsihuan Zhonglu, Chaoyang District,
Beijing 100025, China
Telephone: 0086-10-8538-1892
Fax: 0086-10-8538-1893
E-mail: baishideng@wjgnet.com
http://www.wjgnet.com

EDITING
Editorial Board of *World Journal of Radiology*,
Room 903, Building D, Ocean International Center,
No. 62 Dongsihuan Zhonglu, Chaoyang District,
Beijing 100025, China
Telephone: 0086-10-5908-0036
Fax: 0086-10-8538-1893
E-mail: wjr@wjgnet.com
http://www.wjgnet.com

PUBLISHING
Beijing Baishideng BioMed Scientific Co., Ltd.,
Room 903, Building D, Ocean International Center,
No. 62 Dongsihuan Zhonglu, Chaoyang District,
Beijing 100025, China
Telephone: 0086-10-8538-1892
Fax: 0086-10-8538-1893
E-mail: baishideng@wjgnet.com
http://www.wjgnet.com

SUBSCRIPTION
Beijing Baishideng BioMed Scientific Co., Ltd.,
Room 903, Building D, Ocean International Center,
No. 62 Dongsihuan Zhonglu, Chaoyang District,
Beijing 100025, China
Telephone: 0086-10-8538-1892
Fax: 0086-10-8538-1893
E-mail: baishideng@wjgnet.com
http://www.wjgnet.com

ONLINE SUBSCRIPTION
One-Year Price 216.00 USD

PUBLICATION DATE
December 31, 2009

CSSN
ISSN 1949-8470 (online)

EDITORIAL OFFICE
Na Ma, Director
World Journal of Radiology
Room 903, Building D, Ocean International Center,
No. 62 Dongsihuan Zhonglu, Chaoyang District,
Beijing 100025, China
Telephone: 0086-10-5908-0036
Fax: 0086-10-8538-1893
E-mail: wjr@wjgnet.com
http://www.wjgnet.com

SPECIAL STATEMENT
All articles published in this journal represent the viewpoints of the authors except where indicated otherwise.

INSTRUCTIONS TO AUTHORS
Full instructions are available online at http://www.wjgnet.com/1949-8470/index.htm. If you do not have web access please contact the editorial office.

ONLINE SUBMISSION
http://www.wjgnet.com/1949-8470office

World Journal of Radiology

Online Submissions: http://www.wjgnet.com/1949-8470office
wjr@wjgnet.com
doi:10.4329/wjr.v1.i1.1

World J Radiol 2009 December 31; 1(1): 1-2
ISSN 1949-8470 (online)

EDITORIAL

What is the purpose of launching *World Journal of Radiology?*

Lian-Sheng Ma

Lian-Sheng Ma, Beijing Baishideng BioMed Scientific Co., Ltd., Room 903, Building D, Ocean International Center, No.62 Dongsihuan Zhonglu, Chaoyang District, Beijing 100025, China
Author contributions: Ma LS solely contributed to this paper.
Correspondence to: Lian-Sheng Ma, Professor, President and Editor-in-Chief, Beijing Baishideng BioMed Scientific Co., Ltd., Room 903, Building D, Ocean International Center, No.62 Dongsihuan Zhonglu, Chaoyang District, Beijing 100025, China. l.s.ma@wjgnet.com
Telephone: +86-10-59080036 Fax: +86-10-85381893
Received: September 24, 2009 Revised: October 19, 2009
Accepted: October 26, 2009
Published online: December 31, 2009

Abstract

The first issue of *World Journal of Radiology* (*WJR*), whose preparatory work was initiated on August 24, 2009, will be published on December 31, 2009. The *WJR* Editorial Board has now been established and consists of 303 distinguished experts from 38 countries. Our purpose of launching *WJR* is to publish peer-reviewed, high-quality articles *via* an open-access online publishing model, thereby acting as a platform for communication between peers and the wider public, and maximizing the benefits to editorial board members, authors and readers.

Key words: Maximization of personal benefits; Editorial board members; Authors; Readers; Employees; *World Journal of Radiology*

Peer reviewers: Feng Chen, MD, PhD, Professor, Department of Radiology, Zhong Da Hospital, Southeast University, 87 Ding Jiaqiao, Nanjing 210009, Jiangsu Province, China; Kenneth Coenegrachts, MD, PhD, Department of Radiology, AZ St.-Jan AV, Ruddershove 10, B-8000 Bruges, Belgium

Ma LS. What is the purpose of launching *World Journal of Radiology*? *World J Radiol* 2009; 1(1): 1-2 Available from: URL: http://www.wjgnet.com/1949-8470/full/v1/i1/1.htm DOI: http://dx.doi.org/10.4329/wjr.v1.i1.1

INTRODUCTION

I am very pleased to announce that the first issue of *World Journal of Radiology* (*World J Radiol*, *WJR*, online ISSN 1949-8470, DOI: 10.4329), whose preparatory work was initiated on August 24, 2009, will be published on December 31, 2009. The *WJR* Editorial Board has now been established and consists of 303 distinguished experts from 38 countries. What is the purpose of launching *WJR*? And what is the scope and how are the columns designed?

The role of academic journals is to exhibit the scientific levels of a country, a university, a center, a department, and even a scientist, and build an important bridge for communication between scientists and the public. As we all know, the significance of the publication of scientific articles lies not only in disseminating and communicating innovative scientific achievements and academic views, as well as promoting the application of scientific achievements, but also in formally recognizing the "priority" and "copyright" of innovative achievements published, as well as evaluating research performance and academic levels. To realize these desired attributes of a journal and create a well-recognized journal, the following four types of personal benefits should be maximized.

MAXIMIZATION OF PERSONAL BENEFITS

The maximization of personal benefits refers to the pursuit of the maximum personal benefits in a well-considered optimal manner without violation of the laws, ethical rules and the benefits of others.

Maximization of the benefits of editorial board members

The primary task of editorial board members is to give a peer review of an unpublished scientific article *via* online

office system to evaluate its innovativeness, scientific and practical values and determine whether it should be published or not. During peer review, editorial board members can also obtain cutting-edge information in that field at first hand. As leaders in their field, they have priority to be invited to write articles and publish commentary articles. We will put peer reviewers' names and affiliations along with the article they reviewed in the journal to acknowledge their contribution.

Maximization of the benefits of authors

Since *WJR* is an open-access journal, readers around the world can immediately download and read, free of charge, high-quality, peer-reviewed articles from *WJR* official website, thereby realizing the goals and significance of the communication between authors and peers as well as public reading.

Maximization of the benefits of readers

Readers can read or use, free of charge, high-quality peer-reviewed articles without any limits, and cite the arguments, viewpoints, concepts, theories, methods, results, conclusion or facts and data of pertinent literature so as to validate the innovativeness, scientific and practical values of their own research achievements, thus ensuring that their articles have novel arguments or viewpoints, solid evidence and correct conclusion[1].

Maximization of the benefits of employees

It is an iron law that a first-class journal is unable to exist without first-class editors, and only first-class editors can create a first-class academic journal[2,3]. We insist on strengthening our team cultivation and construction so that every employee, in an open, fair and transparent environment, could contribute their wisdom to edit and publish high-quality articles, thereby realizing the maximization of the personal benefits of editorial board members, authors and readers, and yielding the greatest social and economic benefits.

CONTENTS OF PEER REVIEW

In order to guarantee the quality of articles published in the journal, *WJR* usually invites three experts to comment on the submitted papers. The contents of peer review include: (1) whether the contents of the manuscript are of great importance and novelty; (2) whether the experiment is complete and described clearly; (3) whether the discussion and conclusion are justified; (4) whether the citations of references are necessary and reasonable; and (5) whether the presentation and use of tables and figures are correct and complete.

SCOPE

The major task of *WJR* is to rapidly report the most recent improvement in the research of medical imaging and radiation therapy by the radiologists. *WJR* accepts papers on the following aspects related to radiology: Diagnostic radiology, radiation oncology, radiologic physics, neuroradiology, nuclear radiology, pediatric radiology, vascular/interventional radiology, medical imaging achieved by various modalities and related methods analysis. We also encourage papers that cover all other areas of radiology as well as basic research.

COLUMNS

The columns in the issues of *WJR* will include: (1) Editorial: To introduce and comment on the substantial advance and its importance in the fast-developing areas; (2) Frontier: To review the most representative achievements and comment on the current research status in the important fields, and propose directions for the future research; (3) Topic Highlight: This column consists of three formats, including (A) 10 invited review articles on a hot topic, (B) a commentary on common issues of this hot topic, and (C) a commentary on the 10 individual articles; (4) Observation: To update the development of old and new questions, highlight unsolved problems, and provide strategies on how to solve the questions; (5) Guidelines for Basic Research: To provide Guidelines for basic research; (6) Guidelines for Clinical Practice: To provide guidelines for clinical diagnosis and treatment; (7) Review: To systemically review the most representative progress and unsolved problems in the major scientific disciplines, comment on the current research status, and make suggestions on the future work; (8) Original Articles: To originally report the innovative and valuable findings in radiology; (9) Brief Articles: To briefly report the novel and innovative findings in radiology; (10) Case Report: To report a rare or typical case; (11) Letters to the Editor: To discuss and make reply to the contributions published in *WJR*, or to introduce and comment on a controversial issue of general interest; (12) Book Reviews: To introduce and comment on quality monographs of radiology; and (13) Guidelines: To introduce Consensuses and Guidelines reached by international and national academic authorities worldwide on the research in radiology.

REFERENCES

1 **Zhu DM**. What is the purpose of literature citation? Science Times, 2009-07-17. Available from: URL: http://www.sciencenet.cn/htmlnews/2009/7/221552.shtm
2 **Li ZX**. See the "sallying forth" of Chinese scientific and technical journals from the innovative business model of *WJG*. *Zhongguo Keji Qikan Yanjiu* 2008; **19**: 667-671
3 **Xiao H**. First-class publications can not do without first-class editorial talents. *Keji Yu Chuban* 2008; (**3**): 192

S- Editor Cheng JX **E- Editor** Zheng XM

World Journal of Radiology

Online Submissions: http://www.wjgnet.com/1949-8470office
wjr@wjgnet.com
doi:10.4329/wjr.v1.i1.3

World J Radiol 2009 December 31; 1(1): 3-14
ISSN 1949-8470 (online)

EDITORIAL

Incremental value of magnetic resonance imaging in the advanced management of prostate cancer

Liang Wang

Liang Wang, Department of Radiology, Memorial Sloan-Kettering Cancer Center, 1275 York Avenue, New York, NY 10021, United States
Author contributions: Wang L solely contributed to this paper.
Correspondence to: Liang Wang, MD, PhD, Department of Radiology, Memorial Sloan-Kettering Cancer Center, 1275 York Avenue, New York, NY 10021, United States. wang6@mskcc.org
Telephone: +1-212-6392214 Fax: +1-212-7944010
Received: October 20, 2009 Revised: December 12, 2009
Accepted: December 21, 2009
Published online: December 31, 2009

Abstract

Prostate cancer is a major public health burden throughout the world. The high incidence of prostate cancer, combined with earlier detection and downstaging at the time of diagnosis, and the slow natural progression and biological heterogeneity of the disease, has made its management a complex and controversial issue. There is growing demand for patient-specific therapies that can minimize treatment morbidity while maximizing treatment benefits. There are a number of clinical parameters and clinical nomograms to help with the choice of treatment. Magnetic resonance imaging (MRI) is a technique which makes safer, more individualized therapies possible due to high spatial resolution, superior contrast resolution, multiplanar capability, and a large field of view. Other MRI techniques such as MR spectroscopic imaging, dynamic contrast-enhanced MRI or perfusion MRI, and diffusion-weighted imaging complement MRI by reflecting tissue biochemistry, Brownian motion of water molecules, and capillary wall permeability, respectively. This editorial review highlights the incremental value of MRI in the advanced management of prostate cancer to non-invasively improve cancer staging, biologic potential, treatment planning, therapy response, local recurrence, and to guide target biopsy for clinical suspected cancer with previous negative biopsy. Finally, some future prospects for MRI in prostate cancer management are given.

Key words: Prostate neoplasms; Health care costs; Magnetic resonance imaging; Patient care planning; Clinical nomograms

Peer reviewers: Aytekin Oto, MD, Associate Professor of Radiology, Chief of Abdominal Imaging and Body MRI, Department of Radiology, University of Chicago, 5841 S Maryland Ave, MC 2026, Chicago, IL 60637, United States; Jurgen J Fütterer, MD PhD, Department of Radiology, Radboud University Nijmegen Medical Centre, Geert Grooteplein 10, 6500HB Nijmegen, The Netherlands

Wang L. Incremental value of magnetic resonance imaging in the advanced management of prostate cancer. *World J Radiol* 2009; 1(1): 3-14 Available from: URL: http://www.wjgnet.com/1949-8470/full/v1/i1/3.htm DOI: http://dx.doi.org/10.4329/wjr.v1.i1.3

INTRODUCTION

Prostate cancer affects men of all races, cultures and ethnic backgrounds and is a major public health burden throughout the world[1-3]. It is the most common non-cutaneous cancer and the second/third leading cause of cancer death in men in the United State and European Community[1,3,4]. Asian/Pacific Islanders have a lower incidence of prostate cancer than either African Americans or Caucasians[5] but the death toll from prostate cancer mortality in East Asia continues to rise[6]. A wide discrepancy exists between the number of men diagnosed and those dying from prostate cancer. Prostate cancer is an age-related disease and the increasing natural life expectation will result in a further increase of both the incidence of and the deaths related to prostate cancer[1,7].

The high incidence of prostate cancer, combined with earlier detection and downstaging at the time of diagnosis, and the slow natural progression and biological heterogeneity of the disease, has made its management a complex and controversial issue. The National Cancer Institute's Surveillance, Epidemiology, and End Results Program reported that from 1996 to 2004, 91% of prostate cancer cases were of a local or regional stage at diagnosis, and patients had a 5-year relative survival rate of 100% from 1996 to 2004[1]. The 100% 5-year relative survival rate for all stages indicates that prostate tumors have a slow growth rate and allow for prolonged survival[8]. However, the downstaging resulting from prostatic serum antigen (PSA) screening has been accompanied by an unfortunate trend of overdetection and overtreatment of biologically indolent (low-grade, clinically insignificant) disease[8-11]. Autopsy studies indicated that the "overdetected" cancers never impacted patient longevity[10]. Primary therapies with curative intent (surgery or radiation) provide excellent long-term cancer control but are accompanied by a risk of treatment-related morbidity. Conversely, the understandable appeal of watchful waiting or active surveillance is balanced by the potential harm of missing a window of curative opportunity for a cancer destined to progress[8]. One challenge physicians and patients face is to differentiate men who have disease destined to progress and cause morbidity/mortality from those who will not require immediate, or possibly even delayed, therapeutic intervention[12-14].

Depending on patient age at diagnosis, the stage and aggressiveness of the tumor, the potential side-effects of the treatment, and patient comorbidity[8,15], the options for treatment may include watchful waiting, androgen ablation (chemical or surgical castration), hormone therapy, radical surgery, and various forms of radiation therapy (brachytherapy, external beam irradiation, beam irradiation)[16,17]. In addition, new focal therapies, such as cryotherapy, high-intensity focused ultrasound and radiofrequency ablation is raising clinical interest[18]. There is growing demand for patient-specific therapies that can minimize treatment morbidity while maximizing treatment benefits[19,20]. An important objective prior to any cancer therapy is to obtain a comprehensive and accurate knowledge of tumor location, size, extent, and biologic potential. Better tools are needed to help physicians and patients decide what type of treatment is most appropriate, or whether any treatment is needed at all.

There are a number of clinical parameters and clinical nomograms to help with the choice of treatment[20-26]. To aid in patient counseling, the National Comprehensive Cancer Network guidelines define low risk as a PSA less than 10 ng/mL, a Gleason score of 6 or lower, and a T stage of T2a or lower; the guidelines define high risk as a PSA of more than 20 ng/mL, a Gleason score of 8 or higher, or T2c; intermediate risk is defined as a PSA of 10 to 20 ng/mL, T2b, or a Gleason score of 7[27]. To replace somewhat arbitrary combinations of individual clinical variables, nomograms have been developed and used to give a prediction of the final pathologic stage, the chances of freedom from disease recurrence and an estimate of biologic potential, and to aid in the choice of treatment[20,24-26,28,29]. The Partin staging nomogram (also called the "Partin tables"), which is based on clinical stage, Gleason score, and serum PSA level, was first published in 1993 and was updated in 1997 and again in 2001 to predict the pathological stage at radical prostatectomy[28-30]. Other nomograms, such as Kattan's nomograms, have been developed to predict stage, recurrence, or biologic potential. The nomograms are graphic representations of a statistical model, with scales for calculating the prognostic weight of a value for each individual variable[26,31]. As an important advance in accurate prediction for clinical medicine, the nomograms allow calculation of the continuous probability of a particular outcome and tend to outperform both expert clinicians and risk grouping. The nomograms are validated predictive instruments widely used for individual patient counseling and important decision-making. Despite the strong predictive ability and the cost-effectiveness of the nomograms, there is room for improved accuracy of prediction, particularly as clinical staging in the nomograms is based only on digital rectal examination and biopsy-determined Gleason grade. Although valuable, biopsy is subject to sampling error. Moreover, the nomograms are limited because they do not incorporate the results of imaging studies that could guide interventions to control local disease. Thus, a technique that noninvasively demonstrates the presence, extent, and biologic potential of prostate cancer could contribute incremental value to clinical nomograms and variables and make a substantial contribution to the decision-making process for individualized treatment[32,33].

Magnetic resonance imaging (MRI) is a technique which makes safer, more individualized therapies possible due to high spatial resolution, superior contrast resolution, multiplanar capability (Figure 1)[34-38]. In the last decade, MRI has improved significantly with technologic refinements and increased reader experience. Newer techniques, such as MR spectroscopic imaging (MRSI) (Figure 2), dynamic contrast-enhanced MRI (DCE-MRI) or perfusion MRI (Figure 3), diffusion-weighted imaging (DWI) (Figure 4), high-field strength MRI scanning (Figures 1 and 5), image post-processing and picture and communication systems (PACS) provide greater resources for improved interpretation of MR images of the prostate by experienced radiologists[39,40]. MRSI identifies prostate cancer by an increased ratio of choline plus polyamines plus creatine to citrate (Figure 2)[41]. As a result of increased energy metabolism, the citrate level is reduced in prostate cancer. Owing to a high phospholipid cell membrane turnover the choline level is elevated in proliferating malignant tissue. DWI measures the Brownian motion of water molecules in biologic tissues where increased cellularity and the integrity of cell

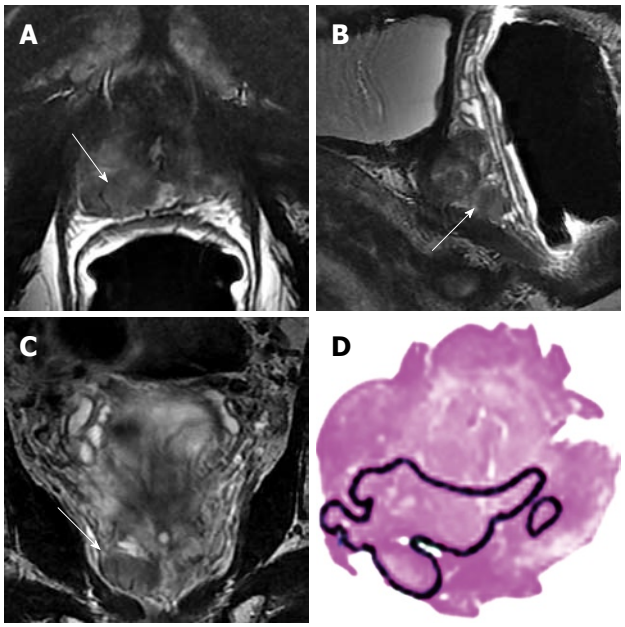

Figure 1 3T magnetic resonance (MR) images of extracapsular extension (ECE) of prostate cancer in a 65-year-old man with clinical stage T1c prostate nodule and prostate specific antigen (PSA) level of 10.7 ng/mL and Gleason grade 4+4 and PT3a. Transverse 3 mm-thick MR (6500/175) image (A), sagittal 3 mm-thick MR (7000/165) image (B) and coronal 3 mm-thick MR (7000/170) image (C) show a hypointense tumor (arrows) with extraprostatic extension in the right apex and mid of the prostate; D: Whole-mount serial section of the removed prostate shows tumor and ECE involving the right apex and mid of the prostate.

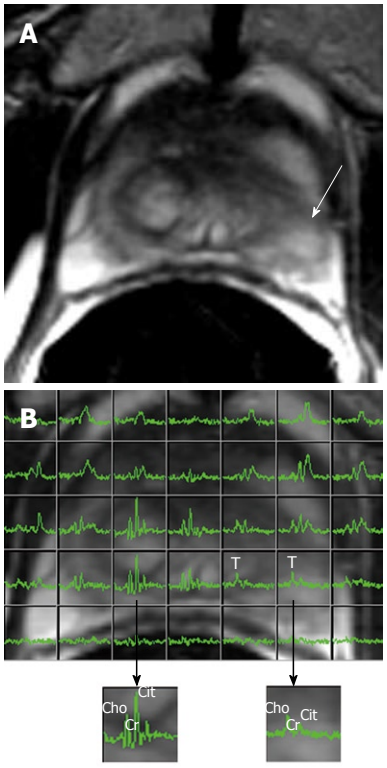

Figure 2 Prostate cancer in a 65-year-old patient with PSA level of 4.76 ng/mL. Transverse T2-weighted MR image (WI) (A) and corresponding MR spectroscopic imaging (MRSI) grid (B) superimposed on the anatomic image show the tumor (arrow) on the left apex. MRSI demonstrates reduced citrate and elevated choline in the left peripheral zone tumor (T) and normal spectra in the healthy right peripheral area. Cho: Choline; Cr: Creatine; Cit: Citrate.

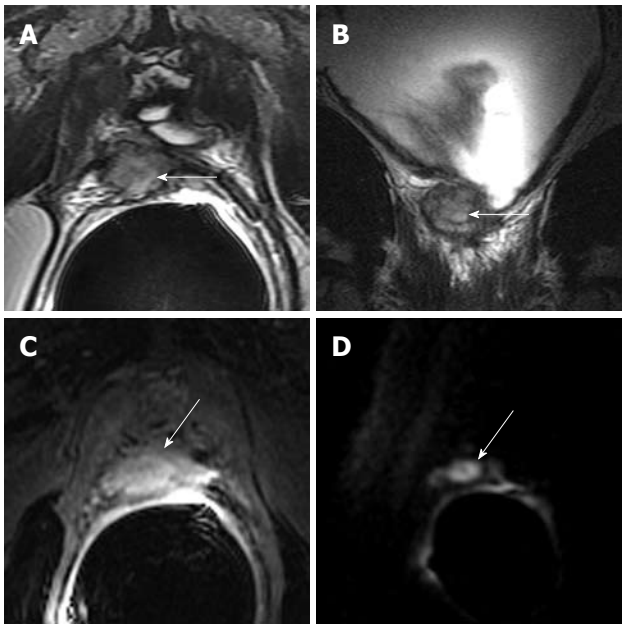

Figure 3 1.5T MR images of locally recurrent prostate cancer in a 63-year-old man with rising PSA levels after radical prostatectomy. Transverse 3 mm-thick T2-WI (4000/125) (A) and coronal 3 mm-thick T2-WI (5300/100) (B) show intermediate SI mass (arrows) to the right posterior aspect of the bladder neck at the anastomosis; C: Transverse 3 mm-thick T1-WI (5.5/2.4) shows significant enhancement of the mass (arrow) after intravenous administration of gadolinium; D: Transverse 3 mm-thick diffusion-weighted image (DWI) (3500/93, b-value of 1000 s/mm^2) shows intense increased signal (restricted diffusion) throughout the mass (arrow).

membranes restrict water diffusion. The apparent diffusion coefficient (ADC) derived from DWI, has been in use for detection of prostate cancer. DWI demonstrated reduced ADC values and increased fractional anisotropy in prostate cancer. DCE-MRI has been used to visualize tumor perfusion and tumor capillary wall permeability and hydrostatic pressure[42]. Vascular endothelial growth factor has a role in increasing tumor capillary wall permeability. This review addresses the incremental value of MRI in the advanced management of prostate cancer to non-invasively improve cancer staging, biologic potential, treatment planning, therapy response, local recurrence, and to guide target biopsy for clinically suspected cancer with previous negative biopsy, and discusses the future prospects of MRI in prostate cancer management.

PROSTATE CANCER STAGING

The staging of prostate cancer was based on the TNM (tumor node metastasis) staging. TNM staging of prostate cancer has undergone a number of modifications, the latest ones having been made in 2010 by the American Joint Committee on Cancer. The 2010 revised TNM system, shown in Table 1, is clinically useful and precisely stratifies newly diagnosed cancer[43]. Most importantly, clinicians must distinguish between patients with pathologically organ-confined prostate cancer (OCPC) (pT2), considered good surgical candidates, and those

Figure 4 MR depiction of malignant adenopathy from prostate cancer in a 63-year-old man with Gleason score 4 + 5 and PSA level of 24 ng/mL. Transverse 5 mm-thick T1-WI (600/8) (A) and transverse 3 mm-thick T2-WI (5450/118) (B) show intermediate SI bulky adenopathy (arrows) with short-axis dimensions of > 10 mm is present in left external iliac and obturator distributions; C: Transverse 3 mm-thick DWI (3500/98, b-value of 1000 s/mm^2) show intense, increased signal (restricted diffusion) throughout the mass (arrow).

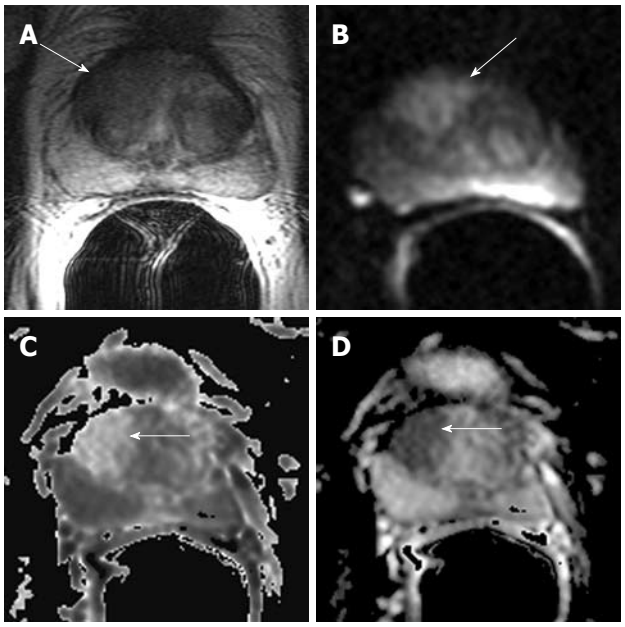

Figure 5 3T MR images of transitional zone tumor in a 59-year-old man with PSA level of 7.6 ng/mL and Gleason grade 3 + 4 and PT4. Transverse T2-WI (A) and transverse diffusion image (B) (b-value of 1000 s/mm^2), exponential apparent diffusion coefficient (ADC) (C) and ADC obtained (D) show an infiltrating tumor (arrows) in the right transitional zone extending from base to mid-gland with anterior extraprostatic extension.

with non-organ-confined prostate cancer (pT3-4). If cancer extends outside the prostate, the chances of cure are substantially diminished and the surgical or radiation treatment planning must be adapted to ensure complete eradication of the cancer[44,45].

Detection of OCPC (pT2)

A cancer completely confined to the prostate is defined as pT2. Pretreatment knowledge of OCPC is important for treatment selection and planning, regardless of whether the treatment method ultimately chosen is watchful waiting, surgery, or radiation therapy. After radical prostatectomy (RP), patients with OCPC have an excellent prognosis, as more than 90% of them are free from biochemical recurrence at 5 years[24,25]. Since the introduction of the Partin tables in 1997, investigators have repeatedly validated the nomograms' capacity to help predict the pathologic stage of clinically localized prostate cancer[46-48]. In 2001, the nomograms were updated based on a more contemporary cohort of disease features[28]. The accuracy of the Partin tables in predicting OCPC is high, with reports of the area under the receiver operating characteristic (ROC) curve ranging from 0.79 to 0.82[46-48]. MR findings (from endorectal MRI or combined endorectal MRI-MRSI) contribute significant incremental value to clinical staging nomograms in the prediction of OCPC. One study on 612 consecutive patients demonstrated that MR findings contributed significant incremental value ($P \leqslant 0.02$) to the Partin tables in the overall study population. The contribution of MR findings was significant in all risk groups but was greatest in the intermediate- and high-risk groups ($P < 0.01$ for both). Overall, in the prediction of OCPC, the area under the ROC curve for the staging nomograms was 0.80, while the area under the ROC curve for the staging nomograms plus MR findings was 0.88; the difference was significant ($P < 0.01$). In the combined endorectal MRI-MRSI group, the areas under the ROC curves were 0.81 for the staging nomograms and 0.90 for the staging nomograms plus MR findings; the difference was significant ($P < 0.01$). A prospective study of 27 patients reported MRI had significantly higher standardized canonical discriminant function coefficients than the Partin tables in prediction of OCPC.

Detection of extracapsular extension (ECE) (pT3a)

A cancer that extends through the prostatic capsule into the periprostatic adipose tissue is defined as a pT3a tumor[49]. ECE is an important predictor of tumor progression because it is associated with greater risk of a positive surgical margin, recurrence and a decreased chance of long-term cancer control[45,49-52]. Awareness of the presence and likely location of ECE would allow surgeons to plan radical prostatectomy more carefully, with

Table 1 Tumor node metastasis staging of prostate cancer (American Joint Committee on Cancer, 7th ed. 2010)[43]

Evaluation of the (primary) tumor ('T')
Clinical
TX: can not evaluate primary tumor
T0: no evidence of primary tumor
T1: clinically inapparent tumor neither palpable nor visible by imaging
T1a: tumor was incidentally found in less than 5% of prostate tissue resected
T1b: tumor was incidentally found in more than 5% of prostate tissue resected
T1c: tumor was found in a needle biopsy performed because of elevated serum PSA
T2: tumor confined within prostate[1]
T2a: the tumor is in half or less than half of one of the prostate gland's 2 lobes
T2b: the tumor is in more than half of one lobe, but not both
T2c: the tumor is in both lobes
T3: the tumor has spread through the prostatic capsule (if it is only part-way through, it is still T2)
T3a: the tumor has spread through the capsule on one or both sides
T3b: the tumor has invaded one or both seminal vesicles
T4: the tumor has invaded adjacent structures other than seminal vesicles (e.g. external sphincter, rectum, bladder, levator muscles, and/or pelvic wall)
Pathologic (pT)[2]
pT2: organ confined
pT2a: unilateral, one-half of one side or less
pT2b: unilateral, involving more than one-half of side but not both sides
pT2c: bilateral disease
pT3: extraprostatic extension
pT3a: extraprostatic extension or microscopic invasion of bladder neck
pT3b: seminal vesicles invasion
pT4: Invasion of rectum, levator muscles, and/or pelvic wall
Evaluation of the regional lymph nodes ('N')
(p)NX: regional lymph nodes were not assessed (sampled)
(p)N0: there has been no spread to the regional lymph nodes
(p)N1: there has been spread to the regional lymph nodes
Evaluation of distant metastasis ('M')
M0: there is no distant metastasis
M1: there is distant metastasis
M1a: the cancer has spread to lymph nodes beyond the regional ones
M1b: the cancer has spread to bone
M1c: the cancer has spread to other sites (regardless of bone involvement)

[1]Tumor found in one or both lobes by needle biopsy, but not palpable or reliably visible by imaging, is classified as T1c; [2]There is no pathologic T1 classification.

the aim of resecting the cancer completely and minimizing the risk of damaging surrounding tissues important to recovery of sexual function[24,53,54]. On endorectal MRI, the criteria for ECE include a contour deformity with a step-off or angulated margin; an irregular bulge or edge retraction; a breach of the capsule with evidence of direct tumor extension; obliteration of the recto-prostatic angle; and asymmetry of the neurovascular bundles (NVBs) (Figures 5 and 6)[36,55,56]. A decision analysis model suggested that preoperative MRI was cost-effective in patients with a moderate or high risk of ECE[57]. A multivariate analysis of endorectal MRI findings and

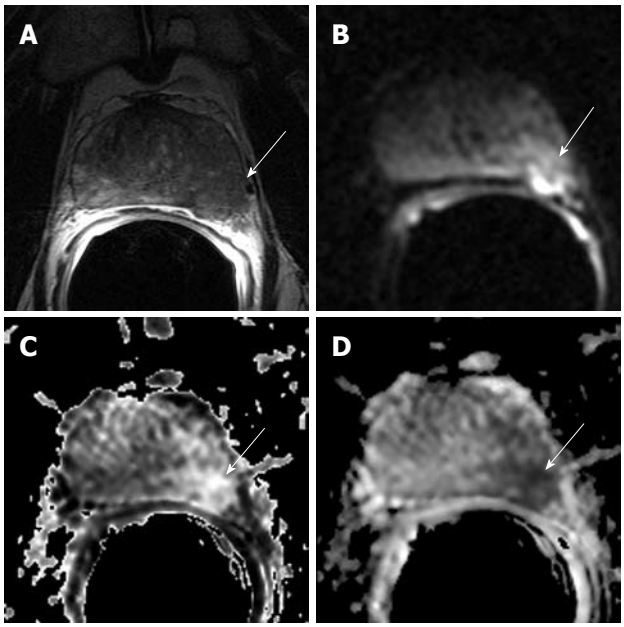

Figure 6 MR images of established ECE of prostate cancer into the periprostatic fat in a 59-year-old man with PSA level of 21.7 ng/mL and Gleason grade 4 + 4 and PT3a. Transverse 3 mm-thick MR (5800/108) image (A) and transverse diffusion image (4000/85. b1000) (B), exponential ADC (C) and ADC (D) of the prostate mid-gland reveal an infiltrative peripheral zone tumor (arrows) that extends into the left periprostatic fat.

other preoperative variables (PSA level, clinical stage, Gleason score, percentage of cancer in biopsy cores, and perineural invasion) in a study of 344 patients showed that endorectal MRI findings were significant presurgical predictors of ECE in patients with prostate cancer, and added incremental value to clinical variables[33]. Areas under the ROC curves for 2 models, with and without endorectal MRI findings, were 0.838 and 0.772, respectively ($P = 0.022$). Endorectal MRI findings had a larger AUC than any of the clinical or histologic variables, a high negative predictive value and a high positive predictive value (0.743, 83.8% and 74.5%, respectively).

While transaxial planes of section are essential in the evaluation of ECE, the utility of combining transaxial and coronal plane images using PACS cross-referencing to facilitate the diagnosis of ECE was shown in the study of Wang *et al*[39]. The study investigated 255 consecutive patients who underwent endorectal MRI before radical prostatectomy. In detecting ECE, the 2 radiologists had higher AUCs using cross-referencing (their AUCs increased from 0.66 to 0.87, and from 0.69 to 0.86; $P < 0.001$ for both). The weighted kappa was 0.56 with MRI alone and 0.76 with cross-referencing, indicating fair to good inter-reader agreement. Sensitivity/specificity for ECE with MRI alone and with cross-referencing, respectively, were 44%/85% and 68%/95% for reader 1 and 56%/78% and 74%/95 for reader 2.

The addition of MRSI to MRI has been shown to significantly increase staging accuracy for inexperienced readers and thus reduce interobserver variability[58]. In a study of 344 consecutive patients preprostatectomy

endorectal MRI findings showed that, overall, endorectal MRI findings were significant predictors of ECE and added significant incremental value to clinical variables when the images were interpreted by genitourinary radiologists experienced in MRI of the prostate (AUC 0.854 *vs* 0.760, $P = 0.019$), but not when they were interpreted by general body MRI radiologists (AUC 0.813 *vs* 0.788, $P = 0.31$)[59]. In the genitourinary MRI radiologists' group of patients, the AUC for endorectal MRI findings (0.833) was superior to that of all other predictors tested (0.566-0.701). In the general body MRI radiologists' group of patients, AUC for endorectal MRI findings (0.646) was similar to that of the clinical predictors (0.582-0.793). This suggests that the recent improvement in the performance of MRI can be attributed to increased reader experience as well as to the maturation of MRI technology (e.g. faster imaging sequences, more powerful gradient coils, and post-processing image correction), and better understanding of morphological criteria used to diagnose ECE. A prospective study of 27 patients reported MRI had significantly higher standardized canonical discriminant function coefficients than the Partin tables in prediction of ECE[60].

Detection of seminal vesicle invasion (SVI) (pT3b)

SVI is defined as the extension of cancer into the muscular layer of the seminal vesicle[49]. SVI is an important predictor of tumor progression because it is associated with increased risks of lymph node metastasis (LNM), recurrence[51,52,61-63]. The criteria for SVI on endorectal MRI include contiguous low-signal-intensity tumor extension from the base of the gland into the seminal vesicles; tumor extension along the ejaculatory duct (non-visualization of the ejaculatory duct); asymmetric decrease in the signal intensity of the seminal vesicles; and decreased conspicuity of the seminal vesicle wall on T2 weighted images[36,64]. Prediction of SVI before treatment may influence treatment selection in favor of radiation therapy instead of surgery. Furthermore, while resection of the seminal vesicles has been a standard component of radical prostatectomy, it has recently been suggested that if SVI can be confidently ruled out, the surgeon may wish to spare the seminal vesicles during radical prostatectomy to prevent long-term loss of urinary continence[65].

A study investigated 573 patients who underwent endorectal MRI before surgery for prostate cancer and had systematic needle biopsy results available for the base of the prostate[66]. The results show that the Kattan nomogram (based on serum PSA, biopsy Gleason grade, clinical staging, and systematic needle biopsy cores from the base of the prostate) plus endorectal MRI (0.87) had a significantly larger AUC than either endorectal MRI alone (0.76) or the Kattan nomogram alone (0.80, $P < 0.05$ for both). These results showed that MRI can add significant incremental value to clinical variables in the prediction of SVI. A study of 283 patients reported the AUC for T2-weighted imaging plus DW imaging (0.897) was significantly larger than that for T2-weighted imaging alone (0.779). T2 images combined with DWI shows significantly more accuracy than T2-weighted imaging alone in the prediction of SVI[67]. A study of 30 patients demonstrated significant improvement in the prediction of SVI for the less experienced readers[68]. DCE MRI may depict extracapsular spread and SVI and NVBs more clearly and improve the staging performance of the less experienced readers[69]. A study of 255 consecutive patients demonstrated the use of PACS cross-referencing, which automatically links axial, coronal and sagittal section planes, to facilitate noninvasive evaluation of SVI[39]. In detecting SVI, the AUCs of 2 radiologists increased with cross-referencing (from 0.62 to 0.87, $P = 0.007$ and from 0.73 to 0.90, $P = 0.056$ for readers 1 and 2, respectively). Sensitivity/specificity for SVI with MRI alone and with cross-referencing, respectively, were 38%/81% and 62%/93% for reader 1 and 62%/84% and 69%/94% for reader 2. PACS cross-referencing is particularly helpful in displaying the junction of the seminal vesicles and the central zone of the prostate. The results showed that PACS cross-referencing significantly improves the detection of prostate cancer SVI by 3D MRI.

Detection of LNM

The presence of LNM at the time of prostate cancer diagnosis is associated with a high probability of progression after treatment and a poor prognosis[70]. The risk of dying of prostate cancer at 10 years is much higher for patients with positive nodes than for patients with negative nodes[71]. Pretreatment knowledge of prostate cancer LNM is important for patient counseling and appropriate treatment selection and planning. The PSA level recommended by the American Urological Association for identifying patients who are at high risk for developing LMN is 15 ng/mL. There is, however, a wide variation in the cut-off values for PSA reported in the literature[72]. The conventional criterion for detection of metastatic lymph nodes on imaging is a short axis of 8 mm[73]. MRI and computed tomography (CT) have similar efficacy in detecting lymph node metastases, with both modalities having low sensitivity. The low sensitivity of MRI has been attributed mainly to the inability of cross-sectional imaging to detect metastases in normal-sized nodes[73,74]. Promising results have been reported for the use of ultra-small, super-paramagnetic iron oxide particles as an aid to diagnosing LNM by MRI[73]. These particles are taken up by normal nodal tissue but not by metastatic tissue, providing tissue contrast within the lymph node and allowing detection of metastases. The sensitivity of MRI for LNM may be increased through use of these compounds, since they appear to permit detection of metastases in normal-sized nodes[73,75]. A study of 411 consecutive patients[32] showed that MRI was an independent statistically significant predictor of LNM

(P = 0.002), with sensitivity and specificity of 27.27% and 98.46%, respectively, and positive predictive value and negative predictive value of 50% and 95.99%, respectively. On multivariate analysis, prediction of lymph node status using the model that included all MRI variables (ECE, SVI, and LNM) along with the Partin nomogram results had a significantly greater AUC than the univariate model that included only MRI LNM findings (AUC = 0.892 *vs* 0.633, respectively, $P < 0.01$). The study data confirmed the high negative predictive value of MRI for LNM and indicated that a combination of endorectal and phased-array MRI with the Partin tables had high accuracy in predicting LNM. As MRI also provides anatomic information that is helpful in treatment planning, these findings suggest that MRI, in conjunction with the Partin tables, may be useful for determining whether further imaging with lymphotropic superparamagnetic nanoparticles is warranted.

PROSTATE CANCER BIOLOGIC POTENTIAL

Noninvasive assessment of prostate cancer biologic potential for prostate cancer management may provide important diagnostic information and therefore help stratify patients for appropriate treatment. The Gleason scoring system assigns increasing pattern grades as the glands formed by the prostate epithelial cells become more poorly differentiated, the margins of the tumor become more poorly defined, and the degree of stromal invasion increases[76,77]. The Gleason scoring system remains one of the most powerful prognostic predictors of prostate cancer nearly 40 years after its initial description. It is endorsed as the primary grading system for prostate cancer by the World Health Organization, the Armed Forces Institute of Pathology Fascicle on Prostate Cancer, the Association of Directors of Anatomic and Surgical Pathology, and the College of American Pathologists[78].

MRI and MRSI may have a role in the evaluation of tumor aggressiveness, because signal intensity ratios from T2-weighted MRI and biochemical data from MRSI correlate with the Gleason grade of prostate cancer[79-81]. A study of 455 patients demonstrated that the signal intensities of prostate cancer on T2w MRI correlated with Gleason grade obtained from surgical pathology, with lower tumor-to-muscle ratios being associated with higher Gleason grades. A recent study demonstrates that MRI derived parameters (ADC and T2 relaxation time) at 3 Tesla correlate with prostate tumor cellularity[80]. A study of 220 patients demonstrated that both MRI and MRI/MRSI have incremental value in the clinical models predicting the probability of insignificant prostate cancer[41].

TREATMENT PLANNING

The surgeon's ultimate goal is to excise the cancer completely while preserving the nearby normal structures, thus avoiding positive surgical margins and minimizing the chances of recurrence and allowing recovery of physiological function. Impotence (erectile dysfunction) is one of the possible complications after RP. Impotence after RP is quantitatively related to the resection of the NVBs that closely run along 2 sides of the prostate and control the blood flow to the penis and erections[82]. Because the recovery of erectile function and the avoidance of positive surgical margins are important but competing outcomes, the decision to preserve or resect a NVB during radical prostatectomy should be based on the most accurate information concerning the location and extent of the tumor. As described in a study of 135 patients, information from MRI can assist in pre-surgical planning[53]. The areas under the ROC curves were 0.741 for pre-MRI and 0.832 for post-MRI surgical planning ($P < 0.01$). MRI findings suggested altering the surgical plan in 39% of NVBs. In 36 high-risk patients, MRI findings changed the surgical plan for 78% of NVBs (the change was found to be appropriate in 93% cases). A study of 75 consecutive patients demonstrated MRI findings successfully changed the operative strategy for NVBs in 44% of patients[83]. MRI can help to refine the surgical plan, to maximize the preservation of periprostatic tissues (important for recovery of urinary and sexual function), and to minimize the risk of positive surgical margins.

In the radiation treatment planning of localized prostate cancer, prostate contouring on MR is associated with less inter-observer variation than on CT[84].

THERAPY RESPONSE

Accurate therapy response assessment is essential for evaluation of either the success or failure of therapy. Early selection of patients who are most likely to benefit from chemotherapy or radiotherapy may prevent unnecessary toxicity in non-responding patients. Early response of prostate carcinoma xenografts to docetaxel chemotherapy is monitored with diffusion MRI. DWI MRI can be used as a biomarker for early detection of prostate cancer xenograft response to docetaxel chemotherapy[85] and is consistent with the therapeutic response in patients with metastatic prostate cancer to bone[86]. In a multivariate analysis of 67 patients, SVI on MRI and MRSI prior to external-beam radiation therapy predicted a worse prognosis[87]. The group demonstrated that the presence and degree of ECE on MRI significantly predicted post-treatment metastatic recurrence[88]. A study of 36 consecutive patients demonstrated a significantly greater area under the ROC curve (Az) for combined T2WI and DWI (Az = 0.879, $P < 0.01$) as compared to T2WI (Az = 0.612). A study demonstrated significant changes in perfusion and extraction coefficient derived from DCE-MRI in monitoring the response to percutaneous intensity-modulated radiotherapy of prostate cancer[89].

TUMOR RECURRENCE

Accurate identification of the risk of disease recurrence would also be particularly useful in clinical trials to assure comparability of treatment and control groups or to identify appropriate candidates for investigational treatment[31,90]. Patients with a PSA ⩽ 1.5 ng/mL after radical prostatectomy are best treated by salvage radiation therapy. Patients with local recurrence after external beam radiation therapy are good candidates for salvage prostatectomy.

An estimated one third of patients treated with radical prostatectomy later experience biochemical recurrence as defined by increases in PSA levels[91]. The natural history of biochemical recurrence after radical prostatectomy can be long but variable. Early identification, before detectable PSA is measured, of men likely to ultimately experience disease progression would be useful in considering early adjuvant therapy[92-95]. Clinical nomograms predicting freedom from biochemical recurrence 5 and 10 years after RP are in use[31,96]. A study of 610 patients demonstrated MRI was a strong predictor of biochemical recurrence after RP with hazard ratios of 1.76 and 1.81 in the 5- and 10-year models of clinical nomograms, respectively, but did not significantly improve prognostic value to standard clinical nomograms[97]. A study of 88 patients demonstrated a Cox model combining all clinical predictors had a C-index of 0.89; the C-index increased to 0.95 when MRI/MRSI was added[41]. In a study of 82 patients, sensitivity of MRI was 95%, and specificity was 100%. A study of 70 patients at high risk of local recurrence after RP demonstrated that combined MRSI and DCE-MRI showed a high sensitivity and specificity in identifying local prostate cancer recurrence in patients with biochemical progression after RP[98]. A study of 51 patients concluded that MRI combined with DCE-MRI is an accurate method to identify local recurrence after radical prostatectomy[99].

A study concluded that prostate cancer local recurrence after radiation therapy occurs at the site of the primary tumor[100]. In a study of 21 patients with biochemical failure after external beam radiation therapy, 3 or more suspicious voxels in a hemiprostate demonstrated a sensitivity and specificity of 89% and 82%, respectively, for the detection of local recurrence.

TO GUIDE TARGET BIOPSY FOR CLINICALLY SUSPECTED CANCER IN PATIENTS WITH NEGATIVE BIOPSY

MRI has been proven to improve tumor detection of prostate cancer in patients with persistently elevated PSA levels and repeated negative biopsies, and rule out cancer[101]. In a study of 54 patients with elevated PSA and negative biopsies, MRI had a sensitivity of 83% and a PPV of 50% for detection of prostate cancer. A study of 92 patients concluded that for patients with elevated PSA and 2 previous negative biopsies, a negative MRI can rule out cancer and avoid subsequent biopsies[102]. In a study of 24 patients, the sensitivity, specificity, positive and negative predictive values, and the accuracy of MRSI for prostate cancer detection were 70.6%, 66.7%, 57.1% and 58.3%, 83.3%[103]. In a study of 42 patients the sensitivity, specificity, positive and negative predictive values, and the accuracy of combined MRI/MRSI for prostate cancer detection were 73.3%, 96.3%, 91.6%, 86.6% and 88%, respectively[104].

FUTURE PROSPECTS

As 3T MR scanners become more available, body imaging at high field strength and improved coil design is becoming the subject of intensive research[105-109]. Theoretically, increasing static magnetic field strength, B_0, from 1.5T to 3T will result in a theoretical doubling of the signal-to-noise ratio (SNR). This in turn can be used to achieve greater spatial resolution and/or reduce scanning time. However, chemical shift and susceptibility artifacts also increase linearly with B_0. Improvements in coil design include the use of rigid coils with higher signal and the introduction of a susceptibility-matched agent into the rectum to reduce distortions relating to the interface of rectal air and tissue. The following advantages can be expected from imaging of prostate cancer with higher field strength and improved coil design: (1) Increased spatial resolution due to increased SNR may improve the detection of microscopic ECE; (2) Higher field strength provide increased spectral and spatial resolution for MRSI, but new pulse sequences will have to be designed for overcoming field inhomogeneities and citrate J-modulation issues. Significant improvement in metabolite resolution in MRSI with prostate cancer should be expected; (3) Faster scanning may help to reduce image artifacts related to patient motion and rectal peristalsis; (4) DCE-MRI may achieve increased SNR and faster image acquisition, with a significantly better trade-off between temporal and spatial resolution; and (5) With 3T and an endorectal coil, the voxel size can be reduced to 0.13 mm^3 as compared to 1.21 mm^3 at 1.5T[40]. Further investigation is needed to develop MRI/MRSI/DWI/DCE-MRI criteria on 3T MRI scanners for prostate cancer detection and staging.

The whole body MRI, one of the advances in MR techniques, may be more sensitive than the traditional work-up for identifying bone metastases. In the future of prostate cancer management, MR-guided prostate interventions such as MRI-guided focused ultrasound surgery will result in major changes.

CONCLUSION

In patients with prostate cancer, there is growing demand for patient-specific therapies that can minimize treatment morbidity while maximizing treatment benefits. MRI non-invasively improves cancer staging,

biologic potential and treatment planning, monitors anti-tumor therapy and local recurrence, and guides target biopsy for clinically suspected cancer with previous negative biopsy. The incorporation of endorectal MR findings into future nomograms for the prediction of prostate cancer stage and freedom from biochemical recurrence is warranted. Advances in technology, such as MRSI, DWI, DCE-MRI, high field strength MRI scanner, and whole body MRI, and in the expertise of radiologists dedicated to the genitourinary field, suggests that MRI can play an increasingly useful role in prostate cancer management.

ACKNOWLEDGMENTS

The author thanks Carolina Montalvo, BA, for preparing the figures.

REFERENCES

1 **Jemal A**, Siegel R, Ward E, Hao Y, Xu J, Thun MJ. Cancer statistics, 2009. *CA Cancer J Clin* 2009; **59**: 225-249
2 **Parkin DM**, Bray F, Ferlay J, Pisani P. Global cancer statistics, 2002. *CA Cancer J Clin* 2005; **55**: 74-108
3 **Kamangar F**, Dores GM, Anderson WF. Patterns of cancer incidence, mortality, and prevalence across five continents: defining priorities to reduce cancer disparities in different geographic regions of the world. *J Clin Oncol* 2006; **24**: 2137-2150
4 **Boyle P**, Ferlay J. Cancer incidence and mortality in Europe, 2004. *Ann Oncol* 2005; **16**: 481-488
5 **Kagotho N**, Tan J. Predictors of prostate cancer screening among older immigrant men. *J Natl Med Assoc* 2008; **100**: 1168-1174
6 **Matsuda T**, Saika K. Comparison of time trends in prostate cancer incidence (1973 1997) in East Asia, Europe and USA, from Cancer Incidence in Five Continents Vols IV VIII. *Jpn J Clin Oncol* 2007; **37**: 556-557
7 **Scardino PT**. New technology and the changing world of cancer. *Nat Clin Pract Urol* 2005; **2**: 403
8 **Eggener SE**, Scardino PT, Carroll PR, Zelefsky MJ, Sartor O, Hricak H, Wheeler TM, Fine SW, Trachtenberg J, Rubin MA, Ohori M, Kuroiwa K, Rossignol M, Abenhaim L. Focal therapy for localized prostate cancer: a critical appraisal of rationale and modalities. *J Urol* 2007; **178**: 2260-2267
9 **Carroll PR**. Early stage prostate cancer--do we have a problem with over-detection, overtreatment or both? *J Urol* 2005; **173**: 1061-1062
10 **Konety BR**, Bird VY, Deorah S, Dahmoush L. Comparison of the incidence of latent prostate cancer detected at autopsy before and after the prostate specific antigen era. *J Urol* 2005; **174**: 1785-1788; discussion 1788
11 **Freedland SJ**, Kane CJ, Amling CL, Aronson WJ, Presti JC Jr, Terris MK. Delay of radical prostatectomy and risk of biochemical progression in men with low risk prostate cancer. *J Urol* 2006; **175**: 1298-1302; discussion 1302-1303
12 **Lieberman R**. Evidence-based medical perspectives: the evolving role of PSA for early detection, monitoring of treatment response, and as a surrogate end point of efficacy for interventions in men with different clinical risk states for the prevention and progression of prostate cancer. *Am J Ther* 2004; **11**: 501-506
13 **Freedland SJ**, Partin AW. Prostate-specific antigen: update 2006. *Urology* 2006; **67**: 458-460
14 **Schröder FH**. Prostate specific antigen and other markers for prostate cancer. *J Urol* 2006; **175**: 1199-1200
15 **Bill-Axelson A**, Holmberg L, Ruutu M, Häggman M, Andersson SO, Bratell S, Spångberg A, Busch C, Nordling S, Garmo H, Palmgren J, Adami HO, Norlén BJ, Johansson JE. Radical prostatectomy versus watchful waiting in early prostate cancer. *N Engl J Med* 2005; **352**: 1977-1984
16 **Gilligan T**, Kantoff PW. Chemotherapy for prostate cancer. *Urology* 2002; **60**: 94-100; discussion 100
17 **Thompson IM**, Seay TM. Will current clinical trials answer the most important questions about prostate adenocarcinoma? *Oncology* (Williston Park) 1997; **11**: 1109-1117; discussion 1117-1118, 1121
18 **Marberger M**, Carroll PR, Zelefsky MJ, Coleman JA, Hricak H, Scardino PT, Abenhaim LL. New treatments for localized prostate cancer. *Urology* 2008; **72**: S36-S43
19 **Bianco FJ Jr**, Scardino PT, Eastham JA. Radical prostatectomy: long-term cancer control and recovery of sexual and urinary function ("trifecta"). *Urology* 2005; **66**: 83-94
20 **Kattan MW**, Scardino PT. Prediction of progression: nomograms of clinical utility. *Clin Prostate Cancer* 2002; **1**: 90-96
21 **Perrotti M**. Understanding PSA and prostate cancer risk assessment. *N J Med* 2001; **98**: 35-38
22 **Graefen M**, Ohori M, Karakiewicz PI, Cagiannos I, Hammerer PG, Haese A, Erbersdobler A, Henke RP, Huland H, Wheeler TM, Slawin K, Scardino PT, Kattan MW. Assessment of the enhancement in predictive accuracy provided by systematic biopsy in predicting outcome for clinically localized prostate cancer. *J Urol* 2004; **171**: 200-203
23 **Parsons JK**, Partin AW. Clinical interpretation of prostate biopsy reports. *Urology* 2006; **67**: 452-457
24 **Ohori M**, Kattan MW, Koh H, Maru N, Slawin KM, Shariat S, Muramoto M, Reuter VE, Wheeler TM, Scardino PT. Predicting the presence and side of extracapsular extension: a nomogram for staging prostate cancer. *J Urol* 2004; **171**: 1844-1849; discussion 1849
25 **Di Blasio CJ**, Rhee AC, Cho D, Scardino PT, Kattan MW. Predicting clinical end points: treatment nomograms in prostate cancer. *Semin Oncol* 2003; **30**: 567-586
26 **Diblasio CJ**, Kattan MW. Use of nomograms to predict the risk of disease recurrence after definitive local therapy for prostate cancer. *Urology* 2003; **62** Suppl 1: 9-18
27 **Scherr D**, Swindle PW, Scardino PT. National Comprehensive Cancer Network guidelines for the management of prostate cancer. *Urology* 2003; **61**: 14-24
28 **Partin AW**, Mangold LA, Lamm DM, Walsh PC, Epstein JI, Pearson JD. Contemporary update of prostate cancer staging nomograms (Partin Tables) for the new millennium. *Urology* 2001; **58**: 843-848
29 **Khan MA**, Partin AW. Partin tables: past and present. *BJU Int* 2003; **92**: 7-11
30 **Partin AW**, Kattan MW, Subong EN, Walsh PC, Wojno KJ, Oesterling JE, Scardino PT, Pearson JD. Combination of prostate-specific antigen, clinical stage, and Gleason score to predict pathological stage of localized prostate cancer. A multi-institutional update. *JAMA* 1997; **277**: 1445-1451
31 **Stephenson AJ**, Scardino PT, Eastham JA, Bianco FJ Jr, Dotan ZA, Fearn PA, Kattan MW. Preoperative nomogram predicting the 10-year probability of prostate cancer recurrence after radical prostatectomy. *J Natl Cancer Inst* 2006; **98**: 715-717
32 **Wang L**, Hricak H, Kattan MW, Schwartz LH, Eberhardt SC, Chen HN, Scardino PT. Combined endorectal and phased-array MRI in the prediction of pelvic lymph node metastasis in prostate cancer. *AJR Am J Roentgenol* 2006; **186**: 743-748
33 **Wang L**, Mullerad M, Chen HN, Eberhardt SC, Kattan MW, Scardino PT, Hricak H. Prostate cancer: incremental value of endorectal MR imaging findings for prediction of extracapsular extension. *Radiology* 2004; **232**: 133-139

34 **Hricak H**. MR imaging and MR spectroscopic imaging in the pre-treatment evaluation of prostate cancer. *Br J Radiol* 2005; **78** Spec No 2: S103-S111

35 **Huzjan R**, Sala E, Hricak H. Magnetic resonance imaging and magnetic resonance spectroscopic imaging of prostate cancer. *Nat Clin Pract Urol* 2005; **2**: 434-442

36 **Claus FG**, Hricak H, Hattery RR. Pretreatment evaluation of prostate cancer: role of MR imaging and 1H MR spectroscopy. *Radiographics* 2004; **24** Suppl 1: S167-S180

37 **Trabulsi EJ**, Merriam WG, Gomella LG. New imaging techniques in prostate cancer. *Curr Urol Rep* 2006; **7**: 175-180

38 **Engelbrecht MR**, Jager GJ, Laheij RJ, Verbeek AL, van Lier HJ, Barentsz JO. Local staging of prostate cancer using magnetic resonance imaging: a meta-analysis. *Eur Radiol* 2002; **12**: 2294-2302

39 **Wang L**, Zhang J, Schwartz LH, Eisenberg H, Ishill NM, Moskowitz CS, Scardino P, Hricak H. Incremental value of multiplanar cross-referencing for prostate cancer staging with endorectal MRI. *AJR Am J Roentgenol* 2007; **188**: 99-104

40 **Fütterer JJ**, Barentsz JO, Heijmink SW. Value of 3-T magnetic resonance imaging in local staging of prostate cancer. *Top Magn Reson Imaging* 2008; **19**: 285-289

41 **Shukla-Dave A**, Hricak H, Moskowitz C, Ishill N, Akin O, Kuroiwa K, Spector J, Kumar M, Reuter VE, Koutcher JA, Zakian KL. Detection of prostate cancer with MR spectroscopic imaging: an expanded paradigm incorporating polyamines. *Radiology* 2007; **245**: 499-506

42 **Wang L**, Van den Bos IC, Hussain SM, Pattynama PM, Vogel MW, Krestin GP. Post-processing of dynamic gadolinium-enhanced magnetic resonance imaging exams of the liver: explanation and potential clinical applications for color-coded qualitative and quantitative analysis. *Acta Radiol* 2008; **49**: 6-18

43 **Edge SB**, Byrd DR, Compton CC, Fritz AG, Greene FL, Trotti A, editors. AJCC Cancer Staging Manual. 7th ed. New York: Springer-Verlag, 2010

44 **Presti JC Jr**. Prostate cancer: assessment of risk using digital rectal examination, tumor grade, prostate-specific antigen, and systematic biopsy. *Radiol Clin North Am* 2000; **38**: 49-58

45 **Scardino PT**. Continuing refinements in radical prostatectomy: more evidence that technique matters. *J Urol* 2005; **173**: 338-339

46 **Blute ML**, Bergstralh EJ, Partin AW, Walsh PC, Kattan MW, Scardino PT, Montie JE, Pearson JD, Slezak JM, Zincke H. Validation of Partin tables for predicting pathological stage of clinically localized prostate cancer. *J Urol* 2000; **164**: 1591-1595

47 **Augustin H**, Eggert T, Wenske S, Karakiewicz PI, Palisaar J, Daghofer F, Huland H, Graefen M. Comparison of accuracy between the Partin tables of 1997 and 2001 to predict final pathological stage in clinically localized prostate cancer. *J Urol* 2004; **171**: 177-181

48 **Graefen M**, Augustin H, Karakiewicz PI, Hammerer PG, Haese A, Palisaar J, Blonski J, Fernandez S, Erbersdobler A, Huland H. Can predictive models for prostate cancer patients derived in the United States of America be utilized in European patients? A validation study of the Partin tables. *Eur Urol* 2003; **43**: 6-10; discussion 11

49 **Ohori M**, Kattan M, Scardino PT, Wheeler TM. Radical prostatectomy for carcinoma of the prostate. *Mod Pathol* 2004; **17**: 349-359

50 **Roach M 3rd**, Chen A, Song J, Diaz A, Presti J Jr, Carroll P. Pretreatment prostate-specific antigen and Gleason score predict the risk of extracapsular extension and the risk of failure following radiotherapy in patients with clinically localized prostate cancer. *Semin Urol Oncol* 2000; **18**: 108-114

51 **Hull GW**, Rabbani F, Abbas F, Wheeler TM, Kattan MW, Scardino PT. Cancer control with radical prostatectomy alone in 1,000 consecutive patients. *J Urol* 2002; **167**: 528-534

52 **Catalona WJ**, Ramos CG, Carvalhal GF. Contemporary results of anatomic radical prostatectomy. *CA Cancer J Clin* 1999; **49**: 282-296

53 **Hricak H**, Wang L, Wei DC, Coakley FV, Akin O, Reuter VE, Gonen M, Kattan MW, Onyebuchi CN, Scardino PT. The role of preoperative endorectal magnetic resonance imaging in the decision regarding whether to preserve or resect neurovascular bundles during radical retropubic prostatectomy. *Cancer* 2004; **100**: 2655-2663

54 **Kamat AM**, Jacobsohn KM, Troncoso P, Shen Y, Wen S, Babaian RJ. Validation of criteria used to predict extraprostatic cancer extension: a tool for use in selecting patients for nerve sparing radical prostatectomy. *J Urol* 2005; **174**: 1262-1265

55 **Outwater EK**, Petersen RO, Siegelman ES, Gomella LG, Chernesky CE, Mitchell DG. Prostate carcinoma: assessment of diagnostic criteria for capsular penetration on endorectal coil MR images. *Radiology* 1994; **193**: 333-339

56 **Yu KK**, Hricak H, Alagappan R, Chernoff DM, Bacchetti P, Zaloudek CJ. Detection of extracapsular extension of prostate carcinoma with endorectal and phased-array coil MR imaging: multivariate feature analysis. *Radiology* 1997; **202**: 697-702

57 **Jager GJ**, Severens JL, Thornbury JR, de La Rosette JJ, Ruijs SH, Barentsz JO. Prostate cancer staging: should MR imaging be used?--A decision analytic approach. *Radiology* 2000; **215**: 445-451

58 **Yu KK**, Scheidler J, Hricak H, Vigneron DB, Zaloudek CJ, Males RG, Nelson SJ, Carroll PR, Kurhanewicz J. Prostate cancer: prediction of extracapsular extension with endorectal MR imaging and three-dimensional proton MR spectroscopic imaging. *Radiology* 1999; **213**: 481-488

59 **Mullerad M**, Hricak H, Wang L, Chen HN, Kattan MW, Scardino PT. Prostate cancer: detection of extracapsular extension by genitourinary and general body radiologists at MR imaging. *Radiology* 2004; **232**: 140-146

60 **Augustin H**, Fritz GA, Ehammer T, Auprich M, Pummer K. Accuracy of 3-Tesla magnetic resonance imaging for the staging of prostate cancer in comparison to the Partin tables. *Acta Radiol* 2009; **50**: 562-569

61 **Masterson TA**, Pettus JA, Middleton RG, Stephenson RA. Isolated seminal vesicle invasion imparts better outcomes after radical retropubic prostatectomy for clinically localized prostate cancer: prognostic stratification of pt3b disease by nodal and margin status. *Urology* 2005; **66**: 152-155

62 **Ramsden AR**, Chodak G. An analysis of risk factors for biochemical progression in patients with seminal vesicle invasion: validation of Kattan's nomogram in a pathological subgroup. *BJU Int* 2004; **93**: 961-964

63 **Ohori M**, Scardino PT, Lapin SL, Seale-Hawkins C, Link J, Wheeler TM. The mechanisms and prognostic significance of seminal vesicle involvement by prostate cancer. *Am J Surg Pathol* 1993; **17**: 1252-1261

64 **Sala E**, Akin O, Moskowitz CS, Eisenberg HF, Kuroiwa K, Ishill NM, Rajashanker B, Scardino PT, Hricak H. Endorectal MR imaging in the evaluation of seminal vesicle invasion: diagnostic accuracy and multivariate feature analysis. *Radiology* 2006; **238**: 929-937

65 **John H**, Hauri D. Seminal vesicle-sparing radical prostatectomy: a novel concept to restore early urinary continence. *Urology* 2000; **55**: 820-824

66 **Wang L**, Hricak H, Kattan MW, Chen HN, Kuroiwa K, Eisenberg HF, Scardino PT. Prediction of seminal vesicle invasion in prostate cancer: incremental value of adding endorectal MR imaging to the Kattan nomogram. *Radiology* 2007; **242**: 182-188

67 **Ren J**, Huan Y, Wang H, Ge Y, Chang Y, Yin H, Sun L. Seminal vesicle invasion in prostate cancer: prediction with combined T2-weighted and diffusion-weighted MR imaging. *Eur Radiol* 2009; **19**: 2481-2486

68 **Kim CK**, Choi D, Park BK, Kwon GY, Lim HK. Diffusion-weighted MR imaging for the evaluation of seminal vesicle invasion in prostate cancer: initial results. *J Magn Reson Imaging* 2008; **28**: 963-969

69 **Fütterer JJ**, Engelbrecht MR, Huisman HJ, Jager GJ, Hulsbergen-van De Kaa CA, Witjes JA, Barentsz JO. Staging prostate cancer with dynamic contrast-enhanced endorectal MR imaging prior to radical prostatectomy: experienced versus less experienced readers. *Radiology* 2005; **237**: 541-549

70 **Ohori M**, Abbas F, Wheeler TM, Kattan MW, Scardino PT, Lerner SP. Pathological features and prognostic significance of prostate cancer in the apical section determined by whole mount histology. *J Urol* 1999; **161**: 500-504

71 **Gervasi LA**, Mata J, Easley JD, Wilbanks JH, Seale-Hawkins C, Carlton CE Jr, Scardino PT. Prognostic significance of lymph nodal metastases in prostate cancer. *J Urol* 1989; **142**: 332-336

72 **Naya Y**, Fritsche HA, Cheli CD, Stamey TA, Bartsch G, Brawer MK, Childs S, Taneja SS, Lepor H, Partin AW, Sokoll LJ, Chan DW, Babaian RJ. Volume indexes of total, free, and complexed prostate-specific antigen enhance prediction of extraprostatic disease extension in men with nonpalpable prostate cancer. *Urology* 2003; **62**: 1058-1062

73 **Harisinghani MG**, Barentsz J, Hahn PF, Deserno WM, Tabatabaei S, van de Kaa CH, de la Rosette J, Weissleder R. Noninvasive detection of clinically occult lymph-node metastases in prostate cancer. *N Engl J Med* 2003; **348**: 2491-2499

74 **Borley N**, Fabrin K, Sriprasad S, Mondaini N, Thompson P, Muir G, Poulsen J. Laparoscopic pelvic lymph node dissection allows significantly more accurate staging in "high-risk" prostate cancer compared to MRI or CT. *Scand J Urol Nephrol* 2003; **37**: 382-386

75 **Bellin MF**, Roy C, Kinkel K, Thoumas D, Zaim S, Vanel D, Tuchmann C, Richard F, Jacqmin D, Delcourt A, Challier E, Lebret T, Cluzel P. Lymph node metastases: safety and effectiveness of MR imaging with ultrasmall superparamagnetic iron oxide particles--initial clinical experience. *Radiology* 1998; **207**: 799-808

76 **Gleason DF**. Classification of prostatic carcinomas. *Cancer Chemother Rep* 1966; **50**: 125-128

77 **Gleason DF**, Mellinger GT. Prediction of prognosis for prostatic adenocarcinoma by combined histological grading and clinical staging. *J Urol* 1974; **111**: 58-64

78 **Epstein JI**, Algaba F, Allsbrook WC Jr, Bastacky S, Boccon-Gibod L, De Marzo AM, Egevad L, Furusto M, Hamper UM, Helpap B, Humphrey PA, Iczkowski KA, Lopez-Beltran A, Montironi R, Rubin MA, Sakr WA, Samaratunga H, Parkin DM. Acinar adenocarcinoma. In: Eble JN, Sauter G, Epstein JI, Sesterhenn IA, editors. WHO Classification of Tumours: Pathology and Genetics of Tumours of the Urinary System and Male Genital Organs. Lyon: IARC Press, 2004: 179-184

79 **Wang L**, Mazaheri Y, Zhang J, Ishill NM, Kuroiwa K, Hricak H. Assessment of biologic aggressiveness of prostate cancer: correlation of MR signal intensity with Gleason grade after radical prostatectomy. *Radiology* 2008; **246**: 168-176

80 **Giusti S**, Caramella D, Fruzzetti E, Lazzereschi M, Tognetti A, Bartolozzi C. Peripheral zone prostate cancer. Pre-treatment evaluation with MR and 3D (1)H MR spectroscopic imaging: correlation with pathologic findings. *Abdom Imaging* 2009; Epub ahead of print

81 **Zakian KL**, Sircar K, Hricak H, Chen HN, Shukla-Dave A, Eberhardt S, Muruganandham M, Ebora L, Kattan MW, Reuter VE, Scardino PT, Koutcher JA. Correlation of proton MR spectroscopic imaging with gleason score based on step-section pathologic analysis after radical prostatectomy. *Radiology* 2005; **234**: 804-814

82 **Rabbani F**, Stapleton AM, Kattan MW, Wheeler TM, Scardino PT. Factors predicting recovery of erections after radical prostatectomy. *J Urol* 2000; **164**: 1929-1934

83 **Labanaris AP**, Zugor V, Takriti S, Smiszek R, Engelhard K, Nutzel R, Kuhn R. The role of conventional and functional endorectal magnetic resonance imaging in the decision of whether to preserve or resect the neurovascular bundles during radical retropubic prostatectomy. *Scand J Urol Nephrol* 2009; **43**: 25-31

84 **Parker CC**, Dearnaley DP. Radical radiotherapy for prostate cancer. *Cancer Treat Rev* 2003; **29**: 161-169

85 **Jennings D**, Hatton BN, Guo J, Galons JP, Trouard TP, Raghunand N, Marshall J, Gillies RJ. Early response of prostate carcinoma xenografts to docetaxel chemotherapy monitored with diffusion MRI. *Neoplasia* 2002; **4**: 255-262

86 **Lee KC**, Bradley DA, Hussain M, Meyer CR, Chenevert TL, Jacobson JA, Johnson TD, Galban CJ, Rehemtulla A, Pienta KJ, Ross BD. A feasibility study evaluating the functional diffusion map as a predictive imaging biomarker for detection of treatment response in a patient with metastatic prostate cancer to the bone. *Neoplasia* 2007; **9**: 1003-1011

87 **Joseph T**, McKenna DA, Westphalen AC, Coakley FV, Zhao S, Lu Y, Hsu IC, Roach M 3rd, Kurhanewicz J. Pretreatment endorectal magnetic resonance imaging and magnetic resonance spectroscopic imaging features of prostate cancer as predictors of response to external beam radiotherapy. *Int J Radiat Oncol Biol Phys* 2009; **73**: 665-671

88 **McKenna DA**, Coakley FV, Westphalen AC, Zhao S, Lu Y, Webb EM, Pickett B, Roach M 3rd, Kurhanewicz J. Prostate cancer: role of pretreatment MR in predicting outcome after external-beam radiation therapy--initial experience. *Radiology* 2008; **247**: 141-146

89 **Franiel T**, Lüdemann L, Taupitz M, Böhmer D, Beyersdorff D. MRI before and after external beam intensity-modulated radiotherapy of patients with prostate cancer: the feasibility of monitoring of radiation-induced tissue changes using a dynamic contrast-enhanced inversion-prepared dual-contrast gradient echo sequence. *Radiother Oncol* 2009; **93**: 241-245

90 **Stephenson AJ**, Scardino PT, Eastham JA, Bianco FJ Jr, Dotan ZA, DiBlasio CJ, Reuther A, Klein EA, Kattan MW. Postoperative nomogram predicting the 10-year probability of prostate cancer recurrence after radical prostatectomy. *J Clin Oncol* 2005; **23**: 7005-7012

91 **Aranha O**, Vaishampayan U. PSA relapse prostate cancer: the importance of tailored therapy. *Urol Oncol* 2004; **22**: 62-69

92 **Freedland SJ**, Humphreys EB, Mangold LA, Eisenberger M, Dorey FJ, Walsh PC, Partin AW. Risk of prostate cancer-specific mortality following biochemical recurrence after radical prostatectomy. *JAMA* 2005; **294**: 433-439

93 **Han M**, Partin AW, Zahurak M, Piantadosi S, Epstein JI, Walsh PC. Biochemical (prostate specific antigen) recurrence probability following radical prostatectomy for clinically localized prostate cancer. *J Urol* 2003; **169**: 517-523

94 **Tewari A**, Gamito EJ, Crawford ED, Menon M. Biochemical recurrence and survival prediction models for the management of clinically localized prostate cancer. *Clin Prostate Cancer* 2004; **2**: 220-227

95 **Moul JW**. Biochemical recurrence of prostate cancer. *Curr Probl Cancer* 2003; **27**: 243-272

96 **Kattan MW**, Eastham JA, Stapleton AM, Wheeler TM, Scardino PT. A preoperative nomogram for disease recurrence following radical prostatectomy for prostate cancer. *J Natl Cancer Inst* 1998; **90**: 766-771

97 **Fuchsjäger MH**, Shukla-Dave A, Hricak H, Wang L, Touijer K, Donohue JF, Eastham JA, Kattan MW. Magnetic resonance imaging in the prediction of biochemical recurrence of prostate cancer after radical prostatectomy. *BJU Int* 2009; **104**: 315-320

98 **Sciarra A**, Panebianco V, Salciccia S, Osimani M, Lisi D, Ciccariello M, Passariello R, Di Silverio F, Gentile V. Role

of dynamic contrast-enhanced magnetic resonance (MR) imaging and proton MR spectroscopic imaging in the detection of local recurrence after radical prostatectomy for prostate cancer. *Eur Urol* 2008; **54**: 589-600

99 **Casciani E**, Polettini E, Carmenini E, Floriani I, Masselli G, Bertini L, Gualdi GF. Endorectal and dynamic contrast-enhanced MRI for detection of local recurrence after radical prostatectomy. *AJR Am J Roentgenol* 2008; **190**: 1187-1192

100 **Pucar D**, Hricak H, Shukla-Dave A, Kuroiwa K, Drobnjak M, Eastham J, Scardino PT, Zelefsky MJ. Clinically significant prostate cancer local recurrence after radiation therapy occurs at the site of primary tumor: magnetic resonance imaging and step-section pathology evidence. *Int J Radiat Oncol Biol Phys* 2007; **69**: 62-69

101 **Yakar D**, Hambrock T, Hoeks C, Barentsz JO, Fütterer JJ. Magnetic resonance-guided biopsy of the prostate: feasibility, technique, and clinical applications. *Top Magn Reson Imaging* 2008; **19**: 291-295

102 **Comet-Batlle J**, Vilanova-Busquets JC, Saladié-Roig JM, Gelabert-Mas A, Barceló-Vidal C. The value of endorectal MRI in the early diagnosis of prostate cancer. *Eur Urol* 2003; **44**: 201-207; discussion 207-208

103 **Yuen JS**, Thng CH, Tan PH, Khin LW, Phee SJ, Xiao D, Lau WK, Ng WS, Cheng CW. Endorectal magnetic resonance imaging and spectroscopy for the detection of tumor foci in men with prior negative transrectal ultrasound prostate biopsy. *J Urol* 2004; **171**: 1482-1486

104 **Amsellem-Ouazana D**, Younes P, Conquy S, Peyromaure M, Flam T, Debré B, Zerbib M. Negative prostatic biopsies in patients with a high risk of prostate cancer. Is the combination of endorectal MRI and magnetic resonance spectroscopy imaging (MRSI) a useful tool? A preliminary study. *Eur Urol* 2005; **47**: 582-586

105 **Rouvière O**, Hartman RP, Lyonnet D. Prostate MR imaging at high-field strength: evolution or revolution? *Eur Radiol* 2006; **16**: 276-284

106 **Hussain SM**, Wielopolski PA, Martin DR. Abdominal magnetic resonance imaging at 3.0 T: problem or a promise for the future? *Top Magn Reson Imaging* 2005; **16**: 325-335

107 **Beyersdorff D**, Taymoorian K, Knösel T, Schnorr D, Felix R, Hamm B, Bruhn H. MRI of prostate cancer at 1.5 and 3.0 T: comparison of image quality in tumor detection and staging. *AJR Am J Roentgenol* 2005; **185**: 1214-1220

108 **Fütterer JJ**, Heijmink SW, Scheenen TW, Jager GJ, Hulsbergen-Van de Kaa CA, Witjes JA, Barentsz JO. Prostate cancer: local staging at 3-T endorectal MR imaging--early experience. *Radiology* 2006; **238**: 184-191

109 **Fütterer JJ**, Scheenen TW, Huisman HJ, Klomp DW, van Dorsten FA, Hulsbergen-van de Kaa CA, Witjes JA, Heerschap A, Barentsz JO. Initial experience of 3 tesla endorectal coil magnetic resonance imaging and 1H-spectroscopic imaging of the prostate. *Invest Radiol* 2004; **39**: 671-680

S- Editor Cheng JX **L- Editor** Cant MR **E- Editor** Zheng XM

World Journal of Radiology

Online Submissions: http://www.wjgnet.com/1949-8470office
wjr@wjgnet.com
doi:10.4329/wjr.v1.i1.15

World J Radiol 2009 December 31; 1(1): 15-24
ISSN 1949-8470 (online)

TOPIC HIGHLIGHT

Hui-Xiong Xu, MD, PhD, *Series Editor*

Contrast-enhanced ultrasound: The evolving applications

Hui-Xiong Xu

Hui-Xiong Xu, Department of Medical Ultrasonics, The First Affiliated Hospital, Sun Yat-Sen University, The Center of Guangdong Province for the Study of Diagnostic Ultrasound and Interventional Therapy, 58 Zhongshan Road 2, Guangzhou 510080, Guangdong Province, China
Author contributions: Xu HX solely contributed to this paper.
Supported by In part by grant No. NCET-06-0723 from the Chinese Ministry of Education and grant 2008-2-10 of Public Welfare Research Special Project from the Chinese Ministry of Health
Correspondence to: Hui-Xiong Xu, MD, PhD, Professor, Department of Medical Ultrasonics, The First Affiliated Hospital, Sun Yat-Sen University, The Center of Guangdong Province for the Study of Diagnostic Ultrasound and Interventional Therapy, 58 Zhongshan Road 2, Guangzhou 510080, Guangdong Province, China. xuhuixiong@hotmail.com
Telephone: +86-20-87765183 Fax: +86-20-87765183
Received: November 5, 2009 Revised: December 17, 2009
Accepted: December 21, 2009
Published online: December 31, 2009

Abstract

Contrast-enhanced ultrasound (CEUS) is a major breakthrough for ultrasound imaging in recent years. By using a microbubble contrast agent and contrast-specific imaging software, CEUS is able to depict the micro- and macro-circulation of the targeted organ, which in turn leads to improved performance in diagnosis. Due to the special dual blood supply system in the liver, CEUS is particularly suitable for liver imaging. It is evident that CEUS facilitates improvement for characterization of focal liver lesions (FLLs), detection of liver malignancy, guidance for interventional procedures, and evaluation of treatment response after local therapies. CEUS has been demonstrated to be equal to contrast-enhanced computed tomography or magnetic resonance imaging for the characterization of FLLs. In addition, the applicability of CEUS has expanded to non-liver structures such as gallbladder, bile duct, pancreas, kidney, spleen, breast, thyroid, and prostate. The usefulness of CEUS in these applications is confirmed by extensive literature production. Novel applications include detecting bleeding sites and hematomas in patients with abdominal trauma, guiding percutaneous injection therapy and therefore achieving the goal of using interventional ultrasonography in managing splenic trauma, assessing the activity of Crohn's disease, and detecting suspected endoleaks after endovascular abdominal aneurysm repair. Contrast-enhanced intraoperative ultrasound (US) and intracavitary use of CEUS have been developed and clinically studied. The potential use of CEUS involves sentinel lymph node detection, drug or gene delivery, and molecular imaging. In conclusion, the advent of CEUS has greatly enhanced the usefulness of US and even changed the status of US in clinical practice. The application of CEUS in the clinic is continuously evolving and it is expected that its use will be expanded further in the future.

Key words: Bile duct; Breast; Gallbladder; Pancreas; Kidney; Liver; Contrast-enhanced ultrasound; Prostate; Spleen; Thyroid

Peer reviewers: Sergio Sartori, MD, Department of Internal Medicine, Section of Interventional Ultrasound, St. Anna Hospital, I-44100 Ferrara, Italy; Sergio Casciaro, PhD, Institute of Clinical Physiology-National Research Council, Campus Universitario Ecotekne, Via Monteroni, 73100 Lecce, Italy

Xu HX. Contrast-enhanced ultrasound: The evolving applications. *World J Radiol* 2009; 1(1): 15-24 Available from: URL: http://www.wjgnet.com/1949-8470/full/v1/i1/15.htm DOI: http://dx.doi.org/10.4329/wjr.v1.i1.15

INTRODUCTION

Ultrasound (US) is one of the most widely used imaging

modalities in the clinic, largely owing to its characteristics such as real-time scanning, no radiation, easy performance, and cost-effectiveness. With the improvement of related technologies, US not only provides high-resolution sectional anatomic images, but also provides detailed blood flow information within the region of interest (ROI), which leads to wide applicability of US in various fields. However, when compared with other tomographic modalities such as computed tomography (CT) or magnetic resonance imaging (MRI), conventional US has been generally regarded to be inferior since it has low ability to depict the microcirculation within the ROI. This is especially true for tumor imaging because the information on microcirculation is essential for imaging diagnosis. Therefore, in the clinic, most patients have to be referred to CT or MRI examination for further confirmation.

The beginning of the new millennium has witnessed a revolutionary evolution of US. Contrast-enhanced US (CEUS), which not only improves the diagnostic performance in numerous pathological conditions, but has also, changed the status of US in some fields. CEUS consists of two basic elements, one is the ultrasound contrast agent (UCA), and the other is contrast-specific imaging technique. The first generation of UCAs such as agitated saline, hydrogen peroxide, air, and carbon dioxide can not pass through the pulmonary circulation, thus only achieve right heart imaging. The second generation of UCAs is stabilized with different substances, the surface of which is made of phospholipid, albumin, or polymers. The mean diameter of the second generation of UCAs is less than 8 μm which guarantees that the UCA can pass through the pulmonary circulation and reach various organs. Second generation UCAs also have prolonged longevity due to their lower solubility in water and have a strong harmonic response.

An UCA in the circulation interacts with the US beam depending on the energy of insonation. At low acoustic powers (low mechanical index), the bubbles reflect US and increase the echoes. As the acoustic power increases, the bubbles develop nonlinear resonance, resulting in the generation of harmonic signals. At higher powers, bubble destruction occurs, producing a strong but transient effect that may be seen as an intense signal. Most of the contrast specific techniques such as pulse and phase inversion discriminate between the nonlinear harmonic response from microbubbles and the response from tissue, thus allowing detection of the signal of microbubbles in a gray-scale image. High MI technologies allow intermittent scanning of the lesion during the various phases of contrast enhancement. Conversely, the contrast-specific imaging technique operates under low MI (i.e. less than 0.2), thus the UCA in the acoustic field would not be destroyed and the scanning fashion is continuous. These nondestructive techniques require administration of second-generation UCAs which are able to reflect the US beam at low acoustic power.

In the CEUS procedure, firstly the UCA is administered through the peripheral veins, and then the ROI is exposed to an acoustic field. When the UCA microbubbles arrive in the ROI, the UCA in the micro- and macro-circulation will interact with the acoustic wave and nonlinear signals will be generated, whereas no or few nonlinear signals are generated from the tissues. Thus an improved signal-to-noise ratio is achieved, and UCA can be used as a tracer to depict the micro- and macro-circulation[1,2].

CEUS FOR LIVER USE

CEUS is particularly suitable for liver imaging, which is largely due to the fact that the liver has a dual blood supply system[3]. The UCAs in the hepatic artery are firstly visualized, followed by those in the portal vein. Hence, the CEUS process is always divided into the arterial phase (< 30 s from the injection of UCA), portal phase (31-121 s), and late phase (> 120 s). The enhancement extent of lesions is divided into hyper-, iso-, hypo-, and non-enhancement compared with the adjacent liver tissue[4].

Characterization

On CEUS, hyperenhancement in the arterial phase and subsequent washout to hypoenhancement often indicates malignancy, and sustained enhancement in the portal or late phase always indicates benignity. This algorithm has been endorsed by the 2008 European Guideline for CEUS[4]. Xu *et al*[5] compared the diagnostic capability of CEUS with baseline US (BUS) in 200 patients with small focal liver lesions (FLLs) (equal or less than 3 cm). The sensitivity, negative predictive value, and accuracy of BUS and CEUS in differentiating between malignant and benign FLLs were 59.6%-71.1% *vs* 89.5%-93.9%, 63.2%-69.2% *vs* 87.4%-91.8% and 73.5%-77.5% *vs* 92.5%, respectively (all $P < 0.001$). A better interobserver agreement was achieved using CEUS ($\kappa = 0.425$ with BUS *vs* $\kappa = 0.716$ with CEUS). Similar results were found by other investigators[6,7].

Besides making the distinction between malignancy and benignity, many FLLs have special enhancement patterns on CEUS, which allow precise lesion type diagnosis for most FLLs. For example, homogeneous or heterogeneous hyperenhancement during the arterial phase and washout in late phase are clues for hepatocellular carcinoma (HCC), and peripheral rim-like hyperenhancement and subsequent washout (or even a "black hole" sign) often indicates metastatic liver cancer. The typical findings of hemangioma in CEUS are peripheral nodular hyperenhancement, centripetal fill in, and sustained enhancement in late phase. The sensitivity and specificity are as high as 96% and 98%, respectively in diagnosing hemangioma. The findings

of focal nodular hyperplasia, the second most common FLL, in CEUS are rapid arterial hyperenhancement with centrifugal radiating or "spoke-wheel" pattern, and sustained hyper- or iso-enhancement in late phase. These specific findings on CEUS greatly improved the ability to determine the nature of the lesions. This is especially clinically relevant in benign lesions or incidental lesions as more expensive examinations such as CT or MRI can be avoided[4-15].

CEUS has the potential to differentiate some FLLs such as HCC. It was suggested that well-differentiated HCC tends to show isoenhancement during portal or late phase and moderately- or poorly-differentiated HCC tends to show hypoenhancement. The former also washes out more quickly in enhancement extent in comparison with the latter on CEUS[16]. CEUS may also be used to evaluate the multi-step carcinogenesis of HCC by evaluating the change in intranodular hemodynamics, which is helpful in detecting premalignant lesions or HCC at an early stage[17]. When compared with CT or MRI, many studies have proven that CEUS is able to achieve the same or even higher characterization of FLLs [18]. This is reasonable when considering that CEUS can document the continuous change in intralesional hemodynamics and UCA is a real blood pool agent so that it is suitable for depicting the microcirculation that is essential for diagnosis.

Detection

Conventional US is less accurate in detecting and staging FLLs than CT, MRI, and intraoperative US. The main reasons for this are that conventional US has decreased ability to visualize small lesions (often less than 1 cm), isoechoic lesions (generally found in small lesions), lesions in coarse livers and lesions located in difficult anatomic areas (e.g. near the diaphragmatic dome).

Most malignant FLLs show hypoenhancement in portal or late phase, which facilitates the detection of small lesions since sufficient contrast between the lesion and the liver is achieved. As a result, many publications have proven that CEUS improves the detection of small lesions with conventional US, and some studies even suggest CEUS is superior to CT in the detection of small lesions[19,20]. When considering the balance between lesion size and location, the overall performance in detection for both CEUS and CT is comparable. The use of the newly launched UCA, Sonazoid further increases the ability of CEUS in FLL detection. Sonazoid allows vascular imaging and Kupffer imaging, and is extremely stable and tolerable for multiple scanning at least up to 60 min in the post-vascular phase, and may further improve the detection rate of HCC with CEUS[21]. CEUS with Sonazoid detected liver malignancy as defects on the sinusoidal phase with a high sensitivity of 95%, specificity of 93%, positive predictive value of 99%, and negative predictive value of 97%. The improved performance makes CEUS a suitable modality for surveillance in patients at high risk for HCC, patients with previous known malignancy, or patients in follow-up after treatment for cancer.

Guidance

Conventional US is the most widely used modality for guidance of tumor biopsy or ablation therapy. However, its role is limited when the target lesion is isoechoic or when the lesion shows infiltrative character and has no definite margin. In patients with liver cancer who have residual tumor after ablation therapy or transarterial chemoembolization (TACE), conventional US has low ability to detect viable tumor when a repeat ablation therapy is scheduled. Under such circumstances, CEUS can be applied for guidance. CEUS may detect more small foci which are invisible on conventional US or CT, thus is useful for patient selection before ablation therapy. CEUS can determine the tumor size and margin more accurately, which might be larger than that depicted by conventional US. Thus, it is helpful for treatment planning or even for excluding some patients not suitable for ablation. Under CEUS guidance, the residual tumor can be well delineated and targeted by recognizing the hyperenhancing area within or adjacent to the treatment zone during the arterial phase or hypoenhancing area during late phase[22].

Treatment response evaluation

Local treatment therapies, mainly TACE and ablation, have been accepted as curative options for early HCC. Recently, anti-angiogenesis methods have also been introduced into the clinic to treat advanced HCC. In these therapies, the tumor is not eradicated, but is devascularized or coagulated. Therefore, it is of paramount importance to evaluate the local treatment response and detect possible viable tumor. Previously, contrast-enhanced CT or MRI has been regarded as the gold standard for treatment response evaluation. Recently, a prospective multi-center study in China has proven that CEUS has the same ability to evaluate treatment response as CT or MRI, thus CEUS can be used as an alternative to CT or MRI for this purpose[23].

Liver CEUS improves depiction of intralesional vascularity and perfusion in FLLs, which always leads to a high contrast between the lesion and the surrounding tissue, especially when the lesion is hypervascular or hypovascular or when the lesion shows washout in late phase, thus it is suitable for three-dimensional US (3DUS). Three-dimensional CEUS (3D-CEUS) combines the advantages of 3DUS and CEUS[24]. Xu *et al*[25] investigated the potential usefulness of 3D-CEUS in evaluating the treatment response in liver cancer after local therapies. 3D-CEUS did not change the diagnosis in any patient compared with 2D-CEUS. However, 3D-CEUS changed the management in 2.8% of lesions, increased confidence but made no change in diagnosis in 79.5% of lesions, added some information but did not change management

or diagnosis in 14.0%, and made no change in 3.7%, respectively. The authors concluded that 3D-CEUS enhanced the diagnostic confidence in the majority of the patients and even changed the management in some patients. 3D-CEUS has potential usefulness in evaluating treatment response in liver cancer after local therapies.

The role of CEUS in evaluating tumor response to anti-angiogenic therapies has promising potential. Clinical trials have shown that CEUS can be used to assess the anticancer efficacy of anti-angiogenic treatment, for which conventional efficacy criteria based on tumor size measurement are unsuitable. Reduction in tumor vascularization can easily be detected in responders after 1-2 wk and is correlated with progression-free survival and overall survival. More sophisticated methods use quantitative approaches to measure the amount and the time course of bolus or reperfusion curves and have shown great promise in revealing effective tumor response to anti-angiogenic drugs in humans before tumor shrinkage occurs[26-28].

CEUS FOR NON-LIVER USE

The advent of CEUS not only enhances the use of US in the liver for tumor diagnosis, guidance and follow-up[29-31], but also provides solutions in many non-liver organs, including the gallbladder, bile duct, pancreas, and kidney.

Gallbladder

Conventional US is the first-line imaging investigation for the diagnosis of gallbladder diseases, but has difficulty in determining the nature of the gallbladder lesions in some cases, especially in differentiating chronic cholecystitis with thickened wall from gallbladder carcinoma with thickened wall or differentiating motionless sludge from gallbladder cancer. Xie *et al*[32] found that hyperenhancement or isoenhancement in the early phase and then fading out to hypoenhancement within 35 s after contrast agent administration was found in 90.9% of carcinomas and 17.0% of benign lesions. Destruction of the intactness of the gallbladder wall, that was, the internal or the outer wall of the gallbladder was discontinuous on CEUS, and was not found in benign diseases, but was present in 84.8% of carcinomas. They summarized that washout of contrast agent within 35 s after injection and destruction of gallbladder wall intactness on CEUS is highly suggestive of gallbladder malignancy. CEUS is particularly useful in differentiating gallbladder carcinomas and motionless biliary sludge or chronic cholecystitis with thickened gallbladder wall.

Bile duct

The use of CEUS has extended to the bile duct in recent years and promising results have been achieved. CEUS is especially useful in the diagnosis of malignancy of the bile duct, including intrahepatic, hilar, and extrahepatic bile ducts. Intrahepatic cholangiocarcinoma (ICC) is a malignant epithelial tumor that originates at the second branch (segmental branch) or the proximal branch of the intrahepatic bile ducts and is the second most common primary malignant tumor in the liver. Xu *et al*[33] summarized the CEUS findings of ICC, and Chen *et al*[34] compared the enhancement patterns of ICC between CEUS and contrast-enhanced CT. They found that during the arterial phases, four enhancement patterns were present on CEUS, which were: (1) peripheral irregular rim-like hyperenhancement (47.5%), (2) diffuse heterogeneous hyperenhancement (22.5%), (3) diffuse homogeneous hyperenhancement (12.5%), and (4) diffuse heterogeneous hypoenhancement (17.5%). When compared with CT, the enhancement patterns of ICC on CEUS were consistent with those on CECT in the arterial phase, whereas in the portal phase, ICC faded out more obviously on CEUS than on CECT. CEUS had the same accuracy as CECT in diagnosing ICCs, and so can be used as a new modality for the characterization of ICC. Although BUS has a low ability in differentiating ICC and HCC, Chen *et al*[35] found that CEUS greatly improved the diagnostic performance in this respect.

The primary investigation for suspected hilar bile duct cancer (i.e. Klatskin tumor) is a transabdominal US examination, which is highly sensitive for confirming biliary duct dilatation, localizing the site of obstruction and excluding gallstones. However, it has a limited role in determining the nature of the obstruction and defining the extent of tumor involvement since the lesion is always isoechoic to surrounding liver and the infiltrative nature of the lesion. Xu *et al*[36] compared the enhancement pattern of Klatskin tumor between CEUS and CECT. They found that the enhancement pattern of hilar cholangiocarcinoma on CEUS was similar to that on CECT in the arterial phase, whereas in the portal phase, hilar cholangiocarcinoma is more likely to show hypoenhancement on CEUS. CEUS and CECT lead to similar results in the evaluation of portal vein infiltration and the diagnosis of this entity. Therefore, CEUS has potential as a tool for the characterization of Klatskin tumors.

The use of CEUS in the extrahepatic bile duct has also been explored. Xu *et al*[37] reported a case of villous adenoma in the extrahepatic bile duct that was successfully diagnosed with CEUS. However, more data are needed on the use of CEUS in this aspect. Theoretically, CEUS may be valuable in distinguishing between tumor and debris or stone without obvious acoustic shadowing.

Pancreas

The study of the pancreas is a new and promising application of CEUS. CEUS can be used to improve delineation of pancreatic lesions compared with conventional US, and to characterize lesions already visible on US. Ductal adenocarcinoma is the most frequent malignancy

in the pancreas. At CEUS, adenocarcinomas are often hypovascularized as compared to the surrounding tissue. Focal pancreatitis has been reported to have similar enhancement extent and pattern with the surrounding pancreas. Contrast quantification software supplements a subjective visual assessment with objective criteria to facilitate the differential diagnosis of focal lesions in pancreatic cancer and chronic pancreatitis[38]. On the other hand, neuroendocrine tumors are hypervascularized lesions. Masses associated with pancreatitis have a different vascularization pattern depending on the degree of inflammation and necrosis. Cystadenomas frequently show many vessels along fibrotic strands. Pseudocysts, the most common cystic lesions of the pancreas, are non-vascularized[39,40]. In the recently launched guideline and good clinical practice recommendation for CEUS, CEUS of the pancreas has been recommended in the following indications: exact dimension depiction and margin depiction of pancreatic lesions and their relationship with adjacent vessels; characterization of focal pancreatic lesions (especially ductal adenocarcinoma, neuroendocrine tumor and focal pancreatitis); differential diagnosis between pseudo cysts and cystic pancreatic tumors; and differentiation of the vascular (solid) or avascular (liquid/necrotic) components of the lesion[4]. CEUS may also be useful in determining treatment efficacy and outcome after chemotherapy[41].

Kidney

Conventional US has been widely used in many centers as the first promising imaging modality for measuring the size of the kidney, confirming or ruling out focal lesions, depicting blood flow perfusion, evaluating the status of transplanted kidneys, and even detecting renal artery stenosis. However, the acoustic properties of conventional US are sometimes not enough to make a distinction between benign and malignant lesions or to evaluate blood flow perfusion. Therefore, significant attention has been paid to CEUS of the kidney[42]. Up to now there have been no reported side effects of contrast agent in the kidney; therefore CEUS is applicable in patients with impaired kidney function or ureteric obstruction which may be contraindications for contrast-enhanced CT or MRI.

CEUS is valuable in distinguishing pseudotumors due to developmental anomaly and neoplasm. The former shows isoenhancement during all phases in relation to the surrounding parenchyma, whereas the latter may show different enhancement patterns compared with normal tissue. The role of CEUS in the characterization of focal renal lesions is equivocal. Some authors think there are no reliable criteria to differentiate benign and malignant focal renal lesions, whereas other authors have the opposite opinion. Xu *et al*[43] believed that hyper- or iso-enhancement during the early phase, subsequent washout in late phase, inhomogeneous enhancement, and perilesional rim-like enhancement are clues for renal cell carcinomas (RCCs), which might be useful for the characterization of RCCs. Complex cysts of the kidney, which are characterized by a thickened or irregular wall, calcifications, septa or solid components, especially those classified as type 2F, 3 or 4 according to the Bosniak classification, are probably the best indication for renal CEUS. CEUS helps to depict blood flow perfusion within the wall, septa and solid components, thus is useful for the characterization of lesions in which CT or MRI studies are inconclusive or contraindicated[4].

CEUS is also valuable in evaluating complications after kidney transplantation. CEUS may help to diagnose vascular stenosis or thrombosis, focal infarction, shunts and hematomas with great confidence. CEUS is also useful in evaluating microvascular renal allograft perfusion[44].

Spleen

CEUS has been used for the characterization of focal splenic lesions. On CEUS, benign lesions appeared predominately non- or isoenhancing relative to splenic parenchyma. The combination of contrast enhancement in the early phase followed by rapid wash-out and demarcation of the lesion without contrast enhancement in the parenchymal phase (60 s after injection) was typical for malignant lesions[45]. For correct diagnosis of benignancy or malignancy, the overall accuracy was 43%-74% before CEUS *vs* 81%-92% after CEUS[46]. CEUS improves the characterization of focal splenic lesions with and without the availability of clinical data.

Breast

US has played a key role in the evaluation of breast lesions in clinical settings. Liu *et al*[47] evaluated the usefulness of CEUS using the microvascular imaging technique in the diagnosis of breast lesions. The authors found that non-enhancement was suggestive of benignity, with a sensitivity of 18.3%, specificity of 97.7%, positive predictive value of 91.7%, negative predictive value of 46.2%, and accuracy of 51.5%. The peripheral enhancement pattern was suggestive of malignancy, with a sensitivity of 39.5%, specificity of 98.3%, positive predictive value of 94.4%, negative predictive value of 69.4%, and accuracy of 73.8%. An accurate assessment of tumor size is necessary when selecting patients for breast-conserving surgery. Underestimation of tumor size may result in incomplete excisions, leading to re-excisions or higher local recurrence rates. Jiang *et al*[48] found that tumor size increase on CEUS compared with conventional US existed in some breast cancers and analyzed the correlation with pathology. However, it is difficult to predict whether the size of the breast cancer measured increases at CEUS based on the margin characteristics shown on conventional US.

Thyroid

The role of CEUS in the thyroid is controversial.

Carraro *et al*[49] calculated the percentage of intranodular contrast agent with the use of 3D-CEUS. They confirmed that malignant nodules had a higher internal vasculature (52.3% ± 15.7%) than benign nodules (14.3% ± 5.3%) and believed this methodology could be useful in improving nodule differentiation in thyroid US exams. On the other hand, Bartolotta *et al*[50] found there was no obvious difference between malignant and benign thyroid nodules and concluded that overlapping findings seem to limit the potential of this technique in the characterization of thyroid nodules.

Prostate

Prostate cancer has increased continuously in recent years. Tang *et al*[51] assessed the value of contrast-enhanced gray-scale transrectal US (CETRUS) in predicting the nature of peripheral zone hypoechoic lesions of the prostate. They found that malignant hypoechoic nodules in the peripheral zone of the prostate are more likely to enhance early and more intensely on CETRUS. A non-enhanced hypoechoic peripheral zone lesion is more likely to be benign.

NOVEL APPLICATIONS

Blunt abdominal trauma

Since UCA can be used as a tracer of blood flow, CEUS is able to detect bleeding sites and hematomas in patients with abdominal trauma[52]. During 5 years of experience in using CEUS to identify traumatic abdominal lesions, the sensitivity, specificity and positive and negative predictive values of US were 70.2%, 59.2%, 74.7% and 53.7%, respectively, whereas those of CEUS were 96.4%, 98%, 98.8% and 94.1%, respectively. The technique is able to detect active bleeding and vascular lesions, avoids exposure to ionizing radiation and is useful for monitoring patients undergoing conservative treatment[53].

CEUS can also be used to guide percutaneous injection therapy and therefore achieve the goal of using interventional ultrasonography in managing splenic trauma. In a study by Tang *et al*[54], six patients with grade 3 or 4 splenic injuries as determined by CEUS and CECT were given hemocoagulase atrox and absorbable cyanoacrylate percutaneously, which were injected into the injured region and active bleeding site, respectively, under CEUS guidance. Among the 6 patients, 4 cases of CEUS-guided hemostatic injection were successful without complications. Re-hemorrhage occurred in 1 patient, and a traumatic arteriovenous fistula occurred in the other patient; repeated injection therapy in these 2 patients was effective. During the follow-up, there were no complications, and spleen perfusion recovered gradually.

Crohn's disease

CEUS provides a new method to assess the activity of Crohn's disease[55]. Mural contrast enhancement shown on CEUS in patients with active disease at endoscopy was markedly increased in comparison with enhancement in patients with inactive disease. Multivariate logistic regression analysis revealed that an increase in wall brightness was a significant and independent variable predictive of severity grade at endoscopy. Quantitative measurements of bowel enhancement obtained by using CEUS correlate with severity grade determined at endoscopy. Thus CEUS could be a useful technique to monitor the activity of Crohn's disease[56].

Detecting suspected endoleaks after endovascular abdominal aneurysm repair

CEUS is able to depict endoleaks accurately after endovascular abdominal aneurysm repair and stent-graft procedure in dissected and ulcerated aorta. It seems to be superior in characterizing the type of endoleak and can be established in order to reduce iodized contrast agent and radiation exposure in follow-up. In a series of 30 patients, 21 endoleaks were identified by CT angiography (CTA) and 22 by CEUS. Thus, the sensitivity of CEUS was 99% and its specificity was 85%[57]. In contrast to CTA, CEUS can be offered to patients with chronic renal insufficiency and allows a dynamic examination and a perfusion analysis.

Contrast-enhanced intraoperative US (CE-IOUS)

The clinical value of CE-IOUS as a novel tool in the hepatic staging of patients undergoing liver resection has been assessed. In a series of 60 patients scheduled to undergo liver resection for metastatic disease, 3 patients were excluded due to disseminated disease on exploration by CE-IOUS. CE-IOUS was more sensitive than CT/MR and IOUS in detecting liver metastases (96.1% *vs* 76.7% and 81.5%, respectively); it altered surgical management in 29.8% of cases due to additional metastases, fewer metastases, benign lesions wrongly diagnosed as metastasis on IOUS/CT, or vascular proximity. CE-IOUS altered combined IOUS/CT/MR staging in 35.1% of cases. These preliminary results suggest that CE-IOUS is an essential tool prior to liver resection for metastases[58].

CE-IOUS was also used in neurosurgery. Malignant brain tumors might not be completely removed in surgery because there is no definite border between the tumor and normal brain tissue. He *et al*[59] investigated the feasibility and value of CE-IOUS in neurosurgery. Their results showed that the tumor border was more distinguishable from normal brain tissue on CEUS than on conventional US. In addition, intraoperative CEUS could improve the definition of residual tumor during surgery.

Gynecological use

Zhou *et al*[60] used CEUS to evaluate response to high intensity focused ultrasound ablation of uterine fibroids,

using CEMRI as the standard of reference. The diagnostic accuracy of CEUS was 100%.

Intracavitary use of CEUS

Besides intravascular use, CEUS is increasingly used for intracavitary purposes. CEUS is used for the diagnosis of vesicoureteric reflux after intravesical instillation. It is especially suitable for children since it can reduce possible ionizing radiation in association with voiding cystourethrography[61]. CEUS is also used to evaluate tubal patency in patients with primary or secondary infertility[62].

In percutaneous drainage procedures, CEUS allows visualization of the location of the drainage duct following intraductal injection. Thus CEUS can be used to determine whether the drainage duct position is appropriate or not, obstructed or not, and can even depict the shape of the biliary tree in percutaneous transhepatic cholangial drainage[63]. CEUS is also useful in the diagnosis of biliary leakage following T-tube removal[64].

POTENTIAL USE

Sentinel lymph node (SLN) detection

Lymphosonography, or CEUS-guided SLN detection, as a technique for demonstrating lymphatic drainage, has been introduced in some experimental studies. In this procedure, transcutaneous injection of an UCA is performed and CEUS is used to identify draining lymphatic channels and SLNs. This use of CEUS is technically feasible, as was demonstrated by various studies[65,66].

Drug or gene delivery

The microbubble contrast agent interacts with the acoustic wave in the acoustic field. The contrast agent itself will serve as a cavitation nucleus and lower the threshold level for cavitation[67,68]. In an experimental study, Nie *et al*[69] found that compared with the group treated by US alone, KDR-tk gene therapy treated by US combined with SonoVue inhibited tumor growth and increased survival time of Hepa1-6 tumor-bearing mice. It was concluded that gene therapy mediated by US exposure enhanced by a microbubble contrast agent may become a new treatment option for HCC. Based on the same principle, UCA was used for drug delivery or in the treatment of acute intravascular thrombi[70,71].

Molecular imaging

Techniques for noninvasive imaging of specific disease-related molecular changes are being developed to enhance diagnosis and therapeutic decision-making. Molecular imaging with CEUS relies on the detection of the acoustic signal produced by microbubble or nanoparticle agents that are targeted to the sites of disease. The potential use of CEUS-based molecular imaging in atherosclerosis, post-ischemic inflammation, angiogenesis, transplant rejection and thrombus formation have been investigated, and is undoubtedly an important development trend[72-76].

CONCLUSION

The role of CEUS in liver imaging is accepted in many clinical settings, such as in the characterization of FLLs, detection of FLLs, treatment response evaluation after local therapy, guidance in interventional procedures for invisible or suboptimal lesions on BUS. Most gallbladder diseases can be correctly diagnosed by conventional US, whereas CEUS is useful in differentiating gallbladder carcinomas and motionless biliary sludge or chronic cholecystitis with thickened gallbladder wall. CEUS also can be used to differentiate between ICC and HCC, and is useful in demarcating Klatskin's tumor. CEUS is useful in the characterization of focal pancreatic lesions, differential diagnosis between pseudo cysts and cystic pancreatic tumors, and differentiation of the vascular (solid) or avascular (liquid/necrotic) components of the lesion. CEUS may also be useful in determining treatment efficacy and outcome after chemotherapy for pancreatic cancer. CEUS is helpful in the characterization of complex cystic lesions and suspected cystic renal carcinoma, and can be used for the evaluation of anatomical variations mimicking renal tumor. CEUS is particularly useful for patients with contraindications for the use of CT or MR contrast agents.

The role of CEUS in other organs such as spleen, breast, and thyroid are still under investigation, and more evidence is needed to validate its usefulness. The novel applications such as use in blunt trauma, Crohn's disease, and gynecology also need further confirmation. The use of CEUS in molecular imaging and in gene therapy still requires further investigation.

In general, the advent of CEUS has greatly enhanced the usefulness of US and even changed the status of US in clinical practice. The application of CEUS in the clinic is continuously evolving and it is expected that its use will be expanded further in the future.

REFERENCES

1 **Correas JM**, Bridal L, Lesavre A, Méjean A, Claudon M, Hélénon O. Ultrasound contrast agents: properties, principles of action, tolerance, and artifacts. *Eur Radiol* 2001; **11**: 1316-1328

2 **Leen E.** The role of contrast-enhanced ultrasound in the characterisation of focal liver lesions. *Eur Radiol* 2001; **11** Suppl 3: E27-E34

3 **Brannigan M**, Burns PN, Wilson SR. Blood flow patterns in focal liver lesions at microbubble-enhanced US. *Radiographics* 2004; **24**: 921-935

4 **Claudon M**, Cosgrove D, Albrecht T, Bolondi L, Bosio M, Calliada F, Correas JM, Darge K, Dietrich C, D'Onofrio M, Evans DH, Filice C, Greiner L, Jäger K, Jong N, Leen E, Lencioni R, Lindsell D, Martegani A, Meairs S, Nolsøe C, Piscaglia F, Ricci P, Seidel G, Skjoldbye B, Solbiati L, Thorelius L, Tranquart F, Weskott HP, Whittingham T. Guidelines and good clinical practice recommendations for contrast enhanced ultrasound (CEUS) - update 2008.

Ultraschall Med 2008; **29**: 28-44
5 **Xu HX**, Liu GJ, Lu MD, Xie XY, Xu ZF, Zheng YL, Liang JY. Characterization of small focal liver lesions using real-time contrast-enhanced sonography: diagnostic performance analysis in 200 patients. *J Ultrasound Med* 2006; **25**: 349-361
6 **Quaia E**, Calliada F, Bertolotto M, Rossi S, Garioni L, Rosa L, Pozzi-Mucelli R. Characterization of focal liver lesions with contrast-specific US modes and a sulfur hexafluoride-filled microbubble contrast agent: diagnostic performance and confidence. *Radiology* 2004; **232**: 420-430
7 **Dai Y**, Chen MH, Yin SS, Yan K, Fan ZH, Wu W, Wang YB, Yang W. Focal liver lesions: can SonoVue-enhanced ultrasound be used to differentiate malignant from benign lesions? *Invest Radiol* 2007; **42**: 596-603
8 **Bartolotta TV**, Midiri M, Quaia E, Bertolotto M, Galia M, Cademartiri F, Lagalla R. Liver haemangiomas undetermined at grey-scale ultrasound: contrast-enhancement patterns with SonoVue and pulse-inversion US. *Eur Radiol* 2005; **15**: 685-693
9 **Bartolotta TV**, Midiri M, Quaia E, Bertolotto M, Galia M, Cademartiri F, Lagalla R, Cardinale AE. Benign focal liver lesions: spectrum of findings on SonoVue-enhanced pulse-inversion ultrasonography. *Eur Radiol* 2005; **15**: 1643-1649
10 **Strobel D**, Seitz K, Blank W, Schuler A, Dietrich C, von Herbay A, Friedrich-Rust M, Kunze G, Becker D, Will U, Kratzer W, Albert FW, Pachmann C, Dirks K, Strunk H, Greis C, Bernatik T. Contrast-enhanced ultrasound for the characterization of focal liver lesions--diagnostic accuracy in clinical practice (DEGUM multicenter trial). *Ultraschall Med* 2008; **29**: 499-505
11 **Dietrich CF**. Characterisation of focal liver lesions with contrast enhanced ultrasonography. *Eur J Radiol* 2004; **51** Suppl: S9-S17
12 **Wang Z**, Xu HX, Xie XY, Xie XH, Kuang M, Xu ZF, Liu GJ, Chen LD, Lin MX, Lu MD. Imaging features of hepatic angiomyolipomas on real-time contrast-enhanced ultrasound. *Br J Radiol* 2009; Epub ahead of print
13 **Lin MX**, Xu HX, Lu MD, Xie XY, Chen LD, Xu ZF, Liu GJ, Xie XH, Liang JY, Wang Z. Diagnostic performance of contrast-enhanced ultrasound for complex cystic focal liver lesions: blinded reader study. *Eur Radiol* 2009; **19**: 358-369
14 **Xu HX**, Xie XY, Lu MD, Liu GJ, Xu ZF, Liang JY, Chen LD. Unusual benign focal liver lesions: findings on real-time contrast-enhanced sonography. *J Ultrasound Med* 2008; **27**: 243-254
15 **Xu HX**, Liu GJ, Lu MD, Xie XY, Xu ZF, Zheng YL, Liang JY. Characterization of focal liver lesions using contrast-enhanced sonography with a low mechanical index mode and a sulfur hexafluoride-filled microbubble contrast agent. *J Clin Ultrasound* 2006; **34**: 261-272
16 **Liu GJ**, Xu HX, Lu MD, Xie XY, Xu ZF, Zheng YL, Liang JY. Correlation between enhancement pattern of hepatocellular carcinoma on real-time contrast-enhanced ultrasound and tumour cellular differentiation on histopathology. *Br J Radiol* 2007; **80**: 321-330
17 **Maruyama H**, Takahashi M, Ishibashi H, Okabe S, Yoshikawa M, Yokosuka O. Changes in tumor vascularity precede microbubble contrast accumulation deficit in the process of dedifferentiation of hepatocellular carcinoma. *Eur J Radiol* 2009; Epub ahead of print
18 **Liu GJ**, Xu HX, Lu MD, Xie XY, Xu ZF, Zheng YL, Liang JY. Enhancement pattern of hepatocellular carcinoma: comparison of real-time contrast-enhanced ultrasound and contrast-enhanced computed tomography. *Clin Imaging* 2006; **30**: 315-321
19 **Hohmann J**, Albrecht T, Hoffmann CW, Wolf KJ. Ultrasonographic detection of focal liver lesions: increased sensitivity and specificity with microbubble contrast agents. *Eur J Radiol* 2003; **46**: 147-159
20 **Solbiati L**, Tonolini M, Cova L, Goldberg SN. The role of contrast-enhanced ultrasound in the detection of focal liver leasions. *Eur Radiol* 2001; **11** Suppl 3: E15-E26
21 **Sugimoto K**, Shiraishi J, Moriyasu F, Saito K, Doi K. Improved detection of hepatic metastases with contrast-enhanced low mechanical-index pulse inversion ultrasonography during the liver-specific phase of sonazoid: observer performance study with JAFROC analysis. *Acad Radiol* 2009; **16**: 798-809
22 **Solbiati L**, Ierace T, Tonolini M, Cova L. Guidance and monitoring of radiofrequency liver tumor ablation with contrast-enhanced ultrasound. *Eur J Radiol* 2004; **51** Suppl: S19-S23
23 **Lu MD**, Yu XL, Li AH, Jiang TA, Chen MH, Zhao BZ, Zhou XD, Wang JR. Comparison of contrast enhanced ultrasound and contrast enhanced CT or MRI in monitoring percutaneous thermal ablation procedure in patients with hepatocellular carcinoma: a multi-center study in China. *Ultrasound Med Biol* 2007; **33**: 1736-1749
24 **Xu HX**, Lu MD, Xie XH, Xie XY, Xu ZF, Chen LD, Liu GJ, Liang JY, Lin MX, Wang Z, Huang B. Three-dimensional contrast-enhanced ultrasound of the liver: experience of 92 cases. *Ultrasonics* 2009; **49**: 377-385
25 **Xu HX**, Lu MD, Xie XH, Xie XY, Kuang M, Xu ZF, Liu GJ, Wang Z, Chen LD, Lin MX. Treatment response evaluation with three-dimensional contrast-enhanced ultrasound for liver cancer after local therapies. *Eur J Radiol* 2009; Epub ahead of print
26 **Lassau N**, Chami L, Benatsou B, Peronneau P, Roche A. Dynamic contrast-enhanced ultrasonography (DCE-US) with quantification of tumor perfusion: a new diagnostic tool to evaluate the early effects of antiangiogenic treatment. *Eur Radiol* 2007; **17** Suppl 6: F89-F98
27 **Cosgrove D**, Lassau N. [Assessment of tumour angiogenesis using contrast-enhanced ultrasound] *J Radiol* 2009; **90**: 156-164
28 **Lavisse S**, Lejeune P, Rouffiac V, Elie N, Bribes E, Demers B, Vrignaud P, Bissery MC, Brulé A, Koscielny S, Péronneau P, Lassau N. Early quantitative evaluation of a tumor vasculature disruptive agent AVE8062 using dynamic contrast-enhanced ultrasonography. *Invest Radiol* 2008; **43**: 100-111
29 **Lencioni R**, Della Pina C, Crocetti L, Bozzi E, Cioni D. Clinical management of focal liver lesions: the key role of real-time contrast-enhanced US. *Eur Radiol* 2007; **17** Suppl 6: F73-F79
30 **Lencioni R**, Piscaglia F, Bolondi L. Contrast-enhanced ultrasound in the diagnosis of hepatocellular carcinoma. *J Hepatol* 2008; **48**: 848-857
31 **Lencioni R**. Impact of European Federation of Societies for Ultrasound in Medicine and Biology (EFSUMB) guidelines on the use of contrast agents in liver ultrasound. *Eur Radiol* 2006; **16**: 1610-1613
32 **Xie XH**, Xu HX, Xie XY, Lu MD, Kuang M, Xu ZF, Liu GJ, Wang Z, Liang JY, Chen LD, Lin MX. Differential diagnosis between benign and malignant gallbladder diseases with real-time contrast-enhanced ultrasound. *Eur Radiol* 2009; Epub ahead of print
33 **Xu HX**, Lu MD, Liu GJ, Xie XY, Xu ZF, Zheng YL, Liang JY. Imaging of peripheral cholangiocarcinoma with low-mechanical index contrast-enhanced sonography and SonoVue: initial experience. *J Ultrasound Med* 2006; **25**: 23-33
34 **Chen LD**, Xu HX, Xie XY, Lu MD, Xu ZF, Liu GJ, Liang JY, Lin MX. Enhancement patterns of intrahepatic cholangiocarcinoma: comparison between contrast-enhanced ultrasound and contrast-enhanced CT. *Br J Radiol* 2008; **81**: 881-889
35 **Chen LD**, Xu HX, Xie XY, Xie XH, Xu ZF, Liu GJ, Wang Z, Lin MX, Lu MD. Intrahepatic cholangiocarcinoma and hepatocellular carcinoma: differential diagnosis with

contrast-enhanced ultrasound. *Eur Radiol* 2009; Epub ahead of print
36 **Xu HX**, Chen LD, Xie XY, Xie XH, Xu ZF, Liu GJ, Lin MX, Wang Z, Lu MD. Enhancement pattern of hilar cholangiocarcinoma: Contrast-enhanced ultrasound versus contrast-enhanced computed tomography. *Eur J Radiol* 2009; Epub ahead of print
37 **Xu HX**, Chen LD. Villous adenoma of extrahepatic bile duct: contrast-enhanced sonography findings. *J Clin Ultrasound* 2008; **36**: 39-41
38 **Kersting S**, Konopke R, Kersting F, Volk A, Distler M, Bergert H, Saeger HD, Grützmann R, Bunk A. Quantitative perfusion analysis of transabdominal contrast-enhanced ultrasonography of pancreatic masses and carcinomas. *Gastroenterology* 2009; **137**: 1903-1911
39 **Badea R**, Seicean A, Diaconu B, Stan-Iuga R, Sparchez Z, Tantau M, Socaciu M. Contrast-enhanced ultrasound of the pancreas--a method beyond its potential or a new diagnostic standard? *J Gastrointestin Liver Dis* 2009; **18**: 237-242
40 **Xie XY**, Xu EJ, Xu HX, Xu ZF, Liu GJ, Zheng YL, Liang JY, Huang B, Lü MD. [Role of contrast-enhanced ultrasound in the differentiation of solid focal lesions of pancreas] *Zhongguo Yixue Kexueyuan Xuebao* 2008; **30**: 35-39
41 **Sofuni A**, Itoi T, Itokawa F, Tsuchiya T, Kurihara T, Ishii K, Tsuji S, Ikeuchi N, Moriyasu F. Usefulness of contrast-enhanced ultrasonography in determining treatment efficacy and outcome after pancreatic cancer chemotherapy. *World J Gastroenterol* 2008; **14**: 7183-7191
42 **Kalantarinia K**, Belcik JT, Patrie JT, Wei K. Real-time measurement of renal blood flow in healthy subjects using contrast-enhanced ultrasound. *Am J Physiol Renal Physiol* 2009; **297**: F1129-F1134
43 **Xu ZF**, Xu HX, Xie XY, Liu GJ, Zheng YL, Liang JY, Lu MD. Renal cell carcinoma: real-time contrast-enhanced ultrasound findings. *Abdom Imaging* 2009; Epub ahead of print
44 **Kihm LP**, Hinkel UP, Michael K, Sommerer C, Seckinger J, Morath C, Zeier M, Schwenger V. Contrast enhanced sonography shows superior microvascular renal allograft perfusion in patients switched from cyclosporine A to everolimus. *Transplantation* 2009; **88**: 261-265
45 **von Herbay A**, Barreiros AP, Ignee A, Westendorff J, Gregor M, Galle PR, Dietrich C. Contrast-enhanced ultrasonography with SonoVue: differentiation between benign and malignant lesions of the spleen. *J Ultrasound Med* 2009; **28**: 421-434
46 **Stang A**, Keles H, Hentschke S, von Seydewitz CU, Dahlke J, Malzfeldt E, Braumann D. Differentiation of benign from malignant focal splenic lesions using sulfur hexafluoride-filled microbubble contrast-enhanced pulse-inversion sonography. *AJR Am J Roentgenol* 2009; **193**: 709-721
47 **Liu H**, Jiang YX, Liu JB, Zhu QL, Sun Q. Evaluation of breast lesions with contrast-enhanced ultrasound using the microvascular imaging technique: initial observations. *Breast* 2008; **17**: 532-539
48 **Jiang YX**, Liu H, Liu JB, Zhu QL, Sun Q, Chang XY. Breast tumor size assessment: comparison of conventional ultrasound and contrast-enhanced ultrasound. *Ultrasound Med Biol* 2007; **33**: 1873-1881
49 **Carraro R**, Molinari F, Deandrea M, Garberoglio R, Suri JS. Characterization of thyroid nodules by 3-D contrast-enhanced ultrasound imaging. *Conf Proc IEEE Eng Med Biol Soc* 2008; **2008**: 2229-2232
50 **Bartolotta TV**, Midiri M, Galia M, Runza G, Attard M, Savoia G, Lagalla R, Cardinale AE. Qualitative and quantitative evaluation of solitary thyroid nodules with contrast-enhanced ultrasound: initial results. *Eur Radiol* 2006; **16**: 2234-2241
51 **Tang J**, Yang JC, Luo Y, Li J, Li Y, Shi H. Enhancement characteristics of benign and malignant focal peripheral nodules in the peripheral zone of the prostate gland studied using contrast-enhanced transrectal ultrasound. *Clin Radiol* 2008; **63**: 1086-1091
52 **Valentino M**, Ansaloni L, Catena F, Pavlica P, Pinna AD, Barozzi L. Contrast-enhanced ultrasonography in blunt abdominal trauma: considerations after 5 years of experience. *Radiol Med* 2009; Epub ahead of print
53 **Valentino M**, Serra C, Pavlica P, Labate AM, Lima M, Baroncini S, Barozzi L. Blunt abdominal trauma: diagnostic performance of contrast-enhanced US in children--initial experience. *Radiology* 2008; **246**: 903-909
54 **Tang J**, Zhang H, Lv F, Li W, Luo Y, Wang Y, Li J. Percutaneous injection therapy for blunt splenic trauma guided by contrast-enhanced ultrasonography. *J Ultrasound Med* 2008; **27**: 925-932; quiz 933
55 **Migaleddu V**, Scanu AM, Quaia E, Rocca PC, Dore MP, Scanu D, Azzali L, Virgilio G. Contrast-enhanced ultrasonographic evaluation of inflammatory activity in Crohn's disease. *Gastroenterology* 2009; **137**: 43-52
56 **Ripollés T**, Martínez MJ, Paredes JM, Blanc E, Flors L, Delgado F. Crohn disease: correlation of findings at contrast-enhanced US with severity at endoscopy. *Radiology* 2009; **253**: 241-248
57 **Pfister K**, Rennert J, Uller W, Schnitzbauer AA, Stehr A, Jung W, Hofstetter P, Zorger N, Kasprzak PM, Jung EM. Contrast harmonic imaging ultrasound and perfusion imaging for surveillance after endovascular abdominal aneurysm repair regarding detection and characterization of suspected endoleaks. *Clin Hemorheol Microcirc* 2009; **43**: 119-128
58 **Leen E**, Ceccotti P, Moug SJ, Glen P, MacQuarrie J, Angerson WJ, Albrecht T, Hohmann J, Oldenburg A, Ritz JP, Horgan PG. Potential value of contrast-enhanced intraoperative ultrasonography during partial hepatectomy for metastases: an essential investigation before resection? *Ann Surg* 2006; **243**: 236-240
59 **He W**, Jiang XQ, Wang S, Zhang MZ, Zhao JZ, Liu HZ, Ma J, Xiang DY, Wang LS. Intraoperative contrast-enhanced ultrasound for brain tumors. *Clin Imaging* 2008; **32**: 419-424
60 **Zhou XD**, Ren XL, Zhang J, He GB, Zheng MJ, Tian X, Li L, Zhu T, Zhang M, Wang L, Luo W. Therapeutic response assessment of high intensity focused ultrasound therapy for uterine fibroid: utility of contrast-enhanced ultrasonography. *Eur J Radiol* 2007; **62**: 289-294
61 **Zimbaro G**, Ascenti G, Visalli C, Bottari A, Zimbaro F, Martino N, Mazziotti S. Contrast-enhanced ultrasonography (voiding urosonography) of vesicoureteral reflux: state of the art. *Radiol Med* 2007; **112**: 1211-1224
62 **Exacoustos C**, Zupi E, Szabolcs B, Amoroso C, Di Giovanni A, Romanini ME, Arduini D. Contrast-tuned imaging and second-generation contrast agent SonoVue: a new ultrasound approach to evaluation of tubal patency. *J Minim Invasive Gynecol* 2009; **16**: 437-444
63 **Ignee A**, Baum U, Schuessler G, Dietrich CF. Contrast-enhanced ultrasound-guided percutaneous cholangiography and cholangiodrainage (CEUS-PTCD). *Endoscopy* 2009; **41**: 725-726
64 **Mao R**, Xu EJ, Li K, Zheng RQ. Usefulness of contrast-enhanced ultrasound in the diagnosis of biliary leakage following T-tube removal. *J Clin Ultrasound* 2010; **38**: 38-40
65 **Curry JM**, Ezzat WH, Merton DA, Goldberg BB, Cognetti DM, Rosen D, Pribitkin EA. Thyroid lymphosonography: a novel method for evaluating lymphatic drainage. *Ann Otol Rhinol Laryngol* 2009; **118**: 645-650
66 **Wang Y**, Cheng Z, Li J, Tang J. Gray-scale contrast-enhanced utrasonography in detecting sentinel lymph nodes: An animal study. *Eur J Radiol* 2009; Epub ahead of print
67 **Wang Y**, Xu HX, Lu MD, Tang Q. Expression of thymidine kinase mediated by a novel non-viral delivery system under the control of vascular endothelial growth factor receptor 2

promoter selectively kills human umbilical vein endothelial cells. *World J Gastroenterol* 2008; **14**: 224-230
68 **Nie F**, Xu HX, Tang Q, Lu MD. Microbubble-enhanced ultrasound exposure improves gene transfer in vascular endothelial cells. *World J Gastroenterol* 2006; **12**: 7508-7513
69 **Nie F**, Xu HX, Lu MD, Wang Y, Tang Q. Anti-angiogenic gene therapy for hepatocellular carcinoma mediated by microbubble-enhanced ultrasound exposure: an in vivo experimental study. *J Drug Target* 2008; **16**: 389-395
70 **Wang Y**, Li X, Zhou Y, Huang P, Xu Y. Preparation of nanobubbles for ultrasound imaging and intracelluar drug delivery. *Int J Pharm* 2010; **384**: 148-153
71 **Xie F**, Lof J, Everbach C, He A, Bennett RM, Matsunaga T, Johanning J, Porter TR. Treatment of acute intravascular thrombi with diagnostic ultrasound and intravenous microbubbles. *JACC Cardiovasc Imaging* 2009; **2**: 511-518
72 **Lindner JR**. Molecular imaging of cardiovascular disease with contrast-enhanced ultrasonography. *Nat Rev Cardiol* 2009; **6**: 475-481
73 **Kaufmann BA**, Sanders JM, Davis C, Xie A, Aldred P, Sarembock IJ, Lindner JR. Molecular imaging of inflammation in atherosclerosis with targeted ultrasound detection of vascular cell adhesion molecule-1. *Circulation* 2007; **116**: 276-284
74 **Böhmer MR**, Klibanov AL, Tiemann K, Hall CS, Gruell H, Steinbach OC. Ultrasound triggered image-guided drug delivery. *Eur J Radiol* 2009; **70**: 242-253
75 **Leong-Poi H**, Kuliszewski MA, Lekas M, Sibbald M, Teichert-Kuliszewska K, Klibanov AL, Stewart DJ, Lindner JR. Therapeutic arteriogenesis by ultrasound-mediated VEGF165 plasmid gene delivery to chronically ischemic skeletal muscle. *Circ Res* 2007; **101**: 295-303
76 **Lankford M**, Behm CZ, Yeh J, Klibanov AL, Robinson P, Lindner JR. Effect of microbubble ligation to cells on ultrasound signal enhancement: implications for targeted imaging. *Invest Radiol* 2006; **41**: 721-728

S- Editor Cheng JX **L- Editor** Webster JR **E- Editor** Zheng XM

World Journal of Radiology

Online Submissions: http://www.wjgnet.com/1949-8470office
wjr@wjgnet.com
doi:10.4329/wjr.v1.i1.25

World J Radiol 2009 December 31; 1(1): 25-36
ISSN 1949-8470 (online)

TOPIC HIGHLIGHT

Hui-Xiong Xu, MD, PhD, *Series Editor*

Detection of focal liver lesions in cirrhotic liver using contrast-enhanced ultrasound

Grace Lai-Hung Wong, Hui-Xiong Xu, Xiao-Yan Xie

Grace Lai-Hung Wong, Institute of Digestive Disease, Department of Medicine and Therapeutics, The Chinese University of Hong Kong, Hong Kong, China
Grace Lai-Hung Wong, Hui-Xiong Xu, Xiao-Yan Xie, Department of Medical Ultrasonics, The First Affiliated Hospital, Institute of Diagnostic and Interventional Ultrasound, Sun Yat-Sen University, Guangzhou 510080, Guangdong Province, China
Author contributions: All authors participated in the preparation of the manuscript; Xu HX provided the ultrasonographic images used in the manuscript.
Supported by (in part) Grant No. NCET-06-0723 from Chinese Ministry of Education and grant 2008-2-10 of Public Welfare Research Special Project from Chinese Ministry of Health
Correspondence to: Hui-Xiong Xu, MD, PhD, Department of Medical Ultrasonics, The First Affiliated Hospital, Institute of Diagnostic and Interventional Ultrasound, Sun Yat-Sen University, Guangzhou 510080, Guangdong Province, China. xuhuixiong@hotmail.com
Telephone: +86-20-28823388 Fax: +86-20-87332908
Received: November 11, 2009 Revised: December 17, 2009
Accepted: December 21, 2009
Published online: December 31, 2009

Abstract

Patients with liver cirrhosis are at increased risk of hepatocellular carcinoma (HCC). Conventional or baseline ultrasound (BUS) is often used as the first-line tool for HCC surveillance or detection, but the accuracy of BUS in HCC detection or differentiation from other focal liver lesions (FLLs) is limited. Contrast-enhanced ultrasound (CEUS) represents a recent revolution in the field of ultrasonography and it has become increasingly important in the detection and evaluation of FLLs. In CEUS, HCC typically exhibits arterial hyper-enhancement and portal-venous washout represented by hypo-enhanced lesions in the portal venous and late phases. The detection rate of HCC was significantly higher with CEUS compared with BUS. Even regenerative or some dysplastic nodules may exhibit arterial hyper-enhancement as they are differentiated from HCC by its iso-enhancing pattern in portal and late phases. The contrast-enhancement patterns of other different types of benign and malignant FLLs, as well as their detection rates with CEUS, were also discussed.

Key words: Contrast-enhanced ultrasound; Cirrhosis; Focal liver lesions; Metastatic liver cancer; Hepatocellular carcinoma

Peer reviewers: Hadi Rokni Yazdi, MD, Central Radiology, Imam Khomeini Hospital, Keshavarz Blvd, Tehran, 1419733141, Iran; Roberto Miraglia, MD, Adjunct Associate Professor of Radiology, Department of Diagnostic and Interventional Radiology, Mediterranean Institute for Transplantation and Advanced Specialized Therapies (IsMeTT), University of Pittsburgh, Via Tricomi 1, Palermo, 90100, Italy

Wong GLH, Xu HX, Xie XY. Detection of focal liver lesions in cirrhotic liver using contrast-enhanced ultrasound. *World J Radiol* 2009; 1(1): 25-36 Available from: URL: http://www.wjgnet.com/1949-8470/full/v1/i1/25.htm DOI: http://dx.doi.org/10.4329/wjr.v1.i1.25

INTRODUCTION

Liver cirrhosis is a potentially life-threatening condition, as it may be complicated by hepatic decompensation and hepatocellular carcinoma (HCC)[1]. Therefore HCC surveillance has been recommended by expert associations to improve survival of patients by identifying tumors in earlier stages[2-4]. Conventional or baseline ultrasound (BUS) is often used as the first-line tool for HCC surveillance, as well as for the detection of HCC or other focal liver lesions (FLLs) because of its

efficiency, availability, non-invasiveness, and relatively low cost[5]. However, in view of the low ability of BUS to demonstrate tumor vascularity, it is sometimes difficult to differentiate benign FLLs (generally having a preferential portal venous blood supply) from malignant ones (generally having a preferential hepatic arterial supply) using BUS alone[6]. This is particularly relevant in the setting of liver cirrhosis, as in the presence of nodular liver parenchyma it can be difficult to differentiate HCC from regenerative, dysplastic nodules or other FLLs.

Contrast-enhanced ultrasound (CEUS) represents a recent breakthrough in the field of ultrasonography and it has becoming increasingly important in the evaluation of FLLs. CEUS involves the use of microbubble contrast agents and specialized imaging techniques such as harmonic and pulse inversion imaging to show sensitive blood flow and tissue perfusion information. The introduction of new generation microbubble contrast agents allows real-time imaging, which further improves the characterization and detection of FLLs[7]. CEUS significantly improved the diagnostic performance in small FLLs compared to BUS[8]. Several other studies also provided evidence that CEUS has sensitivity and specificity similar to computed tomography (CT) and magnetic resonance imaging (MRI) in terms of detection and characterization of FLLs[9-12]. In this article, the application of CEUS for the detection of different benign and malignant FLLs in liver cirrhosis will be described and discussed on the basis of our experience and latest literature data.

ULTRASOUND CONTRAST AGENTS (UCAs) AND CONTRAST-SPECIFIC TECHNIQUES

Microbubbles smaller than 8 μm in diameter have been proved to pass through capillary vessels, and an ultrasound pulse with a frequency of 2 MHz and a negative pressure of about 700 kPa has the ability to disrupt the microbubbles and generate echo signals[13]. Thus, contrast agents with transpulmonary stability, which are administered intravenously into peripheral veins, have become commercially available for use in sonographic enhancement studies. Levovist, Definity, SonoVue, and the latest Sonazoid, are the four UCAs most commonly studied in the liver (Table 1).

The first generation UCAs, such as Levovist, produce a very weak signal when submitted to a low mechanical index ultrasound beam owing to the fragility of the microbubbles containing air with galactose/palmitic acid surfactant[14]. One of the second-generation UCAs, SonoVue, is the most commonly used UCA in China and Europe. Bubbles of SonoVue contain sulfur hexafluoride with a phospholipid shell[15]. The microbubbles are isotonic to human plasma and stable and resistant to pressure. SonoVue improves the display of focal tumor vascularity and normal parenchymal liver vascularity[16]. Sonazoid is another second-generation UCA solely available in Japan. Sonazoid consists of perfluorobutane microbubbles with a median diameter of 2 to 3 μm[17]. A pharmacokinetic study of Sonazoid showed that blood concentrations of perfluorobutane declined biphasically with a distribution half-life of 2 to 3 min and an elimination half-life of 30 to 45 min[18]. The special feature of Sonazoid is the Kupffer imaging in the post-vascular phase, which is stable for at least 60 min post-injection and tolerable for multiple scanning and can be obtained with low acoustic power, because Sonazoid microbubbles are phagocytosed by Kupffer cells[19]. In general, UCAs are very safe with a low incidence of side effects. Serious adverse events in abdominal applications have been reported with a rate of 0.0086%[20]. The common adverse events include pruritus, nonspecific malaise, numbness of limb and dyspnea; while serious adverse events include hypotension and bronchospasm[20].

Table 1 Characteristics of common ultrasound contrast agents used in liver imaging

Agent	Manufacturer	Resonance range (MHz)	Chemical composition	MI level
Levovist®	Schering	2-3	Lipid Air (galactose-based)	High > 0.6
Definity®	BMS	1.5-4	Liposome Perfluorocarbon	Low < 0.4
SonoVue®	Bracco	1.8-3.2	Phospholipid Sulfur hexafluoride	Low < 0.4
Sonazoid®	GE healthcare	2-8	Lipid Perfluorocarbon	Low < 0.4

Contrast-specific techniques suppress linear ultrasound signals coming from tissues and use the nonlinear response of microbubbles to enhance signals from UCAs over the background. The advent of second-generation agents has been significant in improving the ease and the reproducibility of the examination, since low solubility gases offer improved stability and more favorable resonance behavior than air at low acoustic pressure[21]. Hence, contrast-specific imaging can be performed at a low mechanical index (usually less than 0.20), thus preventing microbubble disruption and enabling visualization of the dynamic enhancement pattern in real time over several minutes.

DIFFERENT VASCULAR PHASES OF LIVER IN CEUS

The hepatic artery supply usually starts 10 to 20 s post-injection into a peripheral vein and lasts for approximately 10-15 s. This is followed by the portal venous phase, which usually lasts 2 min after UCA injection. The late phase lasts until clearance of UCA from the liver parenchyma, up to approximately 4-6 min for SonoVue[22]. Another post-vascular or Kupffer phase, up to at least 60 min, is present for Sonazoid (Table 2)[19].

Table 2 Different phases of liver in contrast-enhanced ultrasound

Phase	Start[1]	End[1]
Arterial phase (s)	10-20	20-35
Portal venous phase (s)	30-45	120-180
Late phase (s)	120-180	240-360
Post-vascular or Kupffer phase	Approximately 10 min	At least 60 min

[1]The individual global hemodynamic situation will influence the time of onset of different phases.

Arterial phase

The UCA reaches the liver first *via* the hepatic artery and provides information on the degree and pattern of vascularity. Tumors with substantial arterial blood supply show hyper-enhancement during this phase. This phase is usually defined as the period from 0 to 30 s after UCA injection.

Portal vein phase

After the arterial phase, the UCA has passed through the circulation and spreads through the liver *via* the portal branches. This phase is usually defined as the period from 31 to 120 s after UCA injection.

Late or parenchymal phase

The late or parenchymal phase follows the portal phase, in which UCA is slowly distributed throughout the entire liver parenchyma. The origin of the late phase is the subject of ongoing scientific discussion, and suggested mechanisms include sinusoid pooling and reticulo-endothelial system or Kupffer cell uptake[23]. Both the portal and late phases provide information regarding the washout of contrast agent from the lesion compared with normal liver tissue. In the case of hemangiomas, a progressive filling can be observed during these phases. The portal and late phase enhancement can provide important information regarding the character of the lesions. Most malignant lesions are hypo-enhanced, while the majority of solid benign lesions are iso- or hyper-enhanced[24,25]. This phase is usually defined as the period from 121 to 360 s after UCA injection.

Post-vascular or Kupffer phase

This is an extra phase when Sonazoid is used. Kupffer imaging in the post-vascular phase is stable for at least 60 min post-injection and tolerable for multiple scanning. This can be obtained with low acoustic power, because Sonazoid microbubbles are phagocytosed by Kupffer cells[19].

DETECTION OF MALIGNANT FLLs IN CIRRHOTIC LIVER WITH CEUS

HCC

HCC is the most common primary malignancy of the liver. It usually occurs in patients with chronic liver diseases such as chronic hepatitis B and C, which are highly prevalent in the Asian-Pacific region, Japan and America, respectively. The risk of HCC is substantially increased to 10 times or even more in the presence of cirrhosis when compared to non-cirrhotic patients[1]. The annual detection incidence of HCC ranges from 2% to 5% when cirrhosis is established[26]. On a histopathologic basis, evolving malignant change in a cirrhotic nodular lesion shows that the arterial flow supply progressively increases to the lesion and the portal flow progressively decreases[27]. This progressive neo-angiogenesis provides the clue for clinical diagnosis with imaging techniques[28]. HCC typically exhibits arterial hyper-perfusion compared with the surrounding liver tissue at the time when in the surrounding liver parenchyma no contrast effect is as yet discernible (Figure 1)[29]. Uneven arterial hyper-enhancement of HCC may be noted, because the tumors may have septa, different cell differentiation and arterio-venous shunting patterns among the neo-formed vessels[30]. In the portal and late phase, HCC are usually hypo-enhanced, as the UCA will wash out from HCC to the liver parenchyma rapidly, and the tumor may appear hypo-enhanced with respect to the surrounding liver in the late phase[24,25,29]. As some regenerative nodules may also exhibit additional arterial enrichment, analysis of the portal venous phase makes the differentiation of these iso-enhanced nodules from hypo-enhanced HCC possible.

The detection rates of FLLs are dependent on the sizes of the lesions. While the detection rates are generally higher than 90% with CEUS[9,28]. A summary of CEUS findings of common FLLs was shown in Table 3. The characterization of a hepatic nodule smaller than 2 cm by imaging is more difficult. Detection of small HCCs in the cirrhotic liver is always a great challenge in cirrhotic liver, as multistage processes including regenerative nodules, dysplastic nodules and HCC may co-exist. In general, CEUS improved the sensitivity, negative predictive value, and overall accuracy of detection of HCC $\leqslant$ 2 cm from 29% to 80%, 60% to 91%, and 64% to 87%, respectively, when compared with BUS[31]. A recent investigation has shown that in the setting of cirrhotic patients undergoing HCC surveillance, the sole imaging finding of arterial hyper-vascularization in small solitary nodules of 2 cm or less has a specificity of 86% and a positive predictive value of 92% for the diagnosis of HCC[32]. Small HCCs in cirrhotic liver may be detected as areas of hyper-enhancement in the arterial phase. However, the short duration of the arterial phase does not allow scanning of the whole liver. Hence the portal and late phases may provide more information in the detection of small lesions in cirrhotic liver[24,25]. Evaluation of all three vascular phases has been shown to be superior to the evaluation of enhancement in the late phase alone: the sensitivity increased from 78% to 98%, and the accuracy from 81% to 93%[33]. In a study of 41 cirrhotic patients with small monofocal lesions smaller than 3 cm in diameter using contrast-enhanced Doppler ultrasound, the

Table 3 Summary of contrast-enhanced ultrasound findings of common focal liver lesions[72]

	Arterial	Portal	Late vascular phase	Parenchymal phase
Malignant focal liver lesions				
Hepatocellular carcinoma	Hyperechoic	Isoechoic	Hypo- or isoechoic (30%)	Hypoechoic
Metastases	Hypo- or hyperechoic (hypervascular)	Hypoechoic with or without rim enhancement	Hypoechoic	Hypoechoic
Cholangiocarcinoma	Hypo- or hyperechoic (15%)	Iso- or hypoechoic	Hypoechoic	Hypoechoic
Benign focal liver lesions				
Regenerating nodules	Iso- or hypoechoic	Isoechoic	Isoechoic	Isoechoic
Dysplastic nodules	Hyper, iso- or hypoechoic	Isoechoic	Hypo- or isoechoic	Hypo- or isoechoic
Hemangiomas	Hyperechoic (peripheral nodular enhancement)	Centripetal filling	Isoechoic if filling is complete (intralesional hypoechoic areas in 50%)	Isoechoic (intralesional hypo-echoic areas in 50%)
	Homogenous hyperechoic in 20% of small hemangiomas	Hyper- or isoechoic	Hyper- or isoechoic	Isoechoic
Focal nodular hyperplasia	Hyperechoic	Hyper- or isoechoic; non-enhancing central scar in 45%	Hyper- or isoechoic; non-enhancing central scar in 45%	Hyper- or isoechoic
Hepatocellular adenoma	Hyperechoic	Isoechoic	Isoechoic	Isoechoic
Fatty changes or focal fatty sparing	Isoechoic	Isoechoic	Isoechoic	Isoechoic
Noncomplicated cysts	Absence of enhancement	Absence of enhancement	Absence of enhancement	Absence of enhancement

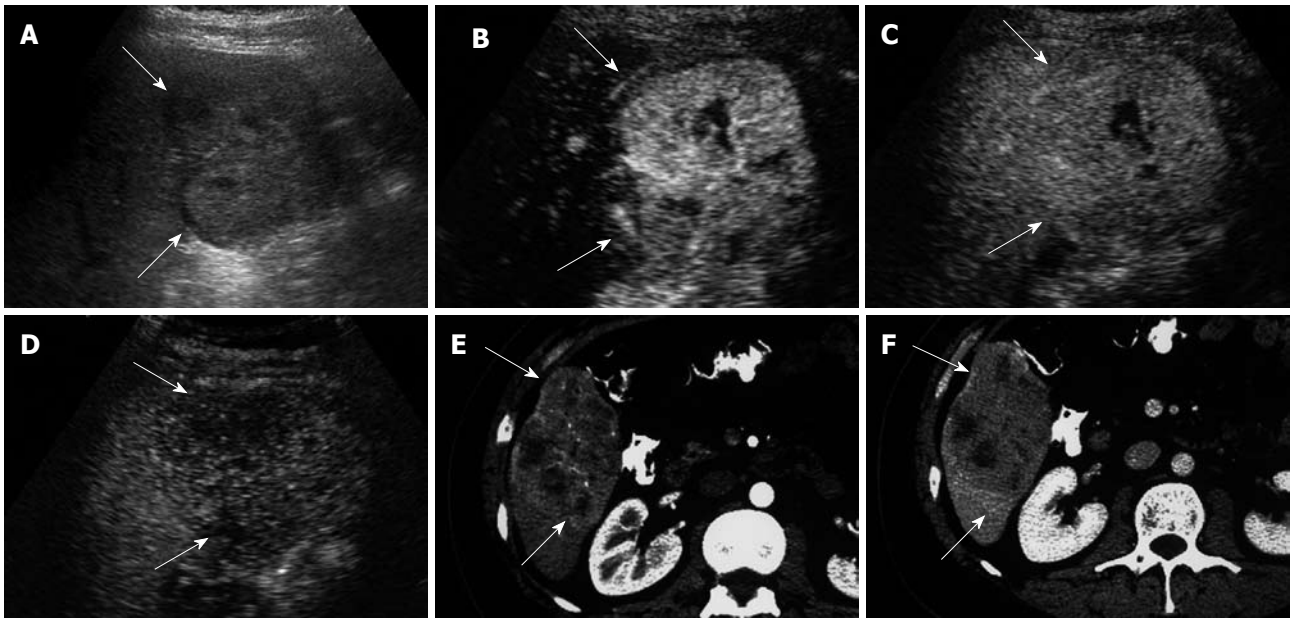

Figure 1 Hepatocellular carcinoma. A: Gray-scale sonogram shows an isoechogenic nodule (arrows); B: Contrast-enhanced ultrasound (CEUS) scan at arterial phase shows homogeneous hyper-enhancement (arrows); C: CEUS scan at portal phase shows iso-enhancement in comparison with adjacent-liver tissue (arrows); D: CEUS scan at late phase shows hypo-enhancement in comparison with adjacent-liver tissue (arrows); E: Computed tomography (CT) scan shows hyper-attenuation of the nodule (arrows) during the arterial phase; F: CT scan during the portal phase shows hypo-attenuation (arrows).

intra-tumoral arterial blood flow was detected in 95% of HCCs, compared with 28% of nonmalignant nodules[34]. All false-positive findings were noted either in high-grade dysplastic nodules or evolving HCCs[34]. CEUS was also found to improve the detection of HCC in patients with chronic hepatitis C related cirrhosis, and it was useful to rule out malignancy in many cases where BUS findings were indeterminate[35]. To increase the specificity of imaging diagnosis, it is mandatory to evaluate contrast washout during the portal venous and the late phases, as recently recommended by the EASL panel of experts on HCC and the AASLD practice guideline[36,37]. These latest guidelines from various panel experts also recommended that the diagnosis of nodules of sizes 1 to 2 cm must be confirmed by two different imaging techniques[36,37].

Despite these promising results and recommendations, detection of small lesions is still a great challenge. A small study involving 30 cirrhotic patients with 30 small FLLs (1 to 2 cm) showed that a combination of characteristics of arterial phase enhancement and absence of delayed phase enhancement in CEUS had a high specificity of 92%, with a relatively low sensitivity of 56%, for detecting

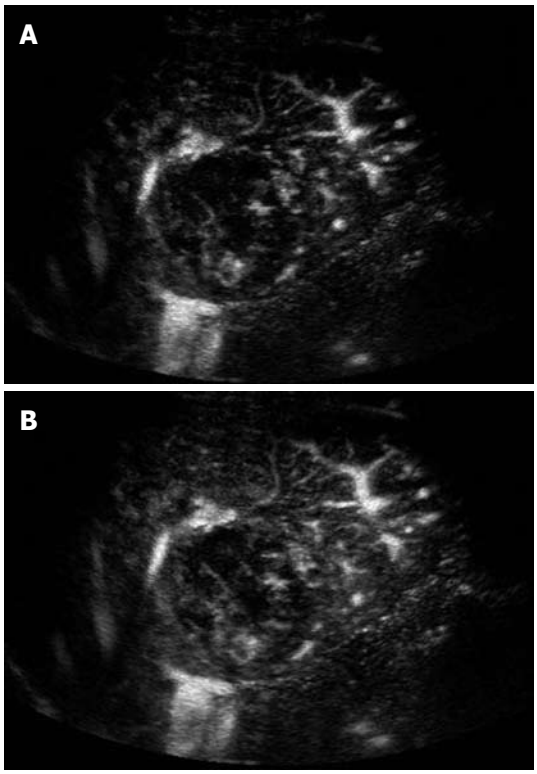

Figure 2 Micro flow imaging (MFI) technique depicts the intra-tumoral vascular architecture.

small HCC in cirrhosis patients[38]. Another recent study showed that the detection rate by coincident arterial hyper-vascularity at CEUS and CT was 44% in nodules of 1 to 2 cm, compared with 84% in larger nodules of sizes 2 to 3 cm in cirrhotic liver[39]. Relying on imaging techniques in nodules of 1 to 2 cm, the missed diagnosis of HCC was up to 38%[39]. This evidence showed that the diagnosis of nodules of 1 to 2 cm in cirrhotic patients is not satisfactory even with arterial hyper-vascularity shown by CEUS and CT. Late-phase pulse-inversion CEUS improved diagnostic sensitivity from 85% to 100% and specificity from 30% to 63% compared with BUS, and with lower inter-observer variability, for the discrimination of malignant versus benign liver lesions[40]. The new UCA Sonazoid provides Kupffer imaging, which is extremely stable and tolerable for multiple scanning at least up to 60 min in the post-vascular phase, and may further improve the detection rate of HCC with CEUS[41]. The analysis of Kupffer function provides essential information compared with other contrast agents[17,42]. CEUS with Sonazoid detects liver malignancy as defects on the sinusoidal phase with a high sensitivity of 95%, specificity of 93%, positive predictive value of 99%, and negative predictive value of 97%[43].

Tumor differentiation was found to be correlated with the pattern of enhancement in the portal and late phases[44]. The timing of HCC becoming hypo-enhanced on CEUS is correlated with tumor cell differentiation; well-differentiated tumors wash out more slowly than poorly differentiated ones[44,45]. The micro flow imaging technique was found to be effective in depicting the intra-tumoral vascular architecture which correlated with pathologic differentiation of HCC (Figure 2)[46]. A minority of HCCs may exhibit sustained hyper-enhancement in the late phase, especially for the small or well-differentiated ones (Figure 3)[30]. This makes the differentiation from other benign lesions such as focal nodular hyperplasia (FNH) or hemangioma impossible. In this scenario, other imaging modalities or biopsy of the nodule may be needed to confirm the diagnosis.

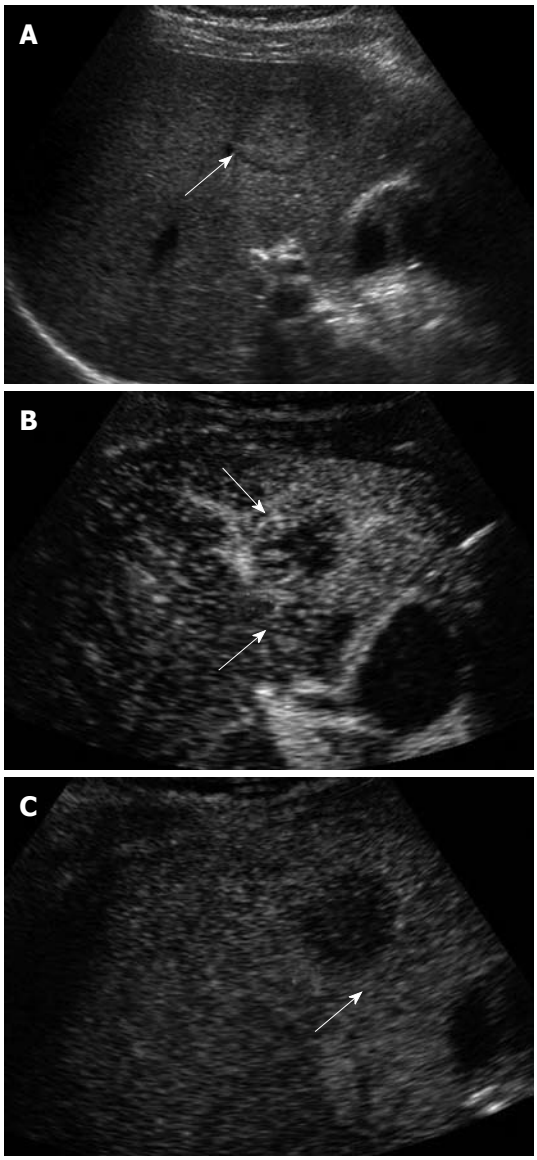

Figure 3 Liver metastasis. A: Gray-scale sonogram shows iso-echoic nodules (arrow); B: CEUS scan obtained in arterial phase shows rim-like enhancement (arrows); C: CEUS scan at late phase shows marked hypo-enhancement (arrow).

Metastatic liver cancer (MLC) and cholangiocarcinoma

Even though the incidence of MLC and cholangiocarcinoma is not increased in the presence of liver cirrhosis, detection of MLC may become more difficult in the presence of the nodular background of liver parenchyma. In the presence of liver cirrhosis, the detection rate of MLC

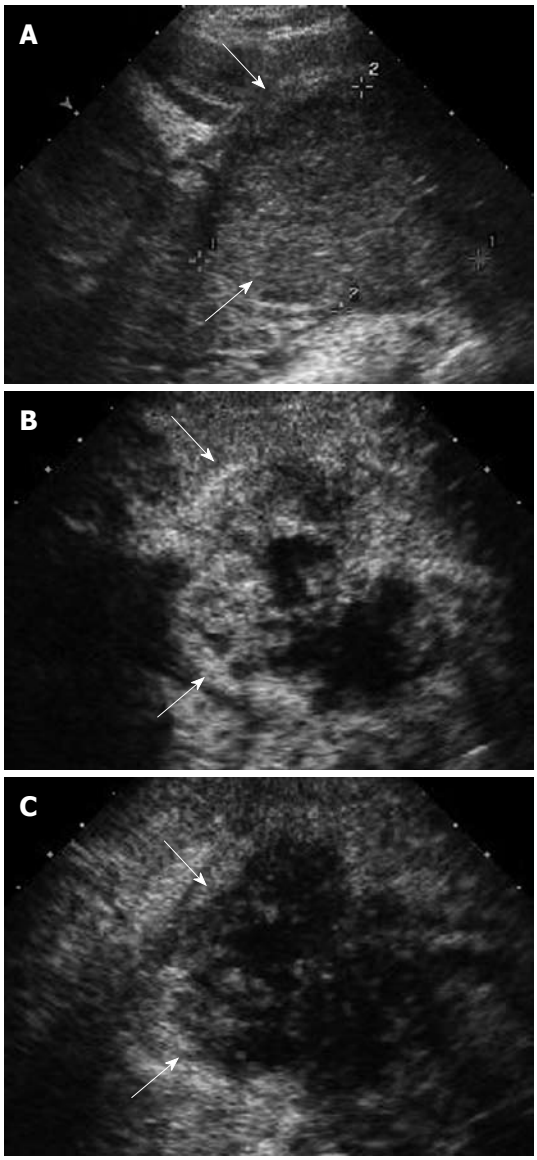

Figure 4 Intrahepatic cholangiocarcinoma. A: Gray-scale sonogram shows hypo-echoic nodule (arrows); B: At CEUS during the arterial phase the lesion shows markedly inhomogeneous enhancement (arrows); C: The lesion appears as hypo-enhancing mass in comparison with adjacent parenchyma in late phase (arrows).

was reported to be 33% in an autopsy series[47], while no data is available for cholangiocarcinoma as it is relatively uncommon. Detection of MLC has an important role in optimizing the therapeutic strategy, particularly in patients suffering from colorectal carcinoma[48,49]. Histologically, metastatic tumors have intratumoral hypo-vascularity and peripheral hyper-vascularity. BUS may miss iso-echoic lesions and lesions smaller than 1 cm[50]. Many studies have confirmed the improvement in accuracy of CEUS in diagnosing MLC[40,51,52]. CEUS also improved the detection of miliary metastases (0.5-1 cm) [53].

In the arterial phase, hypovascular metastases appear as hypo-enhanced lesions, with a typical rim enhancement of varying size ("halo sign", "rim sign"), whereas hypervascular metastases appear as hyper-enhanced and homogeneous lesions[28]. Rapid washout of arterial enhancement is found in the late arterial and portal phases[54]. Therefore, at the beginning of the portal phase, the arterial enhancement fades and the entire hypovascular lesion becomes hypo-echoic. In the late phase, both hypovascular and hypervascular metastases invariably appear dark compared with the enhanced background of normal liver parenchyma ("black-hole sign")[52]. During this late phase, both portal and late-phase imaging markedly increase the contrast between the enhanced normal liver (Figure 3). In the late portal phase very small metastases stand out better, because the artifacts are then less pronounced than directly after the injection of the signal enhancer. Thus, non-enhancing metastases improve detection, especially of small lesions smaller than 1 cm and lesions iso-echoic at BUS[55]. A high diagnostic accuracy in the differentiation between metastases and benign FLLs in the late phase has been reported[56]. A study showed that the addition of CEUS to BUS improved sensitivity for the detection of individual metastases from 71% to 87%. On a per-patient basis, sensitivity improved from 94% to 98% and specificity improved from 60% to 88%[57].

It is often difficult to use BUS alone to differentiate cholangiocarcinoma from other FLLs because its sonographic findings are non-specific. CEUS has much improved the detection rate of this tumor when compared to BUS, and it was found to have the same accuracy as contrast-enhanced CT in diagnosing intrahepatic cholangiocarcinoma (ICC)[58]. ICC usually appeared in inhomogeneous hyper-enhancement of different patterns in arterial phase: peripheral irregular rim-like hyper-enhancement; diffused heterogeneous hyper-enhancement; diffuse homogeneous hyper-enhancement and diffuse heterogeneous hypo-enhancement[58,59]. In the portal phase, most of the ICC was hypo-enhanced and appeared as punched-out defects (Figure 4)[58,59]. CEUS is also useful for differentiating ICC from HCC based on the enhancement pattern[60].

DETECTION OF BENIGN FLLs IN CIRRHOTIC LIVER WITH CEUS

Regenerative and dysplastic nodules

A stepwise carcinogenesis for HCC has been proposed from regenerative nodules, through low-grade dysplastic nodules and high-grade dysplastic nodules, to overt HCC[61]. Occasionally cancerous foci of very well differentiated HCC are encountered within dysplastic nodules, which are called nodule-in-nodule lesions or dysplastic nodules with a focus of HCC[62]. Differentiation between HCC and these nodules is always a major concern in cirrhotic liver, as the appearance in BUS may be similar but their prognosis is substantially different from each other: regenerative nodules are considered as benign lesions; dysplastic nodules are considered as precancerous lesions; while nodule-in-nodule lesions are considered malignant[62]. As definite differentiation among

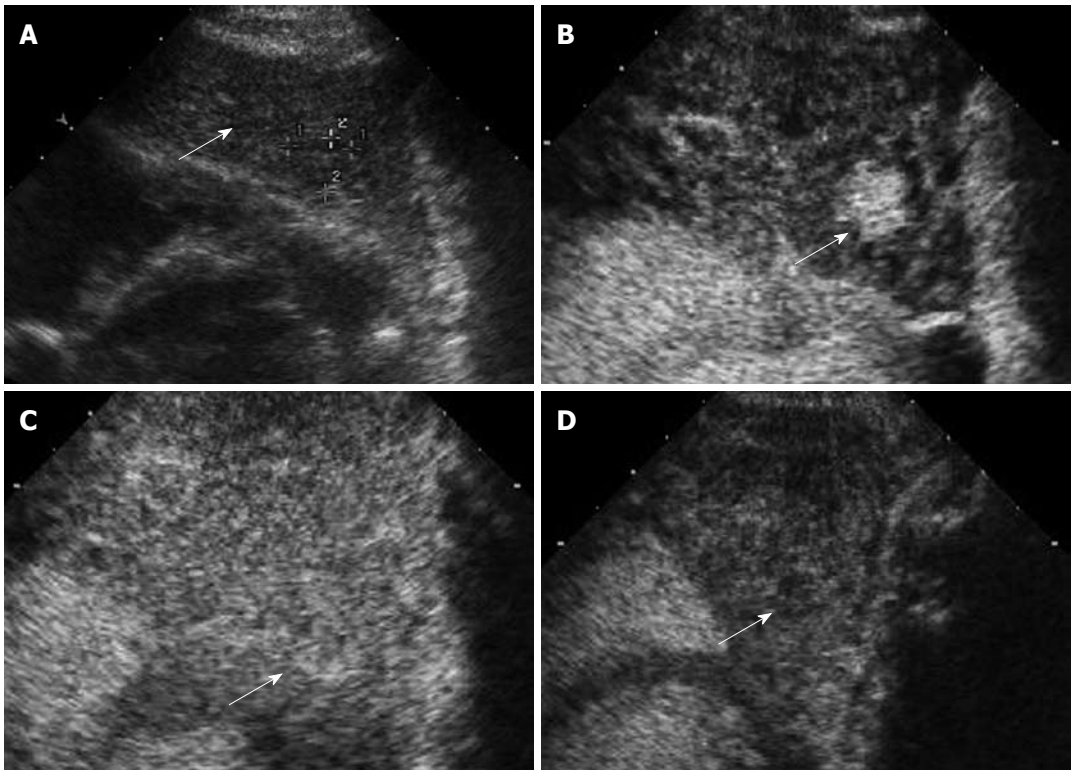

Figure 5 Biopsy-proven dysplastic nodule. A: A well-defined hypo-echoic lesion in the presence of liver cirrhosis (arrow); B: At CEUS during the arterial phase the lesion shows hyper-enhancement (arrow); C: The lesion appears iso-enhanced with respect to surrounding liver parenchyma in the portal phase(arrow); D: The lesion appears hypo-enhanced with respect to surrounding liver parenchyma in later part of the phase (arrow).

these nodules is almost impossible with BUS, CEUS plays an important role in differentiating these lesions because of its ability to demonstrate the vascularity of the lesions[63-65]. Regenerative nodules and dysplastic nodules are differentiated from HCC as the former lesions usually do not show enhancement in the arterial phase and are iso-enhanced similar to the surrounding liver parenchyma in the portal and late phases (Figure 5)[64,65]. Nonetheless, regenerative nodules and some dysplastic nodules may also exhibit additional arterial hyper-enhancement; by analysis of the portal venous and late phases it may be possible to differentiate these iso-enhancing nodules from hypo-enhancing HCC[64,65].

CEUS with Sonazoid is more sensitive for detecting arterial vascularity of target nodules than contrast-enhanced CT and MRI. CEUS with Sonazoid provides the additional post-vascular or Kupffer phase, such that it allows an assumption of the degree of malignancy based on Kupffer function. When uptake of contrast agent is reduced in the Kupffer phase of CEUS with Sonazoid in nodules not depicted as hypervascular lesions by CT or MRI, these lesions should basically be treated as malignant and a biopsy is not indispensable[62]. However, only a part of the liver can be evaluated in the short arterial phase of 20 to 30 s after administration of the contrast agent. As multiple nodules are often present in cirrhotic liver, this is a major limitation of CEUS. This may be overcome by using several doses of contrast agent to scan different segments of the liver. Another way is using CEUS in combination with CT, which was found to increase the accuracy of detecting intra-nodular arterial vascularity, compared to that by a single method[62].

Hemangiomas

Hemangiomas are the most frequent benign tumor found in the liver. Therefore it is also commonly found in cirrhotic liver, and the presence of hemangioma may be misdiagnosed as HCC. On the other hand, with progressive cirrhosis, hemangiomas are likely to decrease in size and become more fibrotic and difficult to diagnose radiologically[63]. The typical findings of hemangioma in CEUS are peripheral nodular contrast-enhancement and centripetal fill in (60% to 80%). However, atypical findings are found in 20% of hemangiomas if thrombosed areas and calcifications are present[66]. In small hemangiomas of diameter less than 2 cm, the arterial phase may show diffuse enhancement, which may occur in hypervascular malignant tumors such as HCC or metastases. Hemangiomas can be differentiated from those malignant lesions as they usually have hyper- or iso-enhancement with respect to the surrounding liver tissue in the portal and late phases, while malignant lesions become hypo-enhanced (Figure 6)[67]. CEUS can be used in the diagnosis of hemangioma, when centripetal fill-in enhancement is a positive finding in hemangioma, and the sensitivity and specificity are 96% and 98%, respectively[68].

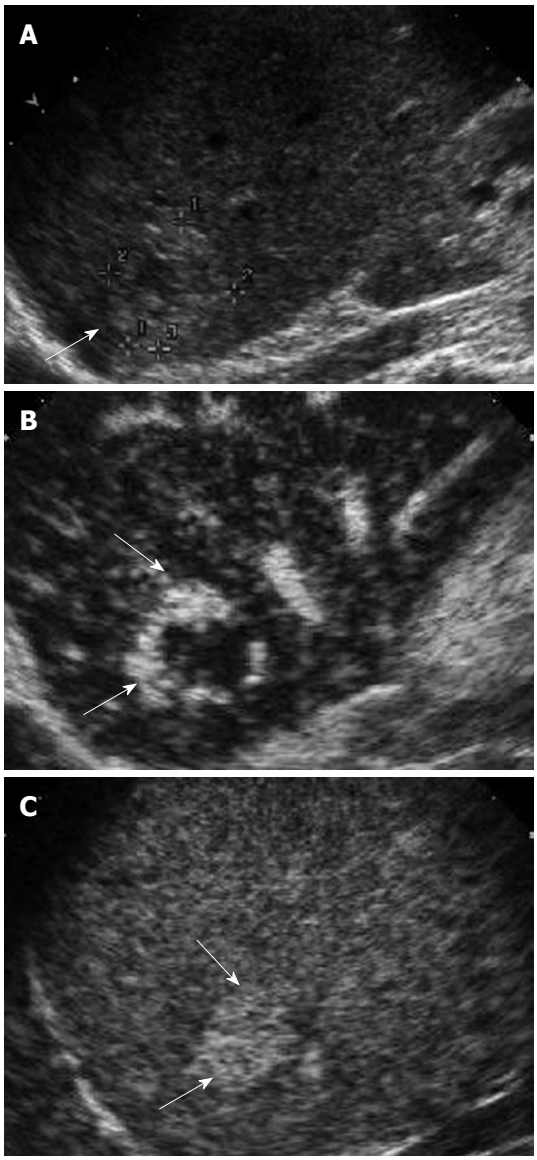

Figure 6 Hemangioma. A: Gray-scale sonogram shows a hyper-echoic nodule (arrow); B: CEUS scan obtained in arterial phase shows peripheral nodular hyper-enhancement (arrows); C: CEUS scan at late phase shows progressive centripetal enhancement and sustained and complete hyperenhancement (arrows).

FNH

FNH is the second most common benign, hyperplastic liver neoplasm composed of all the components of normal liver tissue, and about 45% of cases have a central stellate fibrous scar[69]. FNH was present in 3.4% of cirrhotic patients who received liver transplantation[70]. The findings of FNH in CEUS are rapid arterial hyper-enhancement with atypical centrifugal radiating or "spoke-wheel" pattern, then homogeneous hyper-enhancement in the late arterial phase[71,72]. The spoke-wheel pattern represents a central feeding artery and centrifugal blood supply from the center of the lesion to the periphery. FNH gradually changes to iso-enhanced in portal and late phases as FNH contains all the components of normal liver tissue, while some lesions even show as slightly hyper-enhanced with respect to the surrounding normal liver[40]. A central scar is another characteristic feature of FNH in CEUS due to the central stellate fibrosis scar. With the characteristic features in CEUS, the sensitivity and specificity of diagnosing FNH were 88% to 97% and 95%, respectively[71,73].

Hepatocellular adenoma

Hepatocellular adenoma is a relatively rare benign focal liver lesion, and is mainly found in young women with a history of oral contraceptive use, androgen steroid therapy and glycogen storage disease[74]. Histologically, hepatocellular adenoma is composed of cords of tumor cells, which closely resemble hepatocytes and contain fat and glycogen. In the arterial phase of CEUS, early and homogeneous hyperechoic enhancement is found in most cases. However, no enhancement will be seen if the tumor contains hemorrhage or necrosis[72]. In the portal and late phases, the enhancement of hepatocellular adenoma is almost the same as that of liver parenchyma and remains slightly hypo-enhanced in relation to the adjacent liver tissue in later stages because of varying numbers and activity of Kupffer cells[75]. Studies regarding the detection rate of CEUS in hepatocellular adenoma are not available.

Focal fatty change and focal fatty sparing of liver

Focal fatty change and focal spared areas are usually demonstrated adjacent to the right main portal vein, the gallbladder bed or the falciform ligament. However, a single well-demarcated nodule can be found anywhere in the liver. Because this type of lesion has normal liver components, CEUS shows the same enhancement pattern with respect to the normal liver in all phases and remains iso-enhanced[52]. In the arterial and venous phase the supplying and draining vessels can be imaged[76].

Cystic lesions

Liver cysts are a common ultrasonographic finding and readily diagnosed with BUS features of typical cyst appearance of echo free, round, well-defined borders with lateral shadowing and posterior echo enhancement. Blood vessels have to be excluded by color Doppler imaging ruling out arterio-porto-venous malformations with a cystic appearance. Simple liver cysts typically show no contrast enhancement at all the phases in CEUS[77]. CEUS is usually not necessary to diagnose simple liver cysts. Sometimes, it can play an useful role in the presence of complex, septated cysts to exclude a malignant cystic lesion (Figure 7)[78].

Other benign lesions

CEUS enables a better delineation of liver abscesses, which usually show a peripheral rim of contrast enhancement, surrounding an inner, generally necrotic, hypoechoic non-enhancing area, when compared to BUS. Septa may also enhance after contrast agent administration and show a honeycomb-like appearance (Figure 8)[79]. A recent study of CEUS in infective liver lesions showed that most liver abscesses were irregularly rim-enhanced with non-enhanced central necrotic areas; whereas infect-

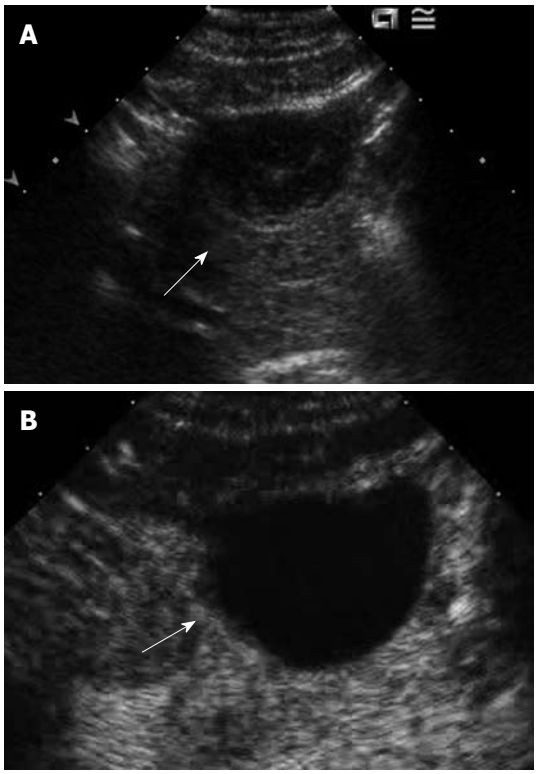

Figure 7 Complicated cyst. A: A slightly hypo-echoic lesion (arrow); B: CEUS at the portal phase of the lesion shows lack of contrast enhancement (arrow), as well as throughout the remaining vascular phases (not shown). Some internal non-enhancing debris within the cyst is still appreciable.

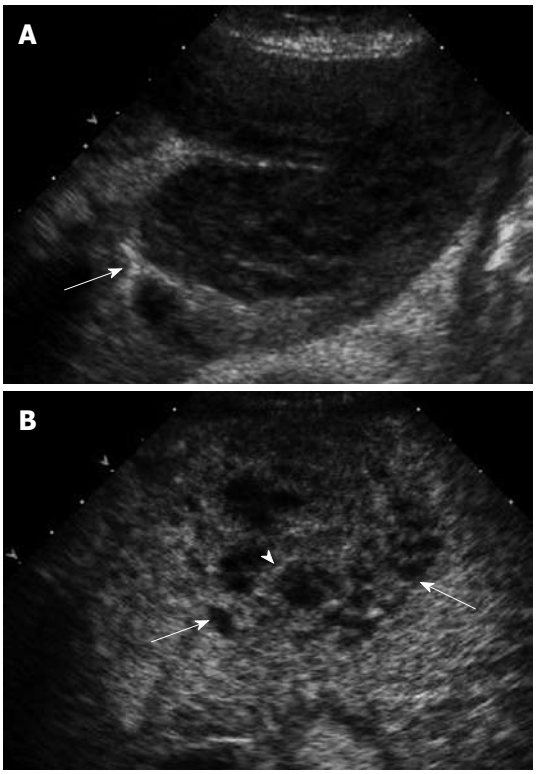

Figure 8 Hepatic abscess. A: An ill-defined lesion with mixed echotexture (arrow); B: The image obtained at CEUS in the portal phase better depicts the real margins of the lesion (arrows). A thin enhancing septum within the lesion is also demonstrated (arrowhead).

ed granulomas and inflammatory pseudotumors exhibit variable CEUS patterns[80]. Biopsy may be required in these lesions as most infected FLLs showed more rapid contrast wash-out than the surrounding liver parenchyma, which is similar to malignant lesions[80].

Some other unusual lesions including intrahepatic biliary cystadenoma, angiomyolipoma, lipoma, biliary epithelial dysplasia, a fungal inflammatory mass, tuberculoma, sarcoidosis, solitary necrotic nodules, peliosis hepatis, and focal fibrosis after surgery were demonstrated in CEUS. The benign nature of some of these lesions was shown as hyper-enhancement during the arterial phase and sustained enhancement during the portal or late phase in CEUS. But some benign lesions (e.g. intrahepatic biliary cystadenoma, sarcoidosis) may have various enhancing patterns during the arterial phase and even hypo-enhancement during the late phase[81].

Insufficiency of CEUS in detection of FLLs

Similar to BUS, CEUS is a dynamic examination that depends on the skill of the sonographers and/or sonologists, hence the accuracy is often operator-dependent[82]. Limited access to certain parts of the liver (e.g. near dome of diaphragm or far from the abdominal wall), especially in obese patients, remains a similar problem as in BUS. As a general rule, if BUS is suboptimal, results from CEUS may be disappointing[21]. Only a part of the liver can be evaluated in the short arterial phase after administration of the contrast agent. In the presence of multiple FLLs, which are particularly common in cirrhotic liver, this may be overcome by using several doses of contrast agent to scan different segments of the liver[83]. The value of scanning in the late phase after contrast administration in cirrhotic patients is limited: while the detection of an hypo-enhanced lesion in the late phase in a cirrhotic patient is very suggestive of HCC, iso-enhanced HCC is not easily detected. Furthermore, due to hemodynamic changes in cirrhotic patients with hyperdynamic circulation and shunting, the parenchymal enhancement in the late phase may appear heterogeneous and less intense than in normal livers, making evaluation difficult[83]. Another major limitation is the inability to evaluate the extrahepatic extension of HCC or other malignant diseases. All these insufficiencies may be overcome by combining CEUS with another dynamic test, such as contrast-enhanced CT or MRI[83].

CONCLUSION

CEUS can clearly demonstrate the vascular pattern and parenchymal contrast in FLLs, hence with CEUS the detection rates of different types of FLLs are much improved compared to BUS, and comparable to CT and MRI. CEUS also improves the diagnostic accuracy of FLLs, even for those as small as 1 to 2 cm. The significantly improved detection and diagnostic values of

CEUS is particularly relevant in the setting of liver cirrhosis because of the nodularity of the liver parenchyma and the coexistence of benign regenerative nodules and malignant HCC. This safe, convenient, low cost and non-invasive diagnostic modality should be promoted in routine clinical practice, especially in cirrhotic patients. Further research should explore the role of CEUS in different clinical applications, such as in the HCC surveillance program.

REFERENCES

1 **Chan HL**, Tse CH, Mo F, Koh J, Wong VW, Wong GL, Chan SL, Yeo W, Sung JJ, Mok TS. High Viral Load and Hepatitis B Virus Subgenotype Ce Are Associated With Increased Risk of Hepatocellular Carcinoma. *J Clin Onco* 2008; **26**: 177-182

2 **European Association For The Study Of The Liver**. EASL Clinical Practice Guidelines: management of chronic hepatitis B. *J Hepatol* 2009; **50**: 227-242

3 **Lok AS**, McMahon BJ. Chronic hepatitis B. *Hepatology* 2007; **45**: 507-539

4 **Wong GL**, Wong VW, Tan GM, Ip KI, Lai WK, Li YW, Mak MS, Lai PB, Sung JJ, Chan HL. Surveillance programme for hepatocellular carcinoma improves the survival of patients with chronic viral hepatitis. *Liver Int* 2008; **28**: 79-87

5 **Ariff B**, Lloyd CR, Khan S, Shariff M, Thillainayagam AV, Bansi DS, Khan SA, Taylor-Robinson SD, Lim AK. Imaging of liver cancer. *World J Gastroenterol* 2009; **15**: 1289-1300

6 **Libbrecht L**, Bielen D, Verslype C, Vanbeckevoort D, Pirenne J, Nevens F, Desmet V, Roskams T. Focal lesions in cirrhotic explant livers: pathological evaluation and accuracy of pretransplantation imaging examinations. *Liver Transpl* 2002; **8**: 749-761

7 **Morin SH**, Lim AK, Cobbold JF, Taylor-Robinson SD. Use of second generation contrast-enhanced ultrasound in the assessment of focal liver lesions. *World J Gastroenterol* 2007; **13**: 5963-5670

8 **Xu HX**, Liu GJ, Lu MD, Xie XY, Xu ZF, Zheng YL, Liang JY. Characterization of small focal liver lesions using real-time contrast-enhanced sonography: diagnostic performance analysis in 200 patients. *J Ultrasound Med* 2006; **25**: 349-361

9 **Quaia E**, Calliada F, Bertolotto M, Rossi S, Garioni L, Rosa L, Pozzi-Mucelli R. Characterization of focal liver lesions with contrast-specific US modes and a sulfur hexafluoride-filled microbubble contrast agent: diagnostic performance and confidence. *Radiology* 2004; **232**: 420-430

10 **Catala V**, Nicolau C, Vilana R, Pages M, Bianchi L, Sanchez M, Bru C. Characterization of focal liver lesions: comparative study of contrast-enhanced ultrasound versus spiral computed tomography. *Eur Radiol* 2007; **17**: 1066-1073

11 **Li R**, Guo Y, Hua X, He Y, Ding J, Guo A, Luo M. Characterization of focal liver lesions: comparison of pulse-inversion harmonic contrast-enhanced sonography with contrast-enhanced CT. *J Clin Ultrasound* 2007; **35**: 109-117

12 **Larsen LP**, Rosenkilde M, Christensen H, Bang N, Bolvig L, Christiansen T, Laurberg S. The value of contrast enhanced ultrasonography in detection of liver metastases from colorectal cancer: a prospective double-blinded study. *Eur J Radiol* 2007; **62**: 302-327

13 **Holland CK**, Apfel RE. An improved theory for the prediction of microcavitation thresholds. *IEEE Trans Ultrason Ferroelectr Freq Control* 1989; **36**: 204-208

14 **Youk JH**, Kim CS, Lee JM. Contrast-enhanced agent detection imaging: value in the characterization of focal hepatic lesions. *J Ultrasound Med* 2003; **22**: 897-910

15 **Schneider M**, Arditi M, Barrau MB, Brochot J, Broillet A, Ventrone R, Yan F. BR1: a new ultrasonographic contrast agent based on sulfur hexafluoride-filled microbubbles. *Invest Radiol* 1995; **30**: 451-457

16 **Leen E**, Angerson WJ, Yarmenitis S, Bongartz G, Blomley M, Del Maschio A, Summaria V, Maresca G, Pezzoli C, Llull JB. Multi-centre clinical study evaluating the efficacy of SonoVue (BR1), a new ultrasound contrast agent in Doppler investigation of focal hepatic lesions. *Eur J Radiol* 2002; **41**: 200-206

17 **Hatanaka K**, Kudo M, Minami Y, Ueda T, Tatsumi C, Kitai S, Takahashi S, Inoue T, Hagiwara S, Chung H, Ueshima K, Maekawa K. Differential diagnosis of hepatic tumors: value of contrast-enhanced harmonic sonography using the newly developed contrast agent, Sonazoid. *Intervirology* 2008; **51** Suppl 1: 61-69

18 **Landmark KE**, Johansen PW, Johnson JA, Johansen B, Uran S, Skotland T. Pharmacokinetics of perfluorobutane following intravenous bolus injection and continuous infusion of sonazoid in healthy volunteers and in patients with reduced pulmonary diffusing capacity. *Ultrasound Med Biol* 2008; **34**: 494-501

19 **Yanagisawa K**, Moriyasu F, Miyahara T, Yuki M, Iijima H. Phagocytosis of ultrasound contrast agent microbubbles by Kupffer cells. *Ultrasound Med Biol* 2007; **33**: 318-325

20 **Piscaglia F**, Bolondi L. The safety of Sonovue in abdominal applications: retrospective analysis of 23188 investigations. *Ultrasound Med Biol* 2006; **32**: 1369-1375

21 **Lencioni R**, Cioni D, Crocetti L, Donati F, Franchini C, Giusti S, Bartolozzi C. Ultrasound imaging of focal liver lesions with a second-generation contrast agent. *Acad Radiol* 2002; **9** Suppl 2: S371-S374

22 **Claudon M**, Cosgrove D, Albrecht T, Bolondi L, Bosio M, Calliada F, Correas JM, Darge K, Dietrich C, D'Onofrio M, Evans DH, Filice C, Greiner L, Jäger K, Jong N, Leen E, Lencioni R, Lindsell D, Martegani A, Meairs S, Nolsøe C, Piscaglia F, Ricci P, Seidel G, Skjoldbye B, Solbiati L, Thorelius L, Tranquart F, Weskott HP, Whittingham T. Guidelines and good clinical practice recommendations for contrast enhanced ultrasound (CEUS) - update 2008. *Ultraschall Med* 2008; **29**: 28-44

23 **Kono Y**, Steinbach GC, Peterson T, Schmid-Schönbein GW, Mattrey RF. Mechanism of parenchymal enhancement of the liver with a microbubble-based US contrast medium: an intravital microscopy study in rats. *Radiology* 2002; **224**: 253-257

24 **Dietrich CF**, Ignee A, Trojan J, Fellbaum C, Schuessler G. Improved characterisation of histologically proven liver tumours by contrast enhanced ultrasonography during the portal venous and specific late phase of SHU 508A. *Gut* 2004; **53**: 401-405

25 **Bryant TH**, Blomley MJ, Albrecht T, Sidhu PS, Leen EL, Basilico R, Pilcher JM, Bushby LH, Hoffmann CW, Harvey CJ, Lynch M, MacQuarrie J, Paul D, Cosgrove DO. Improved characterization of liver lesions with liver-phase uptake of liver-specific microbubbles: prospective multicenter study. *Radiology* 2004; **232**: 799-809

26 **Fattovich G,** Stroffolini T, Zagni I, Donato F. Hepatocellular carcinoma in cirrhosis: incidence and risk factors. *Gastroenterology* 2004; **127**: S35-S50

27 **Roncalli M**, Roz E, Coggi G, Di Rocco MG, Bossi P, Minola E, Gambacorta M, Borzio M. The vascular profile of regenerative and dysplastic nodules of the cirrhotic liver: implications for diagnosis and classification. *Hepatology* 1999; **30**: 1174-1178

28 **Gaiani S**, Celli N, Piscaglia F, Cecilioni L, Losinno F, Giangregorio F, Mancini M, Pini P, Fornari F, Bolondi L. Usefulness of contrast-enhanced perfusional sonography in the assessment of hepatocellular carcinoma hypervascular at spiral computed tomography. *J Hepatol* 2004; **41**: 421-426

29 **Xu HX**, Liu GJ, Lu MD, Xie XY, Xu ZF, Zheng YL, Liang JY. Characterization of focal liver lesions using contrast-enhanced sonography with a low mechanical index mode and a sulfur hexafluoride-filled microbubble contrast agent. *J Clin Ultrasound* 2006; **34**: 261-272

30 **Kim TK**, Kim AY, Choi BI. Hepatocellular carcinoma: harmonic ultrasound and contrast agent. *Abdom Imaging* 2002; **27**: 129-138
31 **Xu HX**, Xie XY, Lu MD, Liu GJ, Xu ZF, Zheng YL, Liang JY, Chen LD. Contrast-enhanced sonography in the diagnosis of small hepatocellular carcinoma < or =2 cm. *J Clin Ultrasound* 2008; **36**: 257-266
32 **Forner A**, Vilana R, Ayuso C, Bianchi L, Solé M, Ayuso JR, Boix L, Sala M, Varela M, Llovet JM, Brú C, Bruix J. Diagnosis of hepatic nodules 20 mm or smaller in cirrhosis: Prospective validation of the noninvasive diagnostic criteria for hepatocellular carcinoma. *Hepatology* 2008; **47**: 97-104
33 **Nicolau C**, Vilana R, Catalá V, Bianchi L, Gilabert R, García A, Brú C. Importance of evaluating all vascular phases on contrast-enhanced sonography in the differentiation of benign from malignant focal liver lesions. *AJR Am J Roentgenol* 2006; **186**: 158-167
34 **Fracanzani AL**, Burdick L, Borzio M, Roncalli M, Bonelli N, Borzio F, Maraschi A, Fiorelli G, Fargion S. Contrast-enhanced Doppler ultrasonography in the diagnosis of hepatocellular carcinoma and premalignant lesions in patients with cirrhosis. *Hepatology* 2001; **34**: 1109-1112
35 **Rahbin N**, Siösteen AK, Elvin A, Blomqvist L, Hagen K, Hultcrantz R, Aleman S. Detection and characterization of focal liver lesions with contrast-enhanced ultrasonography in patients with hepatitis C-induced liver cirrhosis. *Acta Radiol* 2008; **49**: 251-257
36 **Bruix J**, Sherman M, Llovet JM, Beaugrand M, Lencioni R, Burroughs AK, Christensen E, Pagliaro L, Colombo M, Rodés J. Clinical management of hepatocellular carcinoma. Conclusions of the Barcelona-2000 EASL conference. European Association for the Study of the Liver. *J Hepatol* 2001; **35**: 421-430
37 **Bruix J**, Sherman M. Management of hepatocellular carcinoma. *Hepatology* 2005; **42**: 1208-1236
38 **Wang JH**, Lu SN, Hung CH, Chen TY, Chen CH, Changchien CS, Lee CM. Small hepatic nodules (< or =2 cm) in cirrhosis patients: characterization with contrast-enhanced ultrasonography. *Liver Int* 2006; **26**: 928-934
39 **Bolondi L**, Gaiani S, Celli N, Golfieri R, Grigioni WF, Leoni S, Venturi AM, Piscaglia F. Characterization of small nodules in cirrhosis by assessment of vascularity: the problem of hypovascular hepatocellular carcinoma. *Hepatology* 2005; **42**: 27-34
40 **von Herbay A**, Vogt C, Häussinger D. Late-phase pulse-inversion sonography using the contrast agent levovist: differentiation between benign and malignant focal lesions of the liver. *AJR Am J Roentgenol* 2002; **179**: 1273-1279
41 **Kudo M**, Hatanaka K, Maekawa K. Sonazoid-enhanced Ultrasound in the Diagnosis and Treatment of Hepatic Tumors. *J Med Ultrasound* 2008; **16**: 130-139
42 **Kudo M**, Okanoue T. Management of hepatocellular carcinoma in Japan: consensus-based clinical practice manual proposed by the Japan Society of Hepatology. *Oncology* 2007; **72** Suppl 1: 2-15
43 **Sontum PC**, Ostensen J, Dyrstad K, Hoff L. Acoustic properties of NC100100 and their relation with the microbubble size distribution. *Invest Radiol* 1999; **34**: 268-275
44 **Nicolau C**, Catalá V, Vilana R, Gilabert R, Bianchi L, Solé M, Pagés M, Brú C. Evaluation of hepatocellular carcinoma using SonoVue, a second generation ultrasound contrast agent: correlation with cellular differentiation. *Eur Radiol* 2004; **14**: 1092-1099
45 **Liu GJ**, Xu HX, Lu MD, Xie XY, Xu ZF, Zheng YL, Liang JY. Correlation between enhancement pattern of hepatocellular carcinoma on real-time contrast-enhanced ultrasound and tumour cellular differentiation on histopathology. *Br J Radiol* 2007; **80**: 321-330
46 **Yang H**, Liu GJ, Lu MD, Xu HX, Xie XY. Evaluation of the vascular architecture of hepatocellular carcinoma by micro flow imaging: pathologic correlation. *J Ultrasound Med* 2007; **26**: 461-467
47 **Vanbockrijck M**, Klöppel G. Incidence and morphology of liver metastasis from extrahepatic malignancies to cirrhotic livers. *Zentralbl Pathol* 1992; **138**: 91-96
48 **Gillams A**. Minimally invasive treatment for liver and lung metastases in colorectal cancer. *BMJ* 2007; **334**: 1056-1057
49 **Garden OJ**, Rees M, Poston GJ, Mirza D, Saunders M, Ledermann J, Primrose JN, Parks RW. Guidelines for resection of colorectal cancer liver metastases. *Gut* 2006; **55** Suppl 3: iii1-iii8
50 **Oldenburg A**, Hohmann J, Foert E, Skrok J, Hoffmann CW, Frericks B, Wolf KJ, Albrecht T. Detection of hepatic metastases with low MI real time contrast enhanced sonography and SonoVue. *Ultraschall Med* 2005; **26**: 277-284
51 **Harvey CJ**, Blomley MJ, Eckersley RJ, Cosgrove DO, Patel N, Heckemann RA, Butler-Barnes J. Hepatic malignancies: improved detection with pulse-inversion US in late phase of enhancement with SH U 508A-early experience. *Radiology* 2000; **216**: 903-908
52 **Tanaka S**, Ioka T, Oshikawa O, Hamada Y, Yoshioka F. Dynamic sonography of hepatic tumors. *AJR Am J Roentgenol* 2001; **177**: 799-805
53 **Solbiati L**, Tonolini M, Cova L, Goldberg SN. The role of contrast-enhanced ultrasound in the detection of focal liver leasions. *Eur Radiol* 2001; **11** Suppl 3: E15-E26
54 **Hohmann J**, Albrecht T, Hoffmann CW, Wolf KJ. Ultrasonographic detection of focal liver lesions: increased sensitivity and specificity with microbubble contrast agents. *Eur J Radiol* 2003; **46**: 147-159
55 **Konopke R**, Bunk A, Kersting S. The role of contrast-enhanced ultrasound for focal liver lesion detection: an overview. *Ultrasound Med Biol* 2007; **33**: 1515-1526
56 **Quaia E**, Bertolotto M, Forgács B, Rimondini A, Locatelli M, Mucelli RP. Detection of liver metastases by pulse inversion harmonic imaging during Levovist late phase: comparison with conventional ultrasound and helical CT in 160 patients. *Eur Radiol* 2003; **13**: 475-483
57 **Albrecht T**, Blomley MJ, Burns PN, Wilson S, Harvey CJ, Leen E, Claudon M, Calliada F, Correas JM, LaFortune M, Campani R, Hoffmann CW, Cosgrove DO, LeFevre F. Improved detection of hepatic metastases with pulse-inversion US during the liver-specific phase of SHU 508A: multicenter study. *Radiology* 2003; **227**: 361-370
58 **Chen LD**, Xu HX, Xie XY, Lu MD, Xu ZF, Liu GJ, Liang JY, Lin MX. Enhancement patterns of intrahepatic cholangiocarcinoma: comparison between contrast-enhanced ultrasound and contrast-enhanced CT. *Br J Radiol* 2008; **81**: 881-889
59 **Xu HX**, Lu MD, Liu GJ, Xie XY, Xu ZF, Zheng YL, Liang JY. Imaging of peripheral cholangiocarcinoma with low-mechanical index contrast-enhanced sonography and SonoVue: initial experience. *J Ultrasound Med* 2006; **25**: 23-33
60 **Chen LD**, Xu HX, Xie XY, Xie XH, Xu ZF, Liu GJ, Wang Z, Lin MX, Lu MD. Intrahepatic cholangiocarcinoma and hepatocellular carcinoma: differential diagnosis with contrast-enhanced ultrasound. *Eur Radiol* 2009; Epub ahead of print
61 **Hussain SM**, Zondervan PE, IJzermans JN, Schalm SW, de Man RA, Krestin GP. Benign versus malignant hepatic nodules: MR imaging findings with pathologic correlation. *Radiographics* 2002; **22**: 1023-1036; discussion 1037-1039
62 **Kudo M**. Multistep human hepatocarcinogenesis: correlation of imaging with pathology. *J Gastroenterol* 2009; **44** Suppl 19: 112-118
63 **Brancatelli G**, Federle MP, Blachar A, Grazioli L. Hemangioma in the cirrhotic liver: diagnosis and natural history. *Radiology* 2001; **219**: 69-74
64 **Catalano O**, Lobianco R, Cusati B, Siani A. Hepatocellular carcinoma: spectrum of contrast-enhanced gray-scale

harmonic sonography findings. *Abdom Imaging* 2004; **29**: 341-347
65 **Kudo M**. Early detection and characterization of hepatocellular carcinoma: value of imaging multistep human hepatocarcinogenesis. *Intervirology* 2006; **49**: 64-69
66 **Lee JY**, Choi BI, Han JK, Kim AY, Shin SH, Moon SG. Improved sonographic imaging of hepatic hemangioma with contrast-enhanced coded harmonic angiography: comparison with MR imaging. *Ultrasound Med Biol* 2002; **28**: 287-295
67 **Konopke R**, Bunk A, Kersting S. The role of contrast-enhanced ultrasound for focal liver lesion detection: an overview. *Ultrasound Med Biol* 2007; **33**: 1515-1526
68 **Ding H**, Wang WP, Huang BJ, Wei RX, He NA, Qi Q, Li CL. Imaging of focal liver lesions: low-mechanical-index real-time ultrasonography with SonoVue. *J Ultrasound Med* 2005; **24**: 285-297
69 **Wanless IR**, Mawdsley C, Adams R. On the pathogenesis of focal nodular hyperplasia of the liver. *Hepatology* 1985; **5**: 1194-1200
70 **Quaglia A**, Tibballs J, Grasso A, Prasad N, Nozza P, Davies SE, Burroughs AK, Watkinson A, Dhillon AP. Focal nodular hyperplasia-like areas in cirrhosis. *Histopathology* 2003; **42**: 14-21
71 **Di Stasi M**, Caturelli E, De Sio I, Salmi A, Buscarini E, Buscarini L. Natural history of focal nodular hyperplasia of the liver: an ultrasound study. *J Clin Ultrasound* 1996; **24**: 345-350
72 **Nicolau C**, Brú C. Focal liver lesions: evaluation with contrast-enhanced ultrasonography. *Abdom Imaging* 2004; **29**: 348-359
73 **Yen YH**, Wang JH, Lu SN, Chen TY, Changchien CS, Chen CH, Hung CH, Lee CM. Contrast-enhanced ultrasonographic spoke-wheel sign in hepatic focal nodular hyperplasia. *Eur J Radiol* 2006; **60**: 439-444
74 **Petrovic LM**. Benign hepatocellular tumors and tumor-like lesions. *Pathology* (Phila) 1994; **3**: 119-139
75 **Lim AK**, Patel N, Gedroyc WM, Blomley MJ, Hamilton G, Taylor-Robinson SD. Hepatocellular adenoma: diagnostic difficulties and novel imaging techniques. *Br J Radiol* 2002; **75**: 695-699
76 **Solbiati L**, Kirn V, Cova L. Other benign lesions and pseudolesions. In: Solbiati L, editor. Contrast-enhanced ultrasound of liver diseases. Rome: Springer-Verlag, 2003: 60-61
77 **Dietrich CF**. Characterisation of focal liver lesions with contrast enhanced ultrasonography. *Eur J Radiol* 2004; **51** Suppl: S9-S17
78 **Lin MX**, Xu HX, Lu MD, Xie XY, Chen LD, Xu ZF, Liu GJ, Xie XH, Liang JY, Wang Z. Diagnostic performance of contrast-enhanced ultrasound for complex cystic focal liver lesions: blinded reader study. *Eur Radiol* 2009; **19**: 358-369
79 **Catalano O**, Sandomenico F, Raso MM, Siani A. Low mechanical index contrast-enhanced sonographic findings of pyogenic hepatic abscesses. *AJR Am J Roentgenol* 2004; **182**: 447-450
80 **Liu GJ**, Lu MD, Xie XY, Xu HX, Xu ZF, Zheng YL, Liang JY, Wang W. Real-time contrast-enhanced ultrasound imaging of infected focal liver lesions. *J Ultrasound Med* 2008; **27**: 657-666
81 **Xu HX**, Xie XY, Lu MD, Liu GJ, Xu ZF, Liang JY, Chen LD. Unusual benign focal liver lesions: findings on real-time contrast-enhanced sonography. *J Ultrasound Med* 2008; **27**: 243-254
82 **Wilson SR**, Greenbaum LD, Goldberg BB. Contrast-enhanced ultrasound: what is the evidence and what are the obstacles? *AJR Am J Roentgenol* 2009; **193**: 55-60
83 **Nicolau C**, Vilana R, Brú C. The use of contrast-enhanced ultrasound in the management of the cirrhotic patient and for detection of HCC. *Eur Radiol* 2004; **14** Suppl 8: P63-P71

S- Editor Wang JL **L- Editor** O'Neill M **E- Editor** Zheng XM

World Journal of Radiology

Online Submissions: http://www.wjgnet.com/1949-8470office
wjr@wjgnet.com
doi:10.4329/wjr.v1.i1.37

World J Radiol 2009 December 31; 1(1): 37-44
ISSN 1949-8470 (online)

TOPIC HIGHLIGHT

Hui-Xiong Xu, MD, PhD, *Series Editor*

Contrast-enhanced ultrasound in the biliary system: Potential uses and indications

Hui-Xiong Xu

Hui-Xiong Xu, Department of Medical Ultrasonics, The First Affiliated Hospital, Sun Yat-Sen University, The Center of Guangdong Province for the Study of Diagnostic Ultrasound and Interventional Therapy, 58 Zhongshan Road 2, Guangzhou 510080, Guangdong Province, China
Author contributions: Xu HX wrote this paper.
Supported by (in part) Grant No. NCET-06-0723 from the Chinese Ministry of Education and grant 2008-2-10 of Public Welfare Research Special Project from the Chinese Ministry of Health
Correspondence to: Hui-Xiong Xu, MD, PhD, Professor, Department of Medical Ultrasonics, The First Affiliated Hospital, Sun Yat-Sen University, The Center of Guangdong Province for the Study of Diagnostic Ultrasound and Interventional Therapy, 58 Zhongshan Road 2, Guangzhou 510080, Guangdong Province, China. xuhuixiong@hotmail.com
Telephone: +86-20-87765183 Fax: +86-20-87765183
Received: November 26, 2009 Revised: December 11, 2009
Accepted: December 21, 2009
Published online: December 31, 2009

Abstract

Conventional ultrasound (US) is the first-line imaging investigation for biliary diseases. However, it is lack of the ability to depict the microcirculation of some lesions which may lead to failure in diagnosis for some biliary diseases. The use of contrast-enhanced US (CEUS) has reached the field of bile duct disease in recent years and promising results have been achieved. In this review, the methodology, image interpretation, enhancement pattern, clinical usefulness, and indications for CEUS in the biliary system are summarized. CEUS may be indicated in the biliary system under the following circumstances: (1) Where there is a need to make a characterization of intrahepatic cholangiocarcinoma (ICC); (2) For differentiation diagnosis between ICC and other tumors (i.e. hepatocellular carcinoma or liver metastasis) or infectious diseases; (3) For differentiation diagnosis between biliary cystadenoma and biliary cystadenocarcinoma; (4) To detect malignant change in Caroli's disease; (5) To depict the extent of Klatskin's tumor with greater clarity; (6) To make a distinction between gallbladder cholesterol polyp, adenoma and polypoid cancer; (7) To make a distinction between chronic cholecystitis with thickened wall and gallbladder cancer; (8) For differentiation diagnosis between motionless sludge and gallbladder cancer; (9) For differentiation diagnosis between common bile duct cancer and sludge or stone without acoustic shadowing; and (10) In patients who are suspected of having a drop of their percutaneous transhepatic cholangiodrainage tube, US contrast agent can be administered to through the tube detect the site of the tube.

Key words: Contrast-enhanced ultrasound; Bile duct; Gallbladder; Cholangiocarcinoma; Polypoid lesion; Ultrasound contrast agent

Peer reviewer: Herwig R Cerwenka, Professor, MD, Department of Surgery, Medical University of Graz, Auenbruggerplatz 29, A-8036 Graz, Austria

Xu HX. Contrast-enhanced ultrasound in the biliary system: Potential uses and indications. *World J Radiol* 2009; 1(1): 37-44 Available from: URL: http://www.wjgnet.com/1949-8470/full/v1/i1/37.htm DOI: http://dx.doi.org/10.4329/wjr.v1.i1.37

INTRODUCTION

Conventional ultrasound (US) is the first-line imaging investigation for diagnosis of biliary diseases, and most biliary diseases are firstly detected by conventional US. The continuous improvement in imaging quality and the advent of new techniques such as power Doppler

imaging, tissue harmonic imaging, endoscopic US, and three-dimensional US have further enriched the application of US in the biliary system[1-3]. In recent years, a novel technique of contrast-enhanced US (CEUS) has been widely used in various applications and has been accepted in clinical practice. Regarding the abdominal organs, CEUS has been used in the liver, kidney, pancreas, and spleen[4-8]. However, in the 'Guidelines and Good Clinical Practice Recommendations for CEUS - update 2008' which was recently issued, the application of CEUS in the biliary system was not mentioned[9]. The use of CEUS has reached the field of bile duct disease in recent years and promising results have been achieved[10,11]. From 2004, we have carried out biliary CEUS examination in more than 400 patients. In this review, the methodology, image interpretation, enhancement pattern, clinical usefulness, and indications for CEUS in the biliary system are summarized.

CONTRAST AGENT

Ultrasound contrast agent (UCA) is a microbubble-based substance. The diameter of the microbubble is small enough to guarantee its passage through the pulmonary circulation and to reach various organs[12]. Currently, there are five commercially available UCAs that have been approved in clinic. They are Levovist® (air with galactose and palmitic acid as a surfactant; Schering, introduced in 1996), Optison® (octafluoropropane with an albumin shell; GE Healthcare, introduced in 1998), Luminity® (octafluoropropane perflutren with a lipid shell; Bristol-Myers Squibb, introduced in 2006), SonoVue® (sulfur hexafluoride with a phospholipid shell; Bracco, introduced in 2001), Sonazoid® (perfluorobutane with a phosphatidylserine shell; GE Healthcare, introduced in 2007). The diameters of these are approximately 2-8 μm, smaller than that of red cells in the blood. Levovist® works under high acoustic power and is only suitable for intermittent imaging, and is seldom used currently. Optison® and Luminity® are only licensed for cardiac use. Sonazoid® is only approved in Japan. The only licensed UCA in China is SonoVue®, which is also available in Europe[9].

UCA is administrated intravenously and is confined to the intravascular space, which is different from the contrast media for contrast-enhanced computed tomography (CECT) or contrast-enhanced magnetic resonance imaging, where the contrast media is rapidly cleared from the blood pool into the extracellular space[9].

In addition to intravenous use, UCA intracavity applications can be performed in the biliary system. In patients who have undergone percutaneous transhepatic cholangiodrainage (PTCD), UCA can be administered through the drainage tube to visualize the bile duct tree and to locate the position of the tube[13].

IMAGING TECHNIQUE

When the intravenous UCAs are exposed to US, they strongly increase the US backscatter and therefore are useful in the enhancement of echogenicity for the assessment of blood flow, which enables the display of parenchymal microvasculature.

Real-time gray-scale CEUS examination is available with the combinations of UCAs and low acoustic power contrast-specific imaging (CSI) techniques. Under low acoustic power, which is expressed as mechanical index (MI) and is often lower than 0.2, most of the UCAs in the circulation will remain intact and will interact with the acoustic wave. In contrast, under high acoustic power, the microbubbles will be destroyed. Low MI techniques furthermore lead to effective tissue signal suppression, as the non-linear response from the tissue is minimal when low acoustic pressures are used. By using low MI CSI technique, CEUS enables effective investigations over several minutes with the visualization of the dynamic enhancement pattern in real time.

SCANNING METHOD

For all CEUS examinations, baseline US investigations are firstly performed. After identification of the target lesion, the transducer is kept in a stable position and the imaging mode is changed to low MI CSI. The tissue signals are eliminated and the depth, gain and focus are carefully adjusted. UCA is administered intravenously through the antecubital vein as a bolus (within 1-2 s), followed by a flush of 5 mL of normal saline. A stop clock should be started at time of UCA injection.

A simultaneous display of tissue and contrast signals has been implemented in many CSI modes. This modality is recommended in most cases, as it can ensure that the target lesion is kept within the scanning field during CEUS.

To continuously assess the vascular enhancement change, continuous scanning for 60-90 s is recommended in each case. In addition, in the late phase, the scanning may be used intermittently until the disappearance of the UCA from the region of interest (ROI). In patients suspected of malignancy, thorough liver scanning in the late phase is necessary to exclude liver metastasis.

INTRAHEPATIC BILIARY SYSTEM

The intrahepatic bile duct is hard to visualize under normal circumstances, and most lesions of the intrahepatic bile duct are difficult to demarcate from the adjacent parenchyma. Therefore, the entire CEUS process for the intrahepatic biliary system is performed with reference to that for liver, i.e. including arterial (8-30 s from the beginning of contrast agent administration), portal (31-120 s), and late (121-360 s) phases[9]. Also, the enhancement extent is compared with the adjacent liver parenchyma.

Intrahepatic cholangiocarcinoma (ICC)

ICC is a malignant epithelial tumor that originates at the second branch (segmental branch) or the proximal branch

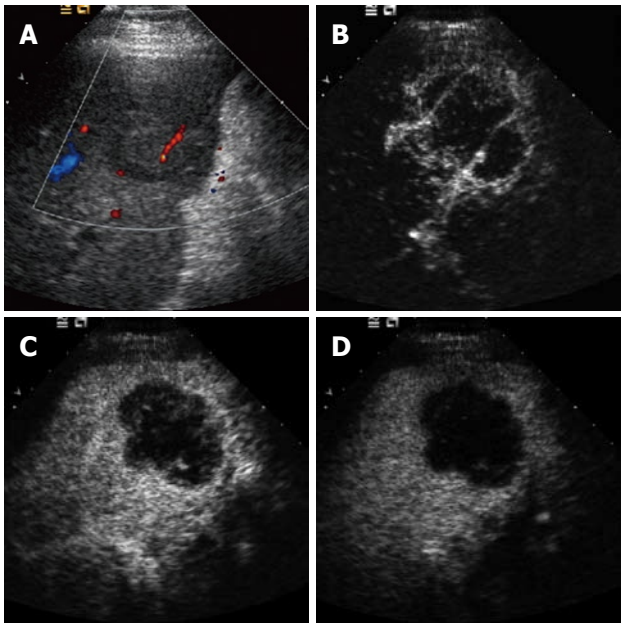

Figure 1 Intrahepatic cholangiocarcinoma. A: Baseline ultrasound shows an isoechoic mass in segment 5 of the liver; B: The lesion shows peripheral rim-like hyper-enhancement 26 s after contrast agent injection on CEUS; C: The lesion becomes hypo-enhanced 52 s after contrast agent injection; D: The lesion continues to be hypo-enhanced 121 s after contrast agent injection.

of the intrahepatic bile ducts and is the second most common primary malignant tumor in the liver. ICC often appears as a large mass because the tumor does not cause clinical symptoms at its early stage. The US features of peripheral cholangiocarcinomas are nonspecific. Most of them show a mass-forming lesion as a hypoechoic mass, and satellite nodules can be seen. Other echo patterns such as isoechoic or hyper-echoic and inhomogeneous masses can also be visualized. Sonographically, it is difficult to differentiate peripheral cholangiocarcinoma from more common diseases such as metastatic liver cancer and hepatocellular carcinoma (HCC) other than the finding that peripheral cholangiocarcinoma is more likely to be associated with peripheral bile duct dilatation.

Xu *et al*[14] summarized the CEUS findings of ICC and Chen *et al*[15] compared the enhancement patterns of ICC between CEUS and contrast-enhanced CT. These authors found that during the arterial phase four enhancement patterns were present on CEUS; these were (1) peripheral irregular rim-like hyper-enhancement (47.5%), (2) diffuse heterogeneous hyper-enhancement (22.5%), (3) diffuse heterogeneous hypo-enhancement (17.5%), and (4) diffuse homogeneous hyper-enhancement (12.5%) (Figure 1). In comparison with CT, the enhancement patterns of ICC on CEUS were consistent with those on CECT in the arterial phase, whereas in the portal phase ICC faded out more obviously on CEUS than on CECT. Chen *et al*[15] reported that CEUS made a correct diagnosis in 80.0% of ICCs before pathological examination and CECT made a correct diagnosis in 67.5%. CEUS therefore had the same accuracy as CECT in diagnosing ICCs, and so can be used as a new modality for the characterization of ICC. Although baseline US has low ability in differentiating ICC and HCC, Chen *et al*[16] found that CEUS greatly improved the diagnostic performance in this use.

The enhancement patterns of ICC correlate with tumor size. That is, most small ICCs ($\leqslant$ 3 cm) are homogeneously enhancing, while those > 3 cm enhance heterogeneously or show a peripherally enhancing rim. This reflects the intratumoral hemodynamic changes in the course of tumor growth. When an ICC is small, it may be abundant in tumor cells with little fibrous tissue, which leads to homogeneous hypervascularity similar to that of HCC. When grown large, more fibrous tissue and central necrosis appear, and the ICC would show peripheral hypervascularity or overall hypovascularity. Consequently, it is difficult to distinguish small ICC from HCC on CEUS, especially in those with homogeneous hyper-enhancement. Under such circumstances, it is important to refer to the clinical background such as liver cirrhosis, blood test for viral hepatitis, and the tumor markers.

In portal and late phase on CEUS, most ICCs show up as hypo-enhancing, which is a prominent feature of malignancy on CEUS. However, on enhanced CT or MRI, most ICCs show delayed hyper-enhancement in the late phase. This phenomenon might be explained by the fact that the UCA is a real blood pool agent and thus it does not diffuse through the vascular endothelium into the interstitium. Conversely, the CT contrast agent can diffuse into the interstitial spaces of the tumor slowly from the intratumoral vessels, and clear up slowly owing to the abundant fibrous tissue and slow blood flow in ICCs; therefore, even delayed tumor enhancement is visualized.

Intrahepatic biliary cystadenoma and cystadenocarcinoma

Intrahepatic biliary cystadenoma is an uncommon multilocular cystic liver mass with malignant potential that usually arises from the epithelium of the intrahepatic bile duct, and which represents less than 5% of intrahepatic cystic masses of biliary origin. Conventional US always reveals a well-defined anechoic cystic mass with echogenic septations or papillary infoldings[6,17].

On CEUS, hyper-enhancement of the cystic wall, internal septations, or a papillary infolding during the arterial phase are seen. The enhancement washes out progressively and is depicted as iso- or hypo-enhancement during the portal and late phases[6,17].

Intrahepatic biliary cystadenocarcinoma is the malignant counterpart of cystadenoma. On CEUS, mural nodule-like hyper-enhancement, thick septa hyper-enhancement, enlarged solid portion hyper-enhancement and non-enhanced central area in the arterial phase are always seen. During portal and late phases, the hyper-enhanced areas wash out and show hypo-enhancement[6].

Biliary epithelial dysplasia of the intrahepatic bile duct

Biliary epithelial dysplasia of the intrahepatic bile duct

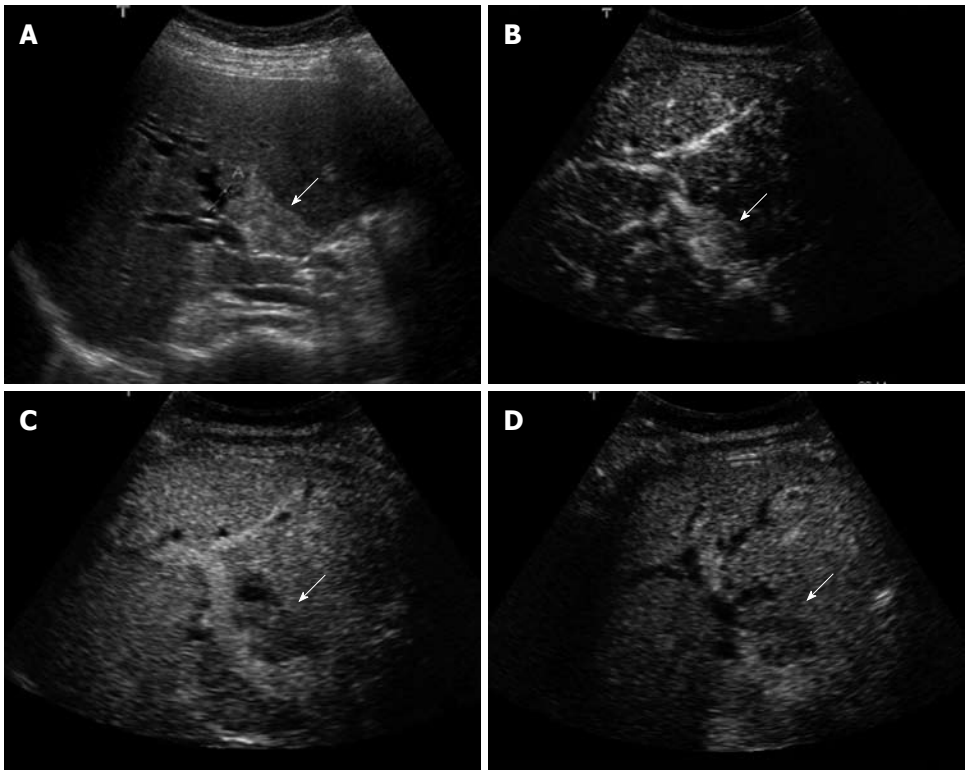

Figure 2 Klatskin tumor. A: Baseline ultrasound shows a hyperechoic mass (arrow) in the hilar bile duct; B: The lesion (arrow) shows homogeneous hyper-enhancement 14 s after contrast agent injection on CEUS; C: The lesion (arrow) becomes hypo-enhanced 45 s after contrast agent injection; D: The lesion (arrow) continues to be hypo-enhanced 126 s after contrast agent injection.

is a premalignant lesion that arises from the epithelium of the intrahepatic bile duct. The imaging features of this entity have seldom been described. In our series, we found one lesion that was slightly hyperechoic and was within a dilated bile duct on baseline US. A peripheral dilated bile duct was visible. On CEUS, the lesion showed homogeneous hyper-enhancement during the arterial phase before liver parenchyma enhancement, which washed out continuously so that the lesion appeared as hypo-enhanced during the portal and late phases and was more conspicuous during those phases[17]. Sonographically, it was hard to differentiate it from its malignant counterpart, ICC.

Periductal inflammation

In patients with intrahepatic cholelithiasis, the continuous irritation of the stone on the wall of the bile duct will cause inflammation, and even lead to periductal inflammation. The patients always complain of fever and right upper quadrant pain. On baseline US, the periductal inflammatory lesion always shows hypoechogenicity around the intrahepatic bile duct. The lesion may be regular or irregular. On CEUS, hyper-enhancement during arterial phase and hypo-enhancement during portal or late phase are the most common findings for this entity. It is difficult to make a distinction between this and liver malignancy solely depending on the findings on US.

HILAR BILE DUCT

The entire CEUS process for the hilar bile duct is also performed with reference to that for liver, i.e. including arterial, portal, and late phases. In addition, the enhancement extent is compared with the adjacent liver parenchyma. Since the lesion in the hilar region is always small, the ROI can be zoomed to display the lesion and the relationship between it and the surrounding vessels more carefully. Simultaneous display of the contrast and tissue mode is recommended to avoid loss of the target lesion.

Klatskin tumor

The most common disease entity in the hilar bile duct is hilar cholangiocarcinoma (i.e. Klatskin tumor). Transabdominal US examination is the primary investigation for suspected Klatskin tumor, which is highly sensitive for confirming biliary duct dilatation, localizing the site of obstruction and excluding gallstones. However, it has a limited role in determining the nature of the obstruction and defining the extent of tumor involvement since the Klatskin tumor is always isoechoic to surrounding liver and the infiltrative nature of the lesion. The use of CEUS in evaluating Klatskin tumor has been investigated. In comparison with the adjacent liver parenchyma, the enhancement of the lesion was earlier (37.5%) or simultaneous (50.0%), and only 12.5% enhanced later. During the arterial phase, hyper-enhancement, iso-enhancement, and hypo-enhancement were visualized in 43.8%, 43.8%, and 12.4% of the lesions, respectively, on CEUS (Figure 2). As to enhancement pattern, peripheral rim-like hyper-enhancement, homogeneous enhancement, and inhomogeneous enhancement were illustrated in 9.4%, 34.4%, and 56.2% of the lesions, respectively. During the portal and late phases of CEUS, 93.8% lesions appeared as hypo-enhancement and the tumor margins became more conspicuous[18].

Xu *et al*[18] compared the enhancement pattern of Klatskin tumor between CEUS and CECT. They found that the enhancement pattern of hilar cholangiocarcinoma on CEUS was similar to that on CECT in the arterial phase, whereas in portal phase hilar cholangiocarcinoma was more likely to show hypo-enhancement on CEUS. CEUS and CECT led to similar results when evaluating portal vein infiltration. CEUS achieved a correct diagnosis in 93.8% of cases whereas CECT was correct in 78.1% of cases. No significant difference was found between these two modalities in diagnosis of this entity. Therefore, CEUS has potential to be a tool for characterization of Klatskin tumor.

GALLBLADDER

The enhancement process of gallbladder lesions on CEUS is classified as early phase (10-30 s after contrast injection) and late phase (31-180 s after contrast injection) since the blood supply of the gallbladder is entirely arterial. The late phase persists for a short time in comparison with that for the liver[19].

Conventional grey-scale US is the first-line imaging investigation for diagnosis of gallbladder diseases, whereas it is insufficient to determine the nature of some complicated gallbladder diseases. Most of the gallbladder cancers present as either a solid mass that occupies the whole gallbladder or as a focal polypoid lesion on conventional US. However, some biliary sludge can generate similar US images and no movement is found[20]. Focal or diffuse thickening of the gallbladder wall is also a common, though nonspecific, US finding. Abnormal thickness can be attributed to diseases such as acute or chronic cholecystitis, benign or malignant tumor. The differentiation between these will become difficult, which is particularly true when the lesions fill the gallbladder or more than two types of lesions are present in gallbladder diseases. The insufficiency of conventional US is largely due to the fact that it has low ability in depicting vascularity in gallbladder diseases. CEUS can thus be applied to overcome the limitations of conventional US, since it can depict the hemodynamics in micro- and macro-circulation[21].

Gallbladder carcinoma

On conventional US, a solid mass that occupies the whole gallbladder, a sessile polypoid mass, focal or diffuse wall thickening, intralesional hypervascularity or infiltration to adjacent liver may be found. On CEUS, branch-like flow pattern or hyper-enhancement during the early phase is always recognized (Figure 3). The arterial branches supplying a gallbladder carcinoma tend to show irregularly tortuous extension. A lesion with tortuous-type tumor vessels on CEUS may be a clue for gallbladder carcinoma[10]. On the other hand, washout of the contrast agent within 35-60 s after contrast agent administration occurs in most gallbladder carcinomas, which seems to be a useful clue for differentiation between malignant and benign gallbladder diseases. Gallbladder carcinoma is usually at an advanced stage when it is firstly detected because it is asymptomatic at early stage. The infiltration to the gallbladder wall and the adjacent liver tissue is common. Accordingly, destruction of the gallbladder wall integrity is also a major sign of gallbladder carcinomas on CEUS[19].

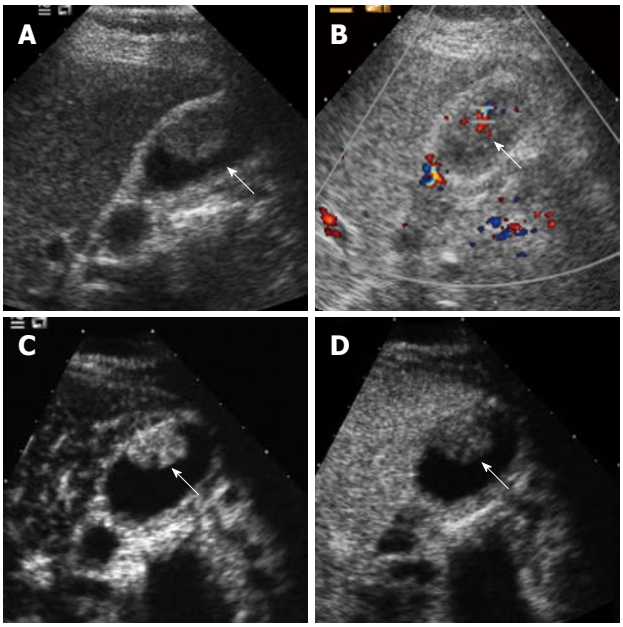

Figure 3 Gallbladder carcinoma. A: Baseline ultrasound shows an isoechoic mass (arrow) in the gallbladder cavity; B: The lesion (arrow) shows hypervascularity on color Doppler flow imaging; C: The lesion (arrow) shows homogeneous hyper-enhancement 19 s after contrast agent injection on CEUS; D: The lesion (arrow) becomes hypo-enhanced 34 s after contrast agent injection.

Gallbladder adenomas

Gallbladder adenomas are relatively uncommon, with an incidence ranging from 0.3% to 0.5% in gallbladders removed by cholecystectomy. The lesions are polypoid, protrude into the gallbladder lumen, and have lobular or cauliflower-like surface. Ninety percent of gallbladder adenomas are single, and 60% are associated with cholecystolithiasis. Gallbladder adenoma appears on US as a sessile polypoid mass, a lesion of an echogenicity slightly greater or similar to the liver, with a smooth or lobulated surface and a relatively homogeneous internal texture, without infiltration to adjacent tissue. On CEUS, homogeneous hyper-enhancement (78%) and iso-enhancement (22%) during the early phase is found. In the late phase, iso- (56%) and hypo-enhancement (44%) are visualized[19].

Cholesterol polyp

Cholesterol polyp shows a pedicle polypoid lesion, a tiny echogenic spot or an aggregation of echogenic spots within the lesion, with no or scarce vascularity on conventional US. On CEUS, hyper-enhancement is found in the majority (93%) of the lesions and the

remaining 7% show iso-enhancement during the early phase. In cholesterol polyp, almost normal-caliber arteries taper normally and subdivide normally into small vessels, and the lesion may show dotted- or branched-type tumor vessels on CEUS. In the late phase, hypo-enhancement is found in 64% and iso-enhancement in 36% of the lesions[19].

Inflammatory polyp

Inflammatory polyp is also a hypervascular lesion which shows hyper-enhancement in the early phase on CEUS. So far no data are available about its pattern in the late phase on CEUS.

Adenomyomatosis

Adenomyomatosis shows focal or diffuse thickened wall, multiple microcysts or comet tail artifact on conventional US. On CEUS, the lesions shows hyper- (20%) or iso-enhancement (80%) in the early phase and all the lesions show hypo-enhancement in the late phase[19].

Biliary sludge

Sometimes, motionless biliary sludge in the gallbladder mimics gallbladder polypoid lesion or cancer on trans-abdominal US. CEUS makes it very easy to differentiate biliary sludge from other polypoid gallbladder diseases on the basis of the finding of the absence of tumor enhancement. This means that evaluating the vascularity of the abnormality may be more useful in defining sludge than evaluating the lesion alterations induced by posture change.

Cholecystitis

Chronic cholecystitis shows thickened wall and no infiltration to adjacent tissue on conventional US and CEUS. When the gallbladder cavity is filled with gallstone or biliary sludge, it is always difficult to differentiate chronic cholecystitis with thickened gallbladder wall from gallbladder carcinoma with conventional US. The intactness of wall is the criterion to differentiate these two diseases. On CEUS, hyper- (86%), iso- (7%), and hypo-enhancement (7%) of the gallbladder wall is found in the early phase and all show hypo-enhancement in the late phase[19].

Baseline US can provide a definite diagnosis in most acute cholecystitis cases, while CEUS may enhance the diagnosis of the complications such as gallbladder perforation. It is easy to show the perforation site on the wall by CEUS, which is visualized as a non-enhancing area. Hypervascularization of the wall may be seen. The hepatic surface of the gallbladder is drained by vessels that communicate with adjacent hepatic veins. Acute inflammation of the gallbladder can extend to the adjacent liver parenchyma through this connection, resulting in contrast enhancement of liver parenchyma in acute cholecystitis.

CEUS may be able to help in differentiation between acute and chronic cholecystitis. Adamietz *et al*[22] found that in 16/20 cases with histologically proven acute cholecystitis, the gallbladder wall showed a strong enhancement. Low enhancement was found in 4/20 patients with acute, and in 6/8 patients with chronic cholecystitis. The gallbladder wall of 2/8 patients with chronic inflammation and all patients (30/30) of the control group showed no enhancement.

Differentiation between benign and malignant gallbladder diseases

The value of CEUS in the differential diagnosis of benign and malignant gallbladder diseases was investigated by Xie *et al*[19]. The extent of enhancement in the early phase did not achieve significant difference between benign and malignant gallbladder diseases. In the early phase at CEUS, hyper-, iso-, hypo-, and non-enhancement were found in 84.8%, 9.1%, 6.1% and 0% of gallbladder carcinomas, and 70.3%, 17.0%, 2.1%, and 10.6% of benign diseases, respectively. Pathologically, gallbladder carcinomas, adenomas, cholesterol polyps, and inflammatory polyps are supplied by arterial flow from branches of the cystic artery. It is therefore not surprising that both lesions show hyper-enhancement. On the other hand, the blood vessel distribution in the lesion may be helpful in differentiation, for benign lesions often show dotted vessel enhancement whereas malignant lesions often show tortuous vessel enhancement.

Hyper- or iso-enhancement in the early phase and then fading out to hypo-enhancement within 35-60 s after contrast agent administration was found in the majority of carcinomas and minority of benign lesions. Destruction of the gallbladder wall intactness was absent in benign diseases, whereas it was present in most carcinomas. It was suggested that the CEUS features of washout within 35-60 s after contrast agent administration and destruction of gallbladder wall intactness are highly suggestive of gallbladder malignancy. CEUS is particularly useful in differentiating gallbladder carcinomas and motionless biliary sludge or chronic cholecystitis with thickened gallbladder wall.

EXTRAHEPATIC BILIARY SYSTEM

Defining the enhancement process of the extrahepatic system is complicated. The blood supply of the extrahepatic bile duct is entirely arterial. It is recommended that the process is classified as early phase (10-30 s after contrast injection) and late phase (31-180 s after contrast injection). However, the enhancement extent of the upper extrahepatic bile duct can be compared with the liver and the lower portion can be compared with the pancreas so as to facilitate the image interpretation.

Villous adenoma

It is not easy to differentiate villous adenoma in the extrahepatic bile duct from biliary sludge since they have similar echogenicity on conventional US. We have

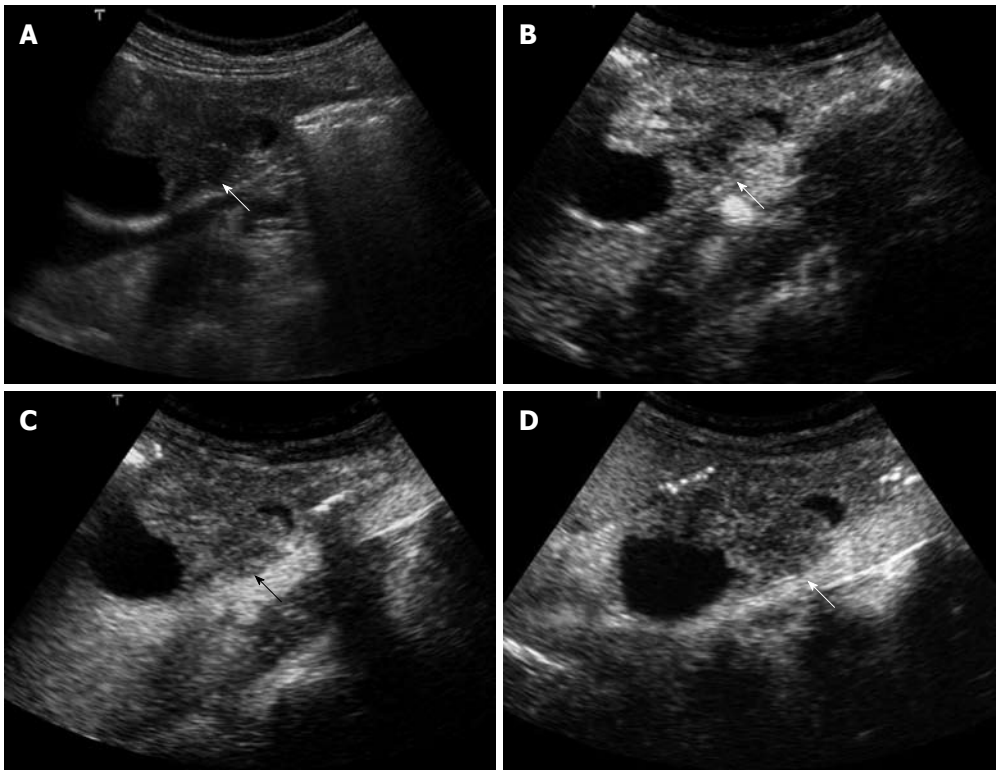

Figure 4 Extrahepatic cholangiocarcinoma. A: Baseline ultrasound shows an isoechoic mass (arrow) in the lower portion of the common bile duct; B: The lesion (arrow) shows heterogeneous iso-enhancement 13 s after contrast agent injection on CEUS; C: The lesion (arrow) continues to be iso-enhanced 56 s after contrast agent injection; D: The lesion (arrow) becomes hypo-enhanced 107 s after contrast agent injection.

reported a case of villous adenoma in the extrahepatic bile duct that was successfully diagnosed with CEUS before surgical resection[23]. On baseline US, the lesion appeared as a homogeneously isoechoic mass filling the bile duct from the confluence of the right and left hepatic ducts to the distal common bile duct. No intralesional flow signal was found on color Doppler imaging and power Doppler imaging. On CEUS, the mass showed homogeneous enhancement during the arterial phase, thus confirming the neoplastic nature of the lesion. The enhancement decreased gradually so that the mass became hypo-enhanced during the late phase.

Extrahepatic cholangiocarcinoma

The extrahepatic cholangiocarcinomas may show hyper-, iso-, or hypo-enhancement in the early phase of CEUS and most of them show hypo-enhancement in the late phase (Figure 4). The major role of CEUS in this regard may be in distinguishing between tumor and debris or stone without obvious acoustic shadowing.

CONCLUSION

In addition to transabdominal CEUS, CEUS can also be performed intraoperatively. Intraoperative CEUS may provide more details about the biliary diseases; however, experience is limited[24-26]. In summary, the application of CEUS in the biliary system is under investigation and needs further validation. CEUS may be indicated under the following circumstances: (1) Where there is a need to make a characterization of ICC; (2) For differentiation diagnosis between ICC and other tumors (i.e. HCC or liver metastasis) or infectious diseases; (3) For differentiation diagnosis between biliary cystadenoma and biliary cystadenocarcinoma; (4) To detect any malignant change in Caroli's disease; (5) To depict the extent of Klatskin' s tumor with great clarity; (6) To make a distinction between gallbladder cholesterol polyp, adenoma and polypoid cancer; (7) To make a distinction between chronic cholecystitis with thickened wall and gallbladder cancer; (8) For differentiation diagnosis between motionless sludge and gallbladder cancer; (9) For differentiation diagnosis between common bile duct cancer and sludge or stone without acoustic shadowing; and (10) In patients who are suspected of having a drop of their PTCD tube, UCA can be administered to through the tube detect the site of the tube.

REFERENCES

1 **Levy AD**, Murakata LA, Rohrmann CA Jr. Gallbladder carcinoma: radiologic-pathologic correlation. *Radiographics* 2001; **21**: 295-314; questionnaire, 549-555
2 **Hirooka Y**, Naitoh Y, Goto H, Ito A, Hayakawa S, Watanabe Y, Ishiguro Y, Kojima S, Hashimoto S, Hayakawa T. Contrast-enhanced endoscopic ultrasonography in gallbladder diseases. *Gastrointest Endosc* 1998; **48**: 406-410
3 **Xu HX**, Yin XY, Lu MD, Liu L, Yue DC, Liu GJ. Comparison of three- and two-dimensional sonography in diagnosis of gallbladder diseases: preliminary experience. *J Ultrasound Med* 2003; **22**: 181-191
4 **Leen E**. The role of contrast-enhanced ultrasound in the characterisation of focal liver lesions. *Eur Radiol* 2001; **11** Suppl 3: E27-E34
5 **Xu HX**, Liu GJ, Lu MD, Xie XY, Xu ZF, Zheng YL, Liang JY. Characterization of small focal liver lesions using real-time contrast-enhanced sonography: diagnostic performance analysis in 200 patients. *J Ultrasound Med* 2006; **25**: 349-361
6 **Lin MX**, Xu HX, Lu MD, Xie XY, Chen LD, Xu ZF, Liu

GJ, Xie XH, Liang JY, Wang Z. Diagnostic performance of contrast-enhanced ultrasound for complex cystic focal liver lesions: blinded reader study. *Eur Radiol* 2009; **19**: 358-369
7 **Xu ZF**, Xu HX, Xie XY, Liu GJ, Zheng YL, Liang JY, Lu MD. Renal cell carcinoma: real-time contrast-enhanced ultrasound findings. *Abdom Imaging* 2009; Epub ahead of print
8 **Xu HX**, Liu GJ, Lu MD, Xie XY, Xu ZF, Zheng YL, Liang JY. Characterization of focal liver lesions using contrast-enhanced sonography with a low mechanical index mode and a sulfur hexafluoride-filled microbubble contrast agent. *J Clin Ultrasound* 2006; **34**: 261-272
9 **Claudon M**, Cosgrove D, Albrecht T, Bolondi L, Bosio M, Calliada F, Correas JM, Darge K, Dietrich C, D'Onofrio M, Evans DH, Filice C, Greiner L, Jäger K, Jong N, Leen E, Lencioni R, Lindsell D, Martegani A, Meairs S, Nolsøe C, Piscaglia F, Ricci P, Seidel G, Skjoldbye B, Solbiati L, Thorelius L, Tranquart F, Weskott HP, Whittingham T. Guidelines and good clinical practice recommendations for contrast enhanced ultrasound (CEUS) - update 2008. *Ultraschall Med* 2008; **29**: 28-44
10 **Inoue T**, Kitano M, Kudo M, Sakamoto H, Kawasaki T, Yasuda C, Maekawa K. Diagnosis of gallbladder diseases by contrast-enhanced phase-inversion harmonic ultrasonography. *Ultrasound Med Biol* 2007; **33**: 353-361
11 **Numata K**, Oka H, Morimoto M, Sugimori K, Kunisaki R, Nihonmatsu H, Matsuo K, Nagano Y, Nozawa A, Tanaka K. Differential diagnosis of gallbladder diseases with contrast-enhanced harmonic gray scale ultrasonography. *J Ultrasound Med* 2007; **26**: 763-774
12 **Correas JM**, Bridal L, Lesavre A, Méjean A, Claudon M, Hélénon O. Ultrasound contrast agents: properties, principles of action, tolerance, and artifacts. *Eur Radiol* 2001; **11**: 1316-1328
13 **Ignee A**, Baum U, Schuessler G, Dietrich CF. Contrast-enhanced ultrasound-guided percutaneous cholangiography and cholangiodrainage (CEUS-PTCD). *Endoscopy* 2009; **41**: 725-726
14 **Xu HX,** Lu MD, Liu GJ, Xie XY, Xu ZF, Zheng YL, Liang JY. Imaging of peripheral cholangiocarcinoma with low-mechanical index contrast-enhanced sonography and SonoVue: initial experience. *J Ultrasound Med* 2006; **25**: 23-33
15 **Chen LD**, Xu HX, Xie XY, Lu MD, Xu ZF, Liu GJ, Liang JY, Lin MX. Enhancement patterns of intrahepatic cholangiocarcinoma: comparison between contrast-enhanced ultrasound and contrast-enhanced CT. *Br J Radiol* 2008; **81**: 881-889
16 **Chen LD**, Xu HX, Xie XY, Xie XH, Xu ZF, Liu GJ, Wang Z, Lin MX, Lu MD. Intrahepatic cholangiocarcinoma and hepatocellular carcinoma: differential diagnosis with contrast-enhanced ultrasound. *Eur Radiol* 2009; Epub ahead of print
17 **Xu HX**, Xie XY, Lu MD, Liu GJ, Xu ZF, Liang JY, Chen LD. Unusual benign focal liver lesions: findings on real-time contrast-enhanced sonography. *J Ultrasound Med* 2008; **27**: 243-254
18 **Xu HX**, Chen LD, Xie XY, Xie XH, Xu ZF, Liu GJ, Lin MX, Wang Z, Lu MD. Enhancement pattern of hilar cholangiocarcinoma: Contrast-enhanced ultrasound versus contrast-enhanced computed tomography. *Eur J Radiol* 2009; Epub ahead of print
19 **Xie XH**, Xu HX, Xie XY, Lu MD, Kuang M, Xu ZF, Liu GJ, Wang Z, Liang JY, Chen LD, Lin MX. Differential diagnosis between benign and malignant gallbladder diseases with real-time contrast-enhanced ultrasound. *Eur Radiol* 2009; Epub ahead of print
20 **Anastasi B**, Sutherland GR. Biliary sludge-ultrasonic appearance simulating neoplasm. *Br J Radiol* 1981; **54**: 679-681
21 **Hattori M**, Inui K, Yoshino J, Miyoshi H, Okushima K, Nakamura Y, Naito T, Imaeda Y, Horibe Y, Hattori T, Nakazawa S. [Usefulness of contrast-enhanced ultrasonography in the differential diagnosis of polypoid gallbladder lesions] *Nippon Shokakibyo Gakkai Zasshi* 2007; **104**: 790-798
22 **Adamietz B**, Wenkel E, Uder M, Meyer T, Schneider I, Dimmler A, Bautz W, Janka R. Contrast enhanced sonography of the gallbladder: a tool in the diagnosis of cholecystitis? *Eur J Radiol* 2007; **61**: 262-266
23 **Xu HX**, Chen LD. Villous adenoma of extrahepatic bile duct: contrast-enhanced sonography findings. *J Clin Ultrasound* 2008; **36**: 39-41
24 **Torzilli G**, Del Fabbro D, Palmisano A, Donadon M, Montorsi M. Contrast-enhanced intraoperative ultrasonography: a valuable and not any more monocentric diagnostic technique performed in different ways. *Ann Surg* 2007; **245**: 152-153; author reply 152-153
25 **Torzilli G**, Del Fabbro D, Olivari N, Calliada F, Montorsi M, Makuuchi M. Contrast-enhanced ultrasonography during liver surgery. *Br J Surg* 2004; **91**: 1165-1167
26 **Cerwenka H**. Intraoperative ultrasonography during planned liver resections remains an important surgical tool. *Surg Endosc* 2008; **22**: 1137-1138

S- Editor Wang JL **L- Editor** Logan S **E- Editor** Zheng XM

World Journal of Radiology

Online Submissions: http://www.wjgnet.com/1949-8470office
wjr@wjgnet.com
doi:10.4329/wjr.v1.i1.45

World J Radiol 2009 December 31; 1(1): 45-49
ISSN 1949-8470 (online)

OBSERVATION

Dimitris Karacostas, MD, PhD, *Series Editor*

Neuroimaging in human prion disease: Searching in the mist

Panayotis Ioannides, Dimitris Karacostas

Panayotis Ioannides, Dimitris Karacostas, B' Department of Neurology, AHEPA University Hospital, Thessaloniki 54636, Greece
Author contributions: Ioannides P and Karacostas D studied the conception, design of the study, collected, analyzed and interpreted the data, wrote and revised the manuscript.
Correspondence to: Dimitris Karacostas, MD, PhD, B' Department of Neurology, AHEPA University Hospital, Thessaloniki 54636, Greece. bneurol@med.auth.gr
Telephone: +30-2310-994677 Fax: +30-2310-994689
Received: November 18, 2009 Revised: December 22, 2009
Accepted: December 25, 2009
Published online: December 31, 2009

Abstract

Human prion disease is a rare, uniformly fatal neurodegenerative disorder.Its precise pathogenesis is obscure. The clinical profile of the disease differs among its various forms. There are no definitive diagnostic tests (except for brain biopsy) or proven treatment. To increase the clinical diagnostic sensitivity and specificity, three laboratory tests, including electroencephalogram, cerebrospinal fluid testing for 14-3-3 protein, and magnetic resonance imaging, are currently used. Additionally, proton magnetic resonance spectroscopy, positron emission tomography and single photon emission computed tomography can provide interesting and novel results in the research of human prion disease.

Key words: Human prion disease; Creutzfeldt-Jakob disease; Neuroimaging; Magnetic resonance imaging

Peer reviewers: Mario Mascalchi, MD, PhD, Professor, Radiodiagnostic Section, Department of Clinical Physiopathology, University of Florence, Viale Morgagni 50134, Florence, Italy; Tarik F Massoud, MB, BCh, BAO, LRCPI, LRCSI, MA, MD, PhD, FRCR, Department of Radiology, University of Cambridge, Addenbrooke's Hospital, Box 219, Hills Road, Cambridge, CB2 2QQ, United Kingdom

Ioannides P, Karacostas D. Neuroimaging in human prion disease: Searching in the mist. *World J Radiol* 2009; 1(1): 45-49 Available from: URL: http://www.wjgnet.com/1949-8470/full/v1/i1/45.htm DOI: http://dx.doi.org/10.4329/wjr.v1.i1.45

INTRODUCTION

Human prion disease is a rare, uniformly fatal progressive neurodegenerative disorder, characterized by the deposition of an abnormal prion protein (PrP) in the central nervous system[1]. The most common form of human prion disease is Creutzfeldt-Jakob disease (CJD) and the whole nosological spectrum has been further divided into four categories. (1) Sporadic CJD (sCJD) arising from either a spontaneous PrP gene mutation or from a stochastic PrP structural change to the abnormal form. The host codon 129 genotype and the molecular strain of the deposited prion agent affect the phenotype[1,2]; (2) Iatrogenic prion disease, caused by infection (prion transmission) from medical (blood transfusion, human growth hormone) or surgical (corneal, dura mater grafts) procedures[1,2]; (3) Variant CJD (vCJD) which is causally linked to bovine (cattle) spongiform encephalopathy prion agent[1-3]; and (4) Inherited or genetic prion disease, caused by autosomal dominant PrP gene mutations (such as *E220k*, *P102L*) or insertions (such as ins144bp, ins24bp) on human chromosome 20[1,2]. The clinicopathological spectrum is further influenced by polymorphisms at codon 129 of the PrP gene[1-3].

The precise pathogenetic mechanism underlying the neurological illness is at present obscure. The clinical profile of the disease differs among its various forms. Early ante-mortem diagnosis is challengingly difficult and no definitive diagnostic tests (except for brain

biopsy) or proven treatment modalities are available. Most importantly, other potentially treatable diseases including infectious, inflammatory, autoimmune, toxic, and metabolic diseases should initially be excluded[1-4].

In addition to abnormal PrP straining, the neuropathological changes are characterized by neuronal loss, astrocytic gliosis, and spongiform change[1-3]. The initial diagnostic suspicion of prion disease is clinical, usually raised by various combinations of rapidly progressive cognitive impairment, psychiatric features, cerebellar ataxia, myoclonus, visual disturbances, pyramidal or extrapyramidal signs and terminal akinetic mutism[3,4]. However, significant clinical heterogeneity and different phenotypes occur in all forms of human prion disease [sCJD, vCJD, genetic and iatrogenic CJD (iCJD)], and are paralleled to variations in neuropathology[1-3,5].

DIAGNOSTIC LABORATORY TESTS

Three laboratory tests, including electroencephalogram (EEG), cerebrospinal fluid (CSF) testing for 14-3-3 protein, and magnetic resonance imaging (MRI) are currently used to increase the clinical diagnostic sensitivity and specificity[2,6,7], and have been included in the World Health Organization (WHO) diagnostic criteria for vCJD[8] and sCJD[9]. The EEG, in around two thirds of cases, may show progressive deterioration with the appearance of periodic sharp wave complexes, the absence of which does not exclude the diagnosis[1,6]. Also, these EEG complexes may be present in other conditions, such as hepatic encephalopathy, drug-heavy metals toxicity and Alzheimer's disease, while they are absent in vCJD[1].

CSF 14-3-3 is a normal neuronal protein that is released into the CSF following neuronal damage, with no specific connection to CJD[1]. However, it shows a surprisingly high specificity and sensitivity (around 94%) to sCJD[6] and therefore it should be only valid in the appropriate clinical setting[1]. When this test is used in unselected patients with rapidly progressive dementia, false positive results can be found in 12% of them[10]. Furthermore, fatal insomnia, a rare inherited form of prion disease, does not increase the CSF levels of 14-3-3 protein, in almost all cases[11].

Over the past decade, the non-invasive nature of MRI, the improved MR sequences used[2] and the availability of clinical-imaging-neuropathological correlations[12,13], have all contributed to an increased importance of MRI in the diagnosis of human prion disease[14], and have been included in the diagnostic criteria for vCJD[8]. Additionally, proton magnetic resonance spectroscopy (MRS)[3], positron emission tomography (PET)[15] and single photon emission computed tomography (SPECT)[16] can provide interesting and novel but sometimes puzzling results in the research of human prion disease.

NEUROIMAGING FINDINGS ON MRI

A symmetric high signal in the caudate and putamen is typical on fluid-attenuated inversion recovery (FLAIR) and diffusion weighted images (DWI) in sCJD[17]. More recent reports have added to the above the significance of "cortical ribbon" hyper-intensity, with a higher sensitivity to DWI[12,18] (Figure 1A and B). Nevertheless, the findings in a comprehensive, multicenter international study, strongly argue that characteristic MR lesion profiles may occur in each molecular subtype of sCJD[12]. However, in another study, no abnormality on any MR sequence was found, in 5 of 8 patients with methionine homozygotes (MM2 subtype)[19]. Although the mechanism underlying the MR signal change is controversial[2], a recent small study found that apparent diffusion coefficient (ADC) values, decrease with increasing spongiform change ($P < 0.001$) and PrP deposition ($P = 0.003$) in deep gray matter[13] and increased signals in DWI are characterized by reduced ADC values, which quantify regional water diffusion[2] (Figure 1B and C). Serial DWI has shown that the extension of high signals increases with disease progression[20,21]. In contrast, initial hyper intensity disappeared in the late disease stages[20,22].

In iCJD, incubation periods range from months to up to 30 years and the imaging patterns observed in recipients seem to differ according to the type of donor materials[2]. In human growth hormone recipients, bilaterally symmetric high signals can be observed in caudate head and putamen[2,23]. Similar findings have been reported in case reports of dura mater recipients[24]. However, atrophy is the only imaging finding in larger series of dural grafts[25]. In prion infection due to blood transfusion from asymptomatic donors who later developed vCJD, the pre-mortem MRI is normal[2] or the pulvinar sign becomes evident as the disease clinically progresses[26].

In vCJD, bilateral symmetric high pulvinar signal, as seen on T2 weighted imaging (T2WI), FLAIR (most sensitive) and DWI has been included in the WHO diagnostic criteria[8]. When this pulvinar sign is associated with hyper-intensity in dorsomedial thalamic nuclei, the "hockey stick" sign develops[27] (Figure 1F-H). The above mentioned pulvinar or hockey stick signs are the most consistent MRI findings in any human prion disease, possibly because only one molecular strain of the disease has been found in vCJD[3]. Finally, in confused or agitated patients with their standard MR sequences degraded by movement artefact, only DWI can provide important diagnostic data[2] (Figure 1I and J).

In inherited prion disease, MR changes are non-specific. However, imaging is required to exclude other prion and non-prion diseases. Imaging reports indicate normal findings[5,28], cortical or cerebellar atrophy or decreased basal ganglia signals[28] (Figure 1D and E). Also,

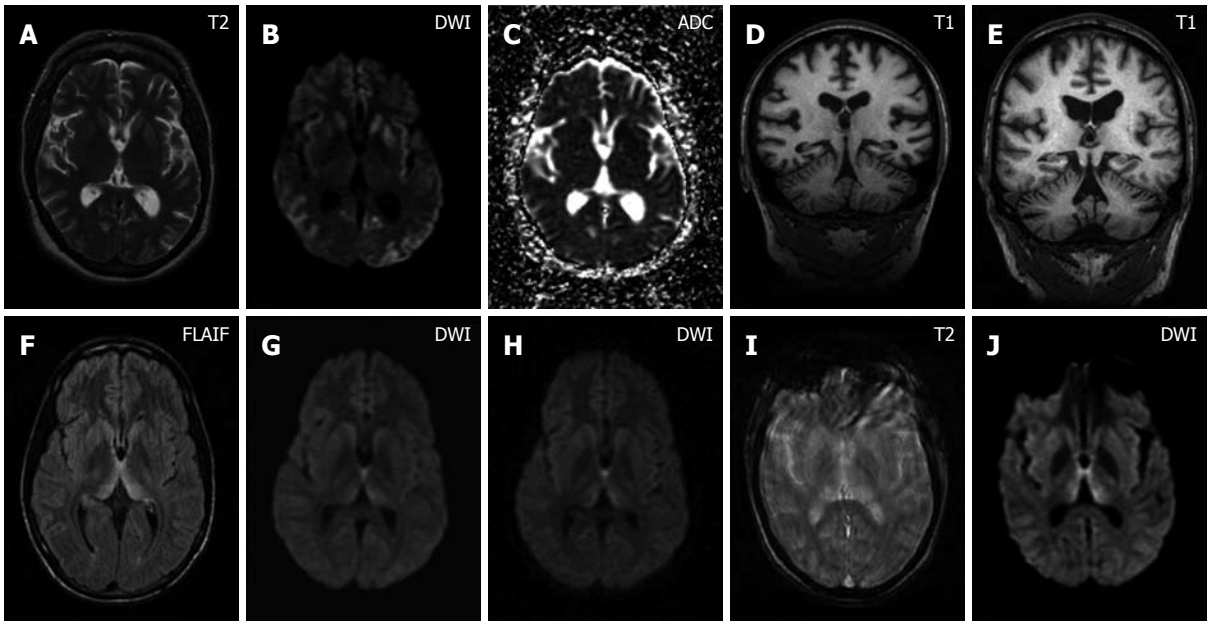

Figure 1 MRI sequences of a patient with sporadic CJD (A-C), inherited CJD (D, E) and variant CJD (F-J). A: Axial T2 weighted image shows a mild signal increase in the left putamen only; B: Axial diffusion weighted images (b = 1000) shows increased signals in both putamina and caudate nuclei (more on left than right),along with cortical hyper-intensity ("ribbons") in both insulae as well as in the frontal, temporal and occipital cortex; C: Apparent diffusion coefficient map demonstrates reduced signals in the areas which were hyperintense on the DWI confirming restricted water diffusion in these regions; D: The coronal T1 MRI shows supratentorial cortical and cerebellar atrophy in an inherited CJD case; E: MRI shows marked supratentorial atrophy with enlarged lateral ventricles accompanying cerebellar atrophy with prominent enlargement of the fourth ventricle in another case with inherited CJD; F: Axial fluid-attenuated inversion recovery image reveals the "hockey stick" sign, with hyper-intensity in the dorsomedial thalamic nuclei and pulvinar bilaterally in a patient with vCJD; G: Axial DWI (b = 1000) also shows increased signals which are less marked than on FLAIR image; H: DWI acquired after 1 mo demonstrates progression of the signal change in the thalami; I: Limited diagnostic value of axial T2 image is degraded by movement in a patient with vCJD; J: DWI (b = 1000) shows a high signal in the dorsomedial thalamic nuclei and pulvinar in the same case as above (All the above images have been reproduced and adapted by permission from BMJ Publishing Group Ltd. Macfarlane RG, Wroe SJ, Collinge J, Yousry TA, Jäger HR. Neuroimaging findings in human prion disease. *J Neurol Neurosurg Psychiatry* 2007; 78: 664-670).

there is no evidence suggesting the most useful MR sequences in the diagnosis of this inherited disorder[2].

FINDINGS ON PROTON MRS

This non-invasive method is used to assess the spectra of several brain metabolites, such as N-acetylaspartate (NAA), creatine and myo-inositol (MI) and to measure these compounds in both absolute values and ratios, in specific brain regions[2,4]. Considering the NAA a neuronal marker[29], and MI a glial marker[4], proton MRS used as an additional tool along with other MR sequences (FLAIR, DWI, T2WI) is of value in the study of human prion disease. Reduced absolute levels or ratios of NAA and increased MI values, have been reported in sporadic[4,30], variant[30,31], iatrogenic[23] and inherited[32] CJD. The pattern of these metabolic changes on MRS matches the MRI findings on FLAIR, T2[30] and DWI[14]. Nevertheless, important questions still remain to be answered. A recent prospective MRS study[4] showed that the most intense metabolic changes are observed in the thalamus and cerebellum of prion patients (sCJD), while the striatum and cerebral cortex are less affected, despite the existence of positive T2 and DWI findings.

PET AND SPECT FINDINGS

At present, the high cost of PET seems to outweigh the benefit obtained in the investigation of human prion disease. In general, PET reveals generalized hypometabolism that is correlated with histological neuronal loss and astrogliosis[15,33] along with spongiform changes[33]. However, this hypo-metabolism is more pronounced in the cerebellum and cortex than in the thalamus and striatum[15], unmatching the distribution of lesions seen on MRI.

Accordingly, widespread hypoperfusion has been demonstrated using SPECT in all forms of human prion disease[2]. The majority of sCJD patients reveal decreased cerebral perfusion, including the occipital cortex, cerebellum or the entire hemisphere[16]. Also, more regional changes in perfusion with SPECT can be detected in early stages of the disease than MRI changes[34].

CONCLUSION

As different types of disease arise, changes in the neuroimaging patterns of human prion disease continue to puzzle clinicians and researchers alike.

At present, the most consistent MRI change is the pulvinar sign in vCJD patients. When the dorsomedial thalamic nuclei are involved, the "hockey stick" sign provides additional clues[3,8,27]. Since bilateral high signals are observed in the caudate and putamen, and "cortical ribbon" hyper-intensity is found on DWI of

sCJD patients[12,17,18], the diagnostic sensitivity of MRI is further augmented. Newer imaging techniques, such as proton MRS and SPECT seem to provide useful data for identifying the patterns in all forms of human prion disease[23,31,32].

Future research should eventually aim at studying the increasing number of "probable" prion cases, through multicenter international studies, utilizing combined imaging modalities, such as serial DWI with MRS, SPECT with MR perfusion imaging and MRI with *in vivo* PET probe to label prion plaques[2,4,33]. Hopefully, this perspective will elucidate some of the debatable issues presented and the "mist" will start to resolve.

REFERENCES

1 **Knight RS**, Will RG. Prion diseases. *J Neurol Neurosurg Psychiatry* 2004; **75** Suppl 1: i36-i42
2 **Macfarlane RG**, Wroe SJ, Collinge J, Yousry TA, Jäger HR. Neuroimaging findings in human prion disease. *J Neurol Neurosurg Psychiatry* 2007; **78**: 664-670
3 **Collinge J**. Prion diseases of humans and animals: their causes and molecular basis. *Annu Rev Neurosci* 2001; **24**: 519-550
4 **Lodi R**, Parchi P, Tonon C, Manners D, Capellari S, Strammiello R, Rinaldi R, Testa C, Malucelli E, Mostacci B, Rizzo G, Pierangeli G, Cortelli P, Montagna P, Barbiroli B. Magnetic resonance diagnostic markers in clinically sporadic prion disease: a combined brain magnetic resonance imaging and spectroscopy study. *Brain* 2009; **132**: 2669-2679
5 **Collinge J**. Human prion diseases: etiology and clinical features. In: Growdon JH, Rossor MN, editors. The Dementias. Boston: Butterworth-Heinemann, 1998: 113-150
6 **Zerr I**, Pocchiari M, Collins S, Brandel JP, de Pedro Cuesta J, Knight RS, Bernheimer H, Cardone F, Delasnerie-Lauprêtre N, Cuadrado Corrales N, Ladogana A, Bodemer M, Fletcher A, Awan T, Ruiz Bremón A, Budka H, Laplanche JL, Will RG, Poser S. Analysis of EEG and CSF 14-3-3 proteins as aids to the diagnosis of Creutzfeldt-Jakob disease. *Neurology* 2000; **55**: 811-815
7 **Steinhoff BJ**, Zerr I, Glatting M, Schulz-Schaeffer W, Poser S, Kretzschmar HA. Diagnostic value of periodic complexes in Creutzfeldt-Jakob disease. *Ann Neurol* 2004; **56**: 702-708
8 **World Health Organization**. The Revision of the Surveillance Case Definition for variant Creutzfeldt-Jakob Disease: Report of a WHO Consultation, Edinburg. *World Health Organ Tech Rep Ser* 2004
9 **Mastrianni JA**. Prion diseases: transmissible spongiform encephalopathies. In: Noseworthy JH, editor. Neurological therapeutics: principles and practice. Oxon: Informa Health Care, 2006: 1163-1168
10 **Burkhard PR**, Sanchez JC, Landis T, Hochstrasser DF. CSF detection of the 14-3-3 protein in unselected patients with dementia. *Neurology* 2001; **56**: 1528-1533
11 **Krasnianski A**, Bartl M, Sanchez Juan PJ, Heinemann U, Meissner B, Varges D, Schulze-Sturm U, Kretzschmar HA, Schulz-Schaeffer WJ, Zerr I. Fatal familial insomnia: Clinical features and early identification. *Ann Neurol* 2008; **63**: 658-661
12 **Meissner B**, Kallenberg K, Sanchez-Juan P, Collie D, Summers DM, Almonti S, Collins SJ, Smith P, Cras P, Jansen GH, Brandel JP, Coulthart MB, Roberts H, Van Everbroeck B, Galanaud D, Mellina V, Will RG, Zerr I. MRI lesion profiles in sporadic Creutzfeldt-Jakob disease. *Neurology* 2009; **72**: 1994-2001
13 **Manners DN**, Parchi P, Tonon C, Capellari S, Strammiello R, Testa C, Tani G, Malucelli E, Spagnolo C, Cortelli P, Montagna P, Lodi R, Barbiroli B. Pathologic correlates of diffusion MRI changes in Creutzfeldt-Jakob disease. *Neurology* 2009; **72**: 1425-1431
14 **Tschampa HJ**, Zerr I, Urbach H. Radiological assessment of Creutzfeldt-Jakob disease. *Eur Radiol* 2007; **17**: 1200-1211
15 **Engler H**, Lundberg PO, Ekbom K, Nennesmo I, Nilsson A, Bergström M, Tsukada H, Hartvig P, Långström B. Multitracer study with positron emission tomography in Creutzfeldt-Jakob disease. *Eur J Nucl Med Mol Imaging* 2003; **30**: 187
16 **Henkel K**, Meller J, Zerr I, Schulz-Schaeffer W, Schroeter A, Tschampa HJ, Kretzschmar HA, Becker W, Poser S. Single photon emission computed tomography (SPECT) in 19 patients with Creutzfeldt-Jakob disease. *J Neurol* 1999; **246** (Suppl 1): 490
17 **Schröter A**, Zerr I, Henkel K, Tschampa HJ, Finkenstaedt M, Poser S. Magnetic resonance imaging in the clinical diagnosis of Creutzfeldt-Jakob disease. *Arch Neurol* 2000; **57**: 1751-1757
18 **Shiga Y**, Miyazawa K, Sato S, Fukushima R, Shibuya S, Sato Y, Konno H, Doh-ura K, Mugikura S, Tamura H, Higano S, Takahashi S, Itoyama Y. Diffusion-weighted MRI abnormalities as an early diagnostic marker for Creutzfeldt-Jakob disease. *Neurology* 2004; **63**: 443-449
19 **Krasnianski A**, Meissner B, Schulz-Schaeffer W, Kallenberg K, Bartl M, Heinemann U, Varges D, Kretzschmar HA, Zerr I. Clinical features and diagnosis of the MM2 cortical subtype of sporadic Creutzfeldt-Jakob disease. *Arch Neurol* 2006; **63**: 876-880
20 **Ukisu R**, Kushihashi T, Kitanosono T, Fujisawa H, Takenaka H, Ohgiya Y, Gokan T, Munechika H. Serial diffusion-weighted MRI of Creutzfeldt-Jakob disease. *AJR Am J Roentgenol* 2005; **184**: 560-566
21 **Russmann H**, Vingerhoets F, Miklossy J, Maeder P, Glatzel M, Aguzzi A, Bogousslavsky J. Sporadic Creutzfeldt-Jakob disease: a comparison of pathological findings and diffusion weighted imaging. *J Neurol* 2005; **252**: 338-342
22 **Matoba M**, Tonami H, Miyaji H, Yokota H, Yamamoto I. Creutzfeldt-Jakob disease: serial changes on diffusion-weighted MRI. *J Comput Assist Tomogr* 2001; **25**: 274-277
23 **Oppenheim C**, Zuber M, Galanaud D, Detilleux M, Bolgert F, Mas JL, Chiras J, Meder JF. Spectroscopy and serial diffusion MR findings in hGH-Creutzfeldt-Jakob disease. *J Neurol Neurosurg Psychiatry* 2004; **75**: 1066-1069
24 **Preusser M**, Ströbel T, Gelpi E, Eiler M, Broessner G, Schmutzhard E, Budka H. Alzheimer-type neuropathology in a 28 year old patient with iatrogenic Creutzfeldt-Jakob disease after dural grafting. *J Neurol Neurosurg Psychiatry* 2006; **77**: 413-416
25 **Martínez-Lage JF**, Poza M, Sola J, Tortosa JG, Brown P, Cervenáková L, Esteban JA, Mendoza A. Accidental transmission of Creutzfeldt-Jakob disease by dural cadaveric grafts. *J Neurol Neurosurg Psychiatry* 1994; **57**: 1091-1094
26 **Wroe SJ**, Pal S, Siddique D, Hyare H, Macfarlane R, Joiner S, Linehan JM, Brandner S, Wadsworth JD, Hewitt P, Collinge J. Clinical presentation and pre-mortem diagnosis of variant Creutzfeldt-Jakob disease associated with blood transfusion: a case report. *Lancet* 2006; **368**: 2061-2067
27 **Zeidler M**, Sellar RJ, Collie DA, Knight R, Stewart G, Macleod MA, Ironside JW, Cousens S, Colchester AC, Hadley DM, Will RG. The pulvinar sign on magnetic resonance imaging in variant Creutzfeldt-Jakob disease. *Lancet* 2000; **355**: 1412-1418
28 **Zerr I**, Giese A, Windl O, Kropp S, Schulz-Schaeffer W, Riedemann C, Skworc K, Bodemer M, Kretzschmar HA, Poser S. Phenotypic variability in fatal familial insomnia (D178N-129M) genotype. *Neurology* 1998; **51**: 1398-1405
29 **Kantarci K**, Knopman DS, Dickson DW, Parisi JE, Whitwell

JL, Weigand SD, Josephs KA, Boeve BF, Petersen RC, Jack CR Jr. Alzheimer disease: postmortem neuropathologic correlates of antemortem 1H MR spectroscopy metabolite measurements. *Radiology* 2008; **248**: 210-220

30 **Pandya HG**, Coley SC, Wilkinson ID, Griffiths PD. Magnetic resonance spectroscopic abnormalities in sporadic and variant Creutzfeldt-Jakob disease. *Clin Radiol* 2003; **58**: 148-153

31 **Cordery RJ**, MacManus D, Godbolt A, Rossor MN, Waldman AD. Short TE quantitative proton magnetic resonance spectroscopy in variant Creutzfeldt-Jakob disease. *Eur Radiol* 2006; **16**: 1692-1698

32 **Waldman AD**, Cordery RJ, MacManus DG, Godbolt A, Collinge J, Rossor MN. Regional brain metabolite abnormalities in inherited prion disease and asymptomatic gene carriers demonstrated in vivo by quantitative proton magnetic resonance spectroscopy. *Neuroradiology* 2006; **48**: 428-433

33 **Goldman S**, Laird A, Flament-Durand J, Luxen A, Bidaut LM, Stanus E, Hildebrand J, Przedborski S. Positron emission tomography and histopathology in Creutzfeldt-Jakob disease. *Neurology* 1993; 43: 1828-1830

34 **Arata H**, Takashima H, Hirano R, Tomimitsu H, Machigashira K, Izumi K, Kikuno M, Ng AR, Umehara F, Arisato T, Ohkubo R, Nakabeppu Y, Nakajo M, Osame M, Arimura K. Early clinical signs and imaging findings in Gerstmann-Sträussler-Scheinker syndrome (Pro102Leu). *Neurology* 2006; **66**: 1672-1678

S- Editor Wang JL **L- Editor** Wang XL **E- Editor** Zheng XM

World Journal of Radiology

Online Submissions: http://www.wjgnet.com/1949-8470office
wjr@wjgnet.com
doi:10.4329/wjr.v1.i1.50

World J Radiol 2009 December 31; 1(1): 50-62
ISSN 1949-8470 (online)

GUIDELINES FOR CLINICAL PRACTICE

Endovascular approach to acute aortic trauma

Riyad Karmy-Jones, Desarom Teso, Nicole Jackson, Lisa Ferigno, Robert Bloch

Riyad Karmy-Jones, Desarom Teso, Nichole Jackson, Division of Cardiac, Thoracic and Vascular Surgery, Southwest Washington Medical Center, Suite 330 400 NE Mother Joseph Place, Vancouver, WA 98664, United States
Riyad Karmy-Jones, Lisa Ferigno, Division of Trauma/Critical Care, Southwest Washington Medical Center, Vancouver, WA 98664, United States
Robert Bloch, Division of Radiology, Southwest Washington Medical Center, Vancouver, WA 98664, United States
Author contributions: Karmy-Jones R, Teso D, Jackson N, Ferigno L and Bloch R all contributed in the writing and editing of this paper.
Correspondence to: Riyad Karmy-Jones, MD, Medical Director, Division of Cardiac, Thoracic and Vascular Surgery, Southwest Washington Medical Center, Suite 330 400 NE Mother Joseph Place, Vancouver, WA 98664, United States. rkarmyjo@swmedicalcenter.com
Telephone: +1-360-5141854 Fax: +1-360-5146063
Received: December 2, 2009 Revised: December 18, 2009
Accepted: December 21, 2009
Published online: December 31, 2009

Abstract

Traumatic thoracic aortic injury remains a major cause of death following motor vehicle accidents. Endovascular approaches have begun to supersede open repair, offering the hope of reduced morbidity and mortality. The available endovascular technology is associated with specific anatomic considerations and complications. This paper will review the current status of endovascular management of traumatic thoracic aortic injuries.

Key words: Aorta; Complications; Outcomes; Traumatic; Endovascular

Peer reviewer: Takao Hiraki, MD, Radiology, Okayama University Medical School, 3-5-1 Shikatacho, Okayama 700-0861, Japan

Karmy-Jones R, Teso D, Jackson N, Ferigno L, Bloch R. Endovascular approach to acute aortic trauma. *World J Radiol* 2009; 1(1): 50-62 Available from: URL: http://www.wjgnet.com/1949-8470/full/v1/i1/50.htm DOI: http://dx.doi.org/10.4329/wjr.v1.i1.50

INTRODUCTION

The treatment of aortic rupture has significantly evolved since Parmley's landmark 1958 paper[1]. Rather than angiography followed by immediate open repair, the use of computed tomography angiogram (CTA), early institution of β-blockade and pressure control to reduce the risk of early rupture, and advances in techniques including left heart bypass has allowed more selective management of patients[2-8]. In addition, increasing use of seat restraints appears to be associated with less severe aortic and associated injury, further enhancing survival[9]. Nevertheless, aortic rupture remains a leading cause of fatalities, particularly after motor vehicle accidents[10].

The incidence of traumatic aortic disruption varies from center to center. Looking at all trauma-related mortality, blunt aortic rupture may be second only to head injury as the primary cause of death. Despite this, accepting that there are approximately 8000 cases/year in the United States, and given that as many as 85% of victims die at the scene, then only 1000-1500 cases/year survive to be treated. In one of the largest contemporary series, 274 patients were admitted to 50 institutions over 2.5 years. If these cases were distributed evenly, the average institution would have seen only 2.2 cases/year[11]. In practice some centers may manage 8-15 cases/year, while the majority may encounter 1-2 at most.

Amidst this era of improved operative outcomes and medical management, endovascular stent grafts have become a possible third option. In North America, the concept of thoracic endografting, as an extension of abdominal endograft technology, was greatly stimulated by the Stanford group[12,13]. Their initial

primary interest, and indeed the bulk of the literature since, was with atherosclerotic aneurysms. We now know that endografting is an attractive option that can avoid the morbidity of a thoracotomy in patients with multiple injuries, and that it appears to reduce the risk of paralysis[14-18]. Some centers have seen dramatic improvements in outcome using the endovascular approach[19-21]. In North America, currently 2/3 of blunt aortic injury are managed endovascularly[22]. As with all invasive procedures, there are specific complications and anatomic considerations that need to be incorporated into the planning of endovascular treatments of traumatic thoracic injuries. The purpose of this paper is to compare outcomes of endovascular approaches to open repair, review pertinent anatomy, imaging techniques and approaches, and to discuss complications and their management.

OUTCOMES OF ENDOVASCULAR STENTS UTILIZED IN THE TRAUMA SETTING

A number of series have been published which support the notion that endovascular stents, in the setting of traumatic aortic disruption, have low mortality (predominantly related to associated injuries) and essentially no risk of post-procedure paralysis. When reviewing these data, it is important to consider the span of time in which the experience was accrued (as stent technology has changed significantly over the past few years), recognize the difference between the acute (whether defined as within 24 h of injury or a longer period) *vs* chronic, and to consider what the indications for stent grafting and contra-indications to open repair were. We have selected those series published between 2002-2006 (11 reports), comprising 167 patients, the youngest being 16 years of age[5,15,16,23-31]. These series ranged from 5 to 30 cases, over time periods ranging from 1 to 7 years. Average follow up among the 10 series with at least one year follow up was 24 mo. Virtually all stents were industry made, although they varied between 'dedicated" thoracic stents to a variety of cuff extenders. There were 7 (4%) deaths, 2 of which were procedure-related (one collapse and rupture, one stroke). Type I endoleak occurred in 8 instances (4.7%), 2 healing spontaneously, 6 requiring further stenting and/or balloon dilation. There were 2 iliac ruptures reported, and 3 (1.7%) cases of acute stent collapse requiring operative intervention. There were 2 cases of non-fatal stroke and 1 of brachial occlusion requiring thrombectomy. These experiences, in combination with an overall major non-fatal complication rate (excluding endoleak) of 4.3% and mortality of 3.6% justifies the excitement that endovascular approaches have provoked in the management of traumatic aortic rupture. Hershberger and colleagues summarized the outcome of 811 patients among 109 publications. Overall technical success rate was 93.6% and mortality 9.5% (72 patients). Eight (1%) of the deaths were directly related to complications of the endovascular procedure, of which two were due to stent collapse, one of aortic enteric fistula and others to continued hemorrhage despite stent placement[17].

In addition, endografts may also be used not as a definitive repair, but in complicated cases as a "bridge" to definitive treatment in selected patients who are not suitable candidates for either operative repair or medical management[23,32].

COMPARISON BETWEEN ENDOVASCULAR AND OPEN REPAIR

It is inherently difficult to retrospectively compare two techniques that are not necessarily applied to the same patient population with respect to risk assessment, operative experience and institutional biases. Each center has sufficiently different patient populations and management strategies to make it difficult to make broad generalizations based on an individual study. Again, recognizing that this is not a complete review of all available works, we reviewed five papers, published between 2004 and 2006, that specifically compared outcomes within their respective institutions between the 2 approaches[5,9,16,24,33]. A total of 108 patients underwent open repair. There were 15 deaths (14%) and 4 (4%) cases of new post-operative paralysis. Ninety-three patients underwent endovascular repair, 9 (9%) died and no paralysis/paraplegia was observed. Only one death was procedure-related among the stent graft group (acute stent collapse).

An American Association for the Surgery of Trauma multicenter study compared the outcomes of endovascular *vs* open repair. One hundred and twenty-five patients underwent endovascular repair with 20% developing stent-related complications. Of 18 patients (14%) with endoleak, 6 required open repair. Paralysis/paraplegia occurred in 0.8% compared to 2.9% among the 68 patients who underwent open repair. When adjusted for extrathoracic injuries, hypotension and age, endovascular repair had a significantly lower mortality compared to open repair[22].

Tang and associates presented the results of a meta-analysis comparing the 30-d outcomes between 278 aortic ruptures managed surgically *vs* 355 managed by endovascular means. There were no significant differences in injury severity or age between the groups. The endovascular group had significantly lower mortality (7.6% *vs* 15.2%, $P = 0.008$), paraplegia (0% *vs* 5.5%, $P < 0.0001$) and stroke (0.81% *vs* 5.1%, $P = 0.003$) compared to the open surgical repair cohort[34].

These small comparisons demonstrate that when feasible, at least in the population over 18 to 20 years, endovascular repair appears to be associated with a markedly lower paralysis rate than open repair, and

length of stay may be reduced compared to open repair, however, acute outcome is probably more related to overall injury severity than approach. It further supports the notion that across many institutions the acute outcomes are as good as open repair, and probably better, but that within institutions with good experience of both approaches outcomes are comparable.

ENDOVASCULAR REPAIR *VS* MEDICAL MANAGEMENT

Institution of strict "anti-impulse" therapy should occur once the diagnosis of aortic rupture is suspected[5,35]. The "ideal" blood pressure depends upon the patient's age and presenting blood pressure. Until recently, the goal was a systolic blood pressure of < 120 mmHg and/or mean arterial pressure < 60-70 mmHg. More recently it has been argued that a blood pressure of "less than what the patient was admitted with" may be more appropriate[10,36]. When strict blood pressure control is implemented, in stable patients, the risk of rupture in the first week may be as low as 5% or less[10]. Some series have noted improved outcomes with both delayed open and endovascular repair, but this may reflect some selection bias[5]. Nevertheless, delayed repair has been shown to be associated with improved outcomes, both for open and endovascular approaches[37].

Reasons for delaying operative intervention include severe head injury, blunt cardiac injury, solid organ injury and/or acute lung injury[7,38]. In these instances, we have favored serial surveillance imaging (usually with CTA) every 48 h for 7-10 d, to detect any change in the size or character of the lesion[2]. While the natural history of residual pseudoaneurysms appears to follow those of non-traumatic atherosclerotic aneurysms, these lesions should not, especially in young patients, be considered completely benign, and we favor early intervention as soon as medically stable.

Tight medical control of blood pressure may not be possible in every case. Many patients require other interventions, and monitoring and controlling blood pressure during these can be difficult. There are some hazards including renal and splanchnic insufficiency, and secondary brain injury especially in the setting of increased cranial pressure[32,39]. Although there is some controversy as to the value of driving up cerebral perfusion pressure, or assuming that an increased pressure translates to improved cerebral perfusion, there is general consensus that "high" pressure is associated with a lower risk of secondary brain injury[40-43]. Thus, closed head injury associated with evidence of increased intracranial pressure [by computed tomography (CT) and/or intracranial pressure monitoring] may actually mandate operative or endovascular repair. One significant advantage of endovascular repair over both operative and non-operative management is that after the stent is placed, in most cases it is possible to allow blood pressure to normalize, or even increase without the risk of bleeding or rupture. We caution that the risk of rupture, even with serial CT angiography and tight hemodynamic control, is not zero. Endovascular stents may be ideally utilized exactly in these patients who cannot undergo open operative repair because of significant co-morbidities.

The extent of injury may also impact the choice between medical and endovascular management. Minor aortic injuries, involving only small intimal defects, often heal without residual defects[4,44]. However, even small lesions can go on to rupture if blood pressure is not controlled[2]. Thus, if blood pressure can be reasonably controlled, and there are no contraindications to medical management, small intimal defects should be managed medically with close follow up. Even small pseudoaneurysms, in some cases, have healed[2]. Thus, while endovascular management appears to be an ideal solution in patients with significant co-morbidities, and who are judged to be at too high risk for prolonged medical management, it is not clear that this approach is better than medical management in patients with minimal injuries. One simple guideline is that if the lesion is minimal enough such that one would not consider open operative repair, than one should not rush to endovascular repair either.

ENDO-GRAFTS CURRENTLY AVAILABLE

The characteristics of an endograft designed for the thoracic aorta, as opposed to the abdominal aorta, include a long enough delivery system to reach the distal arch from the femoral artery, and flexibility to accommodate the curvature of the arch. There are variations between different types of graft in how they deploy, whether or not proximal and/or distal components are bare, whether or not they contain hooks, and how they are actually released from the constraining devices. In general, there has been a shift away from deploying devices in aortic trauma (and type B dissection) which rely on uncovered proximal landing zones because of concerns of aortic perforation[45]. An important consideration is that the average young trauma patient has an aortic diameter in the 20 mm range, which is too small for these devices which were designed for older, atherosclerotic, aortas[46]. Secondly, the use of endografts in the acute trauma setting is considered to be "off label" by the Federal Drug Administration (FDA) outside of trials. Currently, there is only one device approved by the FDA for use in the thoracic aorta, and then only for atherosclerotic aneurysms.

The Gore-TAG® (W.L. Gore & Associates, Flagstaff, AZ, USA) is constructed from ePTFE, wrapped in self-expanding nitinol stents which have a sutureless attachment. These flares can be placed partially across an orifice without occluding the orifice. The device is introduced through a 30-cm sheath, the outer diameter varying depending on the diameter of the graft. The delivery catheter is fairly flexible and 100 cm in length. The device is released by pulling a rip-cord that

unlaces the constraining system with rapid (less than a second) release starting in the center. This central deployment prevents a "wind sock" effect and there is rarely any need to critically lower blood pressure during deployment to beyond normal ranges to prevent distal migration. When advancing the catheter, there can be built-up tension, and so the device should be advanced just beyond the proposed landing zone and then brought back into the proper alignment just before deployment. One characteristic of the TAG device is that it rarely if ever jumps forward. Rather, it may drop a millimeter or two back (distally). In appropriately sized patients, the TAG offers an exceptionally good approach due to its flexibility and rapid deployment characteristics[9,47].

Two other companies, Cook and Medtronic, have also been developing and refining endografts for use in the thoracic aorta, and the early iterations, like the Gore, have proven very useful in trauma patients in Europe, Canada and Australia[26,27,30,33,48,49].

The Cook-Zenith TX2® (Cook, Bloomington, IN, USA) is made of woven polyester fabric over stainless steel Z-stents. The TX2 has a proximal form, which has no bare stents but does have 5 mm long barbs. The distal component does have a bare metal distal segment. The proximal device can be uniform or tapered. The diameters range from 28 to 42 mm (in 2 mm increments) and the lengths vary from 120 to 216 mm. The tapered form narrows at the third Z-stent and the distal diameter is 4 mm less than the proximal. The sheaths are pre-curved and 75 cm long. A 20 Fr sheath (OD 23 Fr) is used for 28-34 mm stents, and a 22 Fr sheath (OD 25 Fr) for 38-42 mm endografts. Although it would be rare to need it in the trauma setting, the TX2 is designed with a distal component, to allow modification of the distal portion of the graft to fit the anatomic requirements of the distal landing zone. This portion has an uncovered bare area. The device is unsheathed, but three trigger wires continue to constrain the device, reducing any "wind sock" effect, and allowing final careful positioning before complete release.

The Medtronic Talent® Thoracic graft has recently been released in Europe in a modified form, the Valiant® (Medtronic, Santa Rosa, CA, USA). The Valiant differs in that while it is still made of a low-profile polyester monofilament material, the nitinol stents are on the outside, and with two proximal configurations, one covered and the other with 12 mm flexible bare stents to allow adaptation to the aortic curvature and greater fixation. In addition, there has been improved conformability of the distal end which may be covered or have a bare extension as well (FreeFlo). The Medtronic company tends to recommend the FreeFlo model over the covered proximal stent as the experience, at least with non-traumatic aortic pathology, is that the increased flexibility allows the uncovered portion to conform well with the aorta, leading to better fixation. Like the Cook-TX2, the Valiant comes in both a proximal and distal (if needed) component, although with short lesions, the proximal component alone is often sufficient. Both come in straight or tapered versions. The delivery system involves an unsheathing maneuver. The device allows retraction and repositioning to permit exact placement. The Talent does come in a slightly smaller model than the Valiant, 22 mm, which may be useful in aortas with diameters of 18-19 mm diameter.

Because of the size constraints in the "typical" trauma patient, and because the arch is often acutely angled, some groups have used abdominal aortic cuff extenders rather than dedicated thoracic aortic stent grafts[28,31,50]. These are not only smaller, but may actually fit the aortic configuration of transected aortas better, albeit at the expense of needing multiple grafts, of an increased risk of Type Ⅲ endoleak, and of having to use the shorter delivery system that is designed for the infra-renal aorta[51]. The AneuRx® (Medtronic, Santa Rosa, CA, USA) cuff extenders range from 20-28 mm diameter, are 4 cm long, and are delivered through a 21 Fr catheter which is 59 cm long. The Gore-Excluder aortic cuffs® (W.L. Gore & Associates, Flagstaff, AZ, USA) are 3.3 cm long, have diameters of 23, 26 and 28.5 mm, and can be delivered *via* an 18 (for the 23 mm device) or 20 Fr sheath which is 61 cm long. On occasion a contra-lateral limb or iliac extender from the abdominal aortic set may fit the specific anatomic requirements.

Borsa and colleagues reviewed the anatomical features of 50 trauma patients with documented traumatic aortic rupture who underwent angiography[46]. The average age was 37 years. The mean distance between the superior aspect of the injury and the origin of the left subclavian artery was 5.8 mm along the inner curve and 14.9 mm along the outer curve. The mean diameter adjacent to the injury was 19.2 mm. The mean degree of curvature from the left subclavian artery and the inferior aspect of the injury was 54.0°. The mean length of the injury was 17 mm along the inner wall and 26 mm along the outer wall. In addition, the injury involved 1/4 of the circumference in 44%, 1/2 in 16%, 3/4 in 18% and the complete circumference in 22%. Finally, 28% had a bovine arch and 10% had aberrant origin of the left vertebral artery from the arch proximal to the left subclavian artery. The implications of this study are that given currently available technology, at least half of patients will require coverage of the left subclavian artery to obtain an even minimally acceptable landing zone, and at least half or more of patients will not be candidates for the TAG but will require smaller diameter devices.

ANATOMICAL CONSIDERATIONS

Anatomic considerations are listed in Table 1. The initial factor to be determined is the diameter of the proximal and distal landing zones. Measurements are taken from inner wall to inner wall. The diameter can be difficult to assess in the distal arch, but one method is to measure the transverse diameter at its widest point. In younger adults the aorta is relatively uniform through the arch.

Table 1 Anatomic considerations

Anatomical features to consider	Implications
Diameter of proximal and distal landing zones	Determines size of endograft that can/should be utilized
Distance from lesion to origin of left subclavian artery	Will obtaining an adequate landing zone require coverage of the left subclavian artery?
Distance from lesion to origin of left common carotid artery	If required, is there room to land distal to the origin of the left common carotid artery? Will there be room, if needed, to clamp distal to the origin or will circulatory arrest be needed if subsequent operative repair is needed?
Degree of curvature across the proximal landing zone	Is there a high likelihood that to avoid malposition along the inner curvature that the graft will have to placed more proximally?
Quality of the aorta	Is there significant thrombus and/or calcification that would pose a risk of stroke or Type I endoleak?
Quality of access vessels	Is the diameter sufficient to permit the required sheath? Are there more proximal calcifications and/or tortuosity that might prevent safe passage of the sheath?
Distance from proposed access vessel to the lesion	Does the system being used have sufficient length to reach the proposed site?
Length of the injury	If using cuffs, how many may be required to ensure fixation
Vascular anomalies	Anomalous origin of left vertebral artery? Patent LIMA graft? Aberrant origin of right subclavian artery?

Three-dimensional reconstruction and measurements of the descending aorta just at the level of the main pulmonary artery can help confirm estimations of the proximal landing zone diameter. The stent graft diameter should be approximately 10%-14% larger than the landing zone diameters.

Because most transections occur in proximity to the left subclavian, the next decision is whether to cover the subclavian origin or not. Deploying the graft within the distal curve ("grey zone") of the arch may result in partial occlusion of the aorta, increase the risk of stent migration and/or collapse, and result in an endoleak. The origin of the left subclavian artery can be marked and both the "drop down" distance measured based on the number of cuts of the CT, and the transverse measurement should be estimated. Ideally at least 2 cm of proximal and distal landing zone is recommended, but in some younger patients, with otherwise normal aortas, 1-cm has proven acceptable.

The proximal aortic landing zone and arch needs to be reviewed to assess for the presence of significant thrombus and/or calcification. Focal areas of calcification can result in elevating a "lip" of endograft, resulting in increased risk of proximal endoleak. Significant thrombus increases the risk of stroke and distal embolization.

The length of the aorta that needs to be covered is based on a minimum of a 2-cm landing zone. If using cuff extenders, usually three will be required to provide stability[31,51].

Having chosen the optimal size and type of endograft, the next consideration is the length of the delivery device. Commercial thoracic endograft delivery systems have sufficient length to reach the entire thoracic aorta from the femorals, but cuff extenders have delivery systems of only 61-cm that may not reach from the groin to the arch. Additionally, the quality and diameter of the proposed access arteries need to be evaluated. The diameter, angulation and degree of calcification should be determined. Calcifications are better seen with non-contrast images. A non-calcified vessel may tolerate a slightly oversized sheath, but a severely calcified vessel may not accept a sheath that would be predicted to fit based on size criteria alone.

PROCEDURE

Imaging

Because the majority of traumatic injuries are located within 2 cm of the origin of the left subclavian artery, they are in proximity to the arch. To visualize the anatomy properly, the most "open" view of the arch should be obtained. In younger patients, usually a left anterior oblique view at the 60-90° range is required. The optimal angle can be estimated from the CTA. During angiography, using a multi-marker pig tail catheter, one can be confident that the optimal view has been obtained when the marks are equidistant throughout the image. This will facilitate the most accurate positioning of the proximal graft and determine the length of coverage needed.

Accessing either the brachial artery for angiograms and or marking with a wire has been advocated by some groups[23]. This can augment precise localization of the graft relative to the origin of the left subclavian. Alternatively, in patients with severe acute arch angulation, placing a stiff wire from the right side may permit "straightening" during deployment[23]. We have not used the right brachial approach in the trauma setting, because of concerns of dissection and/or stroke.

Patient positioning is critical. The arms can obscure visualization of the relevant anatomy. Options include abducting them above the head or placing a roll under the left side to gain some 10°. If it is anticipated that brachial catheterization will be needed, the arm should be prepped out. Prior to prepping and draping the patient, fluoroscopy in key anticipated views should be quickly carried out to make sure that there are no leads in the way, and that the arch can be easily seen without obstruction.

General conduct of the procedure

Endovascular stent-grafting is an operative procedure, and should be performed in a room designed with this in mind, including sterile set up and laminar flow. It can be performed in a standard operating suite, using portable C-arm, but the image quality offered by multi-purpose suites with fixed fluoroscopy units provides significantly better resolution. General anesthesia with a single lumen endotracheal tube is sufficient, but has been done under sedation with local anesthesia in the rare stable patient. A right radial arterial line for blood pressure monitoring is optimal because the left subclavian may be covered or the left brachial artery needed for access. Depending on the angle needed to best visualize the arch, the arms may need to be elevated above the head or a bump placed under the left side. Prior to prepping, fluoroscopy should be performed to ensure that no tubes, lines or boney structures obscure the field. We have found it helpful to place a 5- or 6-Fr sheath and multi-marker pigtail catheter through the femoral artery opposite to the side through which the device will be deployed. This permits final angiographic marking with the non-deployed stent-graft in place. It also allows access for completion pelvic angiogram (although this can be done through the sheath) and access for a balloon occluder in the event of iliac rupture. Great care should be taken to avoid air or atheroembolic. In obese patients, or those with a weak pulse, ultrasound is very helpful in accessing the common femoral artery, and avoiding areas of significant plaque. After arterial access is established, 5000 U of Heparin is administered, although it is possible to avoid heparinization if there is concern for bleeding complications[31]. A 5- or 6-Fr pigtail is advanced over a floppy 3-J wire, and then the wire is exchanged for a stiffer wire (such as an Amplatz or Lunderquist). The location of the rear of the wire should be marked on the table, so that any advancement or withdrawal can be detected. The delivery sheath is then advanced under constant fluoroscopic monitoring, usually in the AP view. Ideally it should lie in the distal aorta. Once the device is in the approximate desired location, the image intensifier is rotated to the ideal angle, and angiography performed with respirations suspended. Usually 20 mL of contrast/s for 2 s is adequate. A "road map" can be obtained and/or the landmarks marked with a felt pen. At this point the stent graft is deployed. We prefer to withdraw the pigtail used for angiogram below the stent prior to deployment. With most devices, deployment is rapid, and adenosine arrest is not needed. Hypertension should be avoided. Using cuff extenders, we do prefer adenosine, at least for the first graft, to avoid distal displacement. When deploying cuffs, in general we have started distally, which we believe helps stabilize subsequent more proximal devices. Once the device(s) is/are deployed, gentle ballooning, starting distally, is performed. When using multiple devices, the ballooning should proceed proximally, covering all areas of overlap. When deploying cuffs, the balloons do occlude the aorta, and even the tri-fasicular balloon when deployed across the curvature of the aorta, can result in acute proximal hypertension and grab the stent-graft. Ideally, in trauma cases, ballooning can be avoided altogether. If needed, rapid inflation and deflation with 1/3 contrats-2/3 saline solution prevents significant hypertension. Vigorous over ballooning should be avoided. The balloon should be withdrawn below the stent, maintaining wire access, and a completion angiogram performed. If there is a small endoleak or if there is a lip of the graft not being apposed to the inner curve of the aorta, repeat ballooning should be performed. If this fails to eradicate the issue, extending the graft with an additional module should be considered. Larger balloons can catch along the edge of the delivery sheath, but gently pulling the balloon and sheath beyond the aorto-iliac junction usually allows the balloon catheter to straighten out and be removed. The sheath is then gently withdrawn to as close to the inguinal ligament as possible (in the case of femoral access) and completion pelvic angiogram *via* the contra-lateral pig tail (or sheath if one was not placed) performed.

Access

Access vessel choice depends upon the size of sheath required for the chosen endograft, length of the delivery system, quality and diameter of the arteries, and clinical setting. Most trauma patients have healthy vasculature, and thus slight mismatch can be tolerated between sheath size and femoral diameter as long as there is no "tugging" and the sheath advances easily under fluoroscopy. If there is any concern, a contra-lateral sheath should be placed so that balloon occlusion can be used in the event of an iliac rupture during sheath removal. A variety of devices have been utilized for percutaneous closures with good results[31]. These devices are designed to place intra-arterial sutures that are then tied down at the end of the case[52]. The most common device used, the Perclose® (Perclose/Abbott Labs, Redwood, CA, USA), places two sutures at right angles to each other. They are placed over a wire at the start of the case, and in general, most clinicians prefer to tie them down over a glide wire at the end so that if there is a failure of closure a sheath can be re-introduced and a cut down performed. There is an approximately 10%-20% failure rate with these devices, which are designed generally for sheaths smaller than those used during endografting procedures. We have found that accessing the femoral artery under ultrasound guidance permits us to be sure we are indeed in the common femoral artery, and are anterior to avoid areas of calcification or thrombus. When using sheaths required for dedicated thoracic stent grafts, we use two placed at 90° to each other. Complications include infection, arterial thrombosis, and pseudoaneurysm, and collectively occur at a rate of about 5%. There are no significant differences between the devices[53-57]. Percutaneous approaches can be performed as quickly as a cut down if the operators have experience but in emergency situations or if there are any concerns

regarding the quality of the femoral artery (calcification, size *etc*.) then a cut down is safer. The groin incision can be oblique, at or above the groin skin crease, or a longitudinal incision. If there are extensive calcifications, endografts such as the TAG have been advanced without using the sheath, but this is not recommended because the graft can catch on an edge and deploy prematurely or be damaged. When withdrawing the sheath at the end of the case, particularly if a percutaneous approach has been used, it is critical that the blood pressure be monitored for 2-3 min as any acute drop is pathognomonic of an iliac rupture.

Retroperitoneal iliac exposure may be required if using cuff extenders and the device is not long enough to reach the location of the tear and/or if the femoral arteries are too small and/or calcified to use. If there has been pelvic trauma, using the side with the least hematoma is desirable. The common iliac can be accessed directly or a 10 mm silo graft is anastomosed end-to-side. If the pelvis is deep, to avoid a problem with angulation, the silo graft can be tunneled through the lower abdominal soft tissue or indeed through the femoral canal to the groin. Patients who have had prior aorto-iliac grafts can be challenging because the iliacs are often imbedded in scar tissue. The ureter should always be mobilized anteriorly, avoiding dissection on both sides to prevent devascularization. In the vast majority of cases, the best that can be achieved is that enough dissection of the iliac limb of the graft allows application of a partial occlusion clamp or direct graft puncture. Having completed the procedure, whether anastomosing to graft or native vessel, the conduit is simply truncated and over sewn as a patch. In some circumstances, it may be advisable to convert the conduit to an ilio-femoral artery bypass. This allows a relatively easier access route for later percutaneous interventions should the need arise.

Some patients may already have an open abdomen, and in these cases direct infra-renal aortic access can be used[51]. This would not be a good choice if there has been visceral spillage.

ILLUSTRATIVE CASE STUDY

An 84-year-old male presented after a motor vehicle accident with multiple deep facial lacerations, right hip dislocation, and traumatic rupture of the thoracic aorta. His history was significant for extensive coronary artery disease and he had electrocardiographic and laboratory evidence for ischemia *vs* blunt cardiac injury (new S-T depressions and elevated cardiac troponin I levels). Because of his co-morbidities we elected to repair the injury in the hybrid operating suite. The injury was very close to the origin of the subclavian artery (Figure 1A). To mark the origin of the subclavian, and because of the short distance across an acutely angled neck, brachial access was obtained to permit exact measurement and allow access for stenting if required (Figure 1B). After deployment, a Type I endoleak was noted (Figure 1C).

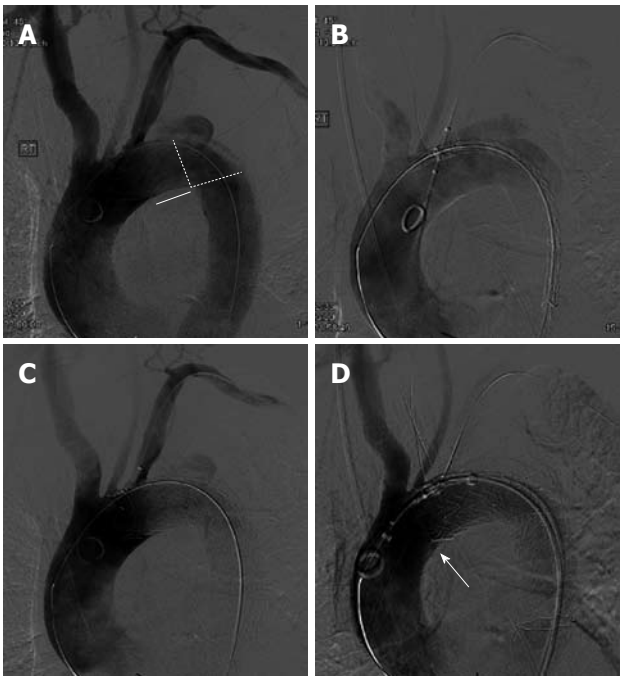

Figure 1 An 84-year-old male's injury was repaired in the hybrid operating suite. A: Traumatic injury. There is one centimeter along the lesser curve in a straight portion of the aorta that could serve as a landing zone, but much less along the outer curve (straight line). The "no-man's land" is indicated by the stippled line, and would also act to destabilize the endograft if such a short landing zone was accepted. Thus, we felt subclavian coverage was required; B: Using the pig tail as a marker the exact location of the subclavian artery is marked during all maneuvers; C: After deployment of a Gore-TAG® 31 mm × 15 cm (W.L. Gore & Associates, Flagstaff, AZ, USA). This length was chosen to gain better distal stability because of the acute aortic curvature. A Type I endoleak is noted. The proximal portion of the graft is in the "proximal no-man's land" of the ascending aorta and does not appose well against the inner curve here; D: After gentle ballooning, the endoleak is obliterated and although a lip still remains (arrow) the graft has improved apposition.

Gentle ballooning to push the inferior lip of the graft into better apposition with the inner curve was successful (Figure 1D). Completion angiogram demonstrated retrograde filling of the subclavian without type II endoleak, thus obviating the need for a kissing stent *via* the subclavian artery or carotid-subclavian bypass. At the end of the procedure his facial injuries were repaired and the hip re-located. The patient was extubated the next morning but spent 2 wk in hospital because of his hip dislocation. At 9 mo follow up he is doing well with no evidence of endoleak.

FOLLOW UP

The protocols for follow up are based on the various clinical trials designed predominantly to evaluate thoracic endografting for atherosclerotic aneurysms. Typical guidelines include CT angiography at 48 h, discharge, 1-, 6- and 12-mo and then annually. These protocols are designed to detect graft collapse, migration or persistent endoleak with aneurysmal growth. To a large extent, these guidelines were laid out because the cases involved patients with diseased landing zones with a potential for

ongoing dilation of the aorta. Obvious concerns include following patients with renal insufficiency, as well as the burden of a large number of radiation exposures. Patients with renal insufficiency can be surveyed with intravascular ultrasound, trans-esophageal echo, magnetic resonance or even CT without contrast. The primary concern is whether or not there is pseudoaneurysm regression or growth. Simple chest radiography can detect stent deformation or migration. For aortic transaction cases we tend to obtain a CT angiography at 48 h, at 1 mo, at one year and then follow with chest radiographs. When obtaining a CT angiogram, it is important to make sure that the study is performed in a uniform manner: triphasic with unenhanced, enhanced and delayed images. Indwelling pressure transducers, placed at the time of abdominal aortic endografting, continue to be studied and may, at least in select patients, provide a useful alternative to serial imaging[58].

We have not used antiplatelet agents for thoracic aortic stent grafting. However, we treat these like any other implant, and recommend antibiotic prophylaxis for any invasive procedure (such as dental work).

COMPLICATIONS

Endoleak and endotension

In brief, endoleak can be categorized as Type I (leak around the proximal, A, or distal, B, ends of the graft), Ⅱ (leak form an artery feeding into the aneurysm sac), Ⅲ (leak between components) or Ⅳ (failure of graft integrity). Typically, distal Type I endoleaks are rare in the trauma setting. These generally are found in patients with extensive atheromatous disease and dilated, short distal landing zones. Proximal Type I endoleaks occur in approximately 5% of cases[17,22]. Persistent Type I endoleak is associated with a risk of late rupture[48]. The predominant mechanism in trauma patients is the combination of a short landing zone and lack of apposition along the inner curvature of the arch. Gentle ballooning should be tried first. If this is not sufficient, then extending proximally with another graft should follow[27,59]. Type I leaks that are visualized only on delayed images immediately following deployment may resolve following heparin reversal. We assess these at 48 h with a repeat CT angiogram. Blood pressure should be controlled with β-blockade during this period. Proximal Type I endoleaks found on follow up imaging can usually be managed by repeat interventions. Significant leaks seen at the time of implant or at follow up, that do not respond to further ballooning or extension should undergo operative repair. There have been attempts to coil embolize the pseudoaneurysm in the hope that thrombosis will ensue, but clinically and experimentally this does not appear to reduce the endotension and is associated with a risk of late rupture. Most Type I endoleaks occur within 30 d, but occasionally can be found up to 2 years later, reinforcing the need for strict surveillance.

Type Ⅱ endoleaks should be managed based on whether or not the left subclavian is the source. If it is, coil occlusion of the subclavian, carotid to subclavian bypass with proximal ligation or carotid subclavian to carotid transposition should be performed. Left subclavian arterial causes of Type Ⅱ endoleak are less common in the trauma setting than the more typical atherosclerotic aneurysm case where there is circumferential dilation and the subclavian is more likely to feed into the aneurysm. Type Ⅱ endoleaks believed to be secondary to patent bronchial or intercostal arteries are more problematic, but again are less problematic in the trauma setting as there are fewer branches in the proximal descending thoracic aorta. Some investigators believe that these are more benign than in the setting of abdominal endografting, and that in the majority of cases they will seal spontaneously[60]. Rarely a branch vessel can be accessed and coiled using micro-catheter techniques.

Type Ⅲ endoleaks represent a leak between endograft components, and thus would be expected to be seen predominantly when cuff extenders are used, particularly if deployed along the curvature of the distal arch/proximal descending aorta. These are usually seen at the time of implant, and are managed by repeat ballooning and/or deploying another cuff across the site of the leak.

Type Ⅳ endoleak has not been described to our knowledge in the trauma population but implies a general failure of the graft material. Endotension refers to persistent pressure within an aneurysm or pseudoaneurysm without a documented endoleak. Clearly, if there is a source that can be defined it should be addressed. If no source is identified, but there is continued aneurysm growth, most surgeons would opt for operative repair rather than re-endografting. There is debate about whether absence of regression without growth represents evidence of endotension. Regardless, this does not appear to be a concern in the majority of trauma patients, and our own bias is that if the pseudoaneurysm is completely thrombosed following endografting, then routine follow up is all that is required.

Stent graft collapse

This is a catastrophic complication that can occur immediately, or within the first 48 h, but it has been seen up to 3 mo post procedure[61]. It is felt that this represents a combination of graft oversizing and a lack of apposition along the inner curve of the aorta[17]. In young hyperdynamic aortas, with their degree of pliability, the force of the cardiac ejection that hits the underside of the graft causes collapse of the graft. This usually leads to immediate aortic occlusion and possibly rupture. If this occurs post-implant, the patient will develop signs of acute coarctation, and the rapid onset of paralysis and renal failure can occur. This may not be immediately apparent if the patient is still on the ventilator and sedated. Alternatively, the collapse may only occur in systole, and require fluoroscopy for detection[62]. Prevention includes

very accurate sizing, choosing a graft that approximates a 10% oversizing rather than 20%. It is also important to plan pre- and intra-operatively to avoid landing in the "no man's land" of the aorta. If the proximal portion of the graft is not apposed or at least close to the inner curve, particularly if there is only a short zone of apposition, perhaps less than 50%, then options include extending the graft proximally and/or repeat ballooning[61]. Uncovered bare metal stents deployed within the stent graft have also been used both acutely and when collapse occurs in a delayed fashion. There has been some concern that these bare stents may either erode over time through the graft fabric or create proximal aortic perforations[45]. There is not enough data to determine the real risk of this occurring, but theoretically a short bare stent will conform more closely to the aortic curvature than a bare proximal portion that is secured to an endograft and has reduced flexibility. Across the country there have been numerous anecdotal reports of bare stent extenders being used for proximal partial or complete collapse with good short term results. There is growing consensuses that perhaps cuff extenders, which may be deployed sequentially and thus fit the curvature of the aorta better, may prove to perform better than longer thoracic stent grafts in patients with aortic diameters smaller than 24 mm.

If stent graft collapse occurs post-operatively, it can often be detected by plain chest radiography, or by non-contrast CT. Immediate intervention is required. If complete collapse has occurred, explanting and operative repair is prudent, but ballooning and extending the device with a bare stent has been used with success[31]. Anecdotally, axillary-femoral-femoral bypass has been used as a temporizing measure, but ultimately the stent must be removed.

Subclavian occlusion

Coverage of the left subclavian artery origin with subclavian to carotid bypass or transposition raises the question of arm ischemia, vertebral-basilar insufficiency and/or type Ⅱ endoleak. Critical arm ischemia is rare, affecting less than 2% of patients, and if it occurs can be managed electively in most cases[15,47,49,63,64]. Type Ⅱ endoleak arising by back flow into the pseudoaneurysm is also uncommon as most tears arise from the inner curve. Should a Type Ⅱ endoleak occur, or if there is concern regarding this prior to the procedure, the left brachial artery can be accessed and once the graft is deployed, the subclavian can be coiled or closed with a peripheral closure device[65]. Vertebral steal phenomenon can also be addressed electively[66]. Patients with patent left internal mammary grafts should undergo carotid-subclavian bypass prior to left subclavian coverage[47,66]. If the proximal landing zone is felt to encroach upon the origin of the left subclavian, but complete coverage is not required, it is possible to access the left brachial artery and leave a wire in the arch, which allows precise placement of the device and can permit stenting of the subclavian origin if narrowing occurs[27].

Stroke

Stroke remains the "Achilles heel" of thoracic endografting, occurring at a rate of 3%-5% of cases[67]. In the trauma population the incidence is lower, at 0%-2% depending on the series[17,22,30]. Occlusion of a critical left vertebral artery is one cause. There is some data that an aberrant vertebral artery arising from the arch directly may be more likely to be a major source of posterior circulation, and in these cases we are more apt to perform vertebral transfer first. In older patients, arch thrombus is a concern for its embolic risk. Manipulation with the stiff wire across the arch can cause embolization. This has not been demonstrated in the trauma population to our knowledge, but should it happen, theoretical options include immediate cerebral angiography and if there is a definitive lesion, intervention with catheter-based techniques. Finally, inadvertent guide wire advancement into the carotid, or air embolism because of a loose connection, can result in cerebrovascular events. Whenever a catheter is proximal to the left subclavian artery, meticulous de-airing of the catheter and equipment is mandatory. Wire position should be monitored and stabilized at all times. Never advance a catheter or wire blindly.

Impeding the flow to the left vertebral may pose a risk of posterior cerebellar circulatory insufficiency or stroke. In our experience, this has never happened in the younger population, but we are concerned in older patients with diffuse vascular disease. Assessing cerebral circulation is clearly difficult under emergent conditions. Anatomic assessments can be made by CT-angiography or MRA of the head and neck, or cerebral angiography either prior to placement or at the time. We have found trans-cranial doppler to be a useful adjunct. If the basilar artery and the posterior communicating artery can be seen, then flow from both vertebral arteries, the basilar arteries and posterior communicating arteries can be measured while temporally occluding the origin of the left subclavian artery with an occlusion balloon. Carotid-subclavian bypass is generally well tolerated, but some investigators have noted an increased stroke risk when this is performed in patients with atherosclerotic aneurysmal disease[66,67]. This may be related to the increased degree of calcification in this older population, and may not apply to the younger trauma patient. Demonstrating intact vertebral-basilar flow upon left subclavian occlusion precludes the need for prophylactic subclavian bypass or transposition[68].

Embolization

Distal embolization is more of a concern in older patients with diffuse atheromata. Rarely, a traumatic injury can present with thrombus arising from the injury site. In any patient where there is a recognized risk that wire or device manipulation might cause distal embolization, one should be prepared to perform distal angiography and to record distal pulses at the start and end of the procedure.

Bronchial obstruction

Grafts placed in the mid descending aorta have rarely

been associated with compression of the left main bronchus[17,69]. This may be detected on follow up CT or chest radiograph, bronchoscopy for other reasons, or clinically with new onset asthma. The optimal management is open repair of the aorta and explanting the device when medically feasible. Bronchial stenting has been used but in our opinion will predispose to the development of aorto-bronchial fistula[17].

Implant syndrome

Occasionally patients will experience persistent or new back pain, fever, malaise and/or a flu-like syndrome following implantation. This has been reported more commonly with abdominal aortic endografting, but Rousseau and associates found it in nearly 1/5 of their series[5,70,71]. It is not clear whether the back pain is due to residual endotension, inflammation secondary to thrombosis in the excluded aorta and/or a systemic inflammatory response to the graft. Repeat CT angiography is required to rule out a complication, but the presence of elevated erythrocyte sedimentation rate, with or without leukocytosis, and a normal CT suggest the diagnosis. Many patients will also complain of various degrees of pleurisy. This condition is self-limited, usually resolving within 7 d, and can be treated with anti-inflammatory medications.

Dissection/rupture

Free rupture can occur at any time. Prevention is strict blood pressure control, particularly during periods of transfer or other procedures that might acutely elevate the heart rate and/or blood pressure. At the time of initial wire passage, great care should be given to watching the wire advance. If there is difficulty negotiating the aortic curvature or there is narrowing at the injury site, a directional catheter such as a vertebral and/or hydrophilic catheter can be invaluable.

There have been cases of delayed or immediate rupture after the graft has been deployed. Endografts which feature a bare metal proximal extension have been implicated in perforating the aortic wall[72]. Even covered grafts which do not have this feature have been implicated if there is poor apposition of the aortic wall with resultant motion against the wall. All three dedicated thoracic endografts discussed here have been implicated in acute or delayed perforation with/or without dissection, at least anecdotally, in the non-trauma experience. Proper graft sizing is essential to facilitate good graft-aortic apposition.

Proximal dissection has also been documented. One mechanism is that during ballooning of the proximal cuff, the ends of the graft can create a dissection flap that rapidly progresses retrograde. To avoid this, initial ballooning should be as gentle as possible, just enough to document profiling of the balloon along the side of the graft. Ballooning should only be done within the graft.

Migration

If the proximal landing zone is not long enough, and the aneurysm itself is large, stents can migrate distally. This may be detected on routine chest radiography, or may present with a new endoleak. In younger patients, as aortic growth occurs, an endograft may loose its fixation. If this should occur, options include both operative explanting and grafting, or proximal extension with another endograft. This is one of the reasons that lifelong surveillance is necessary.

Paralysis

The risk of paralysis with endografting in the trauma setting has not been demonstrated in recent series. This is presumably because in the vast majority of cases only a short segment of the proximal descending aorta is covered. However, based on experience acquired from treating atherosclerotic aneurysms, there may be uncommon circumstances (such as treating a chronic post-traumatic aneurysm in an older patient) where there is increased risk. The major risk factors include covering more than 20 cm of aorta and prior abdominal aortic procedures. These risks are enhanced if the left subclavian must be covered, or if there is extensive iliac disease with hypogastric occlusion. In the elective setting, placement of a lumbar drain and allowing increased pressure after the endograft procedure can both reduce the risk of paralysis or, in as many as 1/3-1/2 of patients who do develop neurological changes, reverse the spinal cord ischemia[73,74]. Clearly this is not a viable option in most acute trauma settings, but may be considered in delayed or elective settings.

Other long term complications

Aortobronchial and/or aortoesophageal fistula have been reported years after endografting[17,75]. Sayed and colleagues reviewed 1518 cases reported in the literature of thoracic endografting (primarily for non-traumatic thoracic aneurysmal disease) and found 6 cases (0.4%) of thoracic graft infection, paralleling the experience with abdominal grafts[21,76]. The primary risk factors were other intravascular sources of infection. Surgical management was associated with a 16% mortality compared with 36% with medical management alone. Any evidence of aneurysmal changes or persistent bacteremia should prompt consideration for surgical intervention.

THE PEDIATRIC AND ADOLESCENT PATIENT

Endovascular aortic stent grafts are not commonly used in pediatric and adolescent patients[77]. These patients usually have aortas that are too small for currently available devices, will likely grow and the lack of long term durability has greater significance in this population. Rarely, an endograft has been used as a "bridge to definitive treatment" in patients who cannot undergo operative repair initially[32].

FUTURE TRENDS

Endograft technology is continuing to evolve, but perhaps

even more significant, experience and longer follow up data is also beginning to accrue. Branched grafts are beginning to be designed for both arch and abdominal visceral vessels. Specific for the trauma population, a variety of grafts which are shorter, pre-curved and smaller are being developed which will allow more precise deployment and potentially reduce complication rates.

CONCLUSION

Endovascular repair of the traumatically injured thoracic aorta has emerged as an exceptionally promising modality that is typically quicker than open repair, with a reduced risk of paralysis. There are a specific set of anatomic criteria that need to be applied, which can be rapidly assessed by the CT angiogram. The enthusiasm for endovascular repair must be tempered by recognition of the complications and lack of long term follow up, particularly in younger patients. Surgeons who are skilled in open aortic repair must not only be involved, but should take on a leadership role during the planning, deployment and follow up of these patients[78]. Familiarity with all of the available devices expands treatment options. As more specific devices become available, and more follow up is accrued, the role of endovascular stents will continue to grow.

REFERENCES

1 **Parmley LF**, Mattingly TW, Manion WC, Jahnke EJ Jr. Nonpenetrating traumatic injury of the aorta. *Circulation* 1958; **17**: 1086-1101
2 **Holmes JH 4th**, Bloch RD, Hall RA, Carter YM, Karmy-Jones RC. Natural history of traumatic rupture of the thoracic aorta managed nonoperatively: a longitudinal analysis. *Ann Thorac Surg* 2002; **73**: 1149-1154
3 **Pate JW**, Gavant ML, Weiman DS, Fabian TC. Traumatic rupture of the aortic isthmus: program of selective management. *World J Surg* 1999; **23**: 59-63
4 **Kepros J**, Angood P, Jaffe CC, Rabinovici R. Aortic intimal injuries from blunt trauma: resolution profile in nonoperative management. *J Trauma* 2002; **52**: 475-478
5 **Rousseau H**, Dambrin C, Marcheix B, Richeux L, Mazerolles M, Cron C, Watkinson A, Mugniot A, Soula P, Chabbert V, Canevet G, Roux D, Massabuau P, Meites G, Tran Van T, Otal P. Acute traumatic aortic rupture: a comparison of surgical and stent-graft repair. *J Thorac Cardiovasc Surg* 2005; **129**: 1050-1055
6 **Miller PR**, Kortesis BG, McLaughlin CA 3rd, Chen MY, Chang MC, Kon ND, Meredith JW. Complex blunt aortic injury or repair: beneficial effects of cardiopulmonary bypass use. *Ann Surg* 2003; **237**: 877-883; discussion 883-884
7 **Karmy-Jones R**, Carter YM, Nathens A, Brundage S, Meissner MH, Borsa J, Demirer S, Jurkovich G. Impact of presenting physiology and associated injuries on outcome following traumatic rupture of the thoracic aorta. *Am Surg* 2001; **67**: 61-66
8 **Forbes AD**, Ashbaugh DG. Mechanical circulatory support during repair of thoracic aortic injuries improves morbidity and prevents spinal cord injury. *Arch Surg* 1994; **129**: 494-497; discussion 497-498
9 **Cook J**, Salerno C, Krishnadasan B, Nicholls S, Meissner M, Karmy-Jones R. The effect of changing presentation and management on the outcome of blunt rupture of the thoracic aorta. *J Thorac Cardiovasc Surg* 2006; **131**: 594-600
10 **Mattox KL**, Wall MJ Jr. Historical review of blunt injury to the thoracic aorta. *Chest Surg Clin N Am* 2000; **10**: 167-182, x
11 **Fabian TC**, Richardson JD, Croce MA, Smith JS Jr, Rodman G Jr, Kearney PA, Flynn W, Ney AL, Cone JB, Luchette FA, Wisner DH, Scholten DJ, Beaver BL, Conn AK, Coscia R, Hoyt DB, Morris JA Jr, Harviel JD, Peitzman AB, Bynoe RP, Diamond DL, Wall M, Gates JD, Asensio JA, Enderson BL. Prospective study of blunt aortic injury: Multicenter Trial of the American Association for the Surgery of Trauma. *J Trauma* 1997; **42**: 374-380; discussion 380-383
12 **Kato N**, Dake MD, Miller DC, Semba CP, Mitchell RS, Razavi MK, Kee ST. Traumatic thoracic aortic aneurysm: treatment with endovascular stent-grafts. *Radiology* 1997; **205**: 657-662
13 **Dake MD**, Miller DC, Mitchell RS, Semba CP, Moore KA, Sakai T. The "first generation" of endovascular stent-grafts for patients with aneurysms of the descending thoracic aorta. *J Thorac Cardiovasc Surg* 1998; **116**: 689-703; discussion 703-704
14 **Fujikawa T**, Yukioka T, Ishimaru S, Kanai M, Muraoka A, Sasaki H, Honma H, Koike S, Kawaguchi S. Endovascular stent grafting for the treatment of blunt thoracic aortic injury. *J Trauma* 2001; **50**: 223-229
15 **Lawlor DK**, Ott M, Forbes TL, Kribs S, Harris KA, DeRose G. Endovascular management of traumatic thoracic aortic injuries. *Can J Surg* 2005; **48**: 293-297
16 **Lebl DR**, Dicker RA, Spain DA, Brundage SI. Dramatic shift in the primary management of traumatic thoracic aortic rupture. *Arch Surg* 2006; **141**: 177-180
17 **Hershberger RC**, Aulivola B, Murphy M, Luchette FA. Endovascular grafts for treatment of traumatic injury to the aortic arch and great vessels. *J Trauma* 2009; **67**: 660-671
18 **Starnes BW**, Arthurs ZM. Endovascular management of vascular trauma. *Perspect Vasc Surg Endovasc Ther* 2006; **18**: 114-129
19 **Kühne CA**, Ruchholtz S, Voggenreiter G, Eggebrecht H, Paffrath T, Waydhas C, Nast-Kolb D. [Traumatic aortic injuries in severely injured patients] *Unfallchirurg* 2005; **108**: 279-287
20 **Uzieblo M**, Sanchez LA, Rubin BG, Choi ET, Geraghty PJ, Flye MW, Curci JA, Moon MR, Sicard GA. Endovascular repair of traumatic descending thoracic aortic disruptions: should endovascular therapy become the gold standard? *Vasc Endovascular Surg* 2004; **38**: 331-337
21 **Sayed S**, Thompson MM. Endovascular repair of the descending thoracic aorta: evidence for the change in clinical practice. *Vascular* 2005; **13**: 148-157
22 **Demetriades D**, Velmahos GC, Scalea TM, Jurkovich GJ, Karmy-Jones R, Teixeira PG, Hemmila MR, O'Connor JV, McKenney MO, Moore FO, London J, Singh MJ, Lineen E, Spaniolas K, Keel M, Sugrue M, Wahl WL, Hill J, Wall MJ, Moore EE, Margulies D, Malka V, Chan LS. Operative repair or endovascular stent graft in blunt traumatic thoracic aortic injuries: results of an American Association for the Surgery of Trauma Multicenter Study. *J Trauma* 2008; **64**: 561-570; discussion 570-571
23 **Wellons ED**, Milner R, Solis M, Levitt A, Rosenthal D. Stent-graft repair of traumatic thoracic aortic disruptions. *J Vasc Surg* 2004; **40**: 1095-1100
24 **Andrassy J**, Weidenhagen R, Meimarakis G, Lauterjung L, Jauch KW, Kopp R. Stent versus open surgery for acute and chronic traumatic injury of the thoracic aorta: a single-center experience. *J Trauma* 2006; **60**: 765-771; discussion 771-772
25 **Thompson CS**, Rodriguez JA, Ramaiah VG, DiMugno L, Shafique S, Olsen D, Diethrich EB. Acute traumatic rupture of the thoracic aorta treated with endoluminal stent grafts. *J Trauma* 2002; **52**: 1173-1177
26 **Orford VP**, Atkinson NR, Thomson K, Milne PY, Campbell WA, Roberts A, Goldblatt J, Tatoulis J. Blunt traumatic

aortic transection: the endovascular experience. *Ann Thorac Surg* 2003; **75**: 106-111; discussion 111-112
27 **Neuhauser B**, Czermak B, Jaschke W, Waldenberger P, Fraedrich G, Perkmann R. Stent-graft repair for acute traumatic thoracic aortic rupture. *Am Surg* 2004; **70**: 1039-1044
28 **Peterson BG**, Matsumura JS, Morasch MD, West MA, Eskandari MK. Percutaneous endovascular repair of blunt thoracic aortic transection. *J Trauma* 2005; **59**: 1062-1065
29 **Marty-Ané CH**, Berthet JP, Branchereau P, Mary H, Alric P. Endovascular repair for acute traumatic rupture of the thoracic aorta. *Ann Thorac Surg* 2003; **75**: 1803-1807
30 **Dunham MB**, Zygun D, Petrasek P, Kortbeek JB, Karmy-Jones R, Moore RD. Endovascular stent grafts for acute blunt aortic injury. *J Trauma* 2004; **56**: 1173-1178
31 **Tehrani HY**, Peterson BG, Katariya K, Morasch MD, Stevens R, DiLuozzo G, Salerno T, Maurici G, Eton D, Eskandari MK. Endovascular repair of thoracic aortic tears. *Ann Thorac Surg* 2006; **82**: 873-877; discussion 877-878
32 **Martin MA**, Barnatan M, Cole F, Long W, Hill J, Karmy-Jones R. A case report of traumatic aortic rupture in a pediatric patient: a possible role for endovascular management as a bridge to definitive repair. *J Trauma* 2009; **67**: E136-E139
33 **Amabile P**, Collart F, Gariboldi V, Rollet G, Bartoli JM, Piquet P. Surgical versus endovascular treatment of traumatic thoracic aortic rupture. *J Vasc Surg* 2004; **40**: 873-879
34 **Tang GL**, Tehrani HY, Usman A, Katariya K, Otero C, Perez E, Eskandari MK. Reduced mortality, paraplegia, and stroke with stent graft repair of blunt aortic transections: a modern meta-analysis. *J Vasc Surg* 2008; **47**: 671-675
35 **Fabian TC**, Davis KA, Gavant ML, Croce MA, Melton SM, Patton JH Jr, Haan CK, Weiman DS, Pate JW. Prospective study of blunt aortic injury: helical CT is diagnostic and antihypertensive therapy reduces rupture. *Ann Surg* 1998; **227**: 666-676; discussion 676-677
36 **Feliciano DV**. Trauma to the aorta and major vessels. *Chest Surg Clin N Am* 1997; **7**: 305-323
37 **Demetriades D**, Velmahos GC, Scalea TM, Jurkovich GJ, Karmy-Jones R, Teixeira PG, Hemmila MR, O'Connor JV, McKenney MO, Moore FO, London J, Singh MJ, Spaniolas K, Keel M, Sugrue M, Wahl WL, Hill J, Wall MJ, Moore EE, Lineen E, Margulies D, Malka V, Chan LS. Blunt traumatic thoracic aortic injuries: early or delayed repair--results of an American Association for the Surgery of Trauma prospective study. *J Trauma* 2009; **66**: 967-973
38 **Maggisano R**, Nathens A, Alexandrova NA, Cina C, Boulanger B, McKenzie R, Harrison AW. Traumatic rupture of the thoracic aorta: should one always operate immediately? *Ann Vasc Surg* 1995; **9**: 44-52
39 **Mattison R**, Hamilton IN Jr, Ciraulo DL, Richart CM. Stent-graft repair of acute traumatic thoracic aortic transection with intentional occlusion of the left subclavian artery: case report. *J Trauma* 2001; **51**: 326-328
40 **Myburgh JA**. Driving cerebral perfusion pressure with pressors: how, which, when? *Crit Care Resusc* 2005; **7**: 200-205
41 **Pace MC**, Cicciarella G, Barbato E, Maisto M, Passavanti MB, Gazzerro G, Barbarisi M, Aurilio C. Severe traumatic brain injury: management and prognosis. *Minerva Anestesiol* 2006; **72**: 235-242
42 **Kinoshita K**, Sakurai A, Utagawa A, Ebihara T, Furukawa M, Moriya T, Okuno K, Yoshitake A, Noda E, Tanjoh K. Importance of cerebral perfusion pressure management using cerebrospinal drainage in severe traumatic brain injury. *Acta Neurochir Suppl* 2006; **96**: 37-39
43 **Czosnyka M**, Hutchinson PJ, Balestreri M, Hiler M, Smielewski P, Pickard JD. Monitoring and interpretation of intracranial pressure after head injury. *Acta Neurochir Suppl* 2006; **96**: 114-118
44 **Fisher RG**, Oria RA, Mattox KL, Whigham CJ, Pickard LR. Conservative management of aortic lacerations due to blunt trauma. *J Trauma* 1990; **30**: 1562-1566
45 **Malina M**, Brunkwall J, Ivancev K, Lindblad B, Malina J, Nyman U, Risberg B. Late aortic arch perforation by graft-anchoring stent: complication of endovascular thoracic aneurysm exclusion. *J Endovasc Surg* 1998; **5**: 274-277
46 **Borsa JJ**, Hoffer EK, Karmy-Jones R, Fontaine AB, Bloch RD, Yoon JK, So CR, Meissner MH, Demirer S. Angiographic description of blunt traumatic injuries to the thoracic aorta with specific relevance to endograft repair. *J Endovasc Ther* 2002; **9** Suppl 2: II84-II91
47 **Wheatley GH 3rd**, Gurbuz AT, Rodriguez-Lopez JA, Ramaiah VG, Olsen D, Williams J, Diethrich EB. Midterm outcome in 158 consecutive Gore TAG thoracic endoprostheses: single center experience. *Ann Thorac Surg* 2006; **81**: 1570-1577; discussion 1577
48 **Fattori R**, Nienaber CA, Rousseau H, Beregi JP, Heijmen R, Grabenwöger M, Piquet P, Lovato L, Dabbech C, Kische S, Gaxotte V, Schepens M, Ehrlich M, Bartoli JM. Results of endovascular repair of the thoracic aorta with the Talent Thoracic stent graft: the Talent Thoracic Retrospective Registry. *J Thorac Cardiovasc Surg* 2006; **132**: 332-339
49 **Scheinert D**, Krankenberg H, Schmidt A, Gummert JF, Nitzsche S, Scheinert S, Bräunlich S, Sorge I, Krakor R, Biamino G, Schuler G, Mohr FW. Endoluminal stent-graft placement for acute rupture of the descending thoracic aorta. *Eur Heart J* 2004; **25**: 694-700
50 **Hoffer EK**, Karmy-Jones R, Bloch RD, Meissner MH, Borsa JJ, Nicholls SC, So CR. Treatment of acute thoracic aortic injury with commercially available abdominal aortic stent-grafts. *J Vasc Interv Radiol* 2002; **13**: 1037-1041
51 **Cheng SG**, Glickerman DJ, Karmy-Jones R, Borsa JJ. Traumatic sternomanubrial dislocation with associated bilateral internal mammary artery occlusion. *AJR Am J Roentgenol* 2003; **180**: 810
52 **Morasch MD**, Kibbe MR, Evans ME, Meadows WS, Eskandari MK, Matsumura JS, Pearce WH. Percutaneous repair of abdominal aortic aneurysm. *J Vasc Surg* 2004; **40**: 12-16
53 **Eggebrecht H**, von Birgelen C, Naber C, Kröger K, Schmermund A, Wieneke H, Bartel T, Wörtgen U, Baumgart D, Haude M, Erbel R. Impact of gender on femoral access complications secondary to application of a collagen-based vascular closure device. *J Invasive Cardiol* 2004; **16**: 247-250
54 **Hoffer EK**, Bloch RD. Percutaneous arterial closure devices. *J Vasc Interv Radiol* 2003; **14**: 865-885
55 **Castelli P**, Caronno R, Piffaretti G, Tozzi M, Lomazzi C. Incidence of vascular injuries after use of the Angio-Seal closure device following endovascular procedures in a single center. *World J Surg* 2006; **30**: 280-284
56 **Biancari F**, Ylönen K, Mosorin M, Lepojärvi M, Juvonen T. Lower limb ischemic complications after the use of arterial puncture closure devices. *Eur J Vasc Endovasc Surg* 2006; **32**: 504-505
57 **Watelet J**, Gallot JC, Thomas P, Douvrin F, Plissonnier D. Percutaneous repair of aortic aneurysms: a prospective study of suture-mediated closure devices. *Eur J Vasc Endovasc Surg* 2006; **32**: 261-265
58 **Ellozy SH**, Carroccio A, Lookstein RA, Minor ME, Sheahan CM, Juta J, Cha A, Valenzuela R, Addis MD, Jacobs TS, Teodorescu VJ, Marin ML. First experience in human beings with a permanently implantable intrasac pressure transducer for monitoring endovascular repair of abdominal aortic aneurysms. *J Vasc Surg* 2004; **40**: 405-412
59 **Orend KH**, Scharrer-Pamler R, Kapfer X, Liewald F, Görich J, Sunder-Plassmann L. [Endoluminal stent-assisted management of acute traumatic aortic rupture] *Chirurg* 2002; **73**: 595-600
60 **Mertens R**, Valdés F, Krämer A, Mariné L, Irarrázaval M, Morán S, Zalaquet R, Schwartz E, Vergara J, Valdebenito M. [Endovascular treatment of descending thoracic aorta aneurysm] *Rev Med Chil* 2003; **131**: 617-622

61 **Idu MM**, Reekers JA, Balm R, Ponsen KJ, de Mol BA, Legemate DA. Collapse of a stent-graft following treatment of a traumatic thoracic aortic rupture. *J Endovasc Ther* 2005; **12**: 503-507

62 **Starnes BW**, Arthurs ZM. Endovascular management of vascular trauma. *Perspect Vasc Surg Endovasc Ther* 2006; **18**: 114-129

63 F**attori R,** Napoli G, Lovato L, Russo V, Pacini D, Pierangeli A, Gavelli G. Indications for, timing of, and results of catheter-based treatment of traumatic injury to the aorta. *AJR Am J Roentgenol* 2002; **179**: 603-609

64 **Görich J**, Asquan Y, Seifarth H, Krämer S, Kapfer X, Orend KH, Sunder-Plassmann L, Pamler R. Initial experience with intentional stent-graft coverage of the subclavian artery during endovascular thoracic aortic repairs. *J Endovasc Ther* 2002; **9** Suppl 2: II39-II43

65 **Hoppe H**, Hohenwalter EJ, Kaufman JA, Petersen B. Percutaneous treatment of aberrant right subclavian artery aneurysm with use of the Amplatzer septal occluder. *J Vasc Interv Radiol* 2006; **17**: 889-894

66 **Peterson BG**, Eskandari MK, Gleason TG, Morasch MD. Utility of left subclavian artery revascularization in association with endoluminal repair of acute and chronic thoracic aortic pathology. *J Vasc Surg* 2006; **43**: 433-439

67 **Appoo JJ**, Moser WG, Fairman RM, Cornelius KF, Pochettino A, Woo EY, Kurichi JE, Carpenter JP, Bavaria JE. Thoracic aortic stent grafting: improving results with newer generation investigational devices. *J Thorac Cardiovasc Surg* 2006; **131**: 1087-1094

68 **Rehders TC**, Petzsch M, Ince H, Kische S, Korber T, Koschyk DH, Chatterjee T, Weber F, Nienaber CA. Intentional occlusion of the left subclavian artery during stent-graft implantation in the thoracic aorta: risk and relevance. *J Endovasc Ther* 2004; **11**: 659-666

69 **Rousseau H**, Soula P, Perreault P, Bui B, Janne d'Othée B, Massabuau P, Meites G, Concina P, Mazerolles M, Joffre F, Otal P. Delayed treatment of traumatic rupture of the thoracic aorta with endoluminal covered stent. *Circulation* 1999; **99**: 498-504

70 **Gerasimidis T**, Sfyroeras G, Trellopoulos G, Skoura L, Papazoglou K, Konstantinidis K, Karamanos D, Filaktou A, Parapanisiou E. Impact of endograft material on the inflammatory response after elective endovascular abdominal aortic aneurysm repair. *Angiology* 2005; **56**: 743-753

71 **Galle C**, De Maertelaer V, Motte S, Zhou L, Stordeur P, Delville JP, Li R, Ferreira J, Goldman M, Capel P, Wautrecht JC, Pradier O, Dereume JP. Early inflammatory response after elective abdominal aortic aneurysm repair: a comparison between endovascular procedure and conventional surgery. *J Vasc Surg* 2000; **32**: 234-246

72 **D'Ancona G**, Bauset R, Normand JP, Turcotte R, Dagenais F. Endovascular stent-graft repair of a complicated penetrating ulcer of the descending thoracic aorta: a word of caution. *J Endovasc Ther* 2003; **10**: 928-931

73 **Cheung AT**, Pochettino A, McGarvey ML, Appoo JJ, Fairman RM, Carpenter JP, Moser WG, Woo EY, Bavaria JE. Strategies to manage paraplegia risk after endovascular stent repair of descending thoracic aortic aneurysms. *Ann Thorac Surg* 2005; **80**: 1280-1288; discussion 1288-1289

74 **Cheung AT**, Weiss SJ, McGarvey ML, Stecker MM, Hogan MS, Escherich A, Bavaria JE. Interventions for reversing delayed-onset postoperative paraplegia after thoracic aortic reconstruction. *Ann Thorac Surg* 2002; **74**: 413-419; discussion 420-421

75 **Eggebrecht H**, Baumgart D, Radecke K, von Birgelen C, Treichel U, Herold U, Hunold P, Gerken G, Jakob H, Erbel R. Aortoesophageal fistula secondary to stent-graft repair of the thoracic aorta. *J Endovasc Ther* 2004; **11**: 161-167

76 **Fiorani P**, Speziale F, Calisti A, Misuraca M, Zaccagnini D, Rizzo L, Giannoni MF. Endovascular graft infection: preliminary results of an international enquiry. *J Endovasc Ther* 2003; **10**: 919-927

77 **Milas ZL**, Milner R, Chaikoff E, Wulkan M, Ricketts R. Endograft stenting in the adolescent population for traumatic aortic injuries. *J Pediatr Surg* 2006; **41**: e27-e30

78 **Karmy-Jones R**, Kouchoukos NT. Endovascular credentialing and assembling the endovascular team. *J Card Surg* 2009; **24**: 334-342

S- Editor Wang JL **L- Editor** Webster JR **E- Editor** Zheng XM

World Journal of Radiology

Online Submissions: http://www.wjgnet.com/1949-8470office
wjr@wjgnet.com
doi:10.4329/wjr.v1.i1.63

World J Radiol 2009 December 31; 1(1): 63-71
ISSN 1949-8470 (online)

Endovascular stent graft repair of abdominal aortic aneurysms: Current status and future directions

Zhonghua Sun

Zhonghua Sun, Discipline of Medical Imaging, Department of Imaging and Applied Physics, Curtin University of Technology, GPO Box U1987, Perth, Western Australia 6845, Australia
Author contributions: Sun Z solely contributed to this paper.
Correspondence to: Dr. Zhonghua Sun, Discipline of Medical Imaging, Department of Imaging and Applied Physics, Curtin University of Technology, GPO Box U1987, Perth, Western Australia 6845, Australia. z.sun@curtin.edu.au
Telephone: +61-8-92667509 Fax: +61-8-92662377
Received: December 3, 2009 Revised: December 22, 2009
Accepted: December 25, 2009
Published online: December 31, 2009

Abstract

Endovascular stent graft repair of abdominal aortic aneurysm (AAA) has undergone rapid developments since it was introduced in the early 1990s. Two main types of aortic stent grafts have been developed and are currently being used in clinical practice to deal with patients with complicated or unsuitable aneurysm necks, namely, suprarenal and fenestrated stent grafts. Helical computed tomography angiography has been widely recognized as the method of choice for both pre-operative planning and post-operative follow-up of endovascular repair (EVAR). In addition to 2D axial images, a number of 2D and 3D reconstructions are generated to provide additional information about imaging of the stent grafts in relation to the aortic aneurysm diameter and extent, encroachment of stent wires to the renal artery ostium and position of the fenestrated vessel stents. The purpose of this article is to provide an overview of applications of EVAR of AAA and diagnostic applications of 2D and 3D image visualizations in the assessment of treatment outcomes of EVAR. Interference of stent wires with renal blood flow from the hemodynamic point of view will also be discussed, and future directions explored.

Key words: Abdominal aortic aneurysm; Stent graft; Computed tomography; Image visualization; Three-dimensional reconstruction; Follow-up

Peer reviewers: Fehmi Kaçmaz, MD, Department of Cardiology, Mesa Hospital, Ozel Mesa Hastanesi, Yasam Cad, No: 5 Sogutozu, 06510 Ankara, Turkey; Ramachandran Prabhakar, PhD, Department of Radiation Oncology, Institute Rotary Cancer Hospital, All India Institute of Medical Sciences, New Delhi 110 029, India

Sun Z. Endovascular stent graft repair of abdominal aortic aneurysms: Current status and future directions. *World J Radiol* 2009; 1(1): 63-71 Available from: URL: http://www.wjgnet.com/1949-8470/full/v1/i1/63.htm DOI: http://dx.doi.org/10.4329/wjr.v1.i1.63

ENDOVASCULAR REPAIR (EVAR) OF ABDOMINAL AORTIC ANEURYSM (AAA)-TECHNICAL DEVELOPMENTS

EVAR of AAA has been confirmed as an effective alternative to open surgery due to its lower invasiveness and reduced morbidity and mortality, and lower overall treatment cost[1,2]. Since its first introduction into the clinical practice in 1991, endovascular stent grafting has been widely used in clinical practice with satisfactory results being achieved[1-5]. Over the last decade, the technique of endovascular stent grafting has progressed rapidly following an improved understanding of the strengths and limitations of various devices and treated patient populations[3-6]. Application of this technology is still limited to patients with suitable proximal and distal sealing zones. It is estimated that up to 40% of patients are unsuitable for conventional infrarenal EVAR as complicated aneurysm necks prevent the patients from being candidates to receive treatment with placement of stent grafts infrarenally due to inadequate sealing zones in the aneurysm neck[5,6].

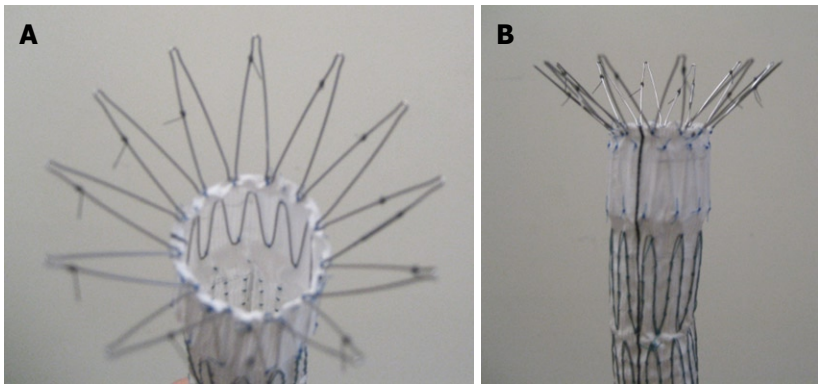

Figure 1 Suprarenal stent grafts with barbs and hooks on the top of uncovered suprarenal component. Views from top (A) and lateral (B) aspect of a commercially available Zenith stent graft.

Unfavorable aneurysm necks (neck length less than 10 mm, severe angulation > 60°, and severe calcification or presence of thrombus in the aneurysm neck) remain challenging for conventional infrarenal EVAR, and this has been addressed by using suprarenal and fenestration endovascular techniques[5-10]. Currently, helical computed tomography (CT) angiography is the preferred method for assessment of suprarenal and fenestrated stent grafting due to its rapid technical developments, which allow for acquisition of high spatial and temporal resolution images[11-13].

In addition to CT imaging, ultrasound and magnetic resonance imaging (MRI) are other two imaging modalities that play an increasing role in follow-up of EVAR of AAA. Ultrasound is less expensive and does not involve ionizing radiation or potentially nephrotoxic contrast[14,15]. Several studies reported the usefulness of contrast-enhanced ultrasound, because it seems to allow better identification and characterization of endoleaks[16-18]. Particularly, contrast-enhanced ultrasound was found to detect a low-flow endoleak classified as endotension on the basis of triple contrast-enhanced CT[16].

MRI is less commonly used than CT and ultrasound in clinical practice for follow-up of EVAR of AAA. This is mainly due to the fact that aortic stent grafts must be MR compatible. Patients with stainless steel devices are unable to be followed with MRI because of the significant metallic artifacts caused by the stainless steel components. The use of MRI for surveillance of EVAR has been evaluated with good results[19,20] in patients with nitinol endografts. Given the fact of lack of availability, long scanning time and cost issue, MRI is not routinely used in EVAR of AAA. MRI is particularly useful in patients with renal impairment.

In the current clinical practice, CT and ultrasound are both used collectively as follow-up imaging tools, especially in the early follow-up periods. Our experience showed that when the aneurysm sac started to shrink it is reasonable to move from CT to ultrasound, reserving CT for patients with suspected aneurysm sac re-enlargement or presence of endoleaks[21].

SUPRARENAL FIXATION OF STENT GRAFTS-TECHNICAL DETAILS

Suprarenal fixation of stent grafts represents a technical modification to conventional infrarenal stent grafts by adding an uncovered suprarenal component on top of the graft material. This allows for proximal fixation of stent grafts with aim of reducing the migration of stent grafts after deployment, thus decreasing the incidence of procedure-related complications, mainly type I endoleak or stent graft migration[5,6]. Attachment may be improved by adding hooks and barbs to the proximal stent (Figure 1)[22,23]. It was reported that stronger fixation could be provided by barbs that perforate the entire aortic wall, enhancing the strength of stent-graft fixation by at least 10 fold[24]. Clinical studies have shown that suprarenal fixation of stent grafts were successfully used to treat patients with suboptimal aneurysm necks with satisfactory results achieved based on short to mid-term follow-up[5,6,25-27], although the long-term safety of this technique is yet to be proven. The main difference between conventional infrarenal and suprarenal stent grafting is the addition of a suprarenal component on top of graft material and presence of suprarenal stent wires in front of the renal artery ostium, which could affect the renal artery perfusion or renal function[25-27]. Accurate assessment of the configuration of suprarenal stent wires in relation to the renal artery is clinically significant, and this is highly dependent on medical image visualization and assessment.

FENESTRATED STENT GRAFTS-TECHNICAL DETAILS

Fenestrated stent grafts represent another technical improvement for treatment of patients with complicated aneurysm necks, especially in patients with short aneurysm necks (less than 10 mm). The principle of fenestrated stent grafting is to create an opening in the graft fabric to accommodate the orifice of the blood vessel that is targeted for preservation[10,28,29]. In most situations, fixation of the fenestration to the renal and the other visceral arteries such as the celiac axis and mesenteric artery can be achieved by implanting bare or covered stents across the graft-artery ostia interfaces. This ensures the stability of stent grafts and guarantees the fenestrated stents are in the correct position in relation to the fenestrated branch vessels. Normally about one-third (5-8 mm in length) of the fenestrated stents protrudes into the abdominal aorta, while the remaining component remains inside the

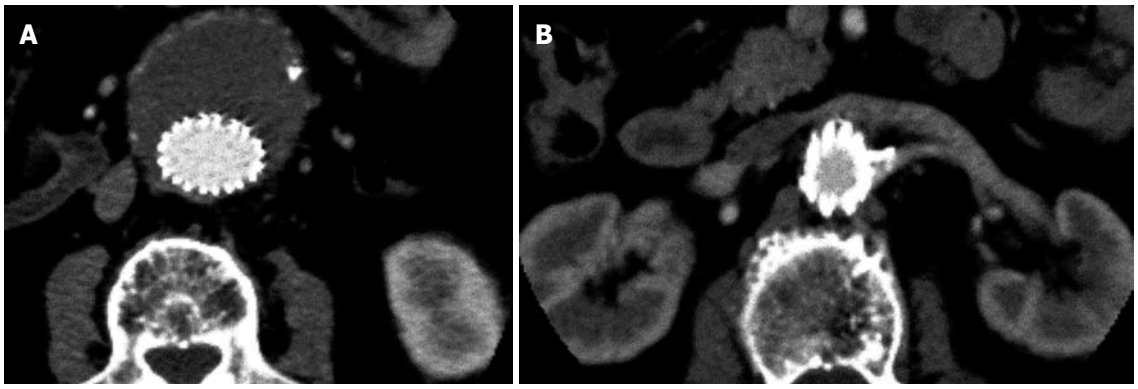

Figure 2 2D axial images in a patient treated with suprarenal stent graft. The aneurysm was successfully excluded from the systemic circulation (A), and the suprarenal stent struts were placed above the left renal artery (B).

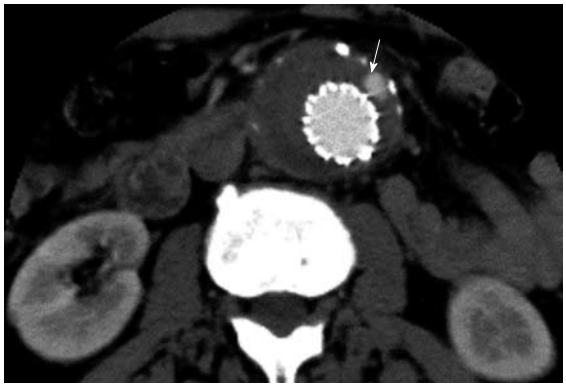

Figure 3 Contrast enhancement was present outside the stent graft but within the aneurysm sac indicating the endoleak (arrow) in a patient with abdominal aortic aneurysm (AAA) following suprarenal fixation of stent graft.

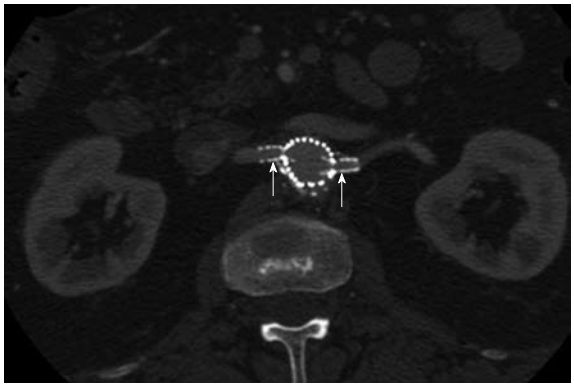

Figure 4 2D axial images show the small fenestrated stents inserted (arrows) into the bilateral renal arteries.

fenestrated arteries. With stents in position, a balloon is inflated to position the stent within the renal and other visceral arteries and begins the flare. This is performed to dilate the fenestrated vessel stents and ensure their fixation against the aortic wall and main body of the stent grafts. It is a routine procedure to perform completion angiography with the aim of confirming normal perfusion of renal arteries and exclusion of the presence of endoleak.

The types of fenestration used in fenestrated repair include scallop (standard and double width scallop) fenestration, and large and small fenestrations[30]. Fenestrations are constructed to match the aortic ostial diameter and maximize the sealing zone. Small fenestration has a width of 6 mm and a height between 6 and 8 mm. The ostia for small fenestrations are placed between stent struts of the aortic device, to allow unrestrained access into the visceral artery. Large fenestrations have greater diameters between 8 and 10 mm, with a strut crossing the fenestration. Standard scallop fenestrations have a minimum width of 10 mm and a height range of 6-12 mm, while double width scallop fenestrations are 20 mm × 20 mm.

2D IMAGE VISUALIZATIONS

In addition to conventional 2D axial images, a number of 2D and 3D reconstructions are generated to provide additional information which is required for accurate evaluation of the spatial relationship between suprarenal/fenestrated stent wires and aortic branches[31]. Of these reconstructed visualizations, multiplanar reformation (MPR), maximum-intensity projection (MIP), and volume rendering (VR) are the most commonly used tools in clinical practice. Another 3D visualization, virtual intravascular endoscopy (VIE) which is a unique tool for providing intraluminal views of the artery wall and stents has been reported to be valuable in the assessment of both suprarenal fixation of stent grafts and fenestrated repair of AAA[32-35].

Conventional 2D axial imaging is the routine image visualization for follow-up of EVAR of AAA. Axial images are useful for detection and measurement of the aortic aneurysm diameter and extent, identification of the position of aortic stent grafts (Figure 2), detection of post-procedural complications such as endoleaks (Figure 3), patency of the stents inserted into the fenestrated vessels (Figure 4), and protrusion of the fenestrated stents into the aortic lumen (Figure 5). However, 2D axial images cannot provide the 3D relationship between stent grafts and aortic branches, which is the main limitation. Another limitation of the 2D axial images lies in the fact that 2D axial views do

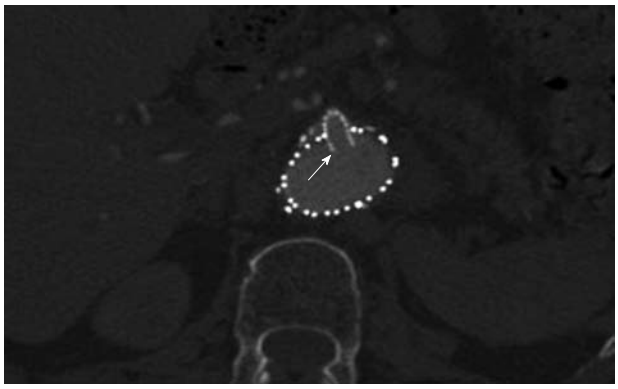

Figure 5 A large fenestrated stent was inserted into the superior mesenteric artery with an intraluminal protrusion (arrow).

Figure 6 Sagittal multiplanar reformatted image shows the stent graft was placed below the celiac axis (short arrows) and SMA (long arrows).

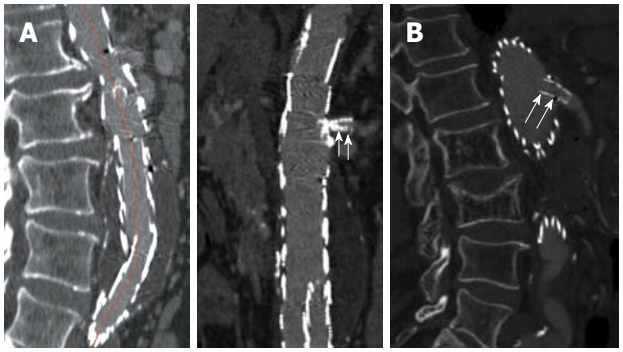

Figure 7 Curved planar reformatted images are produced following the centreline of the abdominal aorta to demonstrate the fenestrated renal stent (arrows in A) and the intra-aortic portion of fenestrated stent deployed into the SMA (arrows in B).

not provide accurate measurements of aneurysm length which is essential for pre-operative planning and aneurysm volume which is useful for follow-up. Traditionally, the preferred imaging method for surveillance of EVAR of AAA is CT angiography, which involves a series of maximal diameter measurements of the aneurysm at regular periods of follow-up, and determining whether the aneurysm is shrinking, enlarging, or remaining unchanged. This has been challenged by some studies which demonstrated the inaccuracy of diameter measurements[36-38]. Studies showed that volume measurement is superior to diameter measurement as it reflects

Figure 8 Computed tomography (CT) coronal maximum-intensity projection (MIP) clearly demonstrates the high-density stent wires and contrast-enhanced blood vessels.

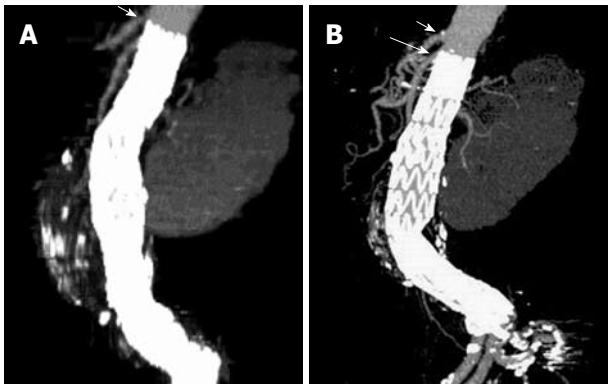

Figure 9 A stent graft migration of 10.2 mm was noticed in a recent sagittal MIP image (B) in a patient treated with suprarenal stent graft 3 years ago (A). Short arrows indicate celiac axis, while long arrow refer to SMA.

all size changes of the aneurysm[37,38]. Thus, accurate evaluation of the aneurysm and stent grafts relative to the aortic branches cannot be assessed based only on 2D axial images. This is complemented by 2D or 3D reconstruction visualizations.

MPR is commonly used to demonstrate the stent grafts relative to the aortic branches through different views, such as coronal and sagittal reformation (Figure 6). Curved planar reformatted images are generated to look at tortuous vessels as these are useful for visualization of the stent grafts position inside the abdominal aorta, as well as the intraluminal portion of suprarenal and fenestrated stents (Figure 7). However, the intraluminal appearance of the suprarenal stent wires in terms of encroachment to the renal artery ostium and fenestrated stents cannot be clearly visualized on MPR views. Moreover, a series of MPR images are required for demonstration of the entire volume dataset as individual MPR views cannot provide all of the anatomical details, which is the main limitation of this visualization tool.

For CT angiography of aortic stent grafting, MIP is the most valuable visualization tool as it produces angiography-like images which clearly shows the high-density aortic stents and contrast-enhanced arterial branches (Figure 8). As a less invasive technique compared to invasive angiography, CT MIP was shown to be more accurate for measurement of stent graft migration than conventional 2D images[34] (Figure 9). CT MIP is a

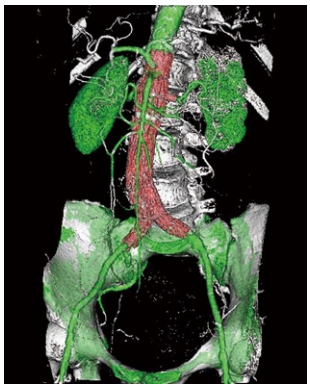

Figure 10 Volume rendering (VR) image demonstrates the 3D relationship between fenestrated renal stents (red color) and aortic branches (green color). Bones are coded with white color.

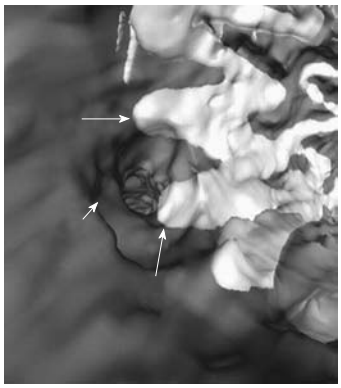

Figure 11 Virtual intravascular endoscopy (VIE) shows the left renal ostium (short arrow) was peripherally crossed by two suprarenal stent struts (long arrows).

widespread useful visualization tool in aortic stent grafting, and its application has been significantly enhanced with the use of 3D software package that is currently available on the workstation of modern CT scanners.

3D VR AND VIE VISUALIZATION

VR is an efficient visualization tool for showing the 3D relationship between stent grafts and arterial branches through use of the all of the information contained inside a volume dataset, thus enhancing readers' understanding of the complex structures of stent grafts and arterial branches. In contrast to the above-mentioned 2D visualizations, VR can easily display various components in a single image with different colors coded to different anatomical structures (Figure 10). VR provides more information than MIP, since a realistic demonstration of the aortic stent grafts and aortic branches can be displayed in a three-dimensional format; thus better appreciation of the stent grafts in relation to the aortic branches can be obtained.

As part of the VR visualization, VIE provides unique information of the intraluminal appearance of the artery wall and aortic stents. Our previous studies showed that VIE provides additional information about suprarenal stents encroachment to the renal artery ostium in terms of the configuration of stent wires and number of stent wires crossing the renal ostium (Figure 11)[31-34]. For fenestrated stent grafting of AAA, VIE is also able to demonstrate the intraluminal configuration and the intra-aortic protrusion of the fenestrated stents (Figure 12).

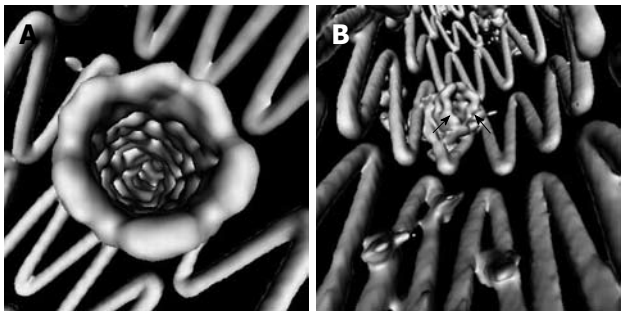

Figure 12 VIE views demonstrate the intraluminal appearance of fenestrated renal stent as circular configuration (A). In addition, the intraluminal portion of the fenestrated stent can be visualised and measured on VIE (arrows in B).

Figure 13 Deformed fenestrated renal stent with irregular appearance is displayed on VIE image (arrows).

This includes the normal appearance of fenestrated stents, as well as deformity or occlusion of the fenestrated stents resulting from the inappropriate fenestrated procedures (Figure 13)[30,35]. In comparison to conventional 2D visualizations, VIE offers valuable information about suprarenal and fenestrated repair since it demonstrates the number of stent wires crossing the renal ostium, confirms the patency of fenestrated vessels, and performs accurate measurement of the intraluminal portion of the fenestrated stents. These details are believed useful for patient follow-up.

INTERFERENCE OF AORTIC STENTS WITH RENAL HEMODYNAMICS

The deployment of a complex multi-component endovascular device in the abdominal aorta is likely to change the local hemodynamics and adversely affects the long-term performance of the device. Researchers studied the fluid-stent graft interaction based on AAA models with a focus on infrarenal fixation of stent grafts[39-41]. Our previous experiments based on realistic aorta models with variable configurations of suprarenal stent wires crossing the renal artery ostium showed that multiple wire configuration leads to a significant decrease in flow velocity to the renal artery, while single wire crossing has a minimal effect on the renal flow changes (Figure 14)[42]. For fenestrated stent grafting, the hemodynamic analysis showed that the interference of fenestrated renal stents with the renal blood flow is

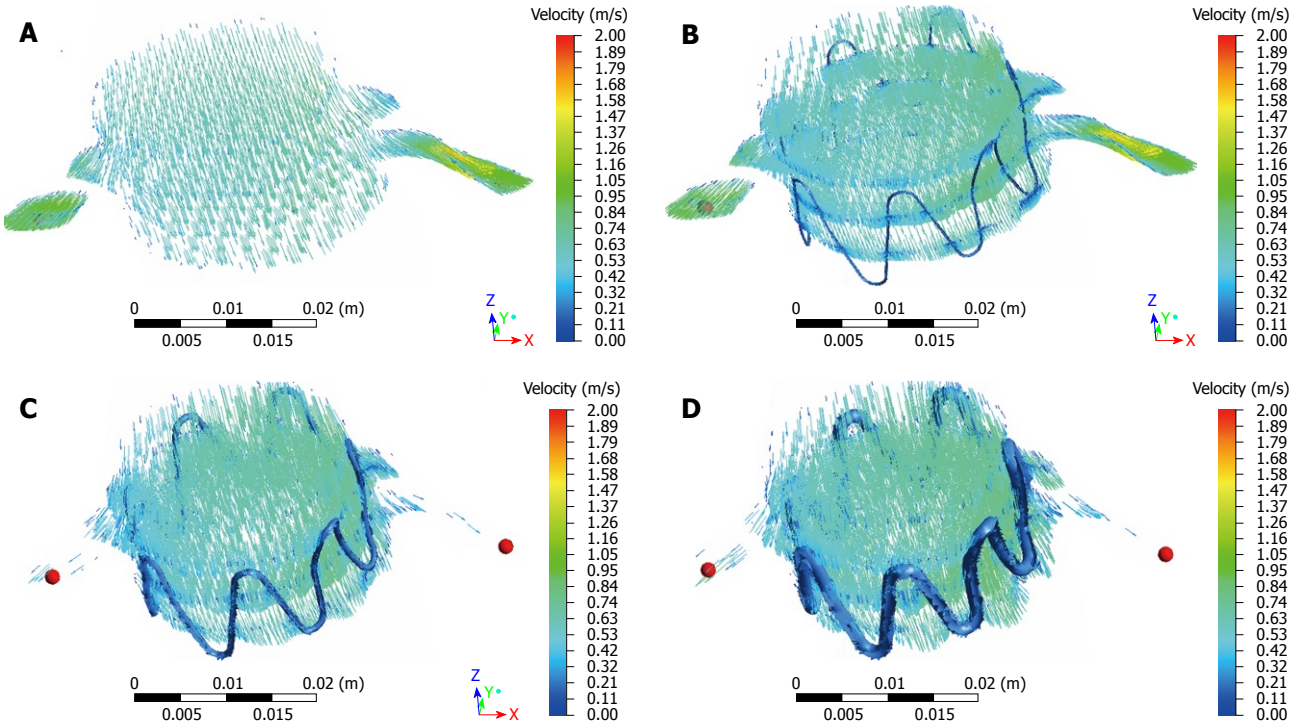

Figure 14 Computational fluid dynamic analysis of the interference of suprarenal stent struts with renal blood flow shows the flow velocity calculated in a realistic aorta model without placement of suprarenal stent struts (A), with simulated stent wire thickness of 0.4 mm (B), 1.0 mm (C) and 2.0 mm (D). The laminar flow pattern from pre-stent grafting was found to change to turbulent with simulated stent struts across the renal arteries, with flow velocity decreased up to 30% when the wire thickness increased to 2.0 mm.

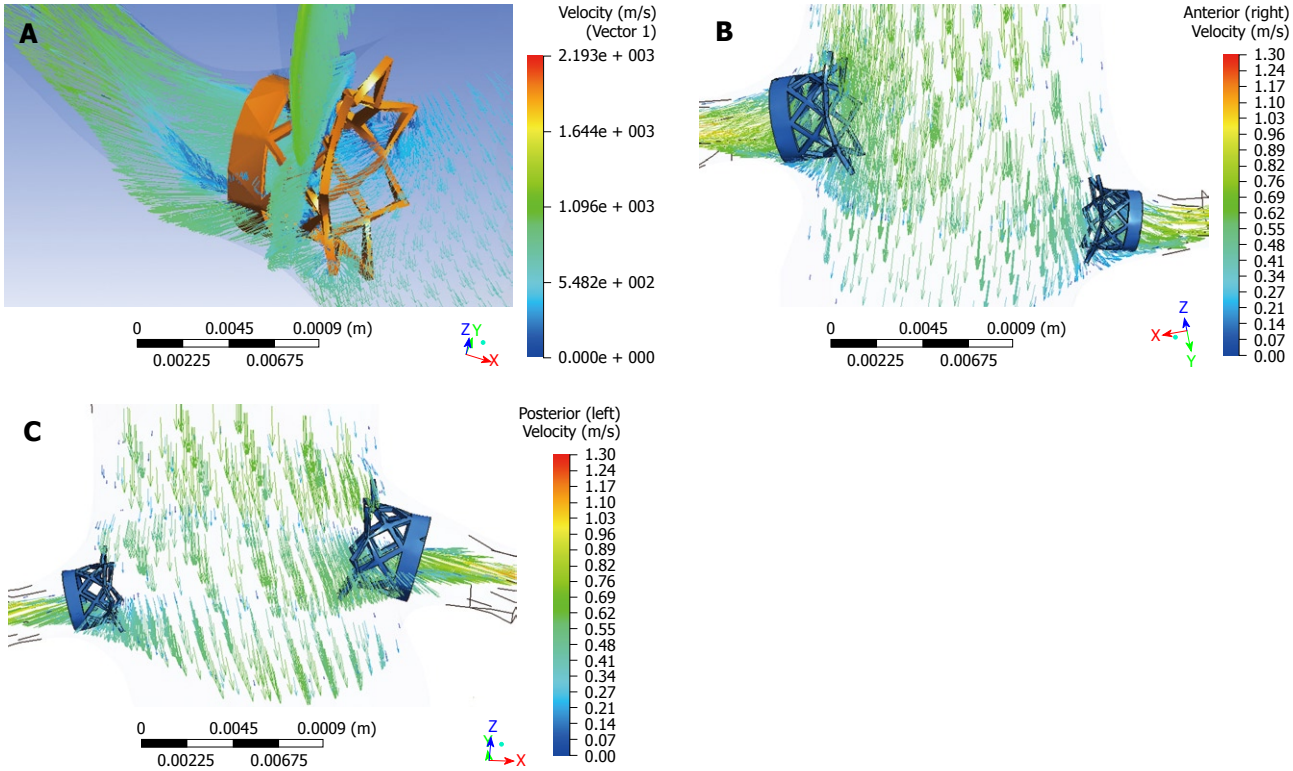

Figure 15 Computational fluid dynamic analysis of the interference of fenestrated renal stent with renal flow was performed with a simulated renal stent inserted into the renal arteries based on an aorta model (A). Flow velocity was not significantly affected after placement of fenestrated renal stents, although flow recirculation was observed at the proximal portion of the renal arteries (B, C).

minimal and insignificant, so this indicates the safety of deploying the fenestrated renal stents inside the renal arteries (Figure 15)[43]. However, wall shear stress at the renal arteries was reduced after implantation of the

fenestrated renal stents, thus this could lead to a potential risk of thrombus formation or stenosis at the renal arteries. Further studies with simulation of different stent wire thicknesses or variable lengths of stent protrusion are necessary to investigate the hemodynamic effects of endovascular stent graft repair of AAA.

FUTURE DIRECTIONS

Since the main concern associated with EVAR of AAA is the patency of renal arteries essential to maintain renal perfusion, future developments of endovascular stent grafts lie in the long-term safety and effects on renal function. This can be achieved through technical modifications of the stent grafts, such as bioengineering of the stent grafts to reduce the proliferation on the stent surface once deployed inside the aorta, or production of drug-eluting stents for fenestrated renal stents[44,45]. In addition to these technical developments, imaging follow-up is another issue that needs to be drawn to endovascular specialists' attention, as patients treated with aortic stent grafts are routinely followed for a long time, thus selection of appropriate imaging modalities is of paramount importance for both monitoring of the success of the procedure and detection of complications.

Helical CT angiography has been widely recognized as the method of choice for follow-up of EVAR of AAA due to its accuracy for measurement of the aneurysm and sensitivity for detection of endoleaks[11-13]. However, CT suffers from the issue of radiation exposure to patients, which is the main disadvantage. Follow-up of patients after EVAR requires multiple examinations at 1, 6 and 12 mo post-procedure, and typically requires the use of thin slices and multiple phase examinations. Thus, patients undergoing EVAR are at potential risk for excessively being exposed to radiation[46]. Optimization of CT scanning protocol is one of the effective strategies to reduce radiation dose. Iezzi *et al*[46] in their study reported that an overall radiation dose reduction of 74% was achieved with low dose protocol when compared to the standard dose protocol, while maintaining image quality. A recent study investigating the radiation exposure during EVAR of AAA concluded that the mean effective dose of CT angiography was 27 mSv, and the entrance skin dose exceeded the threshold value in 29% of patients[47]. This indicates the trend to move from CT follow-up to ultrasound surveillance[48-50], which is another effective approach to reduce radiation dose, since lifelong surveillance is necessary after EVAR. Several studies reported excellent results of ultrasound in the follow-up of EVAR of AAA when compared to CT angiography[16-18,48,49].

Traditional imaging-based follow-up of AAA after EVAR restricted to the detection of endoleaks (the most common complication of EVAR) and changes in AAA morphology have proved unreliable in preventing aneurysm rupture. Pressure measurements of the aneurysm sac are increasingly being recognized as the most accurate indication of AAA exclusion[51-53]. Attempts have been made at assessment of EVAR by intra-aneurysm sac pressure measurements through *in vitro* and *in vivo* studies[51-53]. These studies showed that high intra-aneurysm sac pressure is associated with AAA enlargement and low pressure with shrinkage. Imaging alone requires at least two time interval examinations to determine the trend or treatment outcomes of EVAR. Pressure measurements allow immediate reassurance or indication to intervene. Although it may only apply to few now, pressure measurement is heralded for general use and will provide a scientific basis for the management of common complications such as endoleaks[21].

CONCLUSION

There is no doubt that EVAR will continue to play an increasing role in the treatment of patients with AAA. While its benefits have been widely recognized by clinical practice and thousands of cases are performed every year, the long-term durability is yet to be confirmed. Medical imaging modalities play an essential role in both planning and post-operative follow-up. CT is the preferred imaging modality for following patients treated with endovascular stent grafts; however, ultrasound is being increasingly used to monitor the treatment outcomes at regular follow-up as it does not involve ionizing radiation and its diagnostic accuracy for detection of endoleaks is comparable to CT imaging. Although still under development, pressure measurement is destined for general use and will provide a scientific basis for monitoring treatment outcomes of EVAR and the management of complications such as type Ⅱ endoleaks. Technical improvements are required to ensure the long-term safety of deploying the stent grafts inside the abdominal aorta and artery branches.

REFERENCES

1 **Greenhalgh RM**, Brown LC, Kwong GP, Powell JT, Thompson SG. Comparison of endovascular aneurysm repair with open repair in patients with abdominal aortic aneurysm (EVAR trial 1), 30-day operative mortality results: randomised controlled trial. *Lancet* 2004; **364**: 843-848

2 **Prinssen M**, Verhoeven EL, Buth J, Cuypers PW, van Sambeek MR, Balm R, Buskens E, Grobbee DE, Blankensteijn JD. A randomized trial comparing conventional and endovascular repair of abdominal aortic aneurysms. *N Engl J Med* 2004; **351**: 1607-1618

3 **Parodi JC**, Palmaz JC, Barone HD. Transfemoral intraluminal graft implantation for abdominal aortic aneurysms. *Ann Vasc Surg* 1991; **5**: 491-499

4 **Buth J**, van Marrewijk CJ, Harris PL, Hop WC, Riambau V, Laheij RJ. Outcome of endovascular abdominal aortic aneurysm repair in patients with conditions considered unfit for an open procedure: a report on the EUROSTAR experience. *J Vasc Surg* 2002; **35**: 211-221

5 **Lobato AC**, Quick RC, Vaughn PL, Rodriguez-Lopez J, Douglas M, Diethrich EB. Transrenal fixation of aortic endografts: intermediate follow-up of a single-center experience. *J Endovasc Ther* 2000; **7**: 273-278

6 **Bove PG**, Long GW, Zelenock GB, Bendick PJ, Khoury MD, Burr MO, Bechtel G, Becker F, Huckabone C. Transrenal

fixation of aortic stent-grafts for the treatment of infrarenal aortic aneurysmal disease. *J Vasc Surg* 2000; **32**: 697-703
7 **Browne TF**, Hartley D, Purchas S, Rosenberg M, Van Schie G, Lawrence-Brown M. A fenestrated covered suprarenal aortic stent. *Eur J Vasc Endovasc Surg* 1999; **18**: 445-449
8 **Stanley BM**, Semmens JB, Lawrence-Brown MM, Goodman MA, Hartley DE. Fenestration in endovascular grafts for aortic aneurysm repair: new horizons for preserving blood flow in branch vessels. *J Endovasc Ther* 2001; **8**: 16-24
9 **Anderson JL**, Berce M, Hartley DE. Endoluminal aortic grafting with renal and superior mesenteric artery incorporation by graft fenestration. *J Endovasc Ther* 2001; **8**: 3-15
10 **Muhs BE**, Verhoeven EL, Zeebregts CJ, Tielliu IF, Prins TR, Verhagen HJ, van den Dungen JJ. Mid-term results of endovascular aneurysm repair with branched and fenestrated endografts. *J Vasc Surg* 2006; **44**: 9-15
11 **Stavropoulos SW**, Clark TW, Carpenter JP, Fairman RM, Litt H, Velazquez OC, Insko E, Farner M, Baum RA. Use of CT angiography to classify endoleaks after endovascular repair of abdominal aortic aneurysms. *J Vasc Interv Radiol* 2005; **16**: 663-667
12 **Iezzi R**, Cotroneo AR, Filippone A, Santoro M, Basilico R, Storto ML. Multidetector-row computed tomography angiography in abdominal aortic aneurysm treated with endovascular repair: evaluation of optimal timing of delayed phase imaging for the detection of low-flow endoleaks. *J Comput Assist Tomogr* 2008; **32**: 609-615
13 **Flohr TG**, McCollough CH, Bruder H, Petersilka M, Gruber K, Süss C, Grasruck M, Stierstorfer K, Krauss B, Raupach R, Primak AN, Küttner A, Achenbach S, Becker C, Kopp A, Ohnesorge BM. First performance evaluation of a dual-source CT (DSCT) system. *Eur Radiol* 2006; **16**: 256-268
14 **Zannetti S**, De Rango P, Parente B, Parlani G, Verzini F, Maselli A, Nardelli L, Cao P. Role of duplex scan in endoleak detection after endoluminal abdominal aortic aneurysm repair. *Eur J Vasc Endovasc Surg* 2000; **19**: 531-535
15 **d'Audiffret A**, Desgranges P, Kobeiter DH, Becquemin JP. Follow-up evaluation of endoluminally treated abdominal aortic aneurysms with duplex ultrasonography: validation with computed tomography. *J Vasc Surg* 2001; **33**: 42-50
16 **Napoli V**, Bargellini I, Sardella SG, Petruzzi P, Cioni R, Vignali C, Ferrari M, Bartolozzi C. Abdominal aortic aneurysm: contrast-enhanced US for missed endoleaks after endoluminal repair. *Radiology* 2004; **233**: 217-225
17 **Giannoni MF**, Palombo G, Sbarigia E, Speziale F, Zaccaria A, Fiorani P. Contrast-enhanced ultrasound imaging for aortic stent-graft surveillance. *J Endovasc Ther* 2003; **10**: 208-217
18 **AbuRahma AF**, Welch CA, Mullins BB, Dyer B. Computed tomography versus color duplex ultrasound for surveillance of abdominal aortic stent-grafts. *J Endovasc Ther* 2005; **12**: 568-573
19 **Cejna M**, Loewe C, Schoder M, Dirisamer A, Hölzenbein T, Kretschmer G, Lammer J, Thurnher S. MR angiography vs CT angiography in the follow-up of nitinol stent grafts in endoluminally treated aortic aneurysms. *Eur Radiol* 2002; **12**: 2443-2450
20 **Schwope RB**, Alper HJ, Talenfeld AD, Cohen EI, Lookstein RA. MR angiography for patient surveillance after endovascular repair of abdominal aortic aneurysms. *AJR Am J Roentgenol* 2007; **188**: W334-W340
21 **Lawrence-Brown MM**, Sun Z, Semmens JB, Liffman K, Sutalo ID, Hartley DB. Type II endoleaks: when is intervention indicated and what is the index of suspicion for types I or III? *J Endovasc Ther* 2009; **16** Suppl 1: I106-I118
22 **Lawrence DD Jr**, Charnsangavej C, Wright KC, Gianturco C, Wallace S. Percutaneous endovascular graft: experimental evaluation. *Radiology* 1987; **163**: 357-360
23 **Yoshioka T**, Wright KC, Wallace S, Lawrence DD Jr, Gianturco C. Self-expanding endovascular graft: an experimental study in dogs. *AJR Am J Roentgenol* 1988; **151**: 673-676
24 **Malina M**, Lindblad B, Ivancev K, Lindh M, Malina J, Brunkwall J. Endovascular AAA exclusion: will stents with hooks and barbs prevent stent-graft migration? *J Endovasc Surg* 1998; **5**: 310-317
25 **Alric P**, Hinchliffe RJ, Picot MC, Braithwaite BD, MacSweeney ST, Wenham PW, Hopkinson BR. Long-term renal function following endovascular aneurysm repair with infrarenal and suprarenal aortic stent-grafts. *J Endovasc Ther* 2003; **10**: 397-405
26 **Greenberg RK**, Chuter TA, Sternbergh WC 3rd, Fearnot NE. Zenith AAA endovascular graft: intermediate-term results of the US multicenter trial. *J Vasc Surg* 2004; **39**: 1209-1218
27 **Greenberg RK**, Chuter TA, Lawrence-Brown M, Haulon S, Nolte L. Analysis of renal function after aneurysm repair with a device using suprarenal fixation (Zenith AAA Endovascular Graft) in contrast to open surgical repair. *J Vasc Surg* 2004; **39**: 1219-1228
28 **Verhoeven EL**, Prins TR, Tielliu IF, van den Dungen JJ, Zeebregts CJ, Hulsebos RG, van Andringa de Kempenaer MG, Oudkerk M, van Schilfgaarde R. Treatment of short-necked infrarenal aortic aneurysms with fenestrated stent-grafts: short-term results. *Eur J Vasc Endovasc Surg* 2004; **27**: 477-483
29 **Greenberg RK**, Haulon S, O'Neill S, Lyden S, Ouriel K. Primary endovascular repair of juxtarenal aneurysms with fenestrated endovascular grafting. *Eur J Vasc Endovasc Surg* 2004; **27**: 484-491
30 **Sun Z**, Allen YB, Nadkarni S, Knight R, Hartley DE, Lawrence-Brown MM. CT virtual intravascular endoscopy in the visualization of fenestrated stent-grafts. *J Endovasc Ther* 2008; **15**: 42-51
31 **Sun Z**. 3D multislice CT angiography in post-aortic stent grafting: a pictorial essay. *Korean J Radiol* 2006; **7**: 205-211
32 **Sun Z**, Winder RJ, Kelly BE, Ellis PK, Hirst DG. CT virtual intravascular endoscopy of abdominal aortic aneurysms treated with suprarenal endovascular stent grafting. *Abdom Imaging* 2003; **28**: 580-587
33 **Sun Z**, Winder RJ, Kelly BE, Ellis PK, Kennedy PT, Hirst DG. Diagnostic value of CT virtual intravascular endoscopy in aortic stent-grafting. *J Endovasc Ther* 2004; **11**: 13-25
34 **Sun Z**. Three-dimensional visualization of suprarenal aortic stent-grafts: evaluation of migration in midterm follow-up. *J Endovasc Ther* 2006; **13**: 85-93
35 **Sun Z**, Mwipatayi BP, Allen YB, Hartley DE, Lawrence-Brown MM. Multislice CT angiography of fenestrated endovascular stent grafting for treating abdominal aortic aneurysms: a pictorial review of the 2D/3D visualizations. *Korean J Radiol* 2009; **10**: 285-293
36 **Wever JJ**, Blankensteijn JD, Th M Mali WP, Eikelboom BC. Maximal aneurysm diameter follow-up is inadequate after endovascular abdominal aortic aneurysm repair. *Eur J Vasc Endovasc Surg* 2000; **20**: 177-182
37 **Kritpracha B**, Beebe HG, Comerota AJ. Aortic diameter is an insensitive measurement of early aneurysm expansion after endografting. *J Endovasc Ther* 2004; **11**: 184-190
38 **Bargellini I**, Cioni R, Petruzzi P, Pratali A, Napoli V, Vignali C, Ferrari M, Bartolozzi C. Endovascular repair of abdominal aortic aneurysms: analysis of aneurysm volumetric changes at mid-term follow-up. *Cardiovasc Intervent Radiol* 2005; **28**: 426-433
39 **Chong CK**, How TV. Flow patterns in an endovascular stent-graft for abdominal aortic aneurysm repair. *J Biomech* 2004; **37**: 89-97
40 **Fillinger MF**, Raghavan ML, Marra SP, Cronenwett JL, Kennedy FE. In vivo analysis of mechanical wall stress and abdominal aortic aneurysm rupture risk. *J Vasc Surg* 2002; **36**: 589-597
41 **Deplano V**, Knapp Y, Bertrand E, Gaillard E. Flow behaviour in an asymmetric compliant experimental model

for abdominal aortic aneurysm. *J Biomech* 2007; **40**: 2406-2413
42 **Sun Z**, Chaichana T. Investigation of the hemodynamic effect of stent wires on renal arteries in patients with abdominal aortic aneurysms treated with suprarenal stent-grafts. *Cardiovasc Intervent Radiol* 2009; **32**: 647-657
43 **Sun Z**, Chaichana T. Fenestrated stent graft repair of abdominal aortic aneurysm: hemodynamic analysis of the effect of fenestrated stents on the renal arteries. *Korean J Radiol* 2010; **11**: 1-5
44 **Holmes DR Jr**, Leon MB, Moses JW, Popma JJ, Cutlip D, Fitzgerald PJ, Brown C, Fischell T, Wong SC, Midei M, Snead D, Kuntz RE. Analysis of 1-year clinical outcomes in the SIRIUS trial: a randomized trial of a sirolimus-eluting stent versus a standard stent in patients at high risk for coronary restenosis. *Circulation* 2004; **109**: 634-640
45 **Morice MC**, Colombo A, Meier B, Serruys P, Tamburino C, Guagliumi G, Sousa E, Stoll HP. Sirolimus- vs paclitaxel-eluting stents in de novo coronary artery lesions: the REALITY trial: a randomized controlled trial. *JAMA* 2006; **295**: 895-904
46 **Iezzi R**, Cotroneo AR, Giammarino A, Spigonardo F, Storto ML. Low-dose multidetector-row CT-angiography of abdominal aortic aneurysm after endovascular repair. *Eur J Radiol* 2009; Epub ahead of print
47 **Weerakkody RA**, Walsh SR, Cousins C, Goldstone KE, Tang TY, Gaunt ME. Radiation exposure during endovascular aneurysm repair. *Br J Surg* 2008; **95**: 699-702
48 **McWilliams RG**, Martin J, White D, Gould DA, Rowlands PC, Haycox A, Brennan J, Gilling-Smith GL, Harris PL. Detection of endoleak with enhanced ultrasound imaging: comparison with biphasic computed tomography. *J Endovasc Ther* 2002; **9**: 170-179
49 **Bendick PJ**, Bove PG, Long GW, Zelenock GB, Brown OW, Shanley CJ. Efficacy of ultrasound scan contrast agents in the noninvasive follow-up of aortic stent grafts. *J Vasc Surg* 2003; **37**: 381-385
50 **Sun Z**. Diagnostic value of color duplex ultrasonography in the follow-up of endovascular repair of abdominal aortic aneurysm. *J Vasc Interv Radiol* 2006; **17**: 759-764
51 **Dias NV**, Ivancev K, Malina M, Resch T, Lindblad B, Sonesson B. Intra-aneurysm sac pressure measurements after endovascular aneurysm repair: differences between shrinking, unchanged, and expanding aneurysms with and without endoleaks. *J Vasc Surg* 2004; **39**: 1229-1235
52 **Ellozy SH**, Carroccio A, Lookstein RA, Jacobs TS, Addis MD, Teodorescu VJ, Marin ML. Abdominal aortic aneurysm sac shrinkage after endovascular aneurysm repair: correlation with chronic sac pressure measurement. *J Vasc Surg* 2006; **43**: 2-7
53 **Chaudhuri A**, Ansdell LE, Grass AJ, Adiseshiah M. Intrasac pressure waveforms after endovascular aneurysm repair (EVAR) are a reliable marker of type I endoleaks, but not type II or combined types: an experimental study. *Eur J Vasc Endovasc Surg* 2004; **28**: 373-378

S- Editor Wang JL **L- Editor** O'Neill M **E- Editor** Zheng XM

World Journal of Radiology

Online Submissions: http://www.wjgnet.com/1949-8470office
wjr@wjgnet.com
doi:10.4329/wjr.v1.i1.72

World J Radiol 2009 December 31; 1(1): 72-85
ISSN 1949-8470 (online)

REVIEW

Magnetic resonance imaging of the liver: New imaging strategies for evaluating focal liver lesions

Kenneth Coenegrachts

Kenneth Coenegrachts, Department of Radiology, AZ St.-Jan Brugge-Oostende AV, Ruddershove 10, B-8000 Bruges, Belgium
Author contributions: Coenegrachts K contributed solely to this paper.
Correspondence to: Kenneth Coenegrachts, MD, PhD, Department of Radiology, AZ St.-Jan Brugge-Oostende AV, Ruddershove 10, B-8000 Bruges, Belgium. kenneth.coenegrachts@azbrugge.be
Telephone: +32-50-452103 Fax: +32-50-452146
Received: October 10, 2009 Revised: November 12, 2009
Accepted: November 16, 2009
Published online: December 31, 2009

Abstract

The early detection of focal liver lesions, particularly those which are malignant, is of utmost importance. The resection of liver metastases of some malignancies (including colorectal cancer) has been shown to improve the survival of patients. Exact knowledge of the number, size, and regional distribution of liver metastases is essential to determine their resectability. Almost all focal liver lesions larger than 10 mm are demonstrated with current imaging techniques but the detection of smaller focal liver lesions is still relatively poor. One of the advantages of magnetic resonance imaging (MRI) of the liver is better soft tissue contrast (compared to other radiologic modalities), which allows better detection and characterization of the focal liver lesions in question. Developments in MRI hardware and software and the availability of novel MRI contrast agents have further improved the diagnostic yield of MRI in lesion detection and characterization. Although the primary modalities for liver imaging are ultrasound and computed tomography, recent studies have suggested that MRI is the most sensitive method for detecting small liver metastatic lesions, and MRI is now considered the pre-operative standard method for diagnosis. Two recent developments in MRI sequences for the upper abdomen comprise unenhanced diffusion-weighted imaging (DWI), and keyhole-based dynamic contrast-enhanced (DCE) MRI (4D THRIVE). DWI allows improved detection (b = 10 s/mm^2) of small (< 10 mm) focal liver lesions in particular, and is useful as a road map sequence. Also, using higher b-values, the calculation of the apparent diffusion coefficient value, true diffusion coefficient, D, and the perfusion fraction, f, has been used for the characterization of focal liver lesions. DCE 4D THRIVE enables MRI of the liver with high temporal and spatial resolution and full liver coverage. 4D THRIVE improves evaluation of focal liver lesions, providing multiple arterial and venous phases, and allows the calculation of perfusion parameters using pharmacokinetic models. 4D THRIVE has potential benefits in terms of detection, characterization and staging of focal liver lesions and in monitoring therapy.

Key words: Magnetic resonance imaging; Liver neoplasms; Diffusion-weighted magnetic resonance imaging; 4D THRIVE; Dynamic contrast-enhanced magnetic resonance imaging; Contrast agents

Peer reviewer: Hui-Xiong Xu, MD, PhD, Professor, Department of Medical Ultrasonics, Institute of Diagnostic and Interventional Ultrasound, Sun Yat-Sen University, 58 Zhongshan Road 2, Guangzhou 510080, Guangdong Province, China

Coenegrachts K. Magnetic resonance imaging of the liver: New imaging strategies for evaluating focal liver lesions. *World J Radiol* 2009; 1(1): 72-85 Available from: URL: http://www.wjgnet.com/1949-8470/full/v1/i1/72.htm DOI: http://dx.doi.org/10.4329/wjr.v1.i1.72

INTRODUCTION

The early detection of focal liver lesions, particularly those which are malignant, is of utmost importance. For

example, the resection of liver metastases of some malignancies, including colorectal cancer, has been shown to improve the survival of patients[1]. Exact knowledge of the number, size, and regional distribution of liver metastases is essential to determine their resectability. Almost all focal liver lesions larger than 10 mm can be demonstrated with current imaging techniques but the detection of smaller focal liver lesions is still relatively poor[2-6]. Transabdominal ultrasonography (US) is widely used to assess the liver, but has some limitations: it needs considerable operator expertise and often reveals equivocal results in patients with chemotherapy-induced fatty infiltration of the liver[7]. Contrast-enhanced (CE)-US has increased the potential for characterization of malignant and benign focal liver lesions compared with baseline US. CE-US increased diagnostic confidence in the detection and characterization of liver metastases compared with standard US[8]. Limitations of CE-US are essentially the same as those of US and are related to the presence of bowel gas and to the patient's body habitus[9]. Among radiologic imaging techniques, US and CE-US are relatively inexpensive and therefore are used in many general radiology departments[10,11]. However, for accurate oncologic staging, US examinations often require to be complemented by other imaging techniques.

Diagnostically problematic cases using US are often referred for a computed tomography (CT) or magnetic resonance imaging (MRI) examination. With the introduction of multi-slice CT (MSCT) imaging, the use of MSCT in oncologic patients to search for lung, liver, and lymph node metastases in the body has substantially increased[12,13]. The development of MSCT has substantially increased patient throughput allowing volume coverage of the whole thorax and abdomen in one breath-hold. However, even using MSCT, the sensitivity and ability to discriminate between small liver metastases and other small focal liver lesions is inferior compared to MRI[12].

Combined positron emission tomography (PET)/CT images have significant advantages over either technique alone because it provides both functional and anatomical data. The most significant additional information provided by PET/CT relates to the accurate detection of distant metastases. In a study by Wiering *et al*[14], FDG-PET was clearly superior to CT in predicting extrahepatic disease in patients with colorectal liver metastases.

One of the advantages of MRI in liver imaging is the better soft tissue contrast, which reveals better characterization of focal liver lesions in question. The development of liver-specific MRI contrast agents has further improved the diagnostic yield of MRI in lesion detection and characterization[15,16]. Although the primary modalities for liver imaging are US and CT, recent studies have suggested that CE-MRI is the most sensitive method for detecting small liver metastases and MRI is now considered the pre-operative standard[17-21]. Developments in MRI hardware and software and the availability of novel MRI contrast agents have improved small focal liver lesion detection[22]. During the last few years, MRI enhanced with superparamagnetic iron oxide (SPIO) probably has been considered the most sensitive method for detecting so-called hypovascular liver metastases[22]. In the few studies which have compared different liver-specific agents, SPIO-enhanced MRI has demonstrated varying degrees of superiority, particularly for small focal liver lesions[23,24]. Furthermore, the importance of using ferucarbotran (SPIO contrast agent) by bolus injection, providing the opportunity to obtain dynamic T1-weighted (T1w) images has been described[22]. Ward[22] has found early T1-enhancement on 3D fat-suppressed T1w gradient echo (GE) images to be particularly valuable for depicting small focal liver lesions. The T1-effect is considerably less than occurs with extracellular fluid gadolinium (Gd)-based contrast agents but this is often beneficial in the context of metastatic disease. Liver and vessels often have a similar signal intensity that produces a virtual blank canvas against which small liver metastases are extremely conspicuous and reliably distinguished from vessels. The combination of thin-slice 3D T1w and T2w imaging after SPIO increases diagnostic confidence and is more accurate for small focal liver lesion detection than delayed T2w imaging alone[22].

NEW DEVELOPMENTS IN MRI SEQUENCES FOR THE LIVER

Diffusion-weighted imaging (DWI) [Single-shot spin-echo echo-planar imaging (SS SE-EPI sequence)]

Diffusion-weighted MRI is sensitive to molecular diffusion as a result of random and microscopic translational motion of molecules, known as Brownian motion. Random motion in the field gradient produces incoherent phase shifts that results in signal attenuation. Flowing spins induce the same attenuation effect; the pseudorandom organization of the moving spins at the voxel level, such as perfusion, can also be considered to be an incoherent motion, and this effect can induce much larger signal attenuation than the diffusion effect on an image with very low motion-probing gradients (MPGs)[25,26]. The strength of the applied MPG increases with increasing b-value (expressed in s/mm^2). On the basis of this theory, the apparent diffusion coefficient (ADC) value calculated from the images with no and low MPGs (ADC_{low}) is considered to be more strongly influenced by the flowing spins (microcirculation) than molecular diffusion. The true diffusion coefficient, D, can be obtained from the calculation from images with the higher b-values[25,26]. D as measured at intravoxel incoherent motion (IVIM) MRI is a true parameter of molecular diffusion[25,26]. It therefore permits characterization of tissues and pathologic conditions. Furthermore, the perfusion fraction, f, as measured at IVIM MRI is the (microperfusion) deviation factor representing the fractional

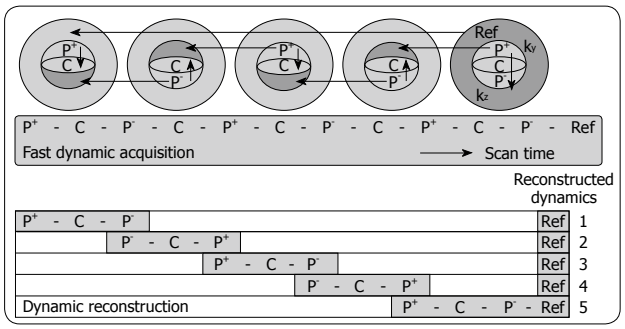

Figure 1 Schematic depiction of the alternating viewsharing technique. The central ky-kz disk defined by the keyhole percentage is subdivided in 3 regions, P^+, C and P^-, where P^+ and P^- cover positive and negative peripheral regions in this central disk and C is the central region as shown. The central region C is acquired in each dynamic scan while regions P^+ and P^- are shared with subsequent dynamic scans according to an alternating viewsharing scheme: P^+-C-P^--C-P^+-C-P^--C-P^+-Ref. The P^- and P^+ parts from subsequent keyhole scans are shared in the reconstruction process.

volume (of spins) occupied in the voxel by flowing spins (= sum of the spins in the microcirculation and spins in turbulent flow)[27].

During recent years, DWI of the liver, using echo planar imaging sequences with low b-values, has been proven to be useful for the detection of focal liver lesions because of the black-blood effect when using low b-values. The black-blood effect renders blood vessels black while focal liver lesions remain bright. The use of the black-blood effect for facilitating detection of focal liver lesions, by better differentiation between small vascular branches and small focal liver lesions, has been described previously[28]. This black-blood effect has proven to be useful in detecting focal liver lesions especially those smaller than 10 mm)[29-32]. Respiratory-triggered SS SE-EPI is preferred for liver MRI as respiratory-triggering increases the signal-to-noise ratio (SNR) and helps to avoid false-negative results but also false-positive results due to noise. In our experience[29], for focal liver lesion detection a b-value of b = 10 s/mm^2 is to be preferred over b = 20 or 50 s/mm^2.

DWI of the liver, using SS SE-EPI with low and high b-values, seems promising for the characterization of focal liver lesions by calculating D, f and ADC_{low}[25-27,33,34].

The SS SE-EPI sequence is prone to artifacts (e.g. air from the bowel loops). Therefore, we recommend giving each patient 0.5 L of tap water just before the start of each MRI examination. We also recommend starting each MRI examination of the upper abdomen with the SS SE-EPI sequence, using respiratory-triggering to optimize the SNR. The SS SE-EPI sequence can then be used as a road map sequence to guide the rest of the MRI examination.

T1w dynamic contrast-enhanced (DCE) MRI (4D THRIVE)

Three-phased DCE MRI is currently accepted as an important imaging tool for detecting and characterizing tumors in abdominal organs such as the liver[35]. The hepatic purely arterial phase is especially important to distinguish fast enhancing lesions from slow contrast uptake in liver parenchyma[36-38]. Also, imaging of the portal venous phase is crucial for characterizing focal liver lesions. However, often the arterial hepatic phase will overlap with enhancement of blood coming from the portal vein during the 20-s acquisition time typically achieved in 3-phased MRI[38]. To address this problem, Beck *et al*[39] recently proposed a fast imaging technique called CENTRA Plus or 4D THRIVE, combining the principles of keyhole imaging with half-Fourier acquisition to achieve a higher temporal resolution with full liver coverage and a minor decrease of the spatial resolution. The elliptical centric keyhole method consists of dynamically acquiring a limited number of central ky-kz-space profiles (disk), and sharing the high spatial resolution information from a single full data set called reference (Figure 1). To further accelerate the technique, an alternating view-sharing technique, as described in references 40 and 41, was applied. With this strategy it was shown that the precision of contrast-enhancement sampling could be improved[39].

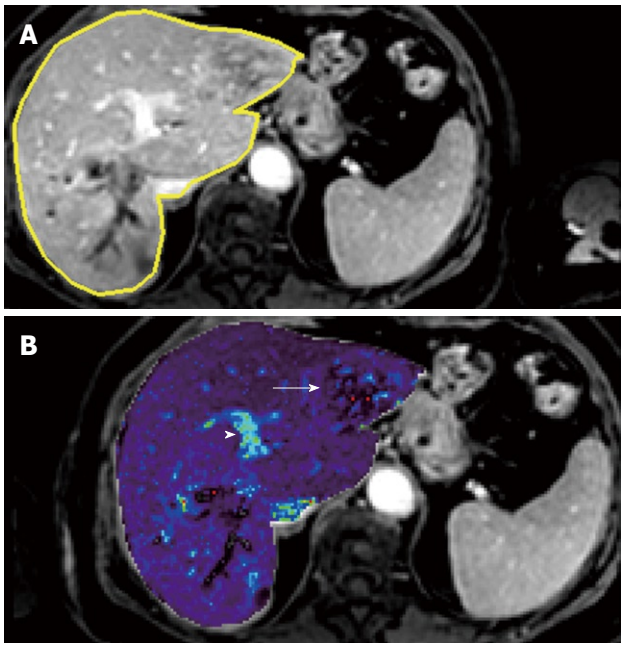

Figure 2 Liver metastasis in a 68-year-old woman using transverse contrast-enhanced 4D THRIVE. The reference image using 4D THRIVE in the delayed phase (A) is shown with corresponding automatically calculated Kep map (B). The parametric map shows the liver metastasis (white arrow) as a heterogeneous lesion with ring enhancement. The portal vein is indicated by the white arrowhead.

DCE MRI sequences (4D THRIVE) with higher temporal resolution can also be used to generate parametric maps (Figure 2) and to compute perfusion and permeability parameters using pharmacokinetic models, with potential benefits in terms of detection, characterization and staging of tumors and in monitoring therapy[42,43]. To date, reports of liver perfusion at MRI are limited in number and vary considerably[44]. T1w dynamic CE-MRI seems a promising method for the detection of cancer[45]. Remarkably, encouraging results

have been obtained despite considerable variation in both the methods of data acquisition and analysis (e.g. visual inspection[46], parametric analysis[47], pharmacokinetic[48] or physiologic[49] modeling). In most cases, only one to a few slices within the whole liver parenchyma have been used to evaluate perfusion parameters.

As a result of new developments in MRI scanning technologies, it is now possible to perform T1w CE-MRI of the entire liver with high spatial and temporal resolution, using the above mentioned T1w DCE 4D THRIVE sequence. This 4D THRIVE sequence has already been evaluated for its ability to differentiate benign from malignant focal liver lesions[41].

MRI CHARACTERISTICS OF DIFFERENT FOCAL LIVER LESIONS

Hepatic cysts

Hepatic cysts, including those without further pathologic importance, almost always can be accurately diagnosed using US. Only rarely are additional imaging sequences needed; non-complicated hepatic cysts can be easily characterized using MRI.

Complex cystic focal liver lesions are lesions containing large fluid-filled areas. They are increasingly commonly found in clinical practice as a result of the increased use of hepatic imaging. Complex cystic focal liver lesions represent a wide spectrum of lesions that include both benign and malignant lesions[50]. The most frequently encountered complex cystic focal liver lesions comprise hepatic cysts complicated by intracystic hemorrhage, abscesses (see description below), hematomas, cystadenomas and cystadenocarcinomas.

Hepatic cysts complicated with acute hemorrhage and acute hematomas are typically hyperintense on unenhanced T1w imaging. The differentiation between cystadenomas and cystadenocarcinomas using only imaging criteria can be very difficult and so-called borderline lesions are frequently encountered. The probability of underlying malignancy in general increases with increased thickening of the septations, increased septal calcifications and increased presence of mural thickening. Using contrast-enhanced MRI, complete non-enhancement using dynamic MRI or slow contrast-enhancement of the septations and mural nodules in the arterial phase and persistent contrast-enhancement in the portal and late venous phases most frequently are exhibited in benign complex cystic focal liver lesions. In contrast, hypo-enhancement in the late venous phases most frequently is seen in malignant complex cystic focal liver lesions[50].

Liver hemangiomas

Liver hemangiomas are the most common benign tumors of the liver, with a reported incidence ranging from 1% to 20%. Hemangiomas occur more commonly in women (female/male ratio 5:1). A hemangioma usually is well circumscribed and blood filled. Hemangiomas larger than 10 cm are designated as giant hemangiomas[51].

On cut sections, hemangiomas almost always are inhomogeneous, with areas of fibrosis, necrosis, and cystic change. Sometimes abundant fibrous tissue completely replaces the lesion. Calcification is rare in this tumor (less than 10%) and can be either large and coarse, with phlebolith-like thrombi within the vascular channels of the hemangioma[52,53]. Microscopically it is composed of multiple vascular channels lined by a single layer of endothelial cells supported by a thin fibrous stroma.

On MRI, hemangiomas characteristically demonstrate marked hyperintensity on T2w images, which may contain low-intensity areas that correlate with zones of fibrosis[54]. In the characterization of hemangiomas, the comparison of T2w images with short echo time (TE) and long TE is important. In most cases, hemangiomas are still displayed as relatively hyperintense, compared with the surrounding liver parenchyma, on long TE T2w images and the contours and volume of the displayed hemangioma are exactly comparable on short TE and long TE T2w imaging. This finding can also be seen in hypervascular liver metastases. Further differentiation of hemangiomas and so-called hypervascular liver metastases is described below.

On unenhanced T1w images, a hemangioma displays most commonly as a well-defined slightly hypo-intense tumor with lobulated borders. The pattern of peripheral "nodular" enhancement after Gd injection was seen as highly specific for hemangioma compared with rim enhancement noted in metastases[54,55].

Three enhancement patterns of hemangioma with Gd-enhanced GE imaging have been noted:

Immediate and complete enhancement of small lesions (so-called capillary hemangiomas): Capillary hemangiomas are rapidly filling hemangiomas that occur significantly more often in small hemangiomas (42% of hemangiomas are less than 1 cm in diameter)[56]. On CT and MRI, capillary hemangiomas show immediate homogenous contrast-enhancement in the arterial phase; thus, differentiation from other hypervascular tumors is difficult. According to various authors, up to 83% of the smaller hemangiomas (less than 3 cm) showed iso-attenuation compared with the arterial system in all 3 phases of enhanced scanning[57,58]. During the portal venous phase of contrast-enhancement, capillary hemangiomas show an attenuation equivalent to that of the aorta. In the delayed phase, on CT or MRI, hemangiomas remain hyperattenuating or hyperintense, whereas hypervascular metastases do not[52].

During the perfusion phase using SPIO-enhanced T1w GE imaging, and persisting during delayed imaging, a significant increase in signal intensity has been reported on T1w GE imaging as a result of pooling of SPIO in the vascular spaces of a hemangioma[59-61]. This pooling of SPIO also explains that hemangiomas often lose signal on delayed T2w imaging[59].

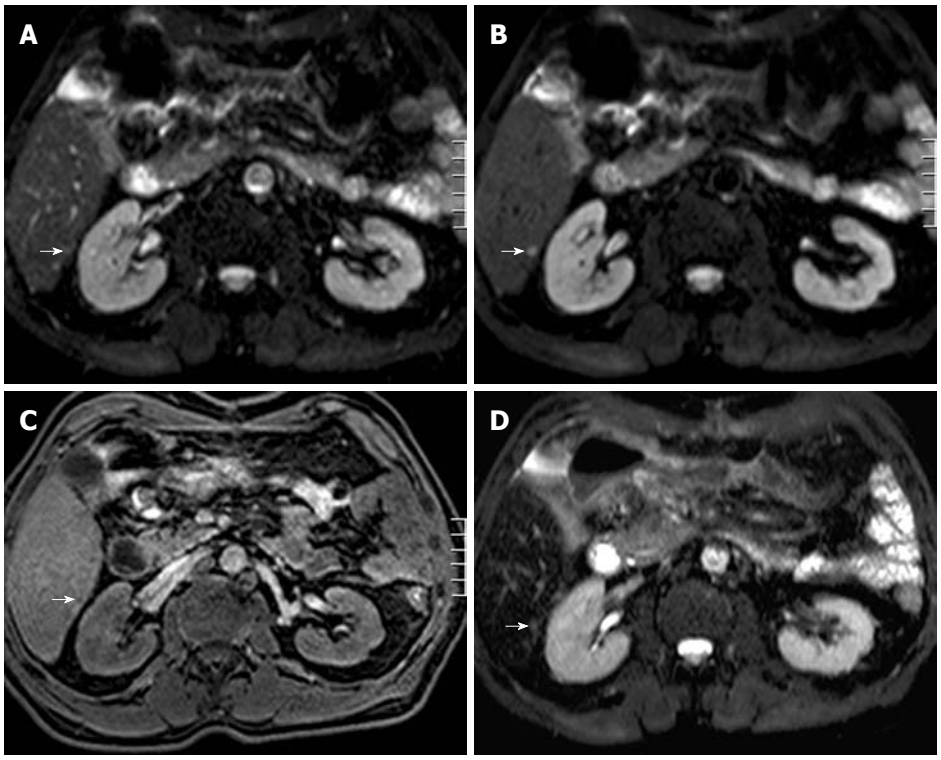

Figure 3 Transverse single-shot spin-echo echo-planar imaging (SS SE-EPI), fat-suppressed T1w 3D GE and SPIO-enhanced T2w TSE (short TE with fat suppression) image in a 62-year-old man. A: A transverse SS SE-EPI image using b = 0 s/mm^2 in a 62-year-old man barely detecting any visible lesion in the area indicated by the white arrow; B: A transverse SS SE-EPI image using b = 10 s/mm^2 in the 62-year-old man clearly detecting the liver metastasis (white arrow); C: A transverse fat-suppressed T1w 3D GE image in the portal-venous phase after intravenous injection of SPIO in the 62-year-old man barely detecting the liver metastasis (white arrow); D: A transverse SPIO-enhanced T2w TSE (short TE with fat suppression) image in the 62-year-old man barely detecting the liver metastasis (white arrow). SS SE-EPI: Single-shot spin-echo echo-planar imaging; GE: Gradient echo; T1w: T1-weighted; SPIO: Superparamagnetic iron oxide; TE: Echo time.

Peripheral nodular enhancement progressing centripetally to uniform enhancement and peripheral nodular enhancement with persistent central hypointensity[62]: These 2 last findings are more frequently depicted in larger (cavernous) hemangiomas. Uniform enhancement throughout the lesion on delayed images should not be used as a criterion for diagnosis because this will only lower the specificity[63]. In the majority of cases, the combination of T2w and serial dynamic Gd images allows a confident diagnosis of hemangiomas[54]. On the delayed liver-specific phase, after Gd-BOPTA (gadobenate dimeglumine), hemangiomas tend to be hypo-intense compared with the surrounding liver parenchyma[64,65].

"Hypovascular" liver metastases

Among solid hypovascular liver lesions, metastases constitute the main group. Hepatic metastases are the most frequent malignancies in the liver. The incidence of hepatic metastases is approximately 40% in patients with colorectal cancer[66]. In the United States, approximately 50 000 cases of hepatic colorectal metastases are seen annually[67]. Lesion detection is size related. When reviewing the literature, a lower threshold for detection is about 1 cm[68]. Unfortunately, postmortem assessment of the size of liver metastases has shown that the ratio between metastases larger than 1 cm and those smaller than 1 cm is approximately 1:1.6 for metastases of colorectal adenocarcinoma and 1:4 for other liver metastases[69]. This clearly indicates that a capacity to accurately detect and characterize metastases smaller than 1 cm is necessary.

Detection and characterization of small (< 1 cm) focal liver lesions using MDCT is inferior to MRI[12]. Furthermore, with the use of the respiratory-triggered SS SE-EPI sequence, detection of focal liver lesions even down to 3 mm is possible using MRI[29]. In a study by Coenegrachts *et al*[29], unenhanced respiratory-triggered SS SE-EPI performed better than SPIO-enhanced MRI (literature gold standard[22]) for detecting so-called hypovascular liver metastases (Figure 3A-D). Therefore, the SS SE-EPI sequence is ideally suited to be used as the first sequence (road map sequence) during an MRI examination of the liver. In most cases, the respiratory-triggered SS SE-EPI depicts the whole liver with good image quality and excellent contrast-to-noise ratio (CNR). In that case, if no focal liver lesions can be detected using the unenhanced respiratory-triggered SS SE-EPI sequence, then the presence of malignant focal liver lesions is extremely unlikely (high negative predictive value of SS SE-EPI). The signal intensity of the metastases is moderately increased compared with the surrounding hepatic tissue on T2w images and decreased on unenhanced T1w images[70]. Malignant tumors tend to have margins that are not sharply defined.

Liquefactive necrosis within the metastasis increases signal intensity on T2w images, whereas coagulative necrosis[71], desmoplastic reaction, or calcifications[72] decrease signal intensity on T2w images.

In some cases, the production of paramagnetic substances modifies the appearance of metastases on T1w images. The melanin present in the metastases from melanoma increases the signal intensity on T1w images. The presence of mucin within metastases can also increase the signal intensity on T1w images[73]. On T1w DCE imaging, in the arterial phase "hypovascular" liver metastases can show a fleeting ring enhancement

that blurs the margins of the lesions and corresponds to a desmoplastic reaction, inflammatory infiltration, and vascular proliferation in the tumor-liver parenchyma margin[74]. Enhancement progresses centrally with concomitant peripheral wash-out[74]. In the venous phase, liver metastases are hypo-intense compared with the surrounding liver parenchyma.

During the perfusion phase using SPIO-enhanced T1w GE imaging, ring enhancement is highly suggestive of malignant liver lesions[61]. Metastases do not contain reticulo-endothelial system cells; thus, after SPIO injection the liver metastasis CNR is improved with increased lesion conspicuity and detection compared with unenhanced T2w images[14,19,75].

In clinical practice, the differentiation between small (< 10 mm), so-called fibrous, liver hemangiomas and hypovascular liver metastases is a frequent problem. For the differentiation of focal liver lesions, the calculation of D, f and ADC_{low} seems promising in reducing liver biopsy procedures in the future. However, for the characterization of small liver hemangiomas and small liver metastases[27], more research is needed. Nonetheless, if an operation is planned, the surgeon has an accurate means of guidance during the operation using intra-operative ultrasound to further characterize these small focal liver lesions in those areas where a focal liver lesion is detected with the SS SE-EPI sequence. This allows the surgeon to locally treat small malignant focal liver lesions with minimally-invasive techniques. This should likely benefit the patients' prognosis by optimizing the removal of all malignant deposits within the liver during one treatment session.

"Hypervascular" liver metastases

Hypervascular metastases are those with an abundant blood supply, typically greater than that of normal liver. These tumors include choriocarcinoma, renal cell carcinoma, thyroid carcinoma, breast carcinoma, melanoma, carcinoid tumor, and islet cell tumor. In general, these tumors may show a hyperintense signal on T2w images, and so potentially could be mistaken for a hemangioma[76]. In addition, most of these tumors have an increased tendency to have an intratumoral hemorrhage. This results in increased signal on unenhanced T1w images as well as T2w images. Melanoma, as a result of the T1 shortening effect of melanin, shows an increased signal on the T1w image even if hemorrhage is not present.

Hypervascular liver metastases show significant enhancement during the arterial phase of ECF agent contrast-enhancement, which is the most important phase for lesion detection, whereas hypovascular metastases are best imaged during the portal venous phase. Detection of smaller hypervascular liver metastases in particular is enhanced with the use of 4D THRIVE - obtaining multiple arterial phases of the whole liver in high spatial resolution - thereby also optimizing the timing of imaging in the appropriate arterial time window for visualizing the sometimes very short arterial hyperenhancing lesions.

In the portal venous phase, hypervascular metastases usually show rapid wash-out, which renders them hypo-intense compared with the surrounding liver parenchyma.

On delayed phase, the ECF accumulates in the center of larger (hypovascular and hypervascular) liver metastases because of its pooling in the extracellular fibrotic component of the lesion, thus becoming progressively hyperintense to the surrounding liver parenchyma (delayed central pooling).

The appearance of a solitary hypervascular liver metastasis and a solitary hepatocellular carcinoma (HCC) can be comparable in some cases. However, differentiation often is facilitated as HCC is almost always encountered in a cirrhotic liver parenchyma whereas a hypervascular liver metastasis is encountered in a "normal" liver parenchyma. Further, specific morphologic criteria can aid in the differentiation of both focal liver lesions (see description in the sections on "hypervascular" liver metastases and HCC).

Focal nodular hyperplasia (FNH)

FNH is a benign tumor-like lesion that results from a hyperplastic rather than a neoplastic process[77]. This explains the nearly iso-intense and homogeneous appearance of FNH with the surrounding liver parenchyma on imaging. When present, the central scar presents as hyperintense on T2w imaging and hypo-intense on unenhanced T1w imaging. In the absence of a central scar, an FNH can hardly be detected using unenhanced imaging. Dynamic Gd-based CE MRI shows a marked enhancement in the arterial phase of the lesion, which persists as slightly hyperintense or iso-intense in the portal venous and distribution phase, whereas the central scar appears hypo-intense in the arterial and portal venous phase to become hyperintense in the distribution phase[74,78]. For detecting smaller FNHs in particular, the use of 4D THRIVE - obtaining multiple arterial phases of the whole liver in high spatial resolution - enhances the visualization of FNHs sometimes showing only very short arterial hyperenhancement.

MRI contrast agents with liver-specific properties are helpful in characterizing FNH. In FNH, there is prolonged and excessive hepatocellular accumulation of hepatocyte-specific contrast agent because of the structural alteration of the biliary canalicular system that does not communicate with or derive from the surrounding normal hepatic biliary system. Two or three hours after IV injection of Gd-BOPTA, typical cases FNHs are hyperintense (to iso-intense) compared with the surrounding liver parenchyma. This behavior is distinct from that seen in adenomas, which do not show significant enhancement compared to the liver parenchyma during the delayed phase[79].

However, accurate characterization of FNH is not always possible because atypical features can confound

the interpretation. While the absence of a scar in small FNHs cannot be considered atypical, it does make it more difficult to distinguish FNH from other hypervascular tumors. Again, delayed phase imaging proved useful in a study by Grazioli *et al*[79]; all 49 small FNHs showed either hyperintense [33 (67%) lesions] or isointense [16 (33%) lesions] enhancement. In addition, a central scar was detected on delayed images in 15 (31%) of the 49 lesions compared with only 7 (14%) of 49 on dynamic phase images. Anecdotal experience by Grazioli *et al*[79] with 4 cases of adenoma and one of adenomatosis (unpublished data) demonstrated a markedly hypointense appearance on delayed images relative to FNH or normal liver. Although adenomas have functioning hepatocytes, they lack bile ducts. It is therefore likely that bilirubin metabolism is blocked in the adenoma, as confirmed by the absence of bile in resected adenomas[80]. Altered hepatocellular metabolism may inhibit the uptake of Gd-BOPTA in the adenoma thereby accounting for its hypo-intense appearance on delayed MRI images. Radionuclide imaging with sulfur colloid is generally considered useful in the characterization of FNH because of the uptake of tracer by the Kupffer cells. However, uptake is seen in only approximately two-thirds of lesions[81] and is limited to the detection only of large lesions.

Kupffer cells usually are observed within FNH and are a major histologic feature of this lesion. Uptake of SPIO by FNH is common, with the lesions showing significant decreases in signal intensity on ferumoxides-enhanced T2w images[82]. Signal drop reflects the presence of Kupffer cells within the lesion. Nevertheless, the amount and distribution of Kupffer cells within the nodule can vary and yield different patterns of signal decrease: some small FNHs (less than 3 cm) show homogenous signal drop similar to that observed in the surrounding parenchyma, whereas large FNHs may show inhomogeneous signal drop. The central scar excludes iron particles and is readily demonstrated as a hyperintense central stellate area. That finding corresponds to the high signal area seen on T2w unenhanced images but higher conspicuity generally is found after the use of SPIO agents[83]. Furthermore, adenomas have also been reported to demonstrate signal drop after SPIO administration using T2w imaging[60].

Telangiectatic FNH

Telangiectatic FNH is an uncommon hepatic neoplasm that demonstrates histologic and imaging features that are different from those of typical FNH[84]. A common finding of telangiectatic FNH in the study of Attal *et al*[84] was strong arterial enhancement, which is also seen in most cases of typical FNH[85]. However, additional imaging characteristics of telangiectatic FNH are described in the literature: (1) A heterogeneous pattern is a very rare feature in FNH and was observed in 2.4% of the cases in a radiologic-pathologic study by Vilgrain *et al*[86]. The main causes of heterogeneity in the study of Attal *et al*[84] were necrosis, the degree of sinusoidal dilatation, and the presence of hemorrhagic foci. Hemorrhage, an unusual finding in FNH, was more commonly observed in larger lesions; (2) Hyperintensity on T1w MRI images is very rare in FNH and was observed in 2.1%-6.0% of cases in previous studies[86,87]. It is well known that hyperintensity on T1w MRI images may be to the result of different pathologic changes, including fat deposition, copper accumulation, high protein concentrations, blood degradation products, or sinusoidal dilatation[88]; (3) Strong hyperintensity on T2w MRI images is also a rare finding in FNH; (4) A central scar was rarely present in the study by Attal *et al*[84]; and (5) Persistent lesion enhancement on delayed phase images was a frequent feature observed by Attal *et al*[84]. This finding has been described only once in FNH, to our knowledge[89]. Persistent contrast agent uptake in telangiectatic FNH could be related to sinusoidal dilatation.

Attal *et al*[84] concluded that telangiectatic FNH is an uncommon entity that differs from typical FNH at imaging. Lesions are multiple in 62% of cases. Atypical features of FNH often observed with telangiectatic FNH are lack of a central scar, lesion heterogeneity, hyperintensity on T1w MRI images, strong hyperintensity on T2w MRI images, and persistent contrast-enhancement on delayed phase T1w MRI images.

Hepatic adenoma

DCE MRI, whether performed with ECF agents or liver targeted agents, can demonstrate early arterial enhancement that becomes iso-intense or hypo-intense in the portal venous phase, although this usually is less marked than in cases of FNH. In cases of previous hemorrhage, the arterial enhancement can be inhomogenous[74]. On Gd-enhanced MRI, most adenomas are hyperintense on arterial and early portal venous phase images, whereas on late portal venous phase images and equilibrium phase images most appear iso-intense overall. For detecting smaller adenomas in particular, the use of 4D THRIVE - obtaining multiple arterial phases of the whole liver in high spatial resolution - also enhances the visualization of adenomas sometimes showing only very short arterial hyperenhancement.

On delayed phase images after injection of Gd-BOPTA, most lesions appear hypo-intense, indicating a lack of uptake by the lesions (see also above; description of FNH)[74]. Therefore, delayed phase imaging using hepatocyte-specific contrast agents can be useful in the differentiation of adenomas and FNHs. Kupffer cells often are found in hepatic adenoma but in reduced numbers and with little or no function, as reflected by the absent or diminished uptake of technetium-99m sulfur colloid[90]. Hepatic adenomas usually do not show uptake of SPIO particles, resulting in increased tumor-liver CNR on T2w images. However, occasionally hepatic adenomas have shown some degree of uptake[82],

with an inhomogeneous signal drop whose entity usually is less than in FNH. Uptake of SPIO in hepatic adenoma appears to be to the result of pooling of the contrast agent within the peliosis-like dilated vessels that characterize them[60]. However, in several cases, no significant difference of signal loss was observed between FNH and hepatic adenoma[83].

HCC

HCC is the most frequent primary tumor of the liver (80%-90%) and represents more than 5% of all cancers, with an incidence of more than 500 000 new cases per year throughout the world[91]. Its incidence in developing countries is 2-3 times higher than in developed countries, although its incidence is rising in Western countries and in Japan[92]. The most significant risk factor, regardless of etiology, is the presence of liver cirrhosis[93], particularly when secondary to viral infection and high alcohol intake. Other risk factors include hemochromatosis and primary biliary cirrhosis[91].

Pathologically, HCC develops *de novo* or most frequently develops in a multistep fashion in the following sequence: from low-grade dysplastic nodule (LGDN), to high-grade dysplastic nodule (HGDN), early HCC, well-differentiated HCC, and finally to a moderately differentiated HCC. Differentiation between early HCC and DN is a very important issue in the clinical setting. CT during arterial portography (CTAP) is the most sensitive tool in the differentiation of premalignant/borderline lesions (LGDN and HGDN) and early HCC[94].

The formation of a pseudocapsule around the lesion (constructed usually from connective fibrous tissue) and of a septum within the tumor is frequently observed with the development of HCC. This may derive from an interaction between the tumor and host liver and may interfere with the growth and invasion of the HCC[95].

On T2w images, most HCCs demonstrate increased signal compared to the surrounding liver, although the tumors tend to be inhomogeneous[96]. The T1 appearance of HCC ranges from hypo-intense to slightly hyperintense, depending on fat content, copper deposition within the tumor, and the degree of differentiation[96].

Several studies have shown that the characteristic HCC profile includes an intense arterial uptake but is followed by contrast agent wash-out in the delayed venous phase[97]. The recognition of the diagnostic value of contrast agent wash-out allowed the refinement of the criteria as reflected in the recent American Association for the Study of Liver Diseases guidelines and in the unpublished consensus of the European Association for the Study of the Liver experts that met in 2005[97].

Dynamic T1w imaging during the arterial phase is of utmost importance for the detection of small (< 10 mm) HCCs, because they may be occult at other pulse sequences and on portal venous and equilibrium phase images[98]. Also, the use of 4D THRIVE (multiple arterial phase imaging) enhances the detection of smaller HCCs in particular.

In these cases, the T1w and T2w appearance of the tumors may not be substantially different from that of the surrounding liver, or the underlying liver heterogeneity may make the tumor difficult to detect[96]. DWI improves the detection of HCCs in particular, and the differentiation of pseudotumoral lesions compared with conventional MRI in liver cirrhosis[99].

Controversies regarding the optimal timing to capture the arterial phase exist[100-102], but as discussed this problem can be solved using 4D THRIVE.

Dysplastic nodules are defined as spontaneously hyperintense on T1w images without (intense) contrast-enhancement in the arterial phase during DCE imaging[97]. However, the differentiation between dysplastic nodules, especially HGDN, and early HCC can often be difficult[94], as early HCC often can have a different appearance on T1w and T2w imaging compared with overt HCC[94]. The most sensitive modality capable of clearly depicting the early carcinogenesis process is CTAP. However, many, well-differentiated, early HCCs appear as hypovascular nodules on CTAP. In cases where portal blood is reduced, but arterial blood flow has not yet increased, both HGDNs as well as early HCCs are depicted as sharply delineated hypo-enhancing nodules compared with the surrounding liver parenchyma[94]. In those cases, differentiation between HGDNs and early HCCs is impossible on imaging.

With SPIO particles, HCCs generally do not show a significant decrease in signal intensity, although signal intensity loss was seen in some individual HCCs[82]. The signal intensity of the normal liver does decrease, however, thereby improving the CNR of malignant focal liver lesions. According to Lim *et al*[103], HCC conspicuity after SPIO depends on differences in the number of Kupffer cells between the lesion and the surrounding cirrhotic liver. Moderately or poorly differentiated HCCs show large differences in the number of Kupffer cells compared with the surrounding cirrhotic liver and thus demonstrate a high CNR at SPIO-enhanced MRI. Dysplastic nodules and most well-differentiated HCCs, on the other hand, contain nearly the same number of Kupffer cells as the surrounding cirrhotic hepatic parenchyma and therefore are not well depicted on T2w MRI[103], although in some cases of well-differentiated HCC there can be decreased uptake of SPIO particles[94].

Some authors have proposed the possibility of a single-visit sequential SPIO-Gd protocol to obtain better diagnostic confidence[104]. Ward *et al*[105] found that the combination of Gd and ferumoxides in double-contrast MRI, compared with ferumoxides-enhanced imaging alone, led to an improvement in the diagnosis of HCC, especially for small (< 1 cm) lesions, for which the sensitivity for detection increased from 14% to 46%, compared with larger lesions (1 cm or larger), for which the sensitivity increased from 81% to 91% with the

addition of Gd-enhanced imaging. Gd-enhanced images obtained during the arterial and portal venous phases of enhancement were essential for differentiating HCC from adjacent fibrosis, which is the most frequent cause of false-positive findings of SPIO-enhanced and SPIO-unenhanced images.

Pauleit *et al*[106] found that for detection of small HCCs, the sensitivity and accuracy with unenhanced and Gd-enhanced imaging were significantly ($P = 0.017$) superior to those with unenhanced and ferumoxides-enhanced imaging, whereas for large HCCs the ferumoxides set was superior to the Gd set, although this difference was not statistically significant. Analysis of all HCCs revealed no significant differences for Gd-enhanced and ferumoxides-enhanced imaging[106].

Fibrolamellar HCC (FL-HCC)

FL-HCC is a distinctive type of HCC that occurs in younger patients (mean age 20 years)[96]. Although it is a malignant lesion, the prognosis is better than that of typical HCC, with 25% of patients having resectable lesions. α-fetoprotein levels are usually not elevated. FL-HCC is typically a well-circumscribed lesion that is hypo-intense on T1w images and hyperintense on T2w images[96]. A central scar may be present. Central calcifications are present in one third of lesions. The differential diagnosis includes mainly FNH.

To our knowledge, there are no reports of FL-HCC enhancement patterns after SPIO. Such lesions would not be expected to enhance significantly.

Cholangiocellular carcinoma (CCC)

CCC is a malignant hepatic tumor of the biliary epithelium and is the second most common form of primary hepatic malignancy in adults after HCC[107]. It represents less than 1% of all newly diagnosed cancers in North America and is usually seen in the seventh decade of life[108].

Several factors have been linked etiologically to the development of CCC, although none of the factors is evident in many patients. CCC is associated with clonorchiasis, intrahepatic stone disease, choledochal cyst, Caroli disease, and primary sclerosing cholangitis (PSC)[109]. Most of these risk factors have in common long-standing inflammation and injury to the bile duct epithelium. PSC is commonly associated with CCC, with as many as 10% of patients with PSC going on to develop CCC[109].

Microscopically the tumor is an adenocarcinoma with a glandular appearance and cells resembling biliary epithelium. Mucin and calcification sometimes can be demonstrated. A large desmoplastic reaction is typical of CCC. Mixed hepato-cholangiocellular carcinomas have been described[110]. Cholangiocarcinoma usually is divided into "intrahepatic" and "extrahepatic", depending on the site of origin. For the purposes of this discussion only the intrahepatic subgroup and the Klatskin tumors are presented:

Intrahepatic ("peripheral") cholangiocarcinoma (ICC): ICC is a malignant neoplasm arising from the epithelium of the intrahepatic bile ducts and represents 10% of all CCC. Hilar (Klatskin) and bile duct CCCs account for the remaining 90%[107]. This neoplasm usually is a large firm mass. In 10%-20% of cases, there are several satellite nodules around the main mass. On cut section, it is characterized by the presence of large amounts of whitish fibrous tissue. A variable amount of central necrosis could be present within the tumor, especially if it is large. Hemorrhage is rare[107].

Klatskin ("perihilar") tumor: The Klatskin ("perihilar") tumor is a small stricturing CCC arising at the junction of the left and right hepatic ducts. These lesions produce bilobar biliary duct obstruction and are nearly always unresectable.

On MRI, ICC has a non-specific appearance. On T2w images, the signal intensity of the tumor ranges from markedly increased to moderately increased, relative to the liver. Tumors with high fibrous content tend to have lower signal intensity on T2w images[107,111]. It is iso-intense to hypo-intense on unenhanced T1w images. The most prominent feature with central CCC on MRI is usually intrahepatic biliary duct dilatation. Morphologic changes may occur late in the disease process, with atrophy of the left lobe of the liver compared with the right lobe. The left-sided hepatic ducts may be more dilated than are those in the right lobe[96]. Vascular invasion and portal nodes should be carefully searched for because these findings preclude resection of the tumor[96].

With serial dynamic ECF-Gd enhanced images, CCCs show minimal or moderate incomplete rim of enhancement at the tumor periphery on early images, with progressive central contrast-enhancement on later images[112]. Contrast-enhancement may be better seen on delayed images because of the fibrous nature of the tumor[113].

DCE imaging with Gd-BOPTA is similar to non-specific vasculo-interstitial Gd-based contrast agents, but in the hepato-biliary phase, the lesion shows contrast-enhancement in the fibrotic area. The degree of enhancement depends on the type of CCC. Greater peripheral enhancement is noted in the early phases in large CCC, whereas greater delayed enhancement is noted in the fibrous core of the "scirrhous" CCCs in the hepatobiliary phase[64]. Occasionally some small peripheral CCCs with a large number of tumor cells and few interstitial fibrous tissues at DCE MRI images reveal strong enhancement of the whole tumor on the early phase[111]. Prolonged enhancement of the tumor on the late venous and delayed phases could be of diagnostic value[114,115].

The hepatobiliary phase after liver-specific contrast agent adds useful information for identification of small satellite lesions. Analogously, after SPIO administration,

because of the absence of Kupffer cells within the lesion, no significant uptake is observed, and there is an increase of liver-to-lesion CNR on T2w images[116].

Liver abscess

Liver abscesses can mimic necrotic liver metastases. DWI might aid in the differentiation between purulent abscesses and necrotic metastases. However, in many cases, drainage is needed for diagnostic and therapeutic purposes.

Angiomyolipoma (AML)

AMLs are mesenchymal tumors composed of varying proportions of blood vessels, smooth muscle and mature adipose tissue. These tumors are common in the kidneys, but hepatic AMLs are very rare[117]. As these lesions are benign, preoperative diagnosis would obviate unnecessary surgery.

In patients with tuberous sclerosis, hepatic AMLs are typically small and multiple and show imaging features consistent with fat on imaging. Contrary to the imaging appearances of hepatic AMLs in patients with tuberous sclerosis, sporadic hepatic AMLs have a varied appearance because of the inconstant proportion of fat, making confident imaging diagnosis difficult and necessitating biopsy in many cases[117]. Sporadic AMLs appear to be radiologically heterogeneous, reflecting the variable proportions of fat, smooth muscle and blood vessels. In contrast to patients with tuberous sclerosis, most sporadic AMLs are solitary. Depending on the components of the sporadic AML, imaging usually shows a hypervascular tumor with heterogeneous areas of fat. In-and-out-of-phase imaging (chemical shift imaging) is useful for the detection of the fatty tissue within AMLs. Contrast-enhanced MRI can be useful to better depict the presence of vessels within AMLs. The presence of fat combined with the presence of (especially central) vessels often is useful for the definite diagnosis of AML. Still, lipid-poor hepatic, sporadic, AML can pose a diagnostic challenge, often requiring biopsy[117].

CONCLUSION

Although the primary modalities for liver imaging are US and CT, recent studies have suggested that CE-MRI is the most sensitive method for detecting small focal liver lesions in particular. One of the advantages of MRI in liver imaging is the better soft tissue contrast, which allows better detection and characterization of benign and malignant focal liver lesions. The development of liver-specific MRI contrast agents has further improved the diagnostic yield of MRI in lesion detection and characterization.

In addition, 2 recent developments in MRI sequences for the upper abdomen comprise unenhanced DWI and keyhole-based DCE MRI (4D THRIVE). Unenhanced DWI has been shown to allow an improved detection (b = 10 s/mm$^{2)}$ of, in particular, small (< 10 mm) focal liver lesions compared with other, more routinely used, MRI sequences and is useful as a road map sequence at the start of each MRI examination of the liver. Also, using higher b-values, the calculation of ADC value, the true diffusion coefficient, D, and the perfusion fraction, f, can be useful for the characterization of focal liver lesions. DCE 4D THRIVE enables MRI of the liver with high temporal and spatial resolution with full liver coverage. 4D THRIVE improves detection and characterization of focal liver lesions providing multiple arterial and venous phases. The characterization of focal liver lesions using parametric maps appears to be promising for differentiating benign and malignant focal liver lesions.

REFERENCES

1 **Lodge JP.** Modern surgery for liver metastases. *Cancer Imaging* 2000; **1**: 77-85
2 **Kuszyk BS**, Bluemke DA, Urban BA, Choti MA, Hruban RH, Sitzmann JV, Fishman EK. Portal-phase contrast-enhanced helical CT for the detection of malignant hepatic tumors: sensitivity based on comparison with intraoperative and pathologic findings. *AJR Am J Roentgenol* 1996; **166**: 91-95
3 **Valls C**, Lopez E, Gumà A, Gil M, Sanchez A, Andía E, Serra J, Moreno V, Figueras J. Helical CT versus CT arterial portography in the detection of hepatic metastasis of colorectal carcinoma. *AJR Am J Roentgenol* 1998; **170**: 1341-1347
4 **Ward J**, Naik KS, Guthrie JA, Wilson D, Robinson PJ. Hepatic lesion detection: comparison of MR imaging after the administration of superparamagnetic iron oxide with dual-phase CT by using alternative-free response receiver operating characteristic analysis. *Radiology* 1999; **210**: 459-466
5 **Valls C**, Andía E, Sánchez A, Gumà A, Figueras J, Torras J, Serrano T. Hepatic metastases from colorectal cancer: preoperative detection and assessment of resectability with helical CT. *Radiology* 2001; **218**: 55-60
6 **Furuhata T**, Okita K, Tsuruma T, Hata F, Kimura Y, Katsuramaki T, Mukaiya M, Hirokawa N, Ichimura T, Yama N, Koito K, Sasaki K, Hirata K. Efficacy of SPIO-MR imaging in the diagnosis of liver metastases from colorectal carcinomas. *Dig Surg* 2003; **20**: 321-325
7 **Wang SS**, Chiang JH, Tsai YT, Lee SD, Lin HC, Chou YH, Lee FY, Wang JS, Lo KJ. Focal hepatic fatty infiltration as a cause of pseudotumors: ultrasonographic patterns and clinical differentiation. *J Clin Ultrasound* 1990; **18**: 401-409
8 **Janica JR**, Lebkowska U, Ustymowicz A, Augustynowicz A, Kamocki Z, Werel D, Polaków J, Kedra B, Pepinski W. Contrast-enhanced ultrasonography in diagnosing liver metastases. *Med Sci Monit* 2007; **13** Suppl 1: 111-115
9 **Della Vigna P**, Cernigliaro F, Monfardini L, Gandini S, Bellomi M. Contrast-enhanced ultrasonography in the follow-up of patients with hepatic metastases from breast carcinoma. *Radiol Med* 2007; **112**: 47-55
10 **Dai Y**, Chen MH, Yin SS, Yan K, Fan ZH, Wu W, Wang YB, Yang W. Focal liver lesions: can SonoVue-enhanced ultrasound be used to differentiate malignant from benign lesions? *Invest Radiol* 2007; **42**: 596-603
11 **Soye JA**, Mullan CP, Porter S, Beattie H, Barltrop AH, Nelson WM. The use of contrast-enhanced ultrasound in the characterisation of focal liver lesions. *Ulster Med J* 2007; **76**: 22-25
12 **Rappeport ED**, Loft A. Liver metastases from colorectal

cancer: imaging with superparamagnetic iron oxide (SPIO)-enhanced MR imaging, computed tomography and positron emission tomography. *Abdom Imaging* 2007; **32**: 624-634
13 **Silverman PM**. Liver metastases: imaging considerations for protocol development with multislice CT (MSCT). *Cancer Imaging* 2006; **6**: 175-181
14 **Wiering B**, Ruers TJ, Krabbe PF, Dekker HM, Oyen WJ. Comparison of multiphase CT, FDG-PET and intra-operative ultrasound in patients with colorectal liver metastases selected for surgery. *Ann Surg Oncol* 2007; **14**: 818-826
15 **Morana G**, Salviato E, Guarise A. Contrast agents for hepatic MRI. *Cancer Imaging* 2007; **7** Spec No A: S24-S27
16 **Zech CJ**, Grazioli L, Jonas E, Ekman M, Niebecker R, Gschwend S, Breuer J, Jönsson L, Kienbaum S. Health-economic evaluation of three imaging strategies in patients with suspected colorectal liver metastases: Gd-EOB-DTPA-enhanced MRI vs. extracellular contrast media-enhanced MRI and 3-phase MDCT in Germany, Italy and Sweden. *Eur Radiol* 2009; **19** Suppl 3: S753-S763
17 **Semelka RC**, Cance WG, Marcos HB, Mauro MA. Liver metastases: comparison of current MR techniques and spiral CT during arterial portography for detection in 20 surgically staged cases. *Radiology* 1999; **213**: 86-91
18 **Hagspiel KD**, Neidl KF, Eichenberger AC, Weder W, Marincek B. Detection of liver metastases: comparison of superparamagnetic iron oxide-enhanced and unenhanced MR imaging at 1.5 T with dynamic CT, intraoperative US, and percutaneous US. *Radiology* 1995; **196**: 471-478
19 **Senéterre E**, Taourel P, Bouvier Y, Pradel J, Van Beers B, Daures JP, Pringot J, Mathieu D, Bruel JM. Detection of hepatic metastases: ferumoxides-enhanced MR imaging versus unenhanced MR imaging and CT during arterial portography. *Radiology* 1996; **200**: 785-792
20 **Müller RD**, Vogel K, Neumann K, Hirche H, Barkhausen J, Stöblen F, Henrich H, Langer R. SPIO-MR imaging versus double-phase spiral CT in detecting malignant lesions of the liver. *Acta Radiol* 1999; **40**: 628-635
21 **Lencioni R**, Della Pina C, Bruix J, Majno P, Grazioli L, Morana G, Filippone A, Laghi A, Bartolozzi C. Clinical management of hepatic malignancies: ferucarbotran-enhanced magnetic resonance imaging versus contrast-enhanced spiral computed tomography. *Dig Dis Sci* 2005; **50**: 533-537
22 **Ward J**. New MR techniques for the detection of liver metastases. *Cancer Imaging* 2006; **6**: 33-42
23 **Kim YK**, Lee JM, Kim CS, Chung GH, Kim CY, Kim IH. Detection of liver metastases: gadobenate dimeglumine-enhanced three-dimensional dynamic phases and one-hour delayed phase MR imaging versus superparamagnetic iron oxide-enhanced MR imaging. *Eur Radiol* 2005; **15**: 220-228
24 **Kim MJ**, Kim JH, Lim JS, Oh YT, Chung JJ, Choi JS, Lee WJ, Kim KW. Detection and characterization of focal hepatic lesions: mangafodipir vs. superparamagnetic iron oxide-enhanced magnetic resonance imaging. *J Magn Reson Imaging* 2004; **20**: 612-621
25 **Le Bihan D**, Breton E, Lallemand D, Aubin ML, Vignaud J, Laval-Jeantet M. Separation of diffusion and perfusion in intravoxel incoherent motion MR imaging. *Radiology* 1988; **168**: 497-505
26 **Yamada I**, Aung W, Himeno Y, Nakagawa T, Shibuya H. Diffusion coefficients in abdominal organs and hepatic lesions: evaluation with intravoxel incoherent motion echo-planar MR imaging. *Radiology* 1999; **210**: 617-623
27 **Coenegrachts K**, Delanote J, Ter Beek L, Haspeslagh M, Bipat S, Stoker J, Steyaert L, Rigauts H. Evaluation of true diffusion, perfusion factor, and apparent diffusion coefficient in non-necrotic liver metastases and uncomplicated liver hemangiomas using black-blood echo planar imaging. *Eur J Radiol* 2009; **69**: 131-138
28 **Nagayama M**, Watanabe Y, Okumura A, Tabuchi T, Mitsui H, Morimoto N, Nakada K, Kumashiro M, Kiyono Y, Amoh Y, Nakashita S, Dodo Y, Geraats D, Van Cauteren M. Black-blood T2-weighted SE-EPI Imaging of the Liver. *Proc Intl SOC Mag Reson Med* 2002; **10**: 1963
29 **Coenegrachts K**, Orlent H, ter Beek L, Haspeslagh M, Bipat S, Stoker J, Rigauts H. Improved focal liver lesion detection: comparison of single-shot spin-echo echo-planar and superparamagnetic iron oxide (SPIO)-enhanced MRI. *J Magn Reson Imaging* 2008; **27**: 117-124
30 **Coenegrachts K**, De Geeter F, ter Beek L, Walgraeve N, Bipat S, Stoker J, Rigauts H. Comparison of MRI (including SS SE-EPI and SPIO-enhanced MRI) and FDG-PET/CT for the detection of colorectal liver metastases. *Eur Radiol* 2009; **19**: 370-379
31 **Hussain SM**, De Becker J, Hop WC, Dwarkasing S, Wielopolski PA. Can a single-shot black-blood T2-weighted spin-echo echo-planar imaging sequence with sensitivity encoding replace the respiratory-triggered turbo spin-echo sequence for the liver? An optimization and feasibility study. *J Magn Reson Imaging* 2005; **21**: 219-229
32 **Nasu K**, Kuroki Y, Nawano S, Kuroki S, Tsukamoto T, Yamamoto S, Motoori K, Ueda T. Hepatic metastases: diffusion-weighted sensitivity-encoding versus SPIO-enhanced MR imaging. *Radiology* 2006; **239**: 122-130
33 **Sun XJ**, Quan XY, Huang FH, Xu YK. Quantitative evaluation of diffusion-weighted magnetic resonance imaging of focal hepatic lesions. *World J Gastroenterol* 2005; **11**: 6535-6537
34 **Koh DM**, Erica S, Collins D, Reinsberg S, Brown G, Leach M, Cunningham D, Husband J. Diffusion coefficients and the perfusion fraction of colorectal hepatic metastases estimated using single-shot echo-planar sensitivity-encoded (SENSE) diffusion-weighted MR imaging. *Proc Intl Soc Mag Reson Med* 2004; **11**: 908
35 **Low RN**. Abdominal MRI advances in the detection of liver tumours and characterisation. *Lancet Oncol* 2007; **8**: 525-535
36 **Rofsky NM**, Lee VS, Laub G, Pollack MA, Krinsky GA, Thomasson D, Ambrosino MM, Weinreb JC. Abdominal MR imaging with a volumetric interpolated breath-hold examination. *Radiology* 1999; **212**: 876-884
37 **Bonaldi VM,** Bret PM, Reinhold C, Atri M. Helical CT of the liver: value of an early hepatic arterial phase. *Radiology* 1995; **197**: 357-363
38 **Lee VS**, Lavelle MT, Rofsky NM, Laub G, Thomasson DM, Krinsky GA, Weinreb JC. Hepatic MR imaging with a dynamic contrast-enhanced isotropic volumetric interpolated breath-hold examination: feasibility, reproducibility, and technical quality. *Radiology* 2000; **215**: 365-372
39 **Beck GM**, De Becker J, Jones AC, von Falkenhausen M, Willinek WA, Gieseke J. Contrast-enhanced timing robust acquisition order with a preparation of the longitudinal signal component (CENTRA plus) for 3D contrast-enhanced abdominal imaging. *J Magn Reson Imaging* 2008; **27**: 1461-1467
40 **Beck G**, Herigault G, Glantenay A, Coenegrachts K, Denolin V. Ultra-fast time resolved contrast enhanced abdominal imaging using an elliptical centric fat suppressed 3D profile sharing acquisition technique, SENSE and partial Fourier. *Proc Intl Soc Mag Reson Med* 2008; **16**: 2622
41 **Coenegrachts K**, Ghekiere J, Denolin V, Gabriele B, Hérigault G, Haspeslagh M, Daled P, Bipat S, Stoker J, Rigauts H. Perfusion maps of the whole liver based on high temporal and spatial resolution contrast-enhanced MRI (4D THRIVE): Feasibility and initial results in focal liver lesions. *Eur J Radiol* 2009; Epub ahead of print
42 **Padhani AR**. MRI for assessing antivascular cancer treatments. *Br J Radiol* 2003; **76** Spec No 1: S60-S80

43 **Wang L**, Van den Bos IC, Hussain SM, Pattynama PM, Vogel MW, Krestin GP. Post-processing of dynamic gadolinium-enhanced magnetic resonance imaging exams of the liver: explanation and potential clinical applications for color-coded qualitative and quantitative analysis. *Acta Radiol* 2008; **49**: 6-18

44 **Pandharipande PV**, Krinsky GA, Rusinek H, Lee VS. Perfusion imaging of the liver: current challenges and future goals. *Radiology* 2005; **234**: 661-673

45 **Evelhoch JL.** Key factors in the acquisition of contrast kinetic data for oncology. *J Magn Reson Imaging* 1999; **10**: 254-259

46 **Kuhl CK**, Mielcareck P, Klaschik S, Leutner C, Wardelmann E, Gieseke J, Schild HH. Dynamic breast MR imaging: are signal intensity time course data useful for differential diagnosis of enhancing lesions? *Radiology* 1999; **211**: 101-110

47 **Mayr NA**, Yuh WT, Zheng J, Ehrhardt JC, Magnotta VA, Sorosky JI, Pelsang RE, Oberley LW, Hussey DH. Prediction of tumor control in patients with cervical cancer: analysis of combined volume and dynamic enhancement pattern by MR imaging. *AJR Am J Roentgenol* 1998; **170**: 177-182

48 **Hawighorst H**, Weikel W, Knapstein PG, Knopp MV, Zuna I, Schönberg SO, Vaupel P, van Kaick G. Angiogenic activity of cervical carcinoma: assessment by functional magnetic resonance imaging-based parameters and a histomorphological approach in correlation with disease outcome. *Clin Cancer Res* 1998; **4**: 2305-2312

49 **Hulka CA**, Edmister WB, Smith BL, Tan L, Sgroi DC, Campbell T, Kopans DB, Weisskoff RM. Dynamic echo-planar imaging of the breast: experience in diagnosing breast carcinoma and correlation with tumor angiogenesis. *Radiology* 1997; **205**: 837-842

50 **Lin MX**, Xu HX, Lu MD, Xie XY, Chen LD, Xu ZF, Liu GJ, Xie XH, Liang JY, Wang Z. Diagnostic performance of contrast-enhanced ultrasound for complex cystic focal liver lesions: blinded reader study. *Eur Radiol* 2009; **19**: 358-369

51 **Valls C**, Reñe M, Gil M, Sanchez A, Narvaez JA, Hidalgo F. Giant cavernous hemangioma of the liver: atypical CT and MR findings. *Eur Radiol* 1996; **6**: 448-450

52 **Vilgrain V**, Boulos L, Vullierme MP, Denys A, Terris B, Menu Y. Imaging of atypical hemangiomas of the liver with pathologic correlation. *Radiographics* 2000; **20**: 379-397

53 **Ros PR**. Benign liver lesion. In: Gore RM, Levin MS, Laufer I, editors. Textbook of Gastrointestinal Radiology. Philadelphia: WB Saunders, 1994: 1861-1896

54 **Semelka RC**, Brown ED, Ascher SM, Patt RH, Bagley AS, Li W, Edelman RR, Shoenut JP, Brown JJ. Hepatic hemangiomas: a multi-institutional study of appearance on T2-weighted and serial gadolinium-enhanced gradient-echo MR images. *Radiology* 1994; **192**: 401-406

55 **Soyer P**, Gueye C, Somveille E, Laissy JP, Scherrer A. MR diagnosis of hepatic metastases from neuroendocrine tumors versus hemangiomas: relative merits of dynamic gadolinium chelate-enhanced gradient-recalled echo and unenhanced spin-echo images. *AJR Am J Roentgenol* 1995; **165**: 1407-1413

56 **Hanafusa K**, Ohashi I, Himeno Y, Suzuki S, Shibuya H. Hepatic hemangioma: findings with two-phase CT. *Radiology* 1995; **196**: 465-469

57 **van Leeuwen MS**, Noordzij J, Feldberg MA, Hennipman AH, Doornewaard H. Focal liver lesions: characterization with triphasic spiral CT. *Radiology* 1996; **201**: 327-336

58 **Kim T**, Federle MP, Baron RL, Peterson MS, Kawamori Y. Discrimination of small hepatic hemangiomas from hypervascular malignant tumors smaller than 3 cm with three-phase helical CT. *Radiology* 2001; **219**: 699-706

59 **Grangier C**, Tourniaire J, Mentha G, Schiau R, Howarth N, Chachuat A, Grossholz M, Terrier F. Enhancement of liver hemangiomas on T1-weighted MR SE images by superparamagnetic iron oxide particles. *J Comput Assist Tomogr* 1994; **18**: 888-896

60 **Denys A**, Arrive L, Servois V, Dubray B, Najmark D, Sibert A, Menu Y. Hepatic tumors: detection and characterization at 1-T MR imaging enhanced with AMI-25. *Radiology* 1994; **193**: 665-669

61 **Kim JH**, Kim MJ, Suh SH, Chung JJ, Yoo HS, Lee JT. Characterization of focal hepatic lesions with ferumoxides-enhanced MR imaging: utility of T1-weighted spoiled gradient recalled echo images using different echo times. *J Magn Reson Imaging* 2002; **15**: 573-583

62 **Yu JS**, Kim MJ, Kim KW, Chang JC, Jo BJ, Kim TH, Lee JT, Yoo HS. Hepatic cavernous hemangioma: sonographic patterns and speed of contrast enhancement on multiphase dynamic MR imaging. *AJR Am J Roentgenol* 1998; **171**: 1021-1025

63 **Whitney WS**, Herfkens RJ, Jeffrey RB, McDonnell CH, Li KC, Van Dalsem WJ, Low RN, Francis IR, Dabatin JF, Glazer GM. Dynamic breath-hold multiplanar spoiled gradient-recalled MR imaging with gadolinium enhancement for differentiating hepatic hemangiomas from malignancies at 1.5 T. *Radiology* 1993; **189**: 863-870

64 **Petersein J**, Spinazzi A, Giovagnoni A, Soyer P, Terrier F, Lencioni R, Bartolozzi C, Grazioli L, Chiesa A, Manfredi R, Marano P, Van Persijn Van Meerten EL, Bloem JL, Petre C, Marchal G, Greco A, McNamara MT, Heuck A, Reiser M, Laniado M, Claussen C, Daldrup HE, Rummeny E, Kirchin MA, Pirovano G, Hamm B. Focal liver lesions: evaluation of the efficacy of gadobenate dimeglumine in MR imaging--a multicenter phase III clinical study. *Radiology* 2000; **215**: 727-736

65 **Oudkerk M**, Torres CG, Song B, König M, Grimm J, Fernandez-Cuadrado J, Op de Beeck B, Marquardt M, van Dijk P, de Groot JC. Characterization of liver lesions with mangafodipir trisodium-enhanced MR imaging: multicenter study comparing MR and dual-phase spiral CT. *Radiology* 2002; **223**: 517-524

66 **Ferrucci JT**. Liver tumor imaging. Current concepts. *Radiol Clin North Am* 1994; **32**: 39-54

67 **Fong Y**, Blumgart LH, Fortner JG, Brennan MF. Pancreatic or liver resection for malignancy is safe and effective for the elderly. *Ann Surg* 1995; **222**: 426-434; discussion 434-437

68 **Wernecke K**, Rummeny E, Bongartz G, Vassallo P, Kivelitz D, Wiesmann W, Peters PE, Reers B, Reiser M, Pircher W. Detection of hepatic masses in patients with carcinoma: comparative sensitivities of sonography, CT, and MR imaging. *AJR Am J Roentgenol* 1991; **157**: 731-739

69 **Schulz W**, Borchard F. [The size of the liver metastases in a low metastatic count. A quantitative study of postmortem livers] *Rofo* 1992; **156**: 320-324

70 **Imam K**, Bluemke DA. MR imaging in the evaluation of hepatic metastases. *Magn Reson Imaging Clin N Am* 2000; **8**: 741-756

71 **Outwater E**, Tomaszewski JE, Daly JM, Kressel HY. Hepatic colorectal metastases: correlation of MR imaging and pathologic appearance. *Radiology* 1991; **180**: 327-332

72 **Semelka RC**, Bagley AS, Brown ED, Kroeker MA. Malignant lesions of the liver identified on T1- but not T2-weighted MR images at 1.5 T. *J Magn Reson Imaging* 1994; **4**: 315-318

73 **Semelka RC**, Kelekis NL. Liver. In: Semelka RC, Ascher SM, Reinhold C, editors. MRI of the abdomen and pelvis: a text-atlas. New York: Wiley-Liss, 1997; 19-135

74 **Morana G**, Grazioli L, Testoni M, Caccia P, Procacci C. Contrast agents for hepatic magnetic resonance imaging. *Top Magn Reson Imaging* 2002; **13**: 117-150

75 **Oudkerk M**, van den Heuvel AG, Wielopolski PA, Schmitz PI, Borel Rinkes IH, Wiggers T. Hepatic lesions: detection with ferumoxide-enhanced T1-weighted MR imaging.

Radiology 1997; **203**: 449-456
76 **Larson RE**, Semelka RC, Bagley AS, Molina PL, Brown ED, Lee JK. Hypervascular malignant liver lesions: comparison of various MR imaging pulse sequences and dynamic CT. *Radiology* 1994; **192**: 393-399
77 **Benhamou JP**. [Oral contraceptives and benign tumors of the liver] *Gastsroenterol Clin Biol* 1997; **21**: 913-915
78 **Grazioli L**, Morana G, Kirchin MA, Caccia P, Romanini L, Bondioni MP, Procacci C, Chiesa A. MRI of focal nodular hyperplasia (FNH) with gadobenate dimeglumine (Gd-BOPTA) and SPIO (ferumoxides): an intra-individual comparison. *J Magn Reson Imaging* 2003; **17**: 593-602
79 **Grazioli L**, Morana G, Federle MP, Brancatelli G, Testoni M, Kirchin MA, Menni K, Olivetti L, Nicoli N, Procacci C. Focal nodular hyperplasia: morphologic and functional information from MR imaging with gadobenate dimeglumine. *Radiology* 2001; **221**: 731-739
80 **Leese T**, Farges O, Bismuth H. Liver cell adenomas. A 12-year surgical experience from a specialist hepato-biliary unit. *Ann Surg* 1988; **208**: 558-564
81 **Boulahdour H**, Cherqui D, Charlotte F, Rahmouni A, Dhumeaux D, Zafrani ES, Meignan M. The hot spot hepatobiliary scan in focal nodular hyperplasia. *J Nucl Med* 1993; **34**: 2105-2110
82 **Paley MR**, Mergo PJ, Torres GM, Ros PR. Characterization of focal hepatic lesions with ferumoxides-enhanced T2-weighted MR imaging. *AJR Am J Roentgenol* 2000; **175**: 159-163
83 **Grandin C**, Van Beers BE, Robert A, Gigot JF, Geubel A, Pringot J. Benign hepatocellular tumors: MRI after superparamagnetic iron oxide administration. *J Comput Assist Tomogr* 1995; **19**: 412-418
84 **Attal P**, Vilgrain V, Brancatelli G, Paradis V, Terris B, Belghiti J, Taouli B, Menu Y. Telangiectatic focal nodular hyperplasia: US, CT, and MR imaging findings with histopathologic correlation in 13 cases. *Radiology* 2003; **228**: 465-472
85 **Carlson SK**, Johnson CD, Bender CE, Welch TJ. CT of focal nodular hyperplasia of the liver. *AJR Am J Roentgenol* 2000; **174**: 705-712
86 **Vilgrain V**, Fléjou JF, Arrivé L, Belghiti J, Najmark D, Menu Y, Zins M, Vullierme MP, Nahum H. Focal nodular hyperplasia of the liver: MR imaging and pathologic correlation in 37 patients. *Radiology* 1992; **184**: 699-703
87 **Lee MJ**, Saini S, Hamm B, Taupitz M, Hahn PF, Seneterre E, Ferrucci JT. Focal nodular hyperplasia of the liver: MR findings in 35 proved cases. *AJR Am J Roentgenol* 1991; **156**: 317-320
88 **Mathieu D**, Paret M, Mahfouz AE, Caseiro-Alves F, Tran Van Nhieu J, Anglade MC, Rahmouni A, Vasile N. Hyperintense benign liver lesions on spin-echo T1-weighted MR images: pathologic correlations. *Abdom Imaging* 1997; **22**: 410-417
89 **Kier R**, Rosenfield AT. Focal nodular hyperplasia of the liver on delayed enhanced CT. *AJR Am J Roentgenol* 1989; **153**: 885-886
90 **Rubin RA**, Lichtenstein GR. Hepatic scintigraphy in the evaluation of solitary solid liver masses. *J Nucl Med* 1993; **34**: 697-705
91 **Bruix J**, Sherman M, Llovet JM, Beaugrand M, Lencioni R, Burroughs AK, Christensen E, Pagliaro L, Colombo M, Rodés J. Clinical management of hepatocellular carcinoma. Conclusions of the Barcelona-2000 EASL conference. European Association for the Study of the Liver. *J Hepatol* 2001; **35**: 421-430
92 **Ince N**, Wands JR. The increasing incidence of hepatocellular carcinoma. *N Engl J Med* 1999; **340**: 798-799
93 **Zaman SN**, Melia WM, Johnson RD, Portmann BC, Johnson PJ, Williams R. Risk factors in development of hepatocellular carcinoma in cirrhosis: prospective study of 613 patients. *Lancet* 1985; **1**: 1357-1360
94 **Kudo M**. Multistep human hepatocarcinogenesis: correlation of imaging with pathology. *J Gastroenterol* 2009; **44** Suppl 19: 112-118
95 **Ishizaki M**, Ashida K, Higashi T, Nakatsukasa H, Kaneyoshi T, Fujiwara K, Nouso K, Kobayashi Y, Uemura M, Nakamura S, Tsuji T. The formation of capsule and septum in human hepatocellular carcinoma. *Virchows Arch* 2001; **438**: 574-580
96 **Kamel IR**, Bluemke DA. MR imaging of liver tumors. *Radiol Clin North Am* 2003; **41**: 51-65
97 **Forner A**, Vilana R, Ayuso C, Bianchi L, Solé M, Ayuso JR, Boix L, Sala M, Varela M, Llovet JM, Brú C, Bruix J. Diagnosis of hepatic nodules 20 mm or smaller in cirrhosis: Prospective validation of the noninvasive diagnostic criteria for hepatocellular carcinoma. *Hepatology* 2008; **47**: 97-104
98 **Krinsky GA**, Lee VS, Theise ND, Weinreb JC, Rofsky NM, Diflo T, Teperman LW. Hepatocellular carcinoma and dysplastic nodules in patients with cirrhosis: prospective diagnosis with MR imaging and explantation correlation. *Radiology* 2001; **219**: 445-454
99 **Vandecaveye V**, De Keyzer F, Verslype C, Op de Beeck K, Komuta M, Topal B, Roebben I, Bielen D, Roskams T, Nevens F, Dymarkowski S. Diffusion-weighted MRI provides additional value to conventional dynamic contrast-enhanced MRI for detection of hepatocellular carcinoma. *Eur Radiol* 2009; **19**: 2456-2466
100 **Earls JP**, Rofsky NM, DeCorato DR, Krinsky GA, Weinreb JC. Hepatic arterial-phase dynamic gadolinium-enhanced MR imaging: optimization with a test examination and a power injector. *Radiology* 1997; **202**: 268-273
101 **Frederick MG**, McElaney BL, Singer A, Park KS, Paulson EK, McGee SG, Nelson RC. Timing of parenchymal enhancement on dual-phase dynamic helical CT of the liver: how long does the hepatic arterial phase predominate? *AJR Am J Roentgenol* 1996; **166**: 1305-1310
102 **Yu JS**, Kim KW, Kim EK, Lee JT, Yoo HS. Contrast enhancement of small hepatocellular carcinoma: usefulness of three successive early image acquisitions during multiphase dynamic MR imaging. *AJR Am J Roentgenol* 1999; **173**: 597-604
103 **Lim JH**, Choi D, Cho SK, Kim SH, Lee WJ, Lim HK, Park CK, Paik SW, Kim YI. Conspicuity of hepatocellular nodular lesions in cirrhotic livers at ferumoxides-enhanced MR imaging: importance of Kupffer cell number. *Radiology* 2001; **220**: 669-676
104 **Kubaska S**, Sahani DV, Saini S, Hahn PF, Halpern E. Dual contrast enhanced magnetic resonance imaging of the liver with superparamagnetic iron oxide followed by gadolinium for lesion detection and characterization. *Clin Radiol* 2001; **56**: 410-415
105 **Ward J**, Guthrie JA, Scott DJ, Atchley J, Wilson D, Davies MH, Wyatt JI, Robinson PJ. Hepatocellular carcinoma in the cirrhotic liver: double-contrast MR imaging for diagnosis. *Radiology* 2000; **216**: 154-162
106 **Pauleit D**, Textor J, Bachmann R, Conrad R, Flacke S, Layer G, Kreft B, Schild H. Hepatocellular carcinoma: detection with gadolinium- and ferumoxides-enhanced MR imaging of the liver. *Radiology* 2002; **222**: 73-80
107 **Craig J**, Peters R, Edmonson H. Tumors of the Liver and Intrahepatic Bile Ducts: Atlas of Tumor Pathology. Washington, DC: Armed Forced Institute of Pathology, 1989
108 **Bloom CM**, Langer B, Wilson SR. Role of US in the detection, characterization, and staging of cholangiocarcinoma. *Radiographics* 1999; **19**: 1199-1218
109 **Sherlock S**, Dooley J, editors. Diseases of the liver and biliary system. London: Blackwell Science, 1997
110 **Hashimoto T**, Nakamura H, Hori S, Tomoda K, Mitani T, Murakami T, Kozuka T, Monden M, Wakasa K, Sakurai M. MR imaging of mixed hepatocellular and cholangiocellular

carcinoma. *Abdom Imaging* 1994; **19**: 430-432
111 **Vilgrain V**, Van Beers BE, Flejou JF, Belghiti J, Delos M, Gautier AL, Zins M, Denys A, Menu Y. Intrahepatic cholangiocarcinoma: MRI and pathologic correlation in 14 patients. *J Comput Assist Tomogr* 1997; **21**: 59-65
112 **Maetani Y**, Itoh K, Watanabe C, Shibata T, Ametani F, Yamabe H, Konishi J. MR imaging of intrahepatic cholangiocarcinoma with pathologic correlation. *AJR Am J Roentgenol* 2001; **176**: 1499-1507
113 **Murakami T**, Nakamura H, Tsuda K, Ishida T, Tomoda K, Hori S, Monden M, Kanai T, Wakasa K, Sakurai M. Contrast-enhanced MR imaging of intrahepatic cholangiocarcinoma: pathologic correlation study. *J Magn Reson Imaging* 1995; **5**: 165-170
114 **Zhang Y**, Uchida M, Abe T, Nishimura H, Hayabuchi N, Nakashima Y. Intrahepatic peripheral cholangiocarcinoma: comparison of dynamic CT and dynamic MRI. *J Comput Assist Tomogr* 1999; **23**: 670-677
115 **Yoshida Y**, Imai Y, Murakami T, Nishikawa M, Kurokawa M, Yonezawa T, Tokunaga K, Fukushima Y, Wakasa K, Kim T, Nakamura H, Sakon M, Monden M. Intrahepatic cholangiocarcinoma with marked hypervascularity. *Abdom Imaging* 1999; **24**: 66-68
116 **Vogl TJ**, Hammerstingl R, Schwarz W, Kümmel S, Müller PK, Balzer T, Lauten MJ, Balzer JO, Mack MG, Schimpfky C, Schrem H, Bechstein WO, Neuhaus P, Felix R. Magnetic resonance imaging of focal liver lesions. Comparison of the superparamagnetic iron oxide resovist versus gadolinium-DTPA in the same patient. *Invest Radiol* 1996; **31**: 696-708
117 **Low SC**, Peh WC, Muttarak M, Cheung HS, Ng IO. Imaging features of hepatic angiomyolipomas. *J Med Imaging Radiat Oncol* 2008; **52**: 118-123

S- Editor Cheng JX **L- Editor** Cant MR **E- Editor** Zheng XM

World Journal of Radiology

Online Submissions: http://www.wjgnet.com/1949-8470office
wjr@wjgnet.com
doi:10.4329/wjr.v1.i1.86

World J Radiol 2009 December 31; 1(1): 86-91
ISSN 1949-8470 (online)

REVIEW

Contrast-enhanced harmonic ultrasound imaging in ablation therapy for primary hepatocellular carcinoma

Yasunori Minami, Masatoshi Kudo

Yasunori Minami, Masatoshi Kudo, Division of Gastroenterology and Hepatology, Department of Internal Medicine, Kinki University School of Medicine, 377-2 Ohno-Higashi Osaka-Sayama, 589-8511, Japan
Author contributions: Minami Y and Kudo M both contributed equally to collecting data and writing this manuscript.
Correspondence to: Masatoshi Kudo, MD PhD, Division of Gastroenterology and Hepatology, Department of Internal Medicine, Kinki University School of Medicine, 377-2 Ohno-Higashi Osaka-Sayama, 589-8511, Japan. m-kudo@med.kindai.ac.jp
Telephone: +81-72-3660221-3525 Fax: +81-72-3672880
Received: November 3, 2009 Revised: December 10, 2009
Accepted: December 21, 2009
Published online: December 31, 2009

Abstract

The success rate of percutaneous radiofrequency (RF) ablation for hepatocellular carcinoma (HCC) depends on correct targeting *via* an imaging technique. However, RF electrode insertion is not completely accurate for residual HCC nodules because B-mode ultrasound (US), color Doppler, and power Doppler US findings cannot adequately differentiate between treated and viable residual tumor tissue. Electrode insertion is also difficult when we must identify the true HCC nodule among many large regenerated nodules in cirrhotic liver. Two breakthroughs in the field of US technology, harmonic imaging and the development of second-generation contrast agents, have recently been described and have demonstrated the potential to dramatically broaden the scope of US diagnosis of hepatic lesions. Contrast-enhanced harmonic US imaging with an intravenous contrast agent can evaluate small hypervascular HCC even when B-mode US cannot adequately characterize tumor. Therefore, contrast-enhanced harmonic US can facilitate RF ablation electrode placement in hypervascular HCC, which is poorly depicted by B-mode US. The use of contrast-enhanced harmonic US in ablation therapy for liver cancer is an efficient approach.

Key words: Contrast-enhanced harmonic ultrasound; Hepatocellular carcinoma; Radiofrequency ablation; Second generation microbubbles

Peer reviewers: Roberto Miraglia, MD, Adjunct Associate Professor of Radiology, Department of Diagnostic and Interventional Radiology, Mediterranean Institute for Transplantation and Advanced Specialized Therapies (IsMeTT), University of Pittsburgh, Via Tricomi 1, Palermo, 90100, Italy; Xiao-Ming Zhang, MD, Professor, Department of Radiology, Affiliated Hospital of North Sichuan Medical College, Wenhua Road 63, Nanchong 637000, Sichuan Province, China

Minami Y, Kudo M. Contrast-enhanced harmonic ultrasound imaging in ablation therapy for primary hepatocellular carcinoma. *World J Radiol* 2009; 1(1): 86-91 Available from: URL: http://www.wjgnet.com/1949-8470/full/v1/i1/86.htm DOI: http://dx.doi.org/10.4329/wjr.v1.i1.86

INTRODUCTION

Hepatocellular carcinoma (HCC) is the most common primary hepatic malignancy[1,2]. Various treatment modalities such as hepatic resection, liver transplantation, transcatheter arterial chemoembolization (TACE), percutaneous ethanol injection, radiofrequency (RF) ablation, microwave coagulative therapy , percutaneous ethanol injection therapy and high intensity focused ultrasound have been developed resulting in improved outcomes[3-9]. Patients with liver tumors not suitable for resection may benefit from minimally invasive treatment that provides good palliation or cure. RF ablation is widely performed as a percutaneous local treatment under real-time sonographic guidance developed for this purpose[4-6]. However, multiple sessions of RF ablation therapy are

often required for hepatic malignancies, including cases in which hepatic nodules are poorly defined by B-mode ultrasound (US) alone[5]. US angiography and computed tomography (CT) fluoroscopy can be used for accurate tumor localization, intra-procedural monitoring, and procedural control[7,8]. These methods, however, increase exposure to radiation because multiple CT scans are obtained and the method is invasive because of the angiographic procedures involved. Moreover, an MR-guided system for RF ablation can show images of hepatic malignancies that cannot be adequately characterized on B-mode US[9]. Though we can use Magnetic resonance imaging (MRI) for reference images, RF ablation procedure is actually performed under sonographic guidance. Therefore, an MR-guided system cannot be used for intraprocedural monitoring and procedural control.

Worldwide, US has functioned as the mainstay of screening efforts to detect small incidental hepatomas in high-risk patients. Nevertheless, the limitations of conventional gray-scale B-mode US for the detection of focal liver lesions have been well documented[10]. Color Doppler and power Doppler increased the sensitivity for hepatic lesion detection compared to that of gray-scale US, but these modalities do not provide levels of sensitivity comparable to those of contrast-enhanced axial imaging (CT and MRI)[10-14]. Two breakthroughs in the field of US technology, harmonic imaging and the development of second-generation contrast agents, have recently been described and have demonstrated the potential to dramatically broaden the scope of US diagnosis of hepatic lesions[12-14]. Contrast-enhanced harmonic US imaging with an intravenous contrast agent is considered useful for assessing the therapeutic response to TACE and RF ablation therapy in patients with hepatic malignancies[15-19], and is able to evaluate small hypervascular HCCs even when B-mode US cannot adequately characterize the tumors[20-26].

Therefore, contrast-enhanced harmonic US is expected to decrease the number of RF ablation treatment sessions in difficult cases[26-31].

This paper will review the former state of the art techniques for contrast-enhanced US in RF ablation for liver cancer, and illustrate the potential of the newer techniques for improving the targeting in percutaneous RF ablation therapy.

CONTRAST-ENHANCED HARMONIC US

Contrast agents

Levovist (Schering, Berlin, Germany) is a first generation US agent consisting of galactose[32]. A trace of palmitic acid is added as a surfactant to stabilize the resultant microbubbles. When Levovist dissolves in blood, air trapped inside the galactose is released as free gas bubbles. These bubbles have a weak encapsulating shell and are easily destroyed by US.

More recently, developed agents made from fluorocarbon gases and albumin, surfactant, lipid, or

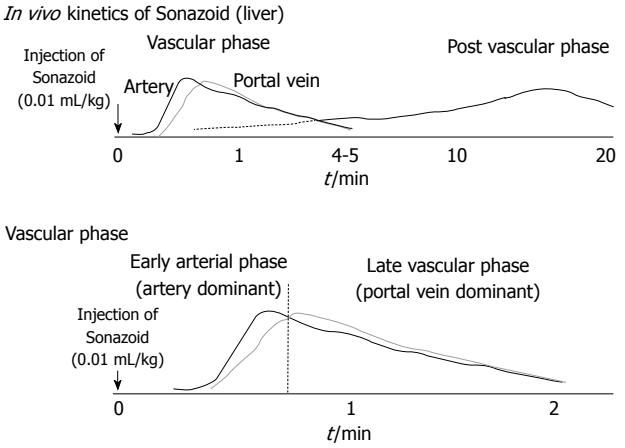

Figure 1 Kinetics of perfluorocarbon microbubbles (Sonazoid) in the liver.

polymer shells offer an increased persistence of the microspheres. These second-generation contrast agents consist of sulfur hexafluoride microbubbles (SonoVue; Bracco SpA, Milan, Italy), perflutren lipid microbubbles (Definity; Bristol- Myers Squibb, North Billerica, MA), and perflutren protein microbubbles (Optison; GE Healthcare, Buckinghamshire, UK). These microbubbles provide stable nonlinear oscillation in a low power acoustic field because of the hard shell of the bubbles, and therefore produce harmonic signals depicting great detail in real-time[33-37]. Perfluorocarbon microbubbles (Sonazoid; Daiichi-Sankyo, Tokyo, Japan) also belong to the second-generation of contrast agents for sonography[38,39]. Unlike other second-generation contrast agents, perfluorocarbon microbubbles are taken up by Kupffer cells in the liver. Therefore, these microbubbles accumulate in the liver parenchyma over time.

Technology and imaging

A gas bubble or encapsulated microsphere will resonate in a highly non-linear fashion, with much of the energy in the returned echo concentrated in harmonics of the insonating frequency[40]. Much of the energy of the backscattered signal is concentrated in or around the second harmonic. Many modern transducer/receiver systems have sufficient bandwidth to exploit this by insonating at the main resonant frequency of the bubble and filtering the returned signal to detect the second harmonic only. This enables separation of the signal derived from the contrast agent from the background tissue signal.

A variety of algorithms are involved in enhancement of the signal coming from the microbubbles and cancellation of signals from tissues. In pulse inversion, also known as phase inversion, two pulses in rapid succession are emitted into the tissue; the second pulse undergoes a 180° phase change so as to be a mirror image of the first. The fundamental response produced in the tissues, which will be phase-inverted compared with the fundamental pulses, is erased because the sum of the two-inverted pulses is zero. In this way, echoes from the microbubbles are enhanced so as to differentiate them from those coming from stationary tissues[41,42].

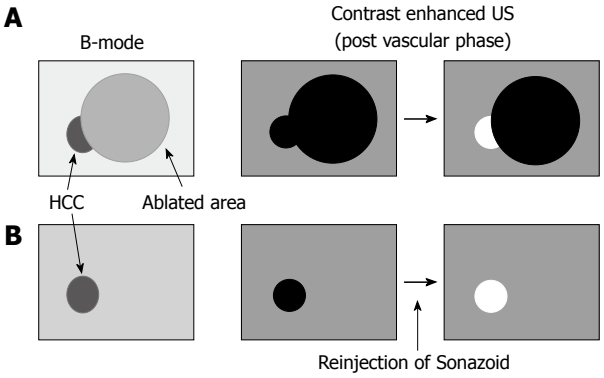

Figure 2 Indications for contrast-enhanced ultrasound (US) in radiofrequency (RF) ablation therapy. A: Local tumor progression or residual hepatic malignancies. Contrast-enhanced US shows not only the tumor but also ablated areas as a defect image in the post vascular phase. However, viable tumor is enhanced by reinjection of Sonazoid; B: Hepatic malignancies with severe cirrhotic change. The true malignant tumor was sited among many large regenerated nodules in cirrhotic liver. On contrast-enhanced US, the tumor was distinguishable by reinjection of Sonazoid.

In contrast-enhanced harmonic US with Sonazoid, the contrast-enhancement pattern of the tumor is determined by evaluations during the vascular and post vascular phases (Figure 1)[20-25]. Vascular findings are shown in the vascular phase (from 10 s to the last 5-7 min after the injection of contrast agent), and liver parenchymal findings are shown in the post vascular phase (about 10 min after the injection of contrast agents) because contrast agents are incorporated into Kupffer cells or liver sinusoids[20-25]. Especially in the vascular phase, the artery-dominant time zone is called early arterial phase, and the portal-dominant time zone is called the late vascular phase. Contrast-enhanced harmonic US using Sonazoid can provide detailed data, not only of the perfusion features in the microvascular bed of the liver parenchyma and tumor during the vascular phase, but also of Kupffer imaging during the post vascular phase. Malignant hepatic tumors may be depicted as defect images in real-time during the post vascular phase.

SONAZOID-ENHANCED HARMONIC US-GUIDED RF ABLATION

Background

The success rate of percutaneous RF ablation for hepatic cancer depends on correct targeting via an imaging technique. However, RF electrode insertion is not completely accurate for residual nodules of hepatic cancer because B-mode US, color Doppler, and power Doppler US findings cannot adequately differentiate between treated and viable residual tumor tissue[27]. Electrode insertion is also difficult when we must identify true malignant tumors among many large regenerated nodules in cirrhotic liver[27]. Therefore, contrast-enhanced harmonic US can faciliatate RF ablation electrode placement in hypervascular HCC, which is poorly depicted by B-mode US (Figure 2).

Procedure

The sonographic contrast agent is perfluorocarbon microbubbles (Sonazoid) with a median diameter of 2-3 μm. This contrast agent is reconstituted with 2 mL distilled water for injection. The anticipated clinical dose for imaging of liver lesions is 0.010 mL encapsulated gas per kilogram of body weight, and this contrast agent is administered as a bolus at a speed of 1 mL/s and then flushed with 10 mL of normal saline via a 22-gauge cannula placed in the antecubital vein.

The contrast harmonic imaging mode is adjusted after the plane showing the area of tumor has been viewed on B-mode US. Thus, we can see two views as contrast-enhanced US images and B-mode US images side by side on the monitor. At the appearance of the first microbubble signal in the liver parenchyma, patients are requested to hold their breath. Real-time images in the optimal scanning plane are displayed by slightly changing the scanning slice showing the nodule. Hepatic malignancies are visualized from the enhancement of intratumoral vessels at the outset (Figure 3) to defects in the liver parenchyma after a short time. We are able to use these defect lesions as a target for insertion of a single RF electrode. Percutaneous insertion of an RF electrode can be guided by real-time contrast harmonic US (Figure 3). In patients previously treated with ablation for hepatic nodules, demonstration of viable nodules among all nodules detected in post-vascular phase is achieved by re-injection of a new dose of Sonazoid, in order to confirm tumor vascularity before electrode insertion. After the RF electrode has penetrated hepatic malignancies, each ablation can be performed for a period of more than 8 min with at least 60 watts at treatment initiation.

CLINICAL OUTCOMES

Miyamoto *et al*[30] reported that conventional sonography identified 30 (57%) of 52 HCCs, whereas Sonazoid-enhanced US detected 50 (96%) of 52 HCCs. Complete ablation was achieved at a single session in 48 of 50 tumors. Thus, Sonazoid-enhanced US is a useful technique for guiding RF ablation of HCCs[30].

Numata *et al*[31] reported that nine (90%) of the 10 lesions that were not detected on conventional US but were depicted on real-time contrast-enhanced harmonic gray-scale US with Levovist (incomplete local treatment, $n = 4$; small new lesion, $n = 6$) were successfully treated with percutaneous ablation therapy guided by this method. The maximal diameter of the tumors ranged from 0.8 to 2.0 cm with a mean maximal diameter of 1.4 ± 0.4 cm (± SD).

The effectiveness of contrast harmonic sonographic guidance for RF ablation of locally progressive HCC has been evaluated prospectively, and the number of treatment sessions was found to be significantly lower in the contrast harmonic US group compared to conventional US (mean: 1.1 ± 0.2 *vs* 1.4 ± 0.6, respectively, $P = 0.037$)[28]. In this study, a series of 40 patients with HCC with

Figure 3 A 66-years-old man with 1.0 cm hepatocellular carcinoma (HCC) (S3) with liver cirrhosis. A: Contrast harmonic US showed HCC nodule as a defect (arrow) in the post vascular phase after administration of Sonazoid; B: Enhancement (arrow) of HCC was obtained in the defect immediately after reinjection of Sonazoid; C: The defect (arrow) was later exhibited again and the RF electrode needle (arrowheads) was inserted.

local tumor progression poorly depicted with B-mode US were randomly treated with RF ablation guided by either contrast harmonic US (n = 20) or conventional B-mode US (n = 20). Treatment analysis showed that the complete ablation rate after a single treatment session was significantly higher in the contrast harmonic US group than in the B-mode US group (94.7% *vs* 65.0%, P = 0.043).

Contrast-enhanced harmonic US using artificial pleural effusion could depict tumor vascularity in locally recurring HCC nodules which are located in the right subphrenic region[29]. Percutaneous RF ablation guided by contrast-enhanced harmonic US with artificial pleural effusion appears to be an efficient approach. Thirteen tumors were treated by percutaneous RF ablation guided by contrast-enhanced harmonic US. Complete tumor necrosis was achieved in a single session of RF ablation in 12 lesions (92.3%), whereas two sessions were required for the remaining lesion (n = 1, 7.7%) in cases treated under contrast-enhanced harmonic US guidance. The maximal diameter of the tumors ranged from 1.0 to 2.5 cm with a mean maximal diameter of 1.7 ± 0.4 cm (± SD). There were no lung injuries, such as pneumothorax, in any patient. It took approximately 1 wk for pleural effusions to spontaneously resolve.

OTHER MODALITIES

CO_2 enhanced US (US angiography)

US angiography enhanced with intraarterial injection of CO_2 microbubbles is a sensitive tool for the depiction of small hypervascular HCCs, especially those that are smaller than 1 cm in diameter[43,44]. US angiography is also useful for the accurate demonstration of vascularity within a tumor and offers useful information for determining the appropriate therapeutic strategy for the treatment of HCC. Thus, RF ablation guided by CO_2 microbubbles-enhanced US is a feasible technique for treating local progression of HCC lesions that cannot be adequately depicted by conventional US[45]. However, nodules may become unclear because bubbles become trapped and accumulate in sinusoids with repeated injections of CO_2 microbubbles. In addition, this method involves angiographic procedures that are invasive.

CT fluoroscopy

Under CT fluoroscopy using either CT arteriography or iodized oil injection, we can target and puncture hepatic malignancies using a percutaneous ethanol injection needle. Real-time CT fluoroscopy is useful to guide the needle puncture and to monitor ethanol injection in small hepatic malignancies[7]. Another merit of this technique is that the efficacy of treatment can be evaluated using contrast-enhanced CT immediately after treatment. However, this therapy would increase exposure to radiation when multiple CT scans are required, and is also invasive because of the subsequent angiographic procedure.

Real-time virtual sonography (RVS)

Virtual CT sonography using magnetic navigation (RVS; HITACHI Medico, Tokyo, Japan) provides cross-sectional images of CT volume data corresponding to the angle of the transducer in the magnetic field in real-time[46,47]. This imaging technique displays a real-time synchronized multiplanar CT image in precisely the same slice of the US plane. Thus, Real-time RVS can be used for real-time needle insertion guidance, especially for nodules demonstrated on CT, but not on US. Needle insertion guidance using RVS is also useful for locally recurring nodules next to previously ablated lesions, which are not usually detected by B-mode US. Furthermore, this technique is useful for ablation of the area, to establish a safety margin surrounding the originally ablated area. However, RVS has some weakness regarding imaging incompatibility which might be attributable to the fact that the depth of breath-holding on CT and US examination varies, and the chances of this problem also increase when the distance is greater between the magnetic sensor attached to the ultrasonic transducer and the magnetic generator.

CONCLUSION

Percutaneous RF ablation guided by contrast-enhanced harmonic US is an efficient approach for HCCs, which are not clearly demarcated by B-mode US, in both untreated and locally recurrent HCC cases. Moreover,

second generation microbubbles could facilitate contrast harmonic US guidance of RF ablation by extending the time limitation, simplifying the procedure, and improving detectability. RF ablation guided by second generation microbubbles-enhanced US could become easier and be an efficient approach for hepatic malignancies that are not clearly depicted on B-mode sonography.

REFERENCES

1 **Parkin DM**, Bray F, Ferlay J, Pisani P. Estimating the world cancer burden: Globocan 2000. *Int J Cancer* 2001; **94**: 153-156
2 **El-Serag HB**, Mason AC. Rising incidence of hepatocellular carcinoma in the United States. *N Engl J Med* 1999; **340**: 745-750
3 **Kudo M**. Local ablation therapy for hepatocellular carcinoma: current status and future perspectives. *J Gastroenterol* 2004; **39**: 205-214
4 **Rossi S**, Di Stasi M, Buscarini E, Cavanna L, Quaretti P, Squassante E, Garbagnati F, Buscarini L. Percutaneous radiofrequency interstitial thermal ablation in the treatment of small hepatocellular carcinoma. *Cancer J Sci Am* 1995; **1**: 73-81
5 **Cioni D**, Lencioni R, Rossi S, Garbagnati F, Donati F, Crocetti L, Bartolozzi C. Radiofrequency thermal ablation of hepatocellular carcinoma: using contrast-enhanced harmonic power doppler sonography to assess treatment outcome. *AJR Am J Roentgenol* 2001; **177**: 783-788
6 **Shiina S**, Teratani T, Obi S, Sato S, Tateishi R, Fujishima T, Ishikawa T, Koike Y, Yoshida H, Kawabe T, Omata M. A randomized controlled trial of radiofrequency ablation with ethanol injection for small hepatocellular carcinoma. *Gastroenterology* 2005; **129**: 122-130
7 **Takayasu K**, Muramatsu Y, Asai S, Muramatsu Y, Kobayashi T. CT fluoroscopy-assisted needle puncture and ethanol injection for hepatocellular carcinoma: a preliminary study. *AJR Am J Roentgenol* 1999; **173**: 1219-1224
8 **Brennan DD**, Appelbaum L, Raptopolous V, Kruskal JB, Goldberg SN. CT artifact introduced by radiofrequency ablation. *AJR Am J Roentgenol* 2006; **186**: S284-S286
9 **Maeda T**, Hong J, Konishi K, Nakatsuji T, Yasunaga T, Yamashita Y, Taketomi A, Kotoh K, Enjoji M, Nakashima H, Tanoue K, Maehara Y, Hashizume M. Tumor ablation therapy of liver cancers with an open magnetic resonance imaging-based navigation system. *Surg Endosc* 2009; **23**: 1048-1053
10 **Kudo M**. Imaging diagnosis of hepatocellular carcinoma and premalignant/borderline lesions. *Semin Liver Dis* 1999; **19**: 297-309
11 **Ding H**, Kudo M, Onda H, Suetomi Y, Minami Y, Maekawa K. Hepatocellular carcinoma: depiction of tumor parenchymal flow with intermittent harmonic power Doppler US during the early arterial phase in dual-display mode. *Radiology* 2001; **220**: 349-356
12 **Ding H**, Kudo M, Maekawa K, Suetomi Y, Minami Y, Onda H. Detection of tumor parenchymal blood flow in hepatic tumors: value of second harmonic imaging with a galactose-based contrast agent. *Hepatol Res* 2001; **21**: 242-251
13 **Kudo M**. Contrast harmonic ultrasound is a breakthrough technology in the diagnosis and treatment of hepatocellular carcinoma. *J Med Ultrasonics* 2001; **28**: 79-81
14 **Ding H**, Kudo M, Onda H, Suetomi Y, Minami Y, Chung H, Kawasaki T, Maekawa K. Evaluation of posttreatment response of hepatocellular carcinoma with contrast-enhanced coded phase-inversion harmonic US: comparison with dynamic CT. *Radiology* 2001; **221**: 721-730
15 **Cioni D**, Lencioni R, Bartolozzi C. Therapeutic effect of transcatheter arterial chemoembolization on hepatocellular carcinoma: evaluation with contrast-enhanced harmonic power Doppler ultrasound. *Eur Radiol* 2000; **10**: 1570-1575
16 **Minami Y**, Kudo M, Kawasaki T, Kitano M, Chung H, Maekawa K, Shiozaki H. Transcatheter arterial chemoembolization of hepatocellular carcinoma: usefulness of coded phase-inversion harmonic sonography. *AJR Am J Roentgenol* 2003; **180**: 703-708
17 **Meloni MF**, Goldberg SN, Livraghi T, Calliada F, Ricci P, Rossi M, Pallavicini D, Campani R. Hepatocellular carcinoma treated with radiofrequency ablation: comparison of pulse inversion contrast-enhanced harmonic sonography, contrast-enhanced power Doppler sonography, and helical CT. *AJR Am J Roentgenol* 2001; **177**: 375-380
18 **Wen YL**, Kudo M, Zheng RQ, Minami Y, Chung H, Suetomi Y, Onda H, Kitano M, Kawasaki T, Maekawa K. Radiofrequency ablation of hepatocellular carcinoma: therapeutic response using contrast-enhanced coded phase-inversion harmonic sonography. *AJR Am J Roentgenol* 2003; **181**: 57-63
19 **Wen YL**, Kudo M, Kawasaki T, Minami Y, Maekawa K. Hepatocellular carcinoma treated with radiofrequency ablation: Evaluation of therapeutic response by contrast-enhanced Coded Harmonic Angio. *Zhongguo Chaosheng Yixue Zazhi* 2002; **18**: 452-455
20 **Kudo M**. Early detection and curative treatment of early-stage hepatocellular carcinoma. *Clin Gastroenterol Hepatol* 2005; **3**: S144-S148
21 **Kudo M**. New sonographic techniques for the diagnosis and treatment of hepatocellular carcinoma. *Hepatol Res* 2007; **37** Suppl 2: S193-S199
22 **Hatanaka K**, Kudo M, Minami Y, Ueda T, Tatsumi C, Kitai S, Takahashi S, Inoue T, Hagiwara S, Chung H, Ueshima K, Maekawa K. Differential diagnosis of hepatic tumors: value of contrast-enhanced harmonic sonography using the newly developed contrast agent, Sonazoid. *Intervirology* 2008; **51** Suppl 1: 61-69
23 **Kudo M**, Hatanaka K, Maekawa K. Defect reperfusion imaing, a newly developed novel technology using Sonazoid in the treatment of hepatocellular carcinoma. *J Med Ultrasound* 2008; **16**: 169-176
24 **Hatanaka K**, Kudo M, Minami Y, Maekawa K. Sonazoid-enhanced ultrasonography for diagnosis of hepatic malignancies: comparison with contrast-enhanced CT. *Oncology* 2008; **75** Suppl 1: 42-47
25 **Xia Y**, Kudo M, Minami Y, Hatanaka K, Ueshima K, Chung H, Hagiwara S, Inoue T, Ishikawa E, Kitai S, Takahashi S, Tatsumi C, Ueda T, Hayaishi S, Maekawa K. Response evaluation of transcatheter arterial chemoembolization in hepatocellular carcinomas: the usefulness of sonazoid-enhanced harmonic sonography. *Oncology* 2008; **75** Suppl 1: 99-105
26 **Kudoa M**, Minamia Y. Radiofrequency ablation therapy under harmonic imaging guidance for the recurring cancer after local therapy for HCC: a randomized controlled study with RFA under B-mode guidance. *Ultrasound Med Biol* 2003; **29**: S145
27 **Minami Y**, Kudo M, Kawasaki T, Chung H, Ogawa C, Shiozaki H. Treatment of hepatocellular carcinoma with percutaneous radiofrequency ablation: usefulness of contrast harmonic sonography for lesions poorly defined with B-mode sonography. *AJR Am J Roentgenol* 2004; **183**: 153-156
28 **Minami Y**, Kudo M, Chung H, Kawasaki T, Yagyu Y, Shimono T, Shiozaki H. Contrast harmonic sonography-guided radiofrequency ablation therapy versus B-mode sonography in hepatocellular carcinoma: prospective randomized controlled trial. *AJR Am J Roentgenol* 2007; **188**: 489-494
29 **Minami Y**, Kudo M, Kawasaki T, Chung H, Ogawa C, Shiozaki H. Percutaneous radiofrequency ablation guided

by contrast-enhanced harmonic sonography with artificial pleural effusion for hepatocellular carcinoma in the hepatic dome. *AJR Am J Roentgenol* 2004; **182**: 1224-1226

30 **Miyamoto N**, Hiramatsu K, Tsuchiya K, Sato Y, Terae S, Shirato H. Sonazoid-enhanced sonography for guiding radiofrequency ablation for hepatocellular carcinoma: better tumor visualization by Kupffer-phase imaging and vascular-phase imaging after reinjection. *Jpn J Radiol* 2009; **27**: 185-193

31 **Numata K**, Isozaki T, Ozawa Y, Sakaguchi T, Kiba T, Kubota T, Ito A, Sugimori K, Shirato K, Morimoto M, Tanaka K. Percutaneous ablation therapy guided by contrast-enhanced sonography for patients with hepatocellular carcinoma. *AJR Am J Roentgenol* 2003; **180**: 143-149

32 **Schlief R**, Schurman R, Niendorf HP. Basic properties and results of clinical trials of ultrasound contrast agents based on galactose. *Ann Acad Med Singapore* 1993; **22**: 762-767

33 **Wilson SR**, Burns PN, Muradali D, Wilson JA, Lai X. Harmonic hepatic US with microbubble contrast agent: initial experience showing improved characterization of hemangioma, hepatocellular carcinoma, and metastasis. *Radiology* 2000; **215**: 153-161

34 **Jang HJ**, Kim TK, Burns PN, Wilson SR. Enhancement patterns of hepatocellular carcinoma at contrast-enhanced US: comparison with histologic differentiation. *Radiology* 2007; **244**: 898-906

35 **Wang Z**, Tang J, An L, Wang W, Luo Y, Li J, Xu J. Contrast-enhanced ultrasonography for assessment of tumor vascularity in hepatocellular carcinoma. *J Ultrasound Med* 2007; **26**: 757-762

36 **Leen E**, Angerson WJ, Yarmenitis S, Bongartz G, Blomley M, Del Maschio A, Summaria V, Maresca G, Pezzoli C, Llull JB. Multi-centre clinical study evaluating the efficacy of SonoVue (BR1), a new ultrasound contrast agent in Doppler investigation of focal hepatic lesions. *Eur J Radiol* 2002; **41**: 200-206

37 **Kono Y**, Lucidarme O, Choi SH, Rose SC, Hassanein TI, Alpert E, Mattrey RF. Contrast-enhanced ultrasound as a predictor of treatment efficacy within 2 weeks after transarterial chemoembolization of hepatocellular carcinoma. *J Vasc Interv Radiol* 2007; **18**: 57-65

38 **Ramnarine KV**, Kyriakopoulou K, Gordon P, McDicken NW, McArdle CS, Leen E. Improved characterisation of focal liver tumours: dynamic power Doppler imaging using NC100100 echo-enhancer. *Eur J Ultrasound* 2000; **11**: 95-104

39 **Korenaga K**, Korenaga M, Furukawa M, Yamasaki T, Sakaida I. Usefulness of Sonazoid contrast-enhanced ultrasonography for hepatocellular carcinoma: comparison with pathological diagnosis and superparamagnetic iron oxide magnetic resonance images. *J Gastroenterol* 2009; **44**: 733-741

40 **Calliada F**, Campani R, Bottinelli O, Bozzini A, Sommaruga MG. Ultrasound contrast agents: basic principles. *Eur J Radiol* 1998; **27** Suppl 2: S157-S160

41 **Burns PN**, Wilson SR, Simpson DH. Pulse inversion imaging of liver blood flow: improved method for characterizing focal masses with microbubble contrast. *Invest Radiol* 2000; **35**: 58-71

42 **Tiemann K**, Veltmann C, Ghanem A, Lohmaier S, Bruce M, Kuntz-Hehner S, Pohl C, Ehlgen A, Schlosser T, Omran H, Becher H. The impact of emission power on the destruction of echo contrast agents and on the origin of tissue harmonic signals using power pulse-inversion imaging. *Ultrasound Med Biol* 2001; **27**: 1525-1533

43 **Kudo M**, Tomita S, Tochio H, Kashida H, Hirasa M, Todo A. Hepatic focal nodular hyperplasia: specific findings at dynamic contrast-enhanced US with carbon dioxide microbubbles. *Radiology* 1991; **179**: 377-382

44 **Kudo M**, Tomita S, Tochio H, Mimura J, Okabe Y, Kashida H, Hirasa M, Ibuki Y, Todo A. Small hepatocellular carcinoma: diagnosis with US angiography with intraarterial CO2 microbubbles. *Radiology* 1992; **182**: 155-160

45 **Miyamoto N**, Hiramatsu K, Tsuchiya K, Sato Y. Carbon dioxide microbubbles-enhanced sonographically guided radiofrequency ablation: treatment of patients with local progression of hepatocellular carcinoma. *Radiat Med* 2008; **26**: 92-97

46 **Minami Y**, Kudo M, Chung H, Inoue T, Takahashi S, Hatanaka K, Ueda T, Hagiwara H, Kitai S, Ueshima K, Fukunaga T, Shiozaki H. Percutaneous radiofrequency ablation of sonographically unidentifiable liver tumors. Feasibility and usefulness of a novel guiding technique with an integrated system of computed tomography and sonographic images. *Oncology* 2007; **72** Suppl 1: 111-116

47 **Minami Y**, Chung H, Kudo M, Kitai S, Takahashi S, Inoue T, Ueshima K, Shiozaki H. Radiofrequency ablation of hepatocellular carcinoma: value of virtual CT sonography with magnetic navigation. *AJR Am J Roentgenol* 2008; **190**: W335-W341

S- Editor Cheng JX **L- Editor** Logan S **E- Editor** Zheng XM

World Journal of Radiology

Online Submissions: http://www.wjgnet.com/1949-8470office
wjr@wjgnet.com
www.wjgnet.com

World J Radiol 2009 December 31; 1(1): I
ISSN 1949-8470 (online)

Acknowledgments to reviewers of *World Journal of Radiology*

Many reviewers have contributed their expertise and time to the peer review, a critical process to ensure the quality of *World Journal of Radiology*. The editors and authors of the articles submitted to the journal are grateful to the following reviewers for evaluating the articles (including those published in this issue and those rejected for this issue) during the last editing time period.

Sergio Casciaro, PhD, Institute of Clinical Physiology-National Research Council, Campus Universitario Ecotekne, Via Monteroni, 73100 Lecce, Italy

Herwig R Cerwenka, Professor, MD, Department of Surgery, Medical University of Graz, Auenbruggerplatz 29, A-8036 Graz, Austria

Feng Chen, MD, PhD, Professor, Department of Radiology, Zhong Da Hospital, Southeast University, 87 Ding Jiaqiao, Nanjing 210009, Jiangsu Province, China

Kenneth Coenegrachts, MD, PhD, Department of Radiology, AZ St.-Jan AV, Ruddershove 10, B-8000 Bruges, Belgium

Abhijit P Datir, MBBS, MD, FRCR, DMRE, Division of Interventional Radiology, Jackson Memorial Hospital, 1611 NW 12th Avenue, West Wing 279, Miami, FL 33136, United States

Jurgen J Fütterer, MD PhD, Department of Radiology, Radboud University Nijmegen Medical Centre, Geert Grooteplein 10, 6500HB Nijmegen, The Netherlands

Takao Hiraki, MD, Radiology, Okayama University Medical School, 3-5-1 Shikatacho, Okayama 700-0861, Japan

Fehmi Kaçmaz, MD, Department of Cardiology, Mesa Hospital, Ozel Mesa Hastanesi, Yasam Cad, No: 5 Sogutozu, 06510 Ankara, Turkey

Mario Mascalchi, MD, PhD, Professor, Radiodiagnostic Section, Department of Clinical Physiopathology, University of Florence, Viale Morgagni 50134, Florence, Italy

Tarik F Massoud, MB, BCh, BAO, LRCPI, LRCSI, MA, MD, PhD, FRCR, Department of Radiology, University of Cambridge, Addenbrooke's Hospital, Box 219, Hills Road, Cambridge, CB2 2QQ, United Kingdom

Roberto Miraglia, MD, Adjunct Associate Professor of Radiology, Department of Diagnostic and Interventional Radiology, Mediterranean Institute for Transplantation and Advanced Specialized Therapies (IsMeTT), University of Pittsburgh, Via Tricomi 1, Palermo, 90100, Italy

Aytekin Oto, MD, Associate Professor of Radiology, Chief of Abdominal Imaging and Body MRI, Department of Radiology, University of Chicago, 5841 S Maryland Ave, MC 2026 Chicago, IL 60637, United States

Ramachandran Prabhakar, PhD, Department of Radiation Oncology, Institute Rotary Cancer Hospital, All India Institute of Medical Sciences, New Delhi 110 029, India

Sergio Sartori, MD, Department of Internal Medicine, Section of Interventional Ultrasound, St. Anna Hospital, I-44100 Ferrara, Italy

Hui-Xiong Xu, MD, PhD, Professor, Department of Medical Ultrasonics, Institute of Diagnostic and Interventional Ultrasound, Sun Yat-Sen University, 58 Zhongshan Road 2, Guangzhou 510080, Guangdong Province, China

Hadi Rokni Yazdi, MD, Central Radiology, Imam Khomeini Hospital, Keshavarz Blvd, Tehran, 1419733141, Iran

Xiao-Ming Zhang, MD, Professor, Department of Radiology, Affiliated Hospital of North Sichuan Medical College, Wenhua Road 63, Nanchong 637000, Sichuan Province, China

WJR World Journal of Radiology

Online Submissions: http://www.wjgnet.com/1949-8470office
wjr@wjgnet.com
www.wjgnet.com

World J Radiol 2009 December 31; 1(1): I
ISSN 1949-8470 (online)

Meetings

Events Calendar 2010

January 04-08
Beaver Creek, Colorado, United States
18th Annual Winter Diagnostic Imaging Update

January 07-09
Leuven, Belgium
4th Leuven Course on Ear Imaging

January 16-17
Hollywood, Florida, United States
The Symposium on Clinical Interventional Oncology

January 17-21
Hollywood, Florida, United States
The International Symposium on Endovascular Therapy

January 21-22
Cairo, Egypt
BGICC Breast Gyne International Cancer Conference

January 21-24
Phoenix, AZ, United States
13th Society for Cardiovascular Magnetic Resonance (SCMR) Annual Scientific Sessions

January 23-23
Atlanta, GA, United States
Emory Winship Cancer Institute: Breast Cancer 2010: Advances in Science, Emerging Data, and Novel Therapeutics

January 25-29
Maui, HI, United States
Musculoskeletal & Neuroradiology MR Imaging Update in Maui

January 27-February 02
Albuquerque, NM, United States
2010 SNM Conjoint Mid-Winter Meetings

January 29-January 30
Barcelona, Spain
7th European Congress: Perspectives in Gynecologic Oncology

February 07-February 12
Vail, CO, United States
15th Annual Vail 2010: Multislice CT in Clinical Practice

February 11-13
Las Vegas, NV, United States
5th Annual Symposium on PET/CT and Molecular Imaging

February 16-19
Park City, UT, United States
6th Interventional/ Neurointerventional Conference

February 18-19
London, United Kingdom
Diagnostic and Interventional Radiology

February 18-21
Las Vegas, NV, United States
American Society of Spine Radiology Annual Symposium

February 20-20
Jacksonville, Florida, United States
Mayo Clinic Molecular Markers and Management of Breast Cancer

February 20-21
Bethesda, Maryland, United States
25th Anniversary Washington Neuroradiology Review

February 21-26
Orlando, FL, United States
The Abdominal Radiology Course

February 21-27
Snowmass, CO, United States
16th Annual Snowmass 2010: Clinical Ultrasound

February 22-26
Bethesda, MD, United States
48th Annual Dr. Kenneth M. Earle Memorial Neuropathology Review

February 24-27
Lake Buena Vista, FL, United States
ACRO 2010 American College of Radiation Oncology Symposium: Clinical Radiation Oncology Challenges

February 25- 27
Chandler, AZ, United States
Multidisciplinary Head and Neck Cancer Symposium

February 26-27
Brussels, Belgium
10èmes Mises au Point en Imagerie Ostéo-Articulaire

February 27-March 01
Cairo, Egypt
7th Gastroenterology Hepatology & Endoscopy Symposium

February 28-March 04
Scottsdale, AZ, United States
International Congress XXIII on Endovascular Interventions

February 28-March 05
Breckenridge, CO, United States
5th Annual Breckenridge 2010: Musculoskeletal MRI

March 03-06
Las Vegas, Nevada, United States
11th Annual Advances in Breast Imaging and Interventions

March 04-08
Vienna, Austria
European Congress of Radiology (ECR 2010) Annual Meeting

March 05-07
Mt Tremblant, QC, Canada
Neuroimaging and Head & Neck Radiology Update in Mt Tremblant

March 07-11
San Diego, CA, United States
SCBT-MR Masters in Body Imaging: "What's New, What's Hot, What You May Not Have Known"

March 10-13
San Antonio, Texas, United States
Clinical Osteoporosis 2010: An ISCD-NOF Symposium

March 11-13
Barcelona, Spain
EORTC Group Meeting: EORTC Radiation Oncology Group

March 11-13
Hannover, Germany
40. Kongress der Deutschen Gesellschaft für Endoskopie und Bildgebende Verfahren e.V.

March 13-18
Tampa, FL, United states
Society of interventional radiology 35th Annual Scientific Meeting

March 14-17
Park City, UT, United States
14th Annual Park City 2010: MRI in Clinical Practice

March 22-26
Beaver Creek, CO, United States
NYU Radiology Spring Skiing Symposium in Beaver Creek

March 22-26
Maui, HI, United States
18th Annual Spring Diagnostic Imaging Update

March 24-27
San Diego, California, United States
2010 American institute of ultrasound in Medicine Annual Convention Preliminary Program

March 24-27
Barcelona, Spain
7th European Breast Cancer Conference

April 8-12
Shanghai, China
The 26th International Congress of Radiology

September 8-12
Guangzhou, China
Chinese Society of Interventional Radiology, 2010 CSIR

November 28-December 03
Chicago, United States
Radiological Society of North America: 2010 Annual Meeting

World Journal of Radiology

Online Submissions: http://www.wjgnet.com/1949-8470office
wjr@wjgnet.com
www.wjgnet.com

World J Radiol 2009 December 31; 1(1): I-V
ISSN 1949-8470 (online)

Instructions to authors

GENERAL INFORMATION

World Journal of Radiology (*World J Radiol*, *WJR*, online ISSN 1949-8470, DOI: 10.4329), is a monthly, open-access (OA), peer-reviewed journal supported by an editorial board of 303 experts in Radiology from 38 countries.

The biggest advantage of the OA model is that it provides free, full-text articles in PDF and other formats for experts and the public without registration, which eliminates the obstacle that traditional journals possess and usually delays the speed of the propagation and communication of scientific research results. The open access model has been proven to be a true approach that may achieve the ultimate goal of the journals, i.e. the maximization of the value to the readers, authors and society.

The role of academic journals is to exhibit the scientific levels of a country, a university, a center, a department, and even a scientist, and build an important bridge for communication between scientists and the public. As we all know, the significance of the publication of scientific articles lies not only in disseminating and communicating innovative scientific achievements and academic views, as well as promoting the application of scientific achievements, but also in formally recognizing the "priority" and "copyright" of innovative achievements published, as well as evaluating research performance and academic levels. So, to realize these desired attributes of *WJR* and create a well-recognized journal, the following four types of personal benefits should be maximized. The maximization of personal benefits refers to the pursuit of the maximum personal benefits in a well-considered optimal manner without violation of the laws, ethical rules and the benefits of others. (1) Maximization of the benefits of editorial board members: The primary task of editorial board members is to give a peer review of an unpublished scientific article *via* online office system to evaluate its innovativeness, scientific and practical values and determine whether it should be published or not. During peer review, editorial board members can also obtain cutting-edge information in that field at first hand. As leaders in their field, they have priority to be invited to write articles and publish commentary articles. We will put peer reviewers' names and affiliations along with the article they reviewed in the journal to acknowledge their contribution; (2) Maximization of the benefits of authors: Since *WJR* is an open-access journal, readers around the world can immediately download and read, free of charge, high-quality, peer-reviewed articles from *WJR* official website, thereby realizing the goals and significance of the communication between authors and peers as well as public reading; (3) Maximization of the benefits of readers: Readers can read or use, free of charge, high-quality peer-reviewed articles without any limits, and cite the arguments, viewpoints, concepts, theories, methods, results, conclusion or facts and data of pertinent literature so as to validate the innovativeness, scientific and practical values of their own research achievements, thus ensuring that their articles have novel arguments or viewpoints, solid evidence and correct conclusion; and (4) Maximization of the benefits of employees: It is an iron law that a first-class journal is unable to exist without first-class editors, and only first-class editors can create a first-class academic journal. We insist on strengthening our team cultivation and construction so that every employee, in an open, fair and transparent environment, could contribute their wisdom to edit and publish high-quality articles, thereby realizing the maximization of the personal benefits of editorial board members, authors and readers, and yielding the greatest social and economic benefits.

The major task of *WJR* is to rapidly report the most recent improvement in the research of medical imaging and radiation therapy by the radiologists. *WJR* accepts papers on the following aspects related to radiology: Abdominal radiology, women health radiology, cardiovascular radiology, chest radiology, genitourinary radiology, neuroradiology, head and neck radiology, interventional radiology, musculoskeletal radiology, molecular imaging, pediatric radiology, experimental radiology, radiological technology, nuclear medicine, PACS and radiology informatics, and ultrasound. We also encourage papers that cover all other areas of radiology as well as basic research.

The columns in the issues of *WJR* will include: (1) Editorial: To introduce and comment on the substantial advance and its importance in the fast-developing areas; (2) Frontier: To review the most representative achievements and comment on the current research status in the important fields, and propose directions for the future research; (3) Topic Highlight: This column consists of three formats, including (A) 10 invited review articles on a hot topic, (B) a commentary on common issues of this hot topic, and (C) a commentary on the 10 individual articles; (4) Observation: To update the development of old and new questions, highlight unsolved problems, and provide strategies on how to solve the questions; (5) Guidelines for Basic Research: To provide Guidelines for basic research; (6) Guidelines for Clinical Practice: To provide guidelines for clinical diagnosis and treatment; (7) Review: To systemically review the most representative progress and unsolved problems in the major scientific disciplines, comment on the current research status, and make suggestions on the future work; (8) Original Articles: To originally report the innovative and valuable findings in radiology; (9) Brief Articles: To briefly report the novel and innovative findings in radiology; (10) Case Report: To report a rare or typical case; (11) Letters to the Editor: To discuss and make reply to the contributions published in *WJR*, or to introduce and comment on a controversial issue of general interest; (12) Book Reviews: To introduce and comment on quality monographs of radiology; and (13) Guidelines: To introduce Consensuses and Guidelines reached by international and national academic authorities worldwide on the research in radiology.

CSSN
ISSN 1949-8470 (online)

Published by
Beijing Baishideng BioMed Scientific Co., Ltd.

SUBMISSION OF MANUSCRIPTS

Manuscripts should be typed in 1.5 line spacing and 12 pt. Book Antiqua with ample margins. Number all pages consecutively, and start each of the following sections on a new page: Title Page, Abstract, Introduction, Materials and Methods, Results, Discussion, Acknowledgements, References, Tables, Figures, and Figure Legends. Neither the editors nor the publisher are responsible for the opinions expressed by contributors. Manuscripts formally accepted for publication become the permanent property of Beijing Baishideng BioMed Scientifc Co., Ltd., and may not be reproduced by any means, in whole or in part, without the written permission of both the authors and the publisher. We reserve the right to copy-edit and put onto our website accepted manuscripts. Authors should follow the relevant guidelines for the care and use of laboratory animals of their institution or national animal welfare committee. For the sake of transparency in regard to the performance and reporting of clinical trials, we endorse the policy of the International Committee of Medical Journal Editors to refuse to publish papers on clinical trial results if the trial was not recorded in a publicly-accessible registry at its outset. The only register now available, to our knowledge, is http://www. clinicaltrials.gov sponsored by the United States National Library of Medicine and we encourage all potential contributors to register with it. However, in the case that other registers become available you will be duly notified. A letter of recommendation from each author's organization should be provided with the contributed article to ensure the privacy and secrecy of research is protected.

Authors should retain one copy of the text, tables, photographs and illustrations because rejected manuscripts will not be returned to the author(s) and the editors will not be responsible for loss or damage to photographs and illustrations sustained during mailing.

Online submissions

Manuscripts should be submitted through the Online Submission System at: http://www.wjgnet.com/1949-8470office. Authors are highly recommended to consult the ONLINE INSTRUCTIONS TO AUTHORS (http://www.wjgnet.com/1949-8470/index.htm) before attempting to submit online. For assistance, authors encountering problems with the Online Submission System may send an email describing the problem to wjr@wjgnet.com, or by telephone: +86-10-59080036. If you submit your manuscript online, do not make a postal contribution. Repeated online submission for the same manuscript is strictly prohibited.

MANUSCRIPT PREPARATION

All contributions should be written in English. All articles must be submitted using word-processing software. All submissions must be typed in 1.5 line spacing and 12 pt. Book Antiqua with ample margins. Style should conform to our house format. Required information for each of the manuscript sections is as follows:

Title page

Title: Title should be less than 12 words.

Running title: A short running title of less than 6 words should be provided.

Authorship: Authorship credit should be in accordance with the standard proposed by International Committee of Medical Journal Editors, based on (1) substantial contributions to conception and design, acquisition of data, or analysis and interpretation of data; (2) drafting the article or revising it critically for important intellectual content; and (3) final approval of the version to be published. Authors should meet conditions 1, 2, and 3.

Institution: Author names should be given first, then the complete name of institution, city, province and postcode. For example, Xu-Chen Zhang, Li-Xin Mei, Department of Pathology, Chengde Medical College, Chengde 067000, Hebei Province, China. One author may be represented from two institutions, for example, George Sgourakis, Department of General, Visceral, and Transplantation Surgery, Essen 45122, Germany; George Sgourakis, 2nd Surgical Department, Korgialenio-Benakio Red Cross Hospital, Athens 15451, Greece

Author contributions: The format of this section should be: Author contributions: Wang CL and Liang L contributed equally to this work; Wang CL, Liang L, Fu JF, Zou CC, Hong F and Wu XM designed the research; Wang CL, Zou CC, Hong F and Wu XM performed the research; Xue JZ and Lu JR contributed new reagents/analytic tools; Wang CL, Liang L and Fu JF analyzed the data; and Wang CL, Liang L and Fu JF wrote the paper.

Supportive foundations: The complete name and number of supportive foundations should be provided, e.g., Supported by National Natural Science Foundation of China, No. 30224801

Correspondence to: Only one corresponding address should be provided. Author names should be given first, then author title, affiliation, the complete name of institution, city, postcode, province, country, and email. All the letters in the email should be in lower case. A space interval should be inserted between country name and email address. For example, Montgomery Bissell, MD, Professor of Medicine, Chief, Liver Center, Gastroenterology Division, University of California, Box 0538, San Francisco, CA 94143, United States. montgomery.bissell@ucsf.edu

Telephone and fax: Telephone and fax should consist of +, country number, district number and telephone or fax number, e.g., Telephone: +86-10-59080039 Fax: +86-10-85381893

Peer reviewers: All articles received are subject to peer review. Normally, three experts are invited for each article. Decision for acceptance is made only when at least two experts recommend an article for publication. Reviewers for accepted manuscripts are acknowledged in each manuscript, and reviewers of articles which were not accepted will be acknowledged at the end of each issue. To ensure the quality of the articles published in *WJR*, reviewers of accepted manuscripts will be announced by publishing the name, title/position and institution of the reviewer in the footnote accompanying the printed article. For example, reviewers: Professor Jing-Yuan Fang, Shanghai Institute of Digestive Disease, Shanghai, Affiliated Renji Hospital, Medical Faculty, Shanghai Jiaotong University, Shanghai, China; Professor Xin-Wei Han, Department of Radiology, The First Affiliated Hospital, Zhengzhou University, Zhengzhou, Henan Province, China; and Professor Anren Kuang, Department of Nuclear Medicine, Huaxi Hospital, Sichuan University, Chengdu, Sichuan Province, China.

Abstract
There are unstructured abstracts (no more than 256 words) and structured abstracts (no more than 480). The specific requirements for structured abstracts are as follows:

An informative, structured abstracts of no more than 480 words should accompany each manuscript. Abstracts for original contributions should be structured into the following sections. AIM (no more than 20 words): Only the purpose should be included. Please write the aim as the form of "To investigate/study/…; MATERIALS AND METHODS (no more than 140 words); RESULTS (no more than 294 words): You should present *P* values where appropriate and must provide relevant data to illustrate how they were obtained, e.g. 6.92 ± 3.86 *vs* 3.61 ± 1.67, $P < 0.001$; CONCLUSION (no more than 26 words). Available from: http://www.wjgnet.com/wjg/help/8.doc

Key words
Please list 5-10 key words, selected mainly from *Index Medicus*, which reflect the content of the study.

Text
For articles of these sections, original articles, rapid communication and case reports, the main text should be structured into the following sections: INTRODUCTION, MATERIALS AND METHODS, RESULTS and DISCUSSION, and should include appropriate Figures and Tables. Data should be presented in the main text or in Figures and Tables, but not in both. The main text format of these sections, editorial, topic highlight, case report, letters to the editors, can be found at: http://www.wjgnet.com/wjg/help/instructions.jsp.

Illustrations
Figures should be numbered as 1, 2, 3, *etc.*, and mentioned clearly in the main text. Provide a brief title for each figure on a separate page. Detailed legends should not be provided under the figures. This part should be added into the text where the figures are applicable. Figures should be either Photoshop or Illustrator files (in tiff, eps, jpeg formats) at high-resolution. Examples can be found at: http://www.wjgnet.com/1007-9327/13/4520.pdf; http://www.wjgnet.com/1007-9327/13/4554.pdf; http://www.wjgnet.com/1007-9327/13/4891.pdf; http://www.wjgnet.com/1007-9327/13/4986.pdf; http://www.wjgnet.com/1007-9327/13/4498.pdf. Keeping all elements compiled is necessary in line-art image. Scale bars should be used rather than magnification factors, with the length of the bar defined in the legend rather than on the bar itself. File names should identify the figure and panel. Avoid layering type directly over shaded or textured areas. Please use uniform legends for the same subjects. For example: Figure 1 Pathological changes in atrophic gastritis after treatment. A: ...; B: ...; C: ...; D: ...; E: ...; F: ...; G: …*etc.* It is our principle to publish high resolution-figures for the printed and E-versions.

Tables
Three-line tables should be numbered 1, 2, 3, *etc.*, and mentioned clearly in the main text. Provide a brief title for each table. Detailed legends should not be included under tables, but rather added into the text where applicable. The information should complement, but not duplicate the text. Use one horizontal line under the title, a second under column heads, and a third below the Table, above any footnotes. Vertical and italic lines should be omitted.

Notes in tables and illustrations
Data that are not statistically significant should not be noted. $^{a}P < 0.05$, $^{b}P < 0.01$ should be noted ($P > 0.05$ should not be noted). If there are other series of *P* values, $^{c}P < 0.05$ and $^{d}P < 0.01$ are used. A third series of *P* values can be expressed as $^{e}P < 0.05$ and $^{f}P < 0.01$. Other notes in tables or under illustrations should be expressed as ^{1}F, ^{2}F, ^{3}F; or sometimes as other symbols with a superscript (Arabic numerals) in the upper left corner. In a multi-curve illustration, each curve should be labeled with ●, ○, ■, □, ▲, △, *etc.*, in a certain sequence.

Acknowledgments
Brief acknowledgments of persons who have made genuine contributions to the manuscript and who endorse the data and conclusions should be included. Authors are responsible for obtaining written permission to use any copyrighted text and/or illustrations.

REFERENCES
Coding system
The author should number the references in Arabic numerals according to the citation order in the text. Put reference numbers in square brackets in superscript at the end of citation content or after the cited author's name. For citation content which is part of the narration, the coding number and square brackets should be typeset normally. For example, "Crohn's disease (CD) is associated with increased intestinal permeability[1,2]". If references are cited directly in the text, they should be put together within the text, for example, "From references[19,22-24], we know that..."

When the authors write the references, please ensure that the order in text is the same as in the references section, and also ensure the spelling accuracy of the first author's name. Do not list the same citation twice.

PMID and DOI
Pleased provide PubMed citation numbers to the reference list, e.g. PMID and DOI, which can be found at http://www.ncbi.nlm.nih.gov/sites/entrez?db=pubmed and http://www.crossref.org/SimpleTextQuery/, respectively. The numbers will be used in E-version of this journal.

Style for journal references
Authors: the name of the first author should be typed in bold-faced letters. The family name of all authors should be typed with the initial letter capitalized, followed by their abbreviated first and middle initials. (For example, Lian-Sheng Ma is abbreviated as Ma LS, Bo-Rong Pan as Pan BR). The title of the cited article and italicized journal title (journal title should be in its abbreviated form as shown in PubMed), publication date, volume number (in black), start page, and end page [PMID: 11819634 DOI: 10.3748/wjg.13.5396].

Style for book references
Authors: the name of the first author should be typed in bold-faced letters. The surname of all authors should be typed with the initial letter capitalized, followed by their abbreviated middle and first initials. (For example, Lian-Sheng Ma is abbreviated as Ma LS, Bo-Rong Pan as Pan BR) Book title. Publication number. Publication place: Publication press, Year: start page and end page.

Format

Journals

English journal article (list all authors and include the PMID where applicable)

1 **Jung EM**, Clevert DA, Schreyer AG, Schmitt S, Rennert J, Kubale R, Feuerbach S, Jung F. Evaluation of quantitative contrast harmonic imaging to assess malignancy of liver tumors: A prospective controlled two-center study. *World J Gastroenterol* 2007; **13**: 6356-6364 [PMID: 18081224 DOI: 10.3748/wjg.13.6356]

Chinese journal article (list all authors and include the PMID where applicable)

2 **Lin GZ**, Wang XZ, Wang P, Lin J, Yang FD. Immunologic effect of Jianpi Yishen decoction in treatment of Pixu-diarrhoea. *Shijie Huaren Xiaohua Zazhi* 1999; **7**: 285-287

In press

3 **Tian D**, Araki H, Stahl E, Bergelson J, Kreitman M. Signature of balancing selection in Arabidopsis. *Proc Natl Acad Sci USA* 2006; In press

Organization as author

4 **Diabetes Prevention Program Research Group**. Hypertension, insulin, and proinsulin in participants with impaired glucose tolerance. *Hypertension* 2002; **40**: 679-686 [PMID: 12411462 PMCID:2516377 DOI:10.1161/01.HYP.0000035706.28494.09]

Both personal authors and an organization as author

5 **Vallancien G**, Emberton M, Harving N, van Moorselaar RJ; Alf-One Study Group. Sexual dysfunction in 1, 274 European men suffering from lower urinary tract symptoms. *J Urol* 2003; **169**: 2257-2261 [PMID: 12771764 DOI:10.1097/01.ju.0000067940.76090.73]

No author given

6 21st century heart solution may have a sting in the tail. *BMJ* 2002; **325**: 184 [PMID: 12142303 DOI:10.1136/bmj.325.7357.184]

Volume with supplement

7 **Geraud G**, Spierings EL, Keywood C. Tolerability and safety of frovatriptan with short- and long-term use for treatment of migraine and in comparison with sumatriptan. *Headache* 2002; **42** Suppl 2: S93-99 [PMID: 12028325 DOI:10.1046/j.1526-4610.42.s2.7.x]

Issue with no volume

8 **Banit DM**, Kaufer H, Hartford JM. Intraoperative frozen section analysis in revision total joint arthroplasty. *Clin Orthop Relat Res* 2002; (**401**): 230-238 [PMID: 12151900 DOI:10.1097/00003086-200208000-00026]

No volume or issue

9 Outreach: Bringing HIV-positive individuals into care. *HRSA Careaction* 2002; 1-6 [PMID: 12154804]

Books

Personal author(s)

10 **Sherlock S**, Dooley J. Diseases of the liver and billiary system. 9th ed. Oxford: Blackwell Sci Pub, 1993: 258-296

Chapter in a book (list all authors)

11 **Lam SK**. Academic investigator's perspectives of medical treatment for peptic ulcer. In: Swabb EA, Azabo S. Ulcer disease: investigation and basis for therapy. New York: Marcel Dekker, 1991: 431-450

Author(s) and editor(s)

12 **Breedlove GK**, Schorfheide AM. Adolescent pregnancy. 2nd ed. Wieczorek RR, editor. White Plains (NY): March of Dimes Education Services, 2001: 20-34

Conference proceedings

13 **Harnden P**, Joffe JK, Jones WG, editors. Germ cell tumours V. Proceedings of the 5th Germ cell tumours Conference; 2001 Sep 13-15; Leeds, UK. New York: Springer, 2002: 30-56

Conference paper

14 **Christensen S**, Oppacher F. An analysis of Koza's computational effort statistic for genetic programming. In: Foster JA, Lutton E, Miller J, Ryan C, Tettamanzi AG, editors. Genetic programming. EuroGP 2002: Proceedings of the 5th European Conference on Genetic Programming; 2002 Apr 3-5; Kinsdale, Ireland. Berlin: Springer, 2002: 182-191

Electronic journal (list all authors)

15 Morse SS. Factors in the emergence of infectious diseases. Emerg Infect Dis serial online, 1995-01-03, cited 1996-06-05; 1(1): 24 screens. Available from: URL: http//www.cdc.gov/ncidod/EID/eid.htm

Patent (list all authors)

16 **Pagedas AC**, inventor; Ancel Surgical R&D Inc., assignee. Flexible endoscopic grasping and cutting device and positioning tool assembly. United States patent US 20020103498. 2002 Aug 1

Statistical data

Write as mean ± SD or mean ± SE.

Statistical expression

Express *t* test as *t* (in italics), *F* test as *F* (in italics), chi square test as χ^2 (in Greek), related coefficient as *r* (in italics), degree of freedom as υ (in Greek), sample number as *n* (in italics), and probability as *P* (in italics).

Units

Use SI units. For example: body mass, m (B) = 78 kg; blood pressure, p (B) = 16.2/12.3 kPa; incubation time, t (incubation) = 96 h, blood glucose concentration, c (glucose) 6.4 ± 2.1 mmol/L; blood CEA mass concentration, p (CEA) = 8.6 24.5 μg/L; CO_2 volume fraction, 50 mL/L CO_2, not 5% CO_2; likewise for 40 g/L formaldehyde, not 10% formalin; and mass fraction, 8 ng/g, *etc.* Arabic numerals such as 23, 243, 641 should be read 23 243 641.

The format for how to accurately write common units and quantums can be found at: http://www.wjgnet.com/wjg/help/15.doc.

Abbreviations

Standard abbreviations should be defined in the abstract and on first mention in the text. In general, terms should not be abbreviated unless they are used repeatedly and the abbreviation is helpful to the reader. Permissible abbreviations are listed in Units, Symbols and Abbreviations: A Guide for Biological and Medical Editors and Authors (Ed. Baron DN, 1988) published by The Royal Society of Medicine, London. Certain commonly used abbreviations, such as DNA, RNA, HIV, LD50, PCR, HBV, ECG, WBC, RBC, CT, ESR, CSF, IgG, ELISA, PBS, ATP, EDTA, mAb, can be used directly without further explanation.

Italics

Quantities: *t* time or temperature, *c* concentration, *A* area, *l* length, *m* mass, *V* volume.

Genotypes: *gyrA*, *arg* 1, *c myc*, *c fos*, *etc.*

Restriction enzymes: *Eco*RI, *Hin*dI, *Bam*HI, *Kbo* I, *Kpn* I, *etc.*
Biology: *H. pylori*, *E coli*, *etc.*

RE-SUBMISSION OF THE REVISED PAPER

Please revise your article according to the revision policies of *WJR*. The revised version including manuscript and high-resolution image figures (if any) should be re-submitted or uploaded online. The author should send copyright transfer letter, and responses to the reviewers and science news to us *via* email.

Editorial Office

World Journal of Radiology

Editorial Department: Room 903, Building D,
Ocean International Center,
No. 62 Dongsihuan Zhonglu,
Chaoyang District, Beijing 100025, China
E-mail: wjr@wjgnet.com
http://www.wjgnet.com
Telephone: +86-10-59080036
Fax: +86-10-85381893

Language evaluation

The language of a manuscript will be graded before it is sent for revision. (1) Grade A: priority publishing; (2) Grade B: minor language polishing; (3) Grade C: a great deal of language polishing needed; and (4) Grade D: rejected. Revised articles should reach Grade A or B.

Copyright assignment form

Please download a Copyright assignment form from http://www.wjgnet.com/1007-9327/news/10.doc.

Responses to reviewers

Please revise your article according to the comments/suggestions provided by the reviewers. The format for responses to the reviewers' comments can be found at: http://www.wjgnet.com/1007-9327/news/12.doc.

Proof of financial support

For paper supported by a foundation, authors should provide a copy of the document and serial number of the foundation.

Science news releases

Authors of accepted manuscripts are suggested to write a science news item to promote their articles. The news will be released rapidly at EurekAlert/AAAS (http://www.eurekalert.org). The title for news items should be less than 90 characters; the summary should be less than 75 words; and main body less than 500 words. Science news items should be lawful, ethical, and strictly based on your original content with an attractive title and interesting pictures.

Publication fee

Authors of accepted articles must pay a publication fee.
EDITORIAL, TOPIC HIGHLIGHTS, BOOK REVIEWS and LETTERS TO THE EDITOR are published free of charge.